UNIVERSITÀ
DEGLI STUDI
DI PADOVA

TESI DI DOTTORATO

Innovative Techniques for Biomechanical Evaluation of Stroke Survivors: Combined fMRI-Gait Analysis Assessment and Fugl-Meyer Clinical Scores Estimation Through Wearable Sensors.

SCUOLA DI DOTTORATO DI RICERCA IN : Ingegneria dell'Informazione

INDIRIZZO : Bioingegneria

CICLO : XXIV

Direttore della Scuola : Ch.mo Prof. Matteo Bertocco

Supervisore : Ch.ma Dott. Ing. Chiara Dalla Man

Dottoranda : Silvia Del Din

Gennaio 2012

UNIVERSITÀ
DEGLI STUDI
DI PADOVA

TESI DI DOTTORATO

Sede Amministrativa: Università degli Studi di Padova

Dipartimento di Ingegneria dell'Informazione

SCUOLA DI DOTTORATO DI RICERCA IN : Ingegneria dell'Informazione

INDIRIZZO : Bioingegneria

CICLO : XXIV

Innovative Techniques for Biomechanical Evaluation of Stroke Survivors: Combined fMRI-Gait Analysis Assessment and Fugl-Meyer Clinical Scores Estimation Through Wearable Sensors.

Direttore della Scuola : Ch.mo Prof. Matteo Bertocco

Supervisore : Ch.ma Dott. Ing. Chiara Dalla Man

Dottorando : Silvia Del Din

Contents

Abstract

Stroke is a leading cause among cerebrovascular injuries responsible for disabilities and social functioning difficulties. This pathology can really affect patients functionality, so that they might not be able to perform the daily simple activities like walking, eating and so on.

So individual rehabilitation programs are designed to address subject-specific motor impairments and functional limitations, therefore it is of paramount importance to optimize the outcomes of rehabilitation on a subject-by-subject basis. What clinicians usually do to assess the effectiveness of rehabilitation programs is to use some clinical scales, which are based on the observation of subjects motor behavior, they are usually time consuming, expensive to perform and quite subjective, so therapists and clinicians often favor increasing the time devoted to therapy at the cost of not performing longitudinal assessments of motor abilities.

Therefore the aim of this work is trying to provide an objective and fast methodology to evaluate stroke survivors performances: the first method is based on a combined functional magnetic resonance imaging (fMRI)-gait analysis study, where fMRI is a MRI procedure that measures brain activity by detecting associated changes in blood flow, and gait analysis is the motion analysis of the human gait; the second one relies on the use of the wearable technology.

The first section of the thesis describes the first method which focuses on an electromyographic biofeedback rehabilitation program for the lower limbs, while the second one develops a method to estimate clinical scores through the use of wearable sensors, centering mostly on the upper limbs.

As regards the first method, one of the primary goals for neurological rehabilitation after stroke is to walk independently with a velocity and endurance which allow the patient to take part in home and community activities of daily living. In particular looking at the gait patterns of hemiparetic stroke survivors they tend to have a severe reduction of ankle power in the push-off phase of the gait cycle, which can lead to an overall reduced gait quality and velocity. The ankle power produced at this stage is a parameter which can be measured only by a laboratory integrated system for gait analysis.

Recent studies have shown that rehabilitation protocols based on electromyographic biofeedback (BFB), in a motor learning context, in post-stroke patients, might improve the ankle joint power production during the push off, increase the speed and enhance the quality of their gait.

The functional magnetic resonance imaging provides an effective approach to analyze brain activity during cognitive and motor tasks in both healthy subjects and, in this context, patients with neurological damages, thanks to the high spatial resolution and safety. So far fMRI has been applied almost exclusively to the upper limbs' analysis, only a few studies have investigated the brain activation during tasks related to the ankle joint. The overall analysis of the current state of art highlights the need to investigate the ankle plantar-dorsiflexion in these patients, from a clinical, kinematic, dynamic point of view and to follow the ankle recovery in relation to possible changes in brain activity. The study involves the recruitment of 1 control

subject and 4 patients with chronic hemiparesis due to ischemic or hemorrhagic stroke, the patients underwent clinical evaluation, instrumented gait analysis and fMRI analysis.

First a preliminary analysis at T0 (i.e. pre-rehabilitation treatment) was performed on post-stroke patients in order to identify the brain activation areas during the motor task of active and passive plantar-dorsiflexion, both for the unaffected and affected side, comparing the obtained results with the healthy subject data.

Afterwards a longitudinal study was carried out on post-stroke patients, before and after a BFB rehabilitation program, aimed at improving the global ankle functionality during gait. Both gait analysis data (kinetics, kinematics and electromyographic activity (EMG)) and fMRI data were collected at T1 (i.e. 2 months after T0) to assess the stabilization of the functional clinical picture and to test the repeatability/reliability of the data collected at T0. Then patients underwent a BFB rehabilitation intervention and they were asked to come back for further assessments within 1 week after the end of rehabilitation (T2) and after 3 months of follow-up (T3) after the initial assessment. The T2 and T3 assessments included the same tests performed at T1.

The healthy subject underwent the fMRI analysis, in order to determine the normative brain activation areas.

Gait analysis was performed by means of an integrated motion analysis system consisting of infrared cameras synchronized with force plates and an EMG device in order to evaluate the subjects' kinematics, kinetics and the patterns of muscle activation.

The data analysis, the functional assessment, the correlation between the gait analysis and the brain activity parameters were used to identify the

possible relationship between the motor ability improvement and the brain reorganization after the BFB treatment; this might become a crucial aspect for the longitudinal assessment of the motor recovery in neurological patients and for the analysis of the mutual interactions between brain activation maps and gait analysis parameters.

In this context clinical assessment scales to evaluate motor abilities in stroke survivors could be used to individualize rehabilitation interventions thus maximizing motor gains. Unfortunately, these scales are not widely utilized in clinical practice because their administration is excessively time-consuming. Wearable sensors could be relied upon to address this issue, so the second method exploits this technology. Sensor data could be unobtrusively gathered during the performance of motor tasks. Features extracted from the sensor data could provide the input to models designed to estimate the severity of motor impairments and functional limitations. In previous work, it has been shown that wearable sensor data collected during the performance of items of the Wolf Motor Function Test (a clinical scale designed to assess functional capability) can be used to estimate scores derived using the Functional Ability Scale, a clinical scale focused on quality of movement. The purpose of the study herein presented was to investigate whether the same dataset could be used to estimate clinical scores derived using the Fugl-Meyer Assessment scale (a clinical scale designed to assess motor impairments). The results showed that Fugl-Meyer Assessment Test scores can be estimated by feeding a Random Forest with features derived from wearable sensor data recorded during the performance of as few as a single item of the Wolf Motor Function Test. Estimates achieved using the proposed method were marked by a root mean squared error as low as 4.7 points of the Fugl-Meyer Assessment Test scale.

This thesis develops two different parts: the first one describes the combined analysis of fmri and gait analysis data for the evaluation of the biofeedback rehabilitation treatment on post-stroke patients, while the second one focuses on a new technique to estimating Fugl-Meyer clinical scores in stroke survivors using wearable sensors.

An overview of the topics of this work with an introduction to Stroke, fMRI, and Gait Analysis is provided in chapter 2. Chapter 3 is centered on the first study: section 3.1 describes the patients' recruitment, section 3.2 focuses on the fMRI instrumental assessment; section 3.3 describes the clinical assessment, section 3.4 is based upon the gait analysis instrumental assessment, section 3.5 focuses on fMRI, gait data analysis, and corelation analysis; in section 3.6 the fMRI, the gait analysis, and the correlation results are reported; finally conclusions and results are the object of section 3.7. The wearable sensors project is the object of chapter 4: an introduction to the wearable sensors and the clinical scores is provided in section 4.1; section 4.2 describes the materials and methods used for the estimation of the clinical scores; in section 4.3 the results obtained from the data gathered from the wearable sensors are reported, finally conclusions and results are the object of section 4.4.

Sommario

La capacità di camminare autonomamente con la velocità e resistenza che permettono le attività di tutti i giorni è uno degli obiettivi primari per la riabilitazione neurologica dopo l'ictus (Stroke) che, tra le lesioni cerebrovascolari, è considerato la principale patologia responsabile di disabilità e di difficoltà nell'inserimento sociale dopo l'evento acuto. Questa patologia può davvero influire sulla funzionalità dei pazienti, che generalmente impedicscono loro di svolgere le semplici attività quotidiane come camminare, mangiare e così via.

Ecco che diventa di fondamentale importanza riuscire a pianificare dei programmi di riabilitazione individuali ad hoc per risolvere gli specifici deficit motori e le limitazioni funzionali, questo, quindi, diventa basilare per ottimizzare i risultati della riabilitazione a livello individuale-soggettivo. Per valutare l'efficacia dei programmi di riabilitazione è pratica comune utilizzare alcune scale cliniche che si basano sull'osservazione delle performances motorie dei soggetti, tuttavia queste valutazioni richiedono molto tempo, sono costose e di fatto soggettive; perciò solitamente i fisioterapisti e i clinici preferiscono aumentare il tempo dedicato alla terapia a scapito di una valutazione longitudinale delle capacità motorie dei pazienti.

L'obiettivo di questo lavoro è di fornire una metodologia oggettiva e veloce per valutare il recupero motorio dei pazienti post-ictus: il primo metodo

si basa su un'analisi combinata di risonanza magnetica funzionale (fMRI)-analisi del cammino, dove l'fMRI è una tecnica di imaging biomedico che misura l'attività cerebrale rilevando i cambiamenti del flusso sanguigno e l'analisi del cammino è definita come l'applicazione dell'analisi del movimento al gesto del cammino; mentre il secondo si focalizza sull'utilizzo della tecnologia indossabile.

La tesi è così strutturata: la prima sezione descrive il primo metodo che si concentra su un programma di riabilitazione basato su biofeedback elettromiografico per gli arti inferiori, mentre la seconda sezione si concentra su un metodo per stimare i punteggi clinici attraverso l'uso di sensori indossabili, centrando l'attenzione maggiormente sugli arti superiori.

Per quanto riguarda il primo studio, è noto che i pazienti con emiparesi causata da ictus tendono ad avere una severa riduzione della potenza prodotta alla caviglia in fase di push-off, con conseguente riduzione della velocità deambulatoria; la potenza prodotta in questa fase è un parametro misurabile solo tramite strumentazione integrata di analisi del cammino effettuata in laboratorio. Studi recenti hanno dimostrato come un protocollo riabilitativo basato su biofeedback elettromiografico (BFB) in un contesto di apprendimento motorio di pazienti con emiparesi post-ictus stabilizzata, sia utile nel migliorare la produzione di potenza alla caviglia al push-off, la velocità e la qualità del cammino. La risonanza magnetica funzionale fornisce un approccio efficace per analizzare l'attività cerebrale relativa a processi motori e cognitivi, sia in soggetti sani che, in questo contesto, in soggetti affetti da danni neurologici, grazie all'elevata risoluzione spaziale e alla sicurezza; essa è stata quasi sempre applicata allo studio dell'arto superiore, pochi studi hanno investigato l'attivazione cerebrale durante task relativi alla caviglia. Nasce da queste considerazioni l'utilità di indagare

la capacità di dorsiflessione plantare della caviglia, sotto il profilo clinico, cinematico-dinamico e di seguirne il recupero in relazione ad una possibile variazione dell'attivazione cerebrale. Lo studio ha previsto il reclutamento di 1 soggetto di controllo e di 4 pazienti cronici con emiparesi da ictus cerebrale (ischemico o emorragico) che sono stati sottoposti ad una valutazione clinica, ad un'analisi strumentata del cammino e ad un'analisi fMRI. In primo luogo è stata effettuata stata effettuata un'analisi preliminare a tempo T0 (ovvero pre-trattamento riabilitativo) nei pazienti post-ictus, per individuare le zone di attivazione cerebrale in seguito al movimento sia attivo che passivo di plantar-dorsiflessione, nell'arto colpito e non, confrontando i risultati ottenuti con i dati soggetto sano. Successivamente, sui pazienti post-ictus, è stato condotto uno studio longitudinale prima e dopo un programma riabilitativo di BFB, mirato al miglioramento della funzionalità della caviglia durante il cammino. Sono stati acquisiti i dati di fMRI e di analisi del cammino (cinetica, cinematica e attività elettromiografia di superficie (EMG)) al tempo T1 (2 mesi dopo T0) per verificare la stabilizzazione del quadro clinico-funzionale e per testare la ripetibilità dei dati raccolti a T0. I pazienti poi sono stati sottoposti ad un programma riabilitativo di BFB e sono stati invitati a ripresentarsi al termine della riabilitazione (entro 1 settimana, T2) e dopo 3 mesi di follow-up (T3) rispetto alla valutazione iniziale. Le valutazioni a T2 e T3 hanno incluso gli stessi test effettuati a T1. Sul soggetto è stata effettuata l'analisi fMRI, per definire le zone di attivazione cerebrale di riferimento da confrontare con i dati ottenuti dai pazienti. L'analisi del cammino cinematica e dinamica è stato sviluppato tramite un sistema integrato di analisi del movimento, rilevazione delle forze al suolo e dei pattern di attivazione muscolare (tramite EMG di superficie). L'analisi dei dati, la valutazione funzionale e la correlazione tra i parametri dell'analisi del movi-

mento e dell'attività cerebrale sono stati utilizzati allo scopo di identificare la possibile relazione tra il miglioramento dell'atto motorio e la capacità di riorganizzazione cerebrale a seguito del trattamento di BFB; questo diventa fondamentale per la valutazione longitudinale del recupero motorio in pazienti neurologici e per lo studio delle interazioni reciproche tra le mappe di attivazione e i parametri di movimento.

In questo contesto, le scale di valutazione clinica per esaminare le abilità motorie nei pazienti post-ictus potrebbero essere utilizzate per individuare e programmare interventi di riabilitazione personalizzati e ad-hoc, con lo scopo di massimizzare il recupero motorio. Purtroppo, queste scale non sono ampiamente utilizzate nella pratica clinica, perchè la loro somministrazione è dispendiosa sia dal punto di vista economico che lunga in termini di tempo. L'utilizzo di sensori indossabili potrebbe essere una possibile soluzione a questo problema, ecco che il secondo metodo sfrutta questa tecnologia. I dati dei sensori possono essere facilmente raccolti durante l'esecuzione di alcuni compiti motori. Le features estratte dai dati dei sensori sono utilizzate come input a modelli costruiti e progettati per valutare la gravità dei deficit motori e delle limitazioni funzionali. In un precedente lavoro è stato dimostrato che i dati dei sensori indossabili raccolti durante l'esecuzione di alcuni task del Wolf Motor Function Test (una scala clinica che serva a valutare le capacità funzionali) possono essere efficacemente utilizzati per stimare i punteggi ottenuti utilizzando la Function Ability Scale, una scala clinica che valuta le performance dei pazienti durante i task del Wolf Motor Function Test, focalizzandosi sulla qualità del movimento. Lo scopo dello studio qui presentato è stato quello di valutare se lo stesso set di dati possano essere utilizzati per stimare i punteggi clinici ottenuti utilizzando la Fugl-Meyer Scale, una scala di valutazione clinica incentrata sulle disabilità motorie dei pazienti e non

sulla funzionalità motoria. I risultati hanno mostrato che i punteggi del test di Fugl-Meyer possono essere stimati utilizzando il metodo delle Random Forest dando come input le features estratte dai dati dei sensori indossabili raccolti durante l'esecuzione di anche solo un singolo task del Wolf Motor Function Test. Le stime degli score clinici della scala clinica di Fugl-Meyer, ottenute utilizzando il metodo proposto, hanno permesso di ottenere uno scarto quadratico medio di 4.7 punti.

Questa tesi si sviluppa in due part: la prima descrive l'analisi combinata fMRI-analisi del cammino per la valutazione del trattamento riabilitativo biofeedback su pazienti post-ictus; mentre la seconda si concentra su una nuova tecnica per stimare i punteggi clinici della scala di Fugl-Meyer in pazienti post-ictus, mediante l'utilizzo di sensori indossabili.

Una panoramica di questo lavoro, una introduzione allo Stroke, all'fMRI, e all'Analisi del Cammino è fornita nel capitolo 2. Il capitolo 3 è centrato sull primo studio: la sezione 3.1 descrive il reclutamento dei pazienti, la sezione 3.2 si concentra sulla valutazione strumentale fMRI, la sezione 3.3 descrive la valutazione clinica, la sezione 3.4 si incentra sulla valutazione strumentale dell'analisi del cammino, la sezione 3.5 si concentra sia sull'analisi dei dati di fMRI, dell'analisi del cammino e sull'analisi di correlazione, nella sezione 3.6 sono riportati i risultati sia dell'analisi fMRI, dell'analisi del cammino che di correlazione, infine le conclusioni ed i risultati sono l'oggetto della sezione 3.7. Il progetto sensori indossabili è l'oggetto del capitolo 4: un'introduzione alla tematicche dei sensori indossabili e dei punteggi clinici è descritta nella sezione 4.1; la sezione 4.2 è incentrata sui i materiali e metodi utilizzati per la stima dei punteggi clinici; nella sezione 4.3 sono riportati i risultati ottenuti dai dati raccolti dai sensori indossabili, infine le conclusioni ed i risultati sono l'oggetto della sezione 4.4.

Chapter 1

Introduction

1.1 Overview

Stroke is a leading cause among cerebrovascular injuries responsible for disabilities and social functioning difficulties after the acute event. The main causes behind the limited mobility impairments and limited functions in post-stroke patients are the side effects of muscle paralysis [1], the loss of balance [2] and the reduced mobility [3], so that stoke can really affect patients functionality: they might not be able to perform the daily simple activities like walking, eating and so on.

Usually individual rehabilitation programs are designed to address subject-specific motor impairments and functional limitations, therefore it is of paramount importance to optimize the outcomes of rehabilitation on a subject-by-subject basis. What clinicians usually do to assess the effectiveness of rehabilitation programs is to use some clinical scales, which are based on the observation of a subjects motor behavior, they are usually time consuming, expensive to perform and quite subjective, so therapists and clinicians often favor increasing the time devoted to therapy at the cost of not performing

longitudinal assessments of motor abilities.

Therefore the aim of this work is trying to provide an objective and fast methodology to evaluate stroke survivors performances: the first method is based on a combined functional magnetic resonance imaging (fMRI)-gait analysis study, the second one relies on the use of the wearable technology.

A primary goal for neurological rehabilitation after stroke is the overall recovery of motor abilities in order to allow stroke survivors to walk independently with a velocity and endurance which allow the patient to take part in home and community activities of daily living. Six months after stroke, patients with persistent hemiparesis walk approximately one third as fast and only 40% the distance of age-matched healthy persons (Dobkin et al., 2004). In this context a lot of rehabilitation treatments based on exercise programs (muscle strengthening exercises and task-oriented) try to improve the balance and the mobility in people with chronic stroke, furthermore gait training treatments can improve walking speed and endurance [4].

The techniques of biofeedback (BFB) have already been used extensively in various areas of rehabilitation, and several studies have used BFB, focusing on improving various aspects of gait in patients with chronic stroke, with encouraging results [5, 6, 7, 8, 9].

Post-stroke patients may experience different motor disorders, for example a upper lesion of the motor neuron may lead to an alteration of muscle control that may vary from patient to patient: some patients have changes in the selective control, the loss of the latter consists of an over-activation of the flexor muscles during the swing phase (hip flexors, knee flexors and tibialis anterior) or of the extensor muscles (quadriceps, triceps and gluteus maximus). An impaired proprioception prevents some patients from experiencing a proper motor control due to the lack of feedback of the position

data. For some patients the only detectable alteration of their gait is the foot drop [10].

Focusing on walking, ankle dorsiflexion (ADF) is of particular interest in patients with hemiparesis of the lower limb, because this movement is often significantly more impaired than the complimentary plantar flexion. ADF is an integral component in gait, so it is not surprising that impairment of this movement is correlated strongly with walking difficulties and therefore predisposing these stroke patients to an increased likelihood of falling [11].

In normal gait, the ankle plantar flexors produce about 80% of the total energy necessary during the gait [12], the work of the ankle plantar flexors is primarily used to contribute to the forward motion during gait, and thus it plays a fundamental role in determining gait velocity [8].

The main role of the plantar flexors during the gait cycle is the push-off during the final phase of the stance.

Patients with hemiparesis tend to have a severe reduction of ankle power in the push-off phase of gait as well as a reduced velocity in gait [8], the ankle power produced at this stage is a parameter which can be measured only by a laboratory integrated system for gait analysis.

In this context gait analysis performed in laboratory settings has shown to provide a great amount of valuable information, whose use for inferring the physical disabilities of post-stroke patients has already been assessed in the literature [13].

Recent studies [14, 15] have shown that a rehabilitation protocol based on electromyographic biofeedback (BFB), in a motor learning context, in post-stroke patients with stabilized hemiparesis, might be useful to improve the ankle joint power production during the push off, to increase the speed and to enhance the quality of their gait.

So far, upon our review, there are no studies that try to correlate the outcomes of the rehabilitation interventions with any possible change of the brain activation, which might be a realistic hypothesis especially when dealing with rehabilitation protocols based on motor learning.

The functional magnetic resonance imaging is one of the most common techniques to analyze brain activity during cognitive and motor tasks in both healthy subjects and, in this context, patients with neurological damages due to high spatial resolution and safety; moreover fMRI may allow for the monitoring of changes in brain activation after rehabilitation programs and it becomes a tool used more widely to study recovery of hemiparesis [16], affecting 89% of stroke patients. So far fMRI has been applied, in this context, almost exclusively to analyze the upper limb, only a few studies have investigated the brain activation during motor tasks performed with the foot or the ankle joint.

Walking is not feasible during fMRI; cerebral activity has been assessed while subjects imagine walking, but the cerebral resources used by an individual to visualize ambulation are open to wide variations across subjects. Prior studies have used toe, foot, or knee movements during fMRI. Such fMRI assessment, if applied serially over time, hopefully could provide information necessary to improve stroke recovery through development of rehabilitation strategies that are tailored to the individual [17].

In this context, during fMRI, ADF could be considered the most similar task to gait analysis. So far fMRI studies were based on the evaluation of cerebral activity during ankle dorsiflexion tasks to assay motor control during walking on healthy subjects [4, 11]; nevertheless, as regards gait analysis, the ability of task-oriented electromyography biofeedback rehabilitation to improve gait in post-stroke patients was assessed [14, 15]. To the authors'

knowledge only a study combined motion capture with fMRI while subjects performed ADF tasks. Although the proposed integrated system showed different advantages with respect to the commonly used technologies, the motion capture system was used to assess ankle kinematics while performing ADF during fMRI [18].

The overall analysis of the current state of art highlights the need to investigate the ankle plantar-dorsiflexion ability in these patients, from a clinical, kinematic, dynamic point of view and to follow the ankle recovery in relation to possible changes in brain activity. The possible benefits are represented by the opportunity to learn more about the changes in the gait of these patients, to study the relationship between the activation of specific brain areas during motor tasks and the effects of the rehabilitation treatment (trying to detect any possible change post-rehabilitation treatment) and to properly plan specific rehabilitation interventions in order to improve the motor outcomes.

1.2 Aims of the thesis

The aim of this work is trying to provide an objective and fast methodology to evaluate stroke survivors performances: the first method is based on a combined fMRI-gait analysis, the second one relies on the use of the wearable technology. The first study developed into different phases, with separate aims per phase.

First, post-stroke patients with hemiparesis underwent a preliminary analysis at T0, which is to say pre-rehabilitation treatment, in order to identify the brain activation pattern during the motor tasks of active and passive plantar-dorsiflexion, both for the unaffected and affected side, comparing

the obtained results with the healthy subject data. The primary goal was to analyze the passive and active voluntary movement of plantar-dorsiflexion.

Afterwards, a longitudinal study was carried out on post-stroke patients before and after a BFB rehabilitation program aimed at improving the global ankle functionality during gait. Both fMRI and gait data were collected at T1 (i.e. 2 months after T0 to ensure the absence of new ictal events, to assess the stabilization of the functional clinical picture and to test the repeatability/reliability of the data collected at T0), then after 15 sessions of BFB rehabilitation (T2) and finally after 3 months of follow-up (T3) after the initial assessment.

In order to evaluate the motor functions and the desirable improvements post rehabilitation treatment, instrumental gait analyses were performed at time T1, T2 and T3. Kinematic and dynamic gait analysis were performed by means of an integrated motion analysis system consisting of infrared cameras synchronized with force plates and a surface electromyography was used in order to evaluate the patterns of muscle activation; the patients' data were compared with the normative bands obtained from a group of healthy control subjects.

The aim of this study was to present a new methodology, based both on fMRI and gait analysis outcomes, in order to investigate the ability of fMRI's to reflect the phases of motor learning pre/post electromyography biofeedback treatment and after 3 months of follow up, and to identify the possible relationship between the motor recovery and the changes in brain activation areas associated with the considered motor functions.

The second study developed a method to estimate clinical scores through the use of wearable sensors, centering mostly on the upper limbs. Clinical assessment scales to evaluate motor abilities in stroke survivors could be used

to individualize rehabilitation interventions thus maximizing motor gain, but unfortunately these scales are not widely utilized in clinical practice because their administration is excessively time-consuming. Wearable sensors could be relied upon to address this issue, so the second method exploits this technology. Sensor data could be unobtrusively gathered during the performance of motor tasks. Features extracted from the sensor data could provide the input to models designed to estimate the severity of motor impairments and functional limitations. In previous work, it has been shown that wearable sensor data collected during the performance of items of the Wolf Motor Function Test (a clinical scale designed to assess functional capability) can be used to estimate scores derived using the Functional Ability Scale, a clinical scale focused on quality of movement. The purpose of the study herein presented was to investigate whether the same dataset could be used to estimate clinical scores derived using the Fugl-Meyer Assessment scale (a clinical scale designed to assess motor impairments). The results showed that Fugl-Meyer Assessment Test scores can be estimated by feeding a Random Forest with features derived from wearable sensor data recorded during the performance of as few as a single item of the Wolf Motor Function Test.

1.3 Outlines of the thesis

This thesis develops two different parts: the first one describes the combined analysis of fMRI and gait analysis data for the evaluation of the biofeedback rehabilitation treatment on post-stroke patients, while the second one focuses on a new technique to estimating Fugl-Meyer clinical scores in stroke survivors using wearable sensors.

An overview of the topics of this work with an introduction to Stroke,

fMRI, and Gait Analysis is provided in chapter 2. Chapter 3 is centered on the first study: section 3.1 describes the patients' recruitment, section 3.2 focuses on the fMRI instrumental assessment; section 3.3 describes the clinical assessment, section 3.4 is based upon the gait analysis instrumental assessment, section 3.5 focuses on fMRI, gait data analysis, and correlation analysis; in section 3.6 the fMRI, the gait analysis, and the correlation results are reported; finally conclusions and results are the object of section 3.7. The wearable sensors project is the object of chapter 4: an introduction to the wearable sensors and the clinical scores is provided in section 4.1; section 4.2 describes the materials and methods used for the estimation of the clinical scores; in section 4.3 the results obtained from the data gathered from the wearable sensors are reported, finally conclusions and results are the object of section 4.4.

Chapter 2

Background

2.1 Stroke

Stroke is defined by the World Health Organization as 'rapidly developed clinical signs of focal or global disturbance of cerebral function, lasting more than 24 hours or until death, with no apparent non-vascular cause' [19]. Stroke is a leading cause of disease and death throughout the world [20], in particular Stroke is the third leading cause of death and the leading cause of long-term disability in the world [19]. Each year there are approximately 196,000 Italians living with the effects of stroke. In addition, there are millions of husbands, wives, children, and friends who care for stroke survivors and whose own lives are personally affected.

A stroke occurs when blood flow to the brain stops. The urgency of this situation cannot be understated. The sooner the blood supply is restored, the greater the likelihood of successful recovery. Stroke can be classified into two major categories: the ischemic stroke and the hemorrhagic stroke, moreover people might experience a third kind of stroke called the transient ischemic attack. In a systematic review of population-based epidemiologic studies

Feigin et al. showed that in 2000-2008 in high-income countries ischemic strokes constituted 82% of strokes and 11% were caused by intracerebral hemorrhage [21]. Therefore the most common is an ischemic stroke, caused by a blood clot that blocks a blood vessel or artery in the brain. The other, less common stroke, is a hemorrhagic stroke, caused when a blood vessel in the brain ruptures and spills blood into the surrounding tissue. Brain cells in the area begin to die, either because they stop getting the oxygen and nutrients they need to function, or they are killed by the rupture of the vessel and sudden spill of blood. The third type of stroke is the transient ischemic attack (TIA), the TIA is a transient stroke that lasts only a few minutes. It occurs when the blood supply to part of the brain is briefly interrupted. TIA symptoms, which usually occur suddenly, are similar to those of stroke but do not last as long. Most symptoms of a TIA disappear within an hour, although they may persist for up to 24 hours. Symptoms can include: numbness or weakness in the face, arm, or leg, especially on one side of the body; confusion or difficulty in talking or understanding speech; trouble seeing in one or both eyes; and difficulty with walking, dizziness, or loss of balance and coordination. TIAs are often warning signs that a person is at risk for a more serious and debilitating stroke. About one-third of those who have a TIA will have an acute stroke some time in the future. Heeding the warning signs of TIAs and treating underlying risk factors can prevent many strokes.

The symptoms of stroke happen immediately:

- Numbness or weakness in the face, arms, or legs (especially on one side of the body);

- Confusion, difficulty speaking or understanding speech;

- Vision disturbances in one or both eyes;
- Dizziness, trouble walking, loss of balance or coordination;
- Severe headache with no known cause.

Stroke appears to run in some families who may either have a genetic mutation that predisposes them to stroke, or share a lifestyle that contributes to stroke risk factors. Other than genetic predisposition, additional risk factors for stroke are high blood pressure, heart disease, smoking, diabetes, and high cholesterol. Controlling these risk factors can decrease the likelihood of stroke. Stroke places a major health burden on our society in terms of mortality, morbidity and economic costs. As for example the National Stroke Association estimates stroke costs the U.S. about 43 billion $ a year. Direct costs for medical care and therapy average 28 billion $ a year. The average cost per patient for the first 90 days after a stroke is 15.000 $ although 10 percent of those cases exceed 35.000$.

2.1.1 Stroke incidence and prevalence

The incidence rate of stroke in the elderly Italian population (age 65-84 years) is equal to 6.5%, and is slightly higher in men (7.4%) than women (5.9%). The new demographic changes, characterized by a marked aging, will bring to Italy to an increased incidence of stroke in the near future [22]. Stroke can also affect, even the incidence is small, also young and it is estimated that each year around 27,000 people in productive age (i.e. <65 years) suffer a stroke. Ischemic stroke is the most common form of stroke (80%). Ischemic stroke affects people of average age 70 years, more often men than women, affects the intraparenchymal bleeding slightly less elderly subjects, always with a slight predominance for males; subarachnoid hemorrhage occurs most

often in females, mean age 50 years or over. The acute mortality (30 days) after stroke is approximately 20% while after 1 year is about 30%, bleeding (parenchymal and sub-arachnoid) have higher rates of early mortality (30% and 40% after the first week, 50% and 45% at 1 month). Within one year after the acute event, about one third of the stroke survivors, whether they suffered an ischemic or a hemorrhagic stroke, experiences some type of disability. According to the National Stroke Association only 10% of stroke survivors recover almost completely, while about 25% recover with minor impairments, 40% experience moderate to severe impairments that require special care, a 10% require care in a nursing home or other long-term facility and 15% die shortly after the stroke. It's important to notice that approximately 14% of stroke survivors experience a second stroke in the first year following a stroke. So, all in all the burden of stroke is growing. Stroke incidence is affected by the management of its risk factors [23].

2.1.2 Risk factors for stroke

Age is the number one risk factor for stroke with steep increases in incidence rates with increasing age and higher rates in men than in women in all age groups. Stroke incidence varies across ethnic groups with higher incidence rates in black people compared with white populations [24, 25], also when adjusted for differences in socioeconomic status [26]. There is a socioeconomic gradient in the incidence of stroke with lower levels of socioeconomic status associated with a higher risk of stroke. This association may partly be explained by stroke risk factors; however, in the Norfolk cohort the association remained significant after adjustment for classical, lifestyle, and psychosocial risk factors [27]. Boysen et al showed that participants in the Copenhagen City Heart Study who were in the lowest level of household income were at

a greater risk of stroke than those in the higher levels (15). The underlying factors of the differences in risk of morbidity and mortality attributed to socioeconomic status are not fully understood [28, 29].

Twenty potentially modifiable risk factors have been identified as leading risk factors contributing to global mortality and global burden of disease [30, 31]. The Most Common Stroke Risk Factors can be summarized as:

- High blood pressure
- Cigarette smoking
- Heart disease
- Carotid artery disease
- Diabetes
- Heavy use of alcohol

High blood pressure is one of the most important modifiable risk factors for stroke with the risk of stroke increasing continuously with increasing levels of blood pressure. Diabetes is a risk factor for stroke with risk of stroke increasing continuously with blood glucose concentrations even below levels set for borderline diabetes [32].

2.1.3 The consequences of a Stroke

As we said about one third of the stroke survivors, whether they suffered an ischemic or a hemorrhagic stroke, experiences some type of disability. The effects of a stroke vary based on the etiology of the stroke, where it occurs and how much of the brain is damaged. The most common effects of a stroke include the following:

- Weakness (hemiparesis) or paralysis (hemiplegia) on one side of the body that may affect the whole side or just the arm or leg. The weakness or paralysis is on the side of the body opposite the side of the brain affected by the stroke.
- Spasticity, stiffness in muscles, painful muscle spasms
- Problems with balance and/or coordination
- Problems using language, including having difficulty understanding speech or writing (aphasia) and knowing the right words but having trouble saying them clearly (dysarthria)
- Being unaware of or ignoring sensations on one side of the body (bodily neglect or inattention)
- Pain, numbness or odd sensations
- Problems with memory, thinking, attention or learning
- Being unaware of the effects of a stroke
- Trouble swallowing (dysphagia)
- Problems with bowel or bladder control
- Fatigue
- Difficulty controlling emotions (emotional lability)
- Depression
- Difficulties with daily tasks

The types and degrees of disability that follow a stroke depend upon which area of the brain is damaged. In more detail, stroke can cause five types of disabilities: paralysis or problems controlling movement, sensory disturbances including pain, problems using or understanding language, problems with thinking and memory, and emotional disturbances.

Paralysis is one of the most common disabilities resulting from stroke. The paralysis is usually on the side of the body opposite the side of the brain damaged by stroke, and may affect the face, an arm, a leg, or the entire side of the body. This one-sided paralysis is called hemiplegia (one-sided weakness is called hemiparesis). Stroke patients with hemiparesis or hemiplegia may have difficulty with everyday activities such as walking or grasping objects. Some stroke patients have problems with swallowing, called dysphagia, due to damage to the part of the brain that controls the muscles for swallowing. Damage to a lower part of the brain, the cerebellum, can affect the body's ability to coordinate movement, a disability called ataxia, leading to problems with body posture, walking, and balance.

Stroke patients may lose the ability to feel touch, pain, temperature, or position. Sensory deficits may also hinder the ability to recognize objects that patients are holding and can even be severe enough to cause loss of recognition of one's own limb. Some stroke patients experience pain, numbness, odd sensations of tingling, prickling in paralyzed or weakened limbs. This condition is known as paresthesia.

At least one-fourth of all stroke survivors experience language impairments, involving the ability to speak, write, and understand spoken and written language. A stroke-induced injury to any of the brain's language control centers can severely impair verbal communication. Damage to a language center located on the dominant side of the brain, known as Broca's

area, causes expressive aphasia. People with this type of aphasia have difficulty conveying their thoughts through words or writing. They lose the ability to speak the words they are thinking and to put words together in coherent, grammatically correct sentences. In contrast, damage to a language center located in a rear portion of the brain, called Wernicke's area, results in receptive aphasia. People with this condition have difficulty understanding spoken or written language and often have incoherent speech. Although they can form grammatically correct sentences, their utterances are often devoid of meaning. The most severe form of aphasia, global aphasia, is caused by extensive damage to several areas involved in language function. People with global aphasia lose nearly all their linguistic abilities; they can neither understand language nor use it to convey thought. A less severe form of aphasia, called anomic or amnesic aphasia, occurs when there is only a minimal amount of brain damage; its effects are often quite subtle. People with anomic aphasia may simply selectively forget interrelated groups of words, such as the names of people or particular kinds of objects.

Stroke can cause damage to parts of the brain responsible for memory, learning, and awareness. Stroke survivors may have dramatically shortened attention spans or may experience deficits in short-term memory. Individuals also may lose their ability to make plans, comprehend meaning, learn new tasks, or engage in other complex mental activities. Two fairly common deficits resulting from stroke are anosognosia, an inability to acknowledge the reality of the physical impairments resulting from stroke, and neglect, the loss of the ability to respond to objects or sensory stimuli located on one side of the body, usually the stroke-impaired side. Stroke survivors who develop apraxia lose their ability to plan the steps involved in a complex task and to carry the steps out in the proper sequence. Stroke survivors

with apraxia may also have problems following a set of instructions. Apraxia appears to be caused by a disruption of the subtle connections that exist between thought and action.

Many people who survive a stroke feel fear, anxiety, frustration, anger, sadness, and a sense of grief for their physical and mental losses. These feelings are a natural response to the psychological trauma of stroke. Some emotional disturbances and personality changes are caused by the physical effects of brain damage. Clinical depression, which is a sense of hopelessness that disrupts an individual's ability to function, appears to be the emotional disorder most commonly experienced by stroke survivors. Signs of clinical depression include sleep disturbances, a radical change in eating patterns that may lead to sudden weight loss or gain, lethargy, social withdrawal, irritability, fatigue, self-loathing, and suicidal thoughts. Post-stroke depression can be treated with antidepressant medications and psychological counseling.

2.1.4 Stroke rehabilitation

Approximately two-thirds of individuals who have a stroke survive and require rehabilitation. Recovery after stroke represents both an exciting and controversial topic in neurology. With theories of recovery emerging only in the last decade, recovery after stroke is a relatively new field of medicine. Recovery is a complex process and may be heterogeneous across patients. Neurologist Bruce H. Dobkin defines recovery as 'the complete return of identical functions that were impaired' [33]. A stroke patient may make functional gains by developing compensation strategies, which are defined as behavioral adaptations. Each of these processes exhibits a spontaneous recovery component, that occurs unaided by therapeutic intervention [34]. In the seminal work by Twitchell, the classical view of recovery is the following

chronological sequence: an initial period of paralysis, reflexes return, muscle tone improves, primitive and reflexive patterns of mass flexion or mass extension movements, followed by voluntary movement control [35]. Currently, a large variety of intervention strategies are used to rehabilitate a stroke survivor: pharmacotherapy, exercise and skill dependent rehabilitation, functional electrical stimulation and virtual reality therapy. No single intervention has emerged as the most efficacious. Even though rehabilitation does not 'cure' stroke in that it does not reverse brain damage, rehabilitation can substantially help people achieve the best possible long-term outcome.

The goal of rehabilitation is to enable an individual who has experienced a stroke to reach the highest possible level of independence and be as productive as possible. Because stroke survivors often have complex rehabilitation needs, progress and recovery are unique for each person. Although a majority of functional abilities may be restored soon after a stroke, recovery is an ongoing process.

Successful rehabilitation depends on:

- Amount of damage to the brain
- Skill on the part of the rehabilitation team
- Cooperation of family and friends. Caring family/friends can be one of the most important factors in rehabilitation
- Timing of rehabilitation the earlier it begins the more likely survivors are to regain lost abilities and skills

Rehabilitation helps stroke survivors relearn skills that are lost when part of the brain is damaged. For example, these skills can include coordinating leg movements in order to walk or carrying out the steps involved

in any complex activity. Rehabilitation also teaches survivors new ways of performing tasks to circumvent or compensate for any residual disabilities. Patients may need to learn how to bathe and dress using only one hand, or how to communicate effectively when their ability to use language has been compromised. There is a strong consensus among rehabilitation experts that the most important element in any rehabilitation program is carefully directed, well-focused, repetitive practice - the same kind of practice used by all people when they learn a new skill, such as playing the piano or pitching a baseball. Rehabilitative therapy begins in the acute-care hospital after the patient's medical condition has been stabilized, often within 24 to 48 hours after the stroke. The first steps involve promoting independent movement because many patients are paralyzed or seriously weakened. Patients are prompted to change positions frequently while lying in bed and to engage in passive or active range-of-motion exercises to strengthen their stroke-impaired limbs: 'passive' range-of-motion exercises are those in which the therapist actively helps the patient move a limb repeatedly, whereas 'active' exercises are performed by the patient with no physical assistance from the therapist. Patients progress from sitting up and transferring between the bed and a chair to standing, bearing their own weight, and walking, with or without assistance. Rehabilitation nurses and therapists help patients perform progressively more complex and demanding tasks, such as bathing, dressing, and using a toilet, and they encourage patients to begin using their stroke-impaired limbs while engaging in those tasks. Beginning to reacquire the ability to carry out these basic activities of daily living represents the first stage in a stroke survivor's return to functional independence.

2.1.5 Motor Training and Motor learning

Motor impairments are the most commonly reported impairments after acute stroke, with upper limb motor deficits present in 77% and lower limb motor deficits present in 72% of patients one week after onset of first-ever stroke [36]. Reduced balance is another common motor impairment, and about 50% of those admitted to further rehabilitation were not able to stand without support one month after onset of stroke [37]. However, spasticity would appear to be a less common problem, as it was present in only 19% of the patients investigated three months after stroke [38]. Motor impairments are associated with reduced self-perceived health and consequently, rehabilitation after stroke has a strong emphasis on physiotherapy and motor training.

A range of physiotherapy approaches based on different ideas about motor recovery following stroke have been implemented. In the 1980s the potential importance of neurophysiology and motor learning was highlighted [39] and the motor learning, or relearning, approach [40] was proposed. The Bobath approach has emphasized the importance of facilitating movement and of tactile stimulation (hands on) [41], while the Motor Relearning Programme emphasizes active patient involvement with focus on goal setting, and task-specific practice to improve function after stroke [40]. Within the Motor Relearning Programme approach, the actions to be learned are practiced in an appropriate context, with exercises directed specifically at the muscles required for the performance of the action, working through the range at which they must generate force. Furthermore, the patients practice movement tasks with the therapist as a coach who encourages the performance by instruction, manual guidance, demonstration or verbal feedback. Instructions are given in such a way as to present a clear goal and to reduce uncertainty. Manual guidance may be used in the early phase to give the patient an idea about

what to do. The action to be executed can be demonstrated either alive or on videotape, and verbal feedback is given to provide information about achievement of the goal and how the movement was performed [40]. The Motor Relearning Programme can be defined as a task-oriented approach based on newer theories of motor control, also referred to as a system approach [42]. However, anecdotal evidence and the results of questionnaire-based studies suggest that it is difficult to distinguish between the practical implementation of the two approaches, this is confirmed in the recent review by Pollock et al. [43], who recommends that further research should focus on investigating clearly defined and described techniques and task-specific interventions regardless of their historical or philosophical origin, in order to develop an evidence-based physiotherapy [43].

Different treatments can be helpful for the post-stroke recovery, here we will discuss some examples, focusing on the Electromyographic Biofeedback treatment.

- Task-specific treatment

  Dean and Shepherd [44] performed the first randomised placebo controlled trial to test the effect of task-specific postural training. They trained chronic stroke patients to increase their upper limb radius while seated and to increase the contribution of the affected lower leg to support balance. At the end of a two-week programme, subjects were able to reach faster and further, to increase the load on the affected foot, and to increase activation of affected lower limb leg muscles compared with the control group. This study provides strong evidence of the efficacy of task-specific motor training in improving the ability to balance during seated reaching activities after stroke [45].

  A more recent randomised controlled trial evaluated the effect of a 3-

month structured, supervised, home-based exercise programme which included task-specific balance training in combination with exercises to improve range of motion, strength and endurance. The results demonstrated improved recovery in patients treated with the home-based programme compared to those treated with usual care [46]. Treadmill training is frequently used to improve endurance in both healthy people and in particular patient groups. Treadmill training is also described as a task-specific method to improve gait function after stroke. For this purpose two different forms of treadmill training exist: bodyweight-supported treadmill training (BWSTT) and unsupported treadmill training. Wood-Dauphinee and Kwakkel [47] have investigated the impact of BWSTT that ranges from no support to 40% support in five randomised controlled trials involving 266 stroke patients. The analysis showed significantly better (29%) gait endurance for the BWSTT group, despite great variability in the intensity of the different studies. No significant differences according to gait speed, balance or walking ability were detected [47]. In contrast, another meta-analysis showed that BWSTT tended to produce a non-significant trend toward higher walking speed compared to other interventions, among stroke patients who could walk independently at the start of treatment [48]. There is no evidence that treadmill training without bodyweight-support has an additional effect on walking compared to conventional gait training programs on the floor [47, 48]. The benefit of task-specific training to improve muscle strength in the affected arm or leg has also been evaluated in some randomized clinical trials [49, 50], showing less impairment and greater isometric strength in the affected arm [49], increased strength in the affected leg, and improved functional outcome [50]. The

intensity of the task-specific intervention varied from 30 minutes progressive resistance strength training for the lower extremity per week for four weeks [50], to task-specific functional training of the upper extremity (e.g. pointing or grasping) of at least 20 hours within six weeks [49]. Although it would appear that task-specific training is effective in enhancing recovery after stroke, there is still no consensus about the appropriate amount or intensity of this training. So it is relevant to ask whether people who receive 'more intensive' as opposed to 'less intensive' rehabilitation in all phases achieve better and faster motor and functional recovery.

- Biofeedback treatment

  Biofeedback is a technique that trains people to improve their health by controlling certain bodily processes that normally happen involuntarily, such as heart rate, blood pressure, muscle tension, and skin temperature. They rely on EMG signals, usually electrodes attached to your skin measure these processes and display them on a monitor. With help from a biofeedback therapist, you can learn to change your heart rate or blood pressure, for example. At first you use the monitor to see your progress, but eventually you will be able to achieve success without the monitor or electrodes. Biofeedback is an effective therapy for many conditions, but it is primarily used to treat high blood pressure, tension headache, migraine headache, chronic pain, and urinary incontinence. The three most commonly used forms of biofeedback therapy are:

  - Electromyography (EMG), which measures muscle tension
  - Thermal biofeedback, which measures skin temperature

- Neuro-feedback or electroencephalography (EEG), which measures brain wave activity

The way biofeedback works and can make patient control their processes is still not well-known. However, there does seem to be at least one common thread: most people who benefit from biofeedback have conditions that are brought on or made worse by stress. For this reason, many scientists believe that relaxation is the key to successful biofeedback therapy. When your body is under chronic stress, internal processes like blood pressure become overactive. Guided by a biofeedback therapist, you can learn to lower your blood pressure through relaxation techniques and mental exercises. When you are successful, you see the results on the monitor, which encourages your efforts. In a normal biofeedback session, electrodes are attached to your skin. They send information to a small monitoring box that translates the measurements into a tone that varies in pitch, a visual meter that varies in brightness, or a computer screen that shows lines moving across a grid. The biofeedback therapist then leads you in mental exercises. Through trial and error, you can soon learn to identify the mental activities that will bring about the physical changes you want. In this study we will focus on the EMG biofeedback treatment (BFB) which has been shown to reduce pain, morning stiffness and help stroke patients to recover and improve their gait by incrementing the ankle power peak and positive work during the push-off phase of the gait cycle [14, 15]. EMG biofeedback is considered safe. No negative side effects have been reported.

The process of recovery after stroke involves few steps:

- Motor recovery after stroke In most stroke patients, recovery follows an exponential progression, with a fast initial improvement during the first six weeks and a slower recovery for the next six weeks [51]. Animal studies have shown that the cerebral cortex undergoes significant functional plasticity for weeks to months following injury [52]. Spared regions adjacent to the infarction and far removed from the infarction undergo functional alterations that are modified by behavioral experience [52]. It has also been shown in an animal model that rehabilitation initiated five days after focal ischaemia was much more effective than waiting for one month before beginning rehabilitation [53]. The mechanisms of this recovery process may be listed in three general changes within the sensorimotor network: restitution, substitution, and compensation [54]. Restitution is relatively independent of external variables such as physical and cognitive stimulation. Restitution includes reduction of edema, absorption of blood, restoration of ionic currents, and restoration of axonal transport [54], and also re-perfusion due to vessel recanalisation [55]. Substitution depends on external stimuli such as practice with the affected hemiparetic arm or leg during rehabilitation. Substitution includes the functional adaptations of diminished, but partially restored, neural networks that compensate for components lost or disrupted by the injury. Substitution may add a cost to the mental or physical energy needed to carry out a relearned motor skill [54]. This may contribute to explaining some of the fatigue experienced by a significant proportion of the stroke population. Compensation aims to improve the mismatch between a patients impaired skills and the demands of the patient or the environment [54].

- Brain plasticity Brain plasticity is defined as lasting change in the func-

tional or morphological properties of neurons in response to environment changes or lesions, occurring at the level of the synapse in neurons [56]. On a more macroscopic level, reorganization may occur as a result of a lesion or infarct and can be thought of as the consequences of plasticity. One example of adaptive changes that exemplify neuronal reorganization occurs in patients with spinal cord injury (SCI). For instance, functional Magnetic Resonance Imaging (fMRI) can be used to localize the foci of activation among different patient populations. One of the most important discoveries of environmentally-induced cortical reorganization after stroke comes from pioneering work by Nudo and colleagues. They found that, after local damage to the motor cortex of the adult primate brain, rehabilitation training helped to reorganize the intact cortex adjacent to the lesion [57]. In patients who have recovered successfully, the unaffected hemisphere shows increased recruitment of the sensorimotor cortex during performance of the affected hand [58]. These observations have helped to cast doubt on the theory that brain structures are static and incapable of reorganizing after injury.

Advances in diagnostic imaging technology have served as primary driving forces for improving stroke care and to characterize changes in activity patterns with recovery and rehabilitation. Electroencephalography (EEG) records electrical activity from electrodes at the scalp, while magnetoencephalography (MEG) records the magnetic changes associated with the changing electrical fields. These approaches offer the advantage of recording signals that are closely related to the underlying neuronal activity, and thus have high temporal resolution; however, their spatial resolution is limited. Relatively new techniques that enable the measurement of diffusion of water in the brain have

been shown to be more sensitive in the visualization of the stroke lesion location than previous methods [59]. Techniques such as functional magnetic resonance imaging (fMRI) or positron emission tomography (PET) record signals related to the metabolic or hemodynamic consequences of such electrical activity [60]. A methodological challenge is the heterogeneity and absence of blood-oxygen-level-dependent (BOLD) signals measured in fMRI observed in some studies in patients with vascular disease [61, 62]. Still, PET and fMRI offer significant advantages in term of spatial resolution, with fMRI as the superior, allowing for fine-grained localization of the remapping that may occur after stroke. Increasingly, Magnetic Resonance Imaging (MRI) is being used for anatomical imaging for acute stroke care and fMRI is also being used to visualize brain activation patterns in recovering stroke patients. A detailed description of fMRI is the topic of next chapter. Several fMRI studies have been undertaken in the past decade to study the role of brain plasticity in the recovery after stroke. Both cross-sectional and longitudinal study designs have been used, but the longitudinal design would appear to be more appropriate to study the evolution of the activity pattern as recovery takes place [63]. The reported patterns of change are variable, but some consistencies have now emerged. These may be classified into three major patterns of change:

1. local remapping within the primary motor cortex;
2. increased activity in non-primary sensorimotor areas;
3. increased activity in the undamaged hemisphere [60].

The local remapping implies a ventral or posterior shift in the location of primary sensorimotor (MISI) cortex activation [63, 64]. There are

recent suggestions that smaller infarction volumes are associated with more ventral and larger infarction volumes with more posterior activation foci. On the other hand, better behavioral outcome would appear to be associated with greater posterior activation, and poorer outcome with a more ventral activity [64]. Increased recruitment of non-primary motor areas, such as inferior parietal cortex, cingulate cortex and premotor cortex has been reported [65, 66]. It is suggested that this pattern represents adaptive plasticity, in which undamaged areas of cortex take over the function of the damaged regions. It is proposed that this pattern will never result in complete recovery [63, 60]. A number of studies have reported increased activity of the unaffected sensorimotor cortex following stroke [67, 68, 69], suggesting a significant role for the non-stroke hemisphere in mediating recovery. Although the majority of corticospinal outputs are crossed, approximately 30% of them remain uncrossed. It is suggested that these fibres bring signals from the undamaged hemisphere to the affected side of the body [70].

- Motor learning and recovery Motor learning is defined as a set of processes associated with practice that lead to relatively permanent change in performance capability [39]. Studies in healthy humans have demonstrated that incremental acquisition of motor skills follows two distinct stages: first, an early, fast learning stage in which considerable improvement in performance can be seen within a single training session, and secondly, a later, slow stage in which further gains can be observed across several sessions (and even weeks) of practice [71]. It is shown in an animal model that motor skill acquisition, or motor learning, is a prerequisite for task-related changes in the activation maps of primary motor cortex [72], and consequently it is suggested that motor learning

is required for both substitution, i.e. when undamaged brain regions are recruited to generate commands to the same muscles as were used before the injury (true recovery), and compensation, i.e. the use of alternative muscles to accomplish the task goal [73]. Several brain structures, including the striatum, cerebellum, and motor cortical regions of the prefrontal lobe, are considered to be critical for acquisition of motor skilled behavior, and it is suggested that the acquisition of motor skills reproduces changes in the cortico-striatal and cortico-cerebellar systems over the course of motor skill learning in healthy subjects [71]. Previous longitudinal brain imaging studies after stroke have mainly focused on the neural correlates to motor recovery, but not on whether these changes share features with brain plasticity in healthy subjects over the course of motor skill learning. The task-oriented approaches, particularly the Motor Relearning Programme, are based on motor learning principles assuming that recovery after stroke i.e. relearning of lost motor skills, are comparable to motor learning in healthy subjects [40]. Whether brain activation corresponding to motor recovery following stroke can be explained by motor learning mechanisms is still undetermined. In the last paper of this thesis, we wanted to study the motor network changes in patients admitted to a comprehensive stroke unit, treated with early mobilization and physiotherapy according to a task-oriented approach, within the framework of motor learning.

2.2 Functional MRI

2.2.1 Magnetic Resonance Imaging - MRI

The MRI technique relies on the inherent magnetic properties of tissue, consequently MRI does not use ionizing radiation; therefore, it can be used with minimal attributable risk. Nuclei with an uneven number of protons or neutrons have a non-zero nuclear spin number. One such example is the hydrogen nucleus, 1H, which is the nucleus used most readily in MRI, because of its high natural abundance in the body in the form of H_2O. Hydrogen nuclei, or protons, have a non-zero angular momentum characterized by a two energy state system and denoted by a spin number $I_z = \pm\frac{1}{2}$. By convention, $I_z = -\frac{1}{2}$ is the lower energy state, and $I_z = \frac{1}{2}$ is the upper energy state.

When a biological sample containing protons is placed in a static magnetic field, it will produce a net magnetization, which is the sum of all the magnetic dipole moments. Protons in a magnetic field, B0, interact with radiofrequency (RF) pulses in a characteristic manner. These RF excitation pulses, applied perpendicular to the direction of B0, create a secondary magnetic field, B1, that tips the magnetization away from the lower energy state if it matches the resonance frequency of the protons. This resonance frequency is called the Larmor frequency, and is defined as γ B0, where γ is the gyromagnetic ratio of 42.576 MHz/T for protons. At 1.5 T, the field strength of most clinical MRI scanners, the proton resonance frequency is 63.86 MHz. Depending on the parameters of the RF pulse, the protons are tipped, partially or fully, into the plane that is orthogonal to the main magnetic field, known as the transverse plane. Typically, this excitation a pulse is small, and a denotes the angle away from B0. Protons tipped in this

manner will be subject to relaxation effects that form the basis for contrast in MR images. The resultant signal measured is called the free-induction decay (FID) and looks like a sine wave modulated by a decay function envelope. The signal decay due to relaxation is typically detected by the RF coil used to generate B1. The resulting MR signal intensities reflect different relaxation properties or proton densities in biological tissues. The next step that is necessary before a full MR image is produced is the addition of time varying gradients that accompany and follow the RF pulses. Gradient coils are used to encode the proton signals by producing time-varying magnetic fields that vary linearly with position to encode the location of protons in three dimensions. Information from a voxel in the image is derived from prescribed and incremental changes in the resonant frequency as a function of position. The application of RF pulses and gradient fields make up the pulse sequence, one of the most usable is the Echo Planar Imaging (EPI), it was developed as a means to acquire an entire image plane in one excitation [74]. EPI with T2*-weighting is the most common acquisition technique for fMRI experiments. However, spiral imaging in fMRI is growing in popularity [75]. Typically, a spiral $T2^*$-weighted image will fill k-space starting in the middle, where low spatial frequencies are located, and follow an Archimedean spiral trajectory. By avoiding the necessity for fast switching gradients associated with EPI [76], spiral imaging is a more efficient use of the gradient system. In addition, it produces less acoustic noise and is less sensitive to motion of the anatomy being scanned [77]. Another major innovation in fMRI has been the realization that higher field strengths will improve $T2^*$ contrast.

2.2.2 fMRI

The last two decades have introduced a trend in diagnostic imaging that goes beyond the use of static anatomical images of the body towards imaging that can provide functional information, be it physiological and/or molecular. Positron Emission Tomography (PET), Diffuse Optical Tomography (DOT), and fMRI are three examples of functional neuroimaging techniques. Although each technique has its strengths and weaknesses, it is without question that fMRI has emerged as the neuroimaging technique that is used more widely for human brain mapping studies. fMRI is a non-invasive technique that relies on the different magnetic properties of hemoglobin in blood, in its oxygenated (HbO) and deoxygenated (Hb) state. Hemoglobin is an endogenous contrast agent in the blood vessels, meaning that no contrast agent is needed to measure functional contrast. Ogawa [78] formulated that the $T2^*$ was related to the concentration of Hb directly, yielding BOLD contrast [78, 79].

The BOLD signal is proportional to the concentration of deoxyhemoglobin, which is a function of three physiological parameters: cerebral blood volume (CBV), cerebral blood flow (CBF) and the cerebral metabolic rate of oxygen consumption ($CMRO_2$). The BOLD fMRI signal is sensitive to the capillary bed and the venous side of the circulation, since arteries and arterioles are very close to 100% saturation and therefore contain no deoxygenated blood. The time series of a BOLD response to a brief stimulus reflects the changes in CBV, CBF and $CMRO_2$. Increases in CBV and $CMRO_2$ decrease the BOLD signal, while increases in CBF increase the BOLD signal (2.1). The summation of the competing physiological effects gives rise to the characteristic hemodynamic response. The BOLD response is composed of three distinct phases [80]: a fast response lasting 1-2 s and sometimes referred to

as the 'initial dip' [81], in which there is a small decrease in the BOLD signal; a relatively large amplitude hyperemia that is caused by the in-flow of fresh oxygenated blood that peaks approximately 4-5 s after the stimulus; a refractory period lasting 5-10 s where the BOLD signal undershoots the baseline. The shape of the hemodynamic response function is characterized by a gamma-variate function [82].

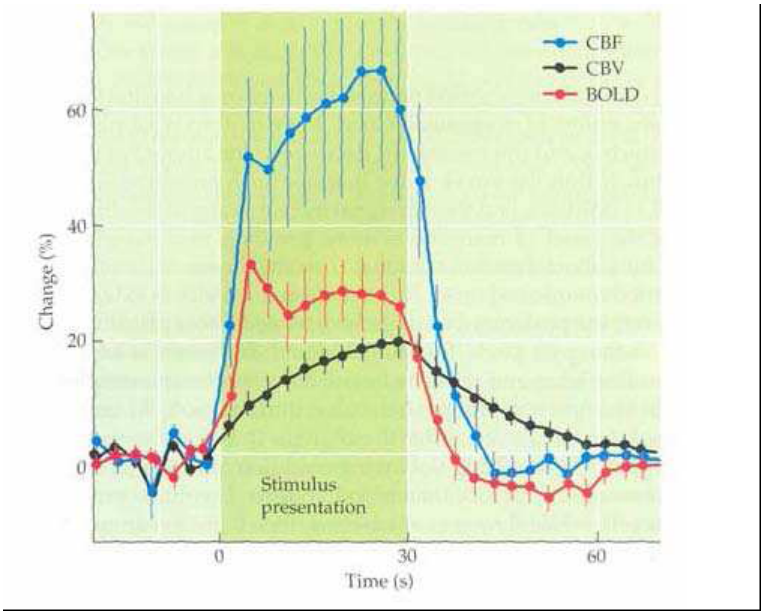

Figure 2.1: Example of the BOLD signal (red) over time during a rest-stimulation; cerebral perfusion (CBF, blue) and blood volume (CBV, black).

In practice, the BOLD fMRI signal is influenced by additional factors. Movement of the chest due to respiration, the beating heart, vascular pulsatility, vasomotor oscillations, and gross head and limb movements all affect the fMRI signal to varying degrees and serve as physiological sources of noise. Knowledge of these effects has led to various techniques to denoise and improve the fMRI analysis [83]. Head motion over and above 2 mm in translation has the potential to ruin an entire fMRI scan [84], so an fMRI

experiment must be designed carefully to minimize head motion. As fMRI technology develops, acquisition and analysis of fMRI data continues to be refined and improved.

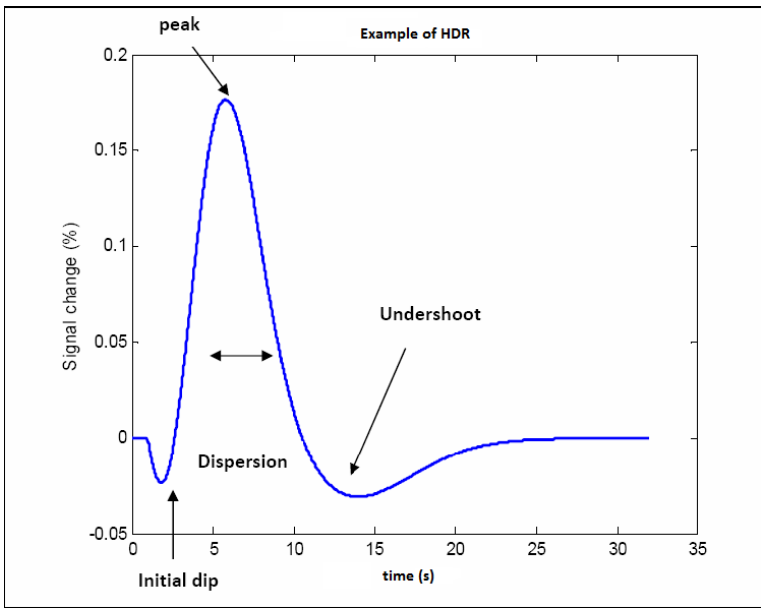

Figure 2.2: Example of hemodynamic response to a pulse stimulus.

The Experimental Design

The goal of mostly of the fMRI studies is to recognize which brain areas are active while the subject is performing a specific task. In order to obtain this information the subject has to undergo an 'ad-hoc' experimental design. Each stimulus is called a task and can be a motor, sensory or cognitive task. To detect the active areas usually the hemodynamic responses while the subject is performing the task with those obtained during the resting state (rest) are compared, or the activation areas during different tasks are taken into account. The two main types of experimental design for stimulation are based on blocked and event related. These two protocols differ in duration

of each stimulus (2.3).

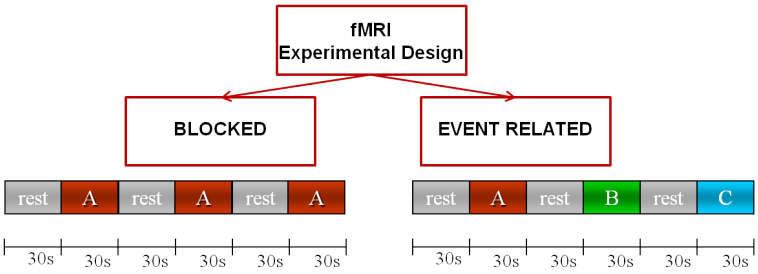

Figure 2.3: Example of block (on the left) and event related design (on the right).

In the first protocol, the duration of each task is set (block) and always the same, while in the second design the stimulus is impulsive. The block experimental design is divided into different parts (blocks) of stimulation, all with the same duration. Within each block are presented many stimuli consecutively. It is possible to compare multiple tasks (stimuli), or to switch between different task / rest blocks.

Thanks to this first design, the obtained BOLD signal is quite high, because the responses of individual stimuli are added together in a linear combination. Conversely hthe protocol is very sensitive to changes in the BOLD signal, is sensitive to the head movements, and it becomes difficult to estimate the hemodynamic response within each bloc because the BOLD signal does not have enough time to come back to the baseline value. The second protocol, defined as event related, each task has a short duration and the stimuli are randomly presented to the subject. The tasks are separated by an inter stimulus interval (ISI) which can vary between 2 and 20 sec. The recorded signal is quite low, and it's really affected by noise, because it represents the answer to a single stimulus. Adopting the event related design it's possible to avoid the effects of task learning, basically because the protocols

are more flexible and the task are randomly chosen, this design allows to estimate the temporal dynamics of the response in between the stimuli, because the BOLD signal can come back to the baseline value. However there are some limitations: you can experience different data according to the ISI, in fact, long ISI intervals do not increase the detection of the stimulus; the decrease in the signal to noise ratio requires a lot of complete brain scans, and finally the hemodynamics response is not known a priori this because different events are presented with a not-optimal timing.

The experimental design can largely influence the hemodynamic response's time course. According to the presented stimuli the hemodynamic can presents different trends, figure TOT shows the hemodynamic response obtained from an input pulse stimulus and from a prolonged one (in this case the response is characterized by a plateau) (2.4).

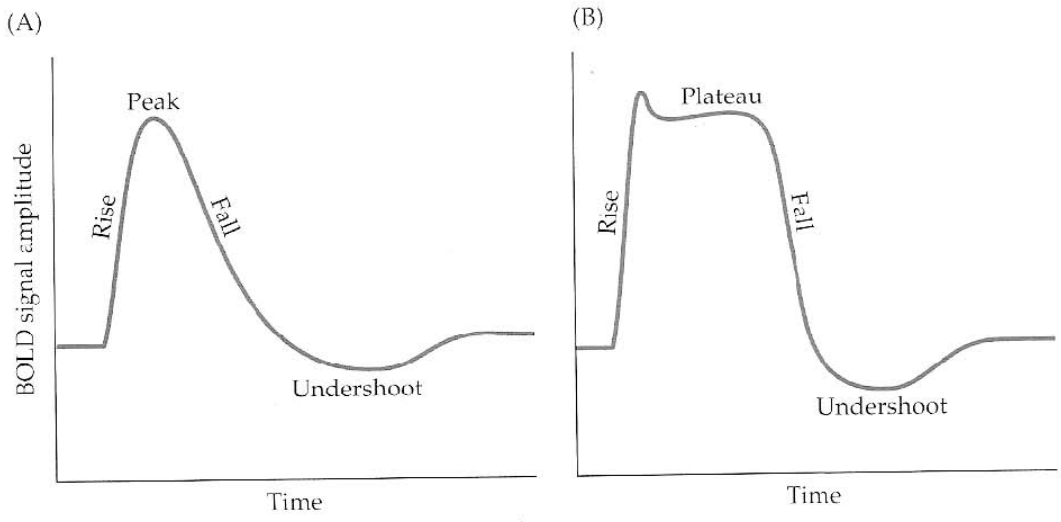

Figure 2.4: Effect of the duration of the stimulus. On the left effect of the pulse stimulus, on the right effect of a longer stimulus.

2.2.3 fMRI Data Analysis

Data analysis has become an important sub-field in fMRI. In all applications of fMRI, researchers collect sets of images sequentially in time while participants perform behavioral tasks or attend to sensory stimuli. The fMRI data have four-dimensions: x, y, z, and time. The usual goal is to find spatial and temporal features in the data that are correlated with the experimental design. For instance, a participant may be asked to perform a task for 30 s and then to rest for 30 s. This process of alternating states, known as block-design, might repeat for 5 10 minutes to build contrast between the two sets of conditions. Often, fMRI data are analyzed and reported as a statistical parameter, such as the goodness of fit between the model and voxel time series data. Simplistically, the result of the statistical test is related to the increased neuronal activity associated with the task the participant performed. There are many strategies on how to analyze fMRI datasets, because there are many ways to represent the fMRI time series data parametrically. It is no surprise then that fMRI analysis has brought together experts from varied fields such as mathematics, statistics, and neuroscience. This subsequent section will focus on analysis techniques that are commonly used.

There are a number of steps that can be carried out prior to the statistical analysis of the row data from any fMRI experiment. Each of these steps is independent and offers different benefits. These steps could be seen as the post-processing/ pre-data analysis steps, which can be applied to the data to improve the detection of the activation areas (2.5).

These include:

- Slice timing correction/ Motion correction: it is performed in order to correct for subject movement during the experiment. Subject head

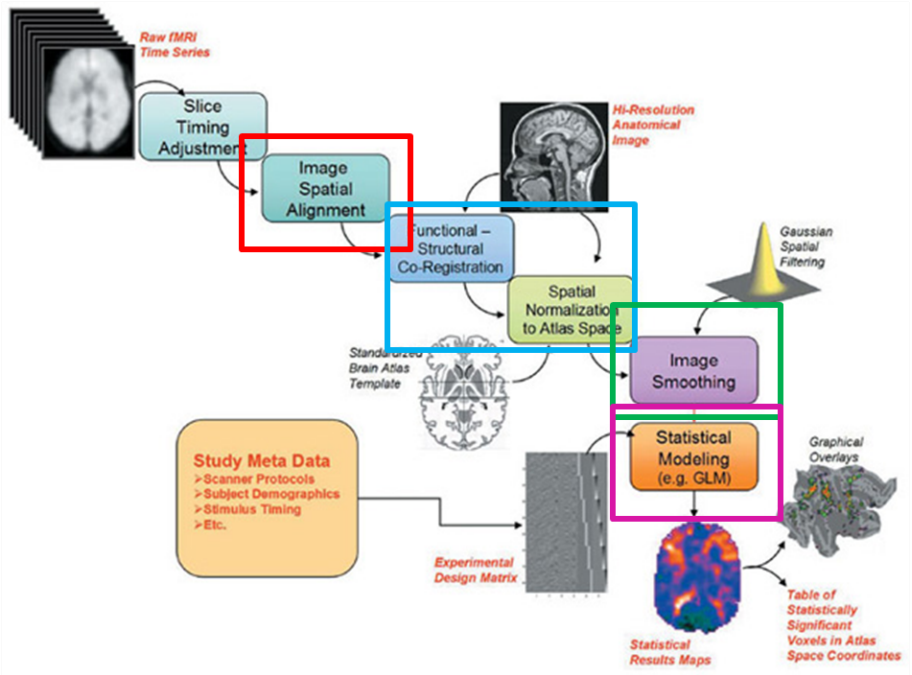

Figure 2.5: Steps of post-processing/ pre data elaboration.

movement, during the experiment is a major source of artifact in fMRI data. The head movement can be limited by using devices that immobilize the head (2.6). It should be noted that a small movement of the head (4-5mm) leads to larger errors in the acquisition of the signal. To reduce fatigue of the subject, and therefore the head movement, usually the whole experiment is divided into small intervals. The head movement is not only caused by involuntary actions (breath, heartbeat), but also by some tasks, such as movement of a limb of the body (i.e. hand, foot). To eliminate the artifacts caused by the movement, the goal is to correct the acquired images so that the brain is always in the same position.

Changes in pixel intensity at the edges of the brain, upon even slight movement, can be far greater than the BOLD activation response.

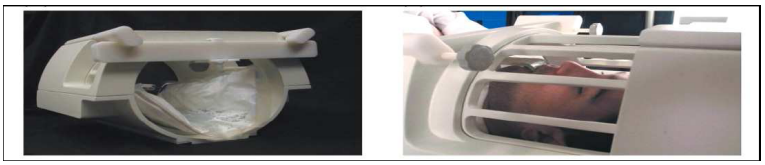

Figure 2.6: Example of devices for the head immobilization.

Therefore in addition to external devices too immobilize the head, it is common in fMRI data analysis to perform some correction which reduces this effect. The approach taken here is to correct only for in-plane translations and rotations of the head within the image. Working on a slice-by-slice basis, the first image is taken to be the reference image, to which all other images of that slice are to be aligned. Two dimensional rotations and translations are applied to the second image, and the sum of the squares of the difference (ssd) between pixels in the first and second image are calculated. Further translations and rotations are applied to the image until the ssd is minimized, using a standard routine. All subsequent images are realigned in the same way (2.7). This technique is quite robust, and does not have difficulty in converging. One obvious extension of this would be to go to a three dimensional technique. This would have the advantage of more fully correcting the head motion, and would also be a faster technique, but introduces the problem of interpolating the data to give isometric voxels. Additional corrections that could be applied include those which remove cardiac and respiratory effects [83], and those which correct for the history of the spins [85].

- Coregistration: fMRI data have a poor resolution, so they are coregistered to the high resolution anatomical T1 images to detect specific areas of the brain. The functional images are blurred image, and

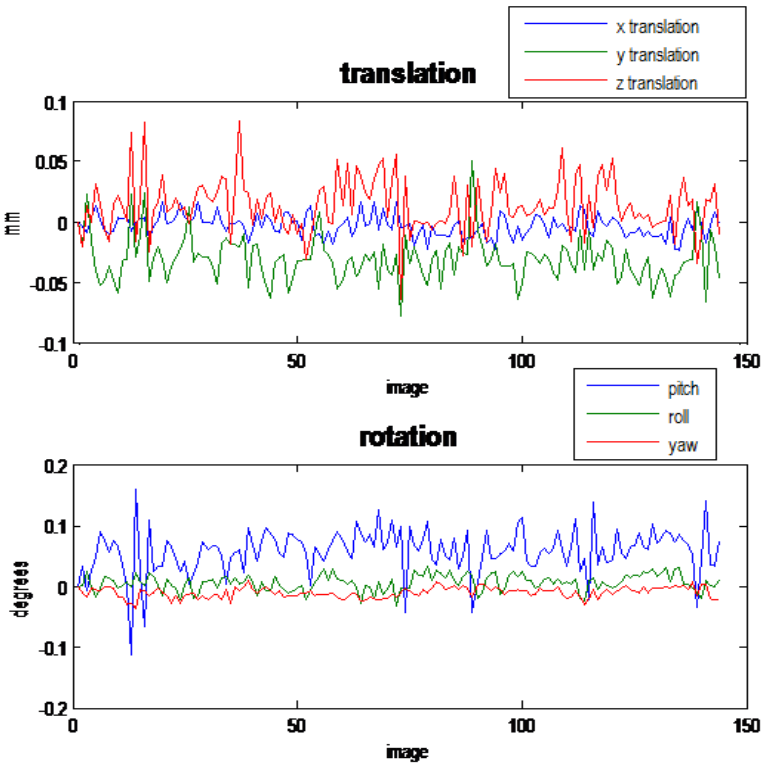

Figure 2.7: Translation and Rotation evaluated for the head motion correction.

have a low spatial resolution. The anatomical images (T1) obtained with MRI, but have a high spatial resolution, being able to identify the different brain areas with precision. In order to exploit the spatial properties of the anatomical images the technique of coregistration can be applied. With coregistration functional images are aligned/matched with anatomical images (T1 weighted MR image) of reference in order to obtain a spatial correspondence of the brain areas (2.8).

- Normalization: images are normalized to a reference stereotaxic atlas in order to compare the brains of different patients. The human brain has a high morphological variability. The volume of a brain adult varies

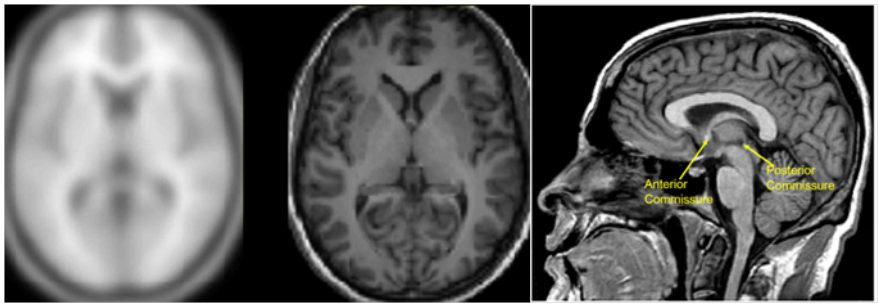

Figure 2.8: On the left the functional image, in the center the T1 anatomical image, on the right the anterior and the posterior commissures localization.

between 1100 cc and 1500 cc, so the variation is about 30%. Changes can occurr not only in the the volume, but also in the shape. Normalization is a procedure used to compensate for differences in shape between different brains, normalized into a common atlas. This common space is defined as stereotaxic atlas and the Talairach atlas was the first used,a drawback is that it is based upon postmortem sections of a 60-year-old French female who had a smaller than average brain size. Currently the Montreal Neurological Institute (MNI) atlas is adopted as the standard atlas; the MNI defined a new standard brain by using a 305 MRI scans on normal controls. The MNI 305 brain is made up of all right handed subjects, 239 M, 66 F, age 23.4 $\pm$ 4.1 years). SPM software for the fMRI data processing bases the normalization ont eh MNI152, that is to say the MNI average of 152 scans.

The normalization into a standardized space is basically performed in order to compare different subjects' brains, the anterior and posterior commissures are the reference brain structures. So you can also specify brain areas using coordinates. You can also apply the operation average across different subjects. The main disadvantage is the reduction of the

resolution space.

- Spatial smoothing: to improve the signal to noise ratio of the data; The spatial smoothing procedure is equivalent to average the value of each voxel with the value of adjacent voxels. Because the data that are acquired are correlated and to eliminate high spatial frequencies images are spatially smoothed. The spatial smoothing improves the signal-to-noise ratio (SNR) of each of the images, but will reduce the resolution in each image, and so a balance must be found between improving the SNR and maintaining the resolution of the functional image (see Fig. 2.9). The most used is the Gaussian filter. The distribution of its kernel is a normal distribution and the spatial dimension is called width, and determines how the data is spatially filtered (see Fig. 2.10). The width is not expressed in terms of standard deviation σ, but by the Full Width at Half Maximum (FWHM). Typical values of FWHM used in functional imaging can vary between 6 and 10 mm.

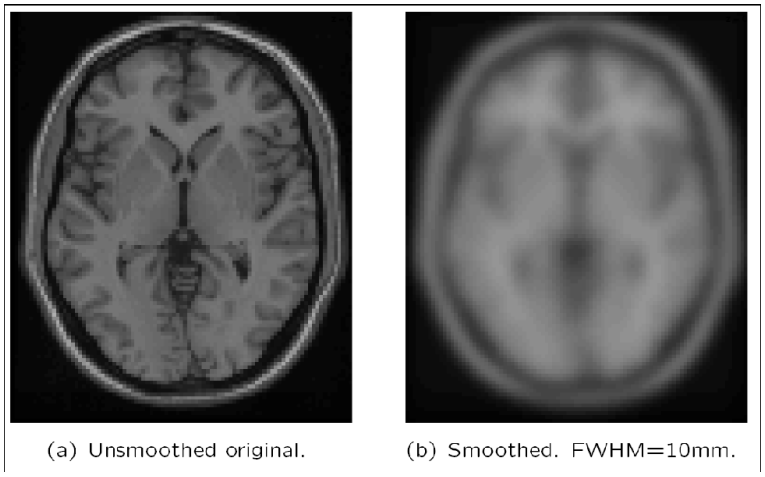

Figure 2.9: On the left the original functional image, on the right the smoothed image.

To carry out the filtering, a smoothing matrix is constructed which is the same size as the image. This image matrix is convolved with the smoothing matrix by Fourier transforming both the image and the filter, with a three dimensional FT. Since fast Fourier transformation (FFT) is considerably faster than a discrete Fourier transform, the image and smoothing matrix are zero filled to the nearest 2n points in each direction. The smoothing matrix is scaled so that its maximum point is equal to one, ensuring that the image is not scaled out of the range of the short data type used to store the smoothed image. The two transformed matrices are multiplied together and then inverse Fourier transformed back to give the smoothed image. Such a method of convolution would attempt to smooth the opposite edges of the image with each other, and so zero filling is carried out to the next largest 2n points to prevent this. There is no straightforward answer to the question of which is the best smoothing width to use in the analysis of the data set. Standard filter theory shows that the best kernel is one which matches the size of the activation region sought. Thus a filter of FWHM of 4 mm would be optimum for regions of this sort of extent, but may reduce the signal from smaller regions. A wider filter will reduce the noise to a greater extent, and so a compromise must be reached.

- Modelling and Statistical Analysis: fMRI signals are modelled using a Generalized Linear Model, the estimated parameters are used for the statistical analysis in order to detect the activation brain areas.

  fMRI data can be modeled on a voxel-by-voxel basis using the General Linear Model (GLM). The GLM incorporates any statistical tests that assume that the data are composed of the linear combination of differ-

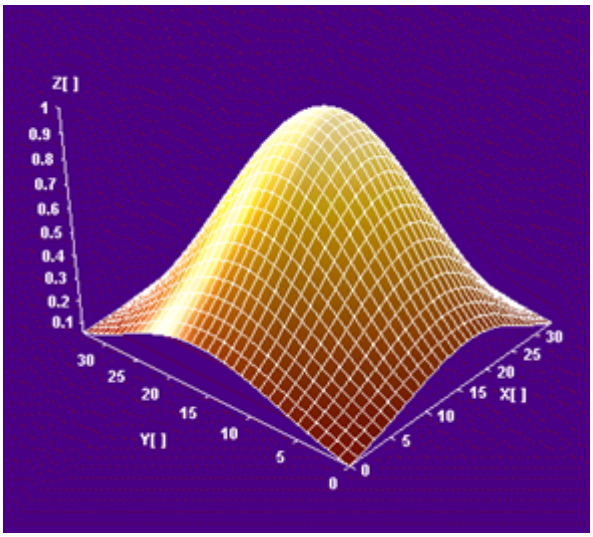

Figure 2.10: Example of a tridimentional Gaussian Filter.

ence model factors, in addition to an uncorrelated noise source. The GLM assumes that: 1) each scan or temporal measurement is an independent observation, 2) the system behaves linearly and 3) the system is time-invariant. The signal intensity for each voxel time course, Y, can be approximated by the product of model factors, X, and a scaling factor or parameter weight, β, which accounts for how much each factor contributes to the data, Y, plus a noise term [86]. This is expressed mathematically as the following:

$$Y = X\beta + \epsilon \tag{2.1}$$

where now Y is the vector of observed pixel values, β is the vector of parameters and ϵ is the vector of the error terms, where the error is thought to be uncorrelated, independent and Normally distributed N(0, σ^2I) 2.11).

The matrix X is known as the design matrix. It has one row for every time point in the original data, and one column for every explanatory

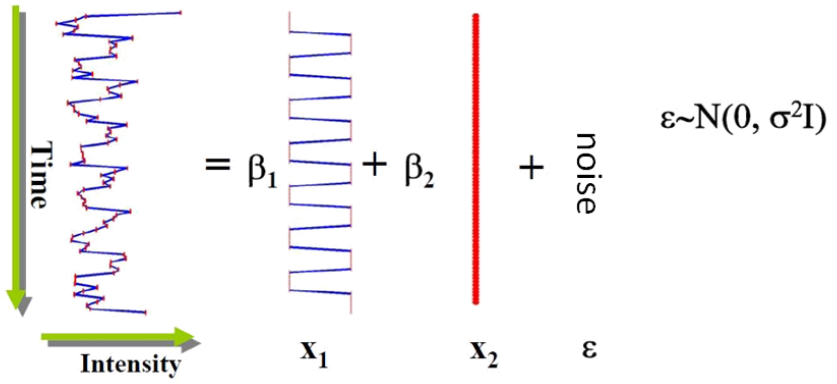

Figure 2.11: Example of the GLM model.

variable in the model. Analysing an fMRI experiment, the columns of X contain vectors corresponding to the 'on' and 'off' elements of the stimulus presented. The matrix X contains the independent variables and it is called design matrix, which corresponds to the model of the hemodynamic response. This matrix is built based on the experimental protocol used for the experimental setup. Each column of this matrix is composed of a basic function that represents a possible contribution to the signal obtained with fMRI, it has been suggested that each column is the expected time course of the BOLD signal due to evoked neuronal activity. The functions used have known shape but unknown amplitude, this will be the β vector to estimate. In order to build the X matrix the model of the hemodynamic response (HRF) and the experimental design are needed. As previously said, the hemodynamic response h(t) is the result of a stimulus pulse $\delta(t)$ and it can show the following time course.

The external stimulus applied through the experimental design affects the signal BOLD x(t), because the signal is obtained from the convo-

lution between the external stimulus u(t) and impulse hemodynamic response h(t):

$$x(t) = \int_0^\infty h(\tau)u(t-\tau)\delta\tau \tag{2.2}$$

Therefore it can be noticed that the BOLD signal depends on the hemodynamic response h(t) and the experimental design associated with the study of stimulation u(t). As the BOLD signal relies on the experimental design, the importance f a correct stimulation is basic in order to obtain a signal to represent that precise activation.

As we said, the X matrix is based both on the experimental design and on the choose of the model hemodynamic response. In this context, there are several models to represent the hemodynamic response (2.12):

- Canonical
- Canonical temporal derivatives
- Canonical dispersion derivatives

The Canonical model, which is the most commonly used, was introduced by Friston [87], it's based on the use of two gamma functions:

$$h(t) = \frac{t}{d1}^{a_1} \exp\frac{-(t-d_1)}{b_1} - c\frac{t}{d_2}^{a_2} \exp\frac{-(t-d_2)}{b_1} \tag{2.3}$$

The values of a_i, b_i, are properly chosen and in the case of the Canonical model these values are equal to a1=6, a2 = 12, b1 = b2 = 0.9, c = 0.35. The second model, temporal Canonical derivatives, is the sum of Canonical function and its first-order Taylor expansion. Using this model, the performance of the BOLD signal can be improved. In fact, as stated above, the slices are not acquired all simultaneously, so that the signal from each voxel has a small delay. To consider the presence

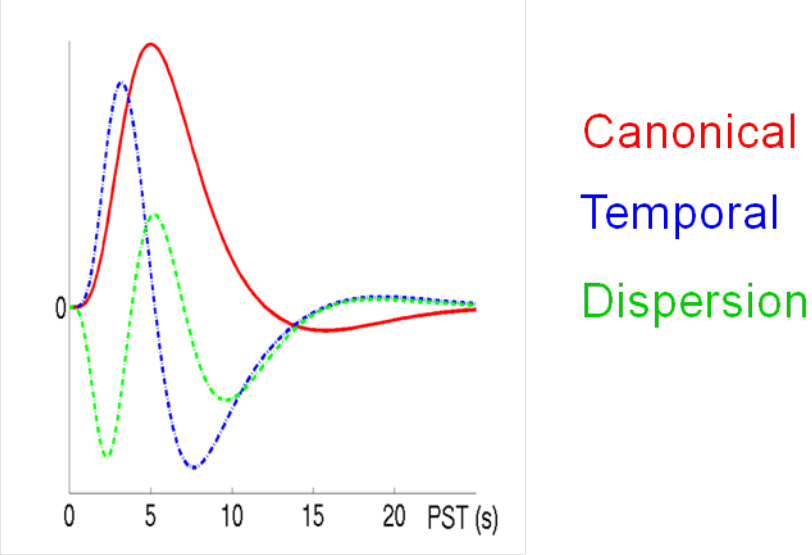

Figure 2.12: The three different models for the hemodynamic response: canonical, temporal and dispersion.

of this delay in the hemodynamic response a new model of the HRF can be used. This function improves the fit of the data because it has a new parameter β that must be estimated. The third model for the hemodynamic response, i.e. the dispersion Canonical derivatives,can be obtained by the Canonical function added up to the the multivariate Taylor's expansion both in time (temporal derivative), and in amplitude (dispersion derivative). A third parameter β is introduced with this model which is useful to model the presence of the initial undershoot that characterizes the hemodynamic response.

Now, built the known X matrix, the only values we have to estimate are the amplitudes of the parameters in the β vector, the presence or absence of an activation can be detected.

β can be determined by solving the 'normal equations':

$$X^T Y = (X^T X)\widehat{\beta} \tag{2.4}$$

where $\widehat{\beta}$ is the best linear estimate of b. Provided that $(X^T X)$ is invertible then is given by:

$$\widehat{\beta} = (X^T X)^{-1} X^T Y \tag{2.5}$$

Such parameter estimates are normally distributed, and since the error term can be determined, statistical inference can be made as to whether the β parameter corresponding to the model of an activation response is significantly different from the null hypothesis. The general linear model provides a framework for most kinds of modeling of the data, and can eliminate effects that may confound the analysis, such as drift or respiration, provided that they can be modelled.

The previous assumptions regarding the measurement error, that is to say additive, uncorrelated and normally distributed N(0, σ^2I), are not fully verified in fMRI.

In particular in the fMRI data, serial correlation can be due to low frequency physiological (respiratory and cardiac) noise, and to the neuronal activity which cannot be modeled. So by assuming the uncorrelated error, the estimated $\widehat{\beta}$ parameters are affected by a bias error.

So by using the correct assumption, in the following equation:

$$Y = X\beta + \epsilon \tag{2.6}$$

the error ϵ is thought to be independent and Normally distributed N(0, σ^2 V), where V is NOT a diagonal matrix. In order to get unbiased estimates we need to premultiply the model X by the matrix W:

$$W = V^{-\frac{1}{2}} \tag{2.7}$$

The result is:

$$W \cdot Y = W \cdot X\beta + W \cdot \epsilon = W \cdot X\beta + w \tag{2.8}$$

where now the error w is really uncorrelated, independent and Normally distributed N(0, σ^2 I).

In this way, by defining $\widetilde{Y} = W \cdot Y$ and $\widetilde{X} = W \cdot X$, the estimation problem is still described as:

$$\widetilde{Y} = \widetilde{X}\beta + w \tag{2.9}$$

and the error w is uncorrelated, independent and Normally distributed N(0, σ^2 I).

The V matrix is built using the Yule-Walker equations coefficients (ρ): the correlation structure of the error (ϵ) is modeled as an autoregressive process of degree 1.

$$\epsilon(t) = \rho \cdot \epsilon(t-1) + \xi_{t1} \tag{2.10}$$

where

$$|\rho| \leq 1 \tag{2.11}$$

and $\xi_{t1} \sim$ N(0,σ_1^2).

The autocorrelation parameter (ρ) is assumed to be the same for each voxel and it is estimated from the least squares residuals using the Yule-Walker equations.

Finally to detect the activation areas, the last step is to compare the various β calculated adopting the t-test. The differences between the β

vector are specified by the contrast vector: c. This vector is made up of integer values, negative and positive. Each contrast vector is orthogonal to the others, which means that each contrast is independent. For example, to test whether the task hemodynamic response is different from the rest condition one or not, the used contrast will be (1 0). Once the contrast is chosen, the second step is to run the t-test, the goal is to check whether the detected signal in a voxel satisfies or not the null hypothesis H0 (Task = rest) when applied to the obtained estimates of the parameters. The t statistic, also known as t-contrast, is:

$$t = \frac{c^T \beta}{\sigma \sqrt{c^T (X^T X)^{-} 1 c}} \tag{2.12}$$

The numerator represents the effect size, i.e. the estimates weighted with the c contrast, while the denominator is the uncertainty of effect size, i.e. the residuals weighted for the c contrast. To proceed with the t-test you have to define the degrees of freedom, as the t distribution depends only on this parameter. In the case of the fMRI data, it can be shown that the degrees of freedom are equal to (N - p), with N = number of volumes acquired and p is equal to the rank of X. In addition to the degrees of freedom a threshold of significance α is selected, the p-value is usually set equals to 0.05, this means that only 5% of the non-active areas are misclassified as active. The matrices that represent the brain slices are 64x64 pixels matrix, so the number of voxels for each slice is equal to 4096, so even considering p = 0.05, the number of voxels false positives is high. It is necessary to take into account a new correction which reduces the value of α, the Bonferroni Correction.

The Bonferroni Correction, known also as Family-Wise Error (FWE), is used in multiple comparisons tests. As said before it is necessary to

change the value of α, to decrease the number of false positive (Type I error), it decreases the number of statistical independent tests:

Bonferroni corrected α = p-value / # voxel slice

If we consider that each slice is composed of 4096 voxels and the p-value is equal to 0.05, then the new α value is equal to the correct α: 0.05/4096 = 1.2207e-005. This method seeks to control Type I errors (false positive), i.e. classifying a voxel active when there is no activation. In fact, the correction decreases the Type I error, however as a drawback Type II error increases.

2.3 Gait Analysis

2.3.1 Introduction

The observation and analysis of the natural phenomenon 'human movement' calls for a prerequisite to be met, which consists in collecting data that allow for the reconstruction, in the 3-D space and in each sampled instant of time, of the subject-specific bones involved in the analysis. Human Movement Analysis requires the gathering of quantitative information about the relative movement between adjacent bones, the intersegmental loads, and the forces transmitted by individual body tissues such as muscles, tendons, ligaments, etc. These quantities are estimated using mathematical models of the musculo-skeletal system and measures of observable quantities and allow the graphical rendering of the movement of the musculo-skeletal system as a virtual reality 3-D realistic representation.

The anthropomorphic model consists of a kinematic chain of links representing the portion of the locomotor apparatus under analysis. These links

are made of soft tissues and a bony part (segment). Whereas the latter is considered non-deformable and, therefore, represented using rigid bodies, soft tissues may or may not be considered deformable; most of the literature chooses the latter option. However, in recent years, some authors have started to advocate for soft tissue deformability to be accounted for in human movement modeling. It has in fact been shown that, by ignoring this deformability, bony segment kinematics reconstructed using non-invasive photogrammetric data of skin-markers is affected by inaccuracies that may hinder the practical usability of the results [88, 89]. To reconstruct the 3-D kinematics of each body or bony segment during the execution of a motor task, two pieces of information are necessary: bone pose (i.e. position and orientation) and bone morphology. Pose is time-variant while morphology is hypothesized as invariant, that is the bone is considered non-deformable. The description of the skeletal-system pose involves the definition of a local frame, relative to a global or laboratory frame of reference, rigidly associated with the bony segment involved, which is referred to as technical frame [90] These quantities are most commonly measured using stereophotogrammetric systems. Positions of target points of either light emitting diodes or retro-reflective cluster of markers, placed on the surface of a body segment, are measured and used to construct instantaneous position vectors relative to a frame of reference. Relevant results are affected by instrumental errors [91, 92] and soft tissue artifacts, [88, 93]. These errors are time variant and affect the reconstructed positions of the markers both in an uncorrelated and correlated manner, thus giving rise to marker cluster deformation and rigid movement relative to the underlying bone, respectively. In the literature, there is ample evidence that the propagation of the photogrammetric errors to the end results of a movement analysis is far less disruptive to the information involved than that of

the soft tissue artifacts [94, 95]. In addition, minimizing the propagation of the uncorrelated error using least squares optimal pose estimators that exploit information redundancy of the reconstructed coordinates of three or more markers is known to be relatively easy [96, 97].

So the aim of Human movement analysis is to gather quantitative information about the mechanics of the musculo-skeletal system during the execution of a motor task. In particular, information is sought concerning the movement of the whole-body center of mass; the relative movement between adjacent bones, or joint kinematics; the forces exchanged with the environment; the resultant loads transmitted across sections of body segments or between body segments, or transmitted by individual body tissues such as muscles, tendons, ligaments, bones, and body segment, energy variation and muscular work. The quantities that provide the above listed information are either measured or estimated using mathematical models of the musculo-skeletal system. In this way, quantitative descriptions of the functions of the locomotor system, the assessment of enhancement or impairment and of the way an individual executes a motor activity (assessment of activity limitation) are obtained. Normally, the following quantities are measured. Instantaneous positions of markers located on the skin surface are obtained using stereophotogrammetry (motion capture) either based on conventional photography or optoelectronic sensors. External forces are measured using dynamometers, such as force plates. Electrical activity of muscles is recorded through electromyography. Anthropometric quantities are acquired either using a scale, a tape measure and calipers, or more sophisticated methods such as 3-D scanners. Following the work by Braune and Fischer, the anthropomorphic model used to estimate the quantities that are not directly observable consists of a kinematic chain of links. Each link represents a por-

tion of the human body referred to as body segment. These segments are made of a bony part (segments) and by soft tissues. Bony segments are considered non-deformable and, therefore, are represented using rigid bodies, in the Classical Mechanics sense. So far, no author has disputed this choice or assessed the inaccuracy that it may introduce in the analysis, provided, of course, that the bony segment represents a single bone. Bony segments are connected by joints with 1 to 5 degrees of freedom. The limit cases of 0 and 6 degrees of freedom may be included for the sake of generalization. The number of bony segments and constraints imposed by the joints contribute to the number of degrees of freedom of the model and its structural faithfulness to reality. Soft tissues around the bony segments may or may not be considered deformable. Most of the literature chooses the latter option, that is the entire body segment is regarded as a rigid body. In principle, under these circumstances, the analysis described above is straightforward: for the most part, Classical Mechanics can solve any related problem and, with the aid of modern computers, can do this without difficulty.

The data obtained from the gait analysis of the movement can be divided into three groups:

- Kinematic data: the spatial position, velocity and acceleration of the body. These data are usually obtained by using motion capture systems.

- Kinetic data: the forces and moments that generate the movement. These information can be obtained using the force platforms.

- Electromyographic data: the activation signals of muscles involved in the movement.

In order to gather the kinematic data, from which we can derive some

kinetic information, is necessary to use a motion capture system, which is therefore the most important instrument for the gait analysis. The motion capture systems can be divided into two categories: optical systems (with or without markers) and non-optical systems (electromechanical, optical, inertial, magnetic, acoustic). [98]

2.3.2 Optoelectronic Systems

Stereophotogrammetric methods, whose applications cover wide-range (as in the earth sciences) and close-range (as in biomechanics) measurements, are used to reconstruct 3-D landmark coordinates from photographs , radiography and video images. Photogrammetry has been developed as a photography-oriented science since Muybridges well-known sequence of a horse in motion dating 1878, and is now under continuous development with the aid of computer vision, pattern recognition and artificial intelligence techniques. Video images have several potential advantages over the other techniques in terms of time consumption, cost, and potential image distortion of the development process, so that optoelectronic systems are nowadays largely the most popular in movement analysis. More specifically, OSS are used to track, by means of a system of CCD cameras, the 3-D position of a set of fiducial points, constituted from either retro-reflective (passive) or light-emitting (active) markers. Analytical close-range photogrammetry then allows the estimation of 3-D position data from digitized, noisy image data, using the geometrical properties of central projection from multi-camera observations. Retroreflective passive markers are used together with infrared stroboscopic illumination produced by an array of light-emitting diodes mounted around the lens of each camera. The process of recognizing passive markers in the video frames can be performed either via pattern recognition software or by

dedicated hardware circuits. Conversely, active markers are pulsed sequentially, so the system can detect automatically each marker by virtue of the pulse timing, and marker tracking is more easily performed. The 3-D coordinates of each marker are finally computed based upon the 2-D data from two or more cameras, their known location and internal parameters. For the reconstruction of 3-D coordinates, each marker must be seen simultaneously by at least two cameras, but in practice more than two are recommended, since markers can become obscured from camera views because of arm swings, walking aids, subject rotation, etc. Several sources of inaccuracy affect photogrammetric measurements, resulting in an error on marker coordinates. Instrumental errors are of two types:

1. systematic (instrumental systematic error, ISE)

2. andom (instrumental random error, IRE)

The former type is in any case associated with a model of the measurement system of limited validity, due either to photogrammetric calibration inaccuracies (bad estimation of model parameters) or to non-linearities that this calibration could not take care of (inadequate model). The magnitude of the systematic errors depends on the size of the measurement field and on the position that the marker assumes within it. Random errors may be due to electronic noise, marker flickering, i.e. the imprecision with which marker images are converted into image points, and the quantization inherent to the digitizing process, which transforms marker image coordinates into their numerical values [91].

2.3.3 Camera calibration methods

The task of calibration, aims at estimating both the internal and external parameters of each camera. Internal parameters determine how the image coordinates of a point are derived, given the spatial position of the point with respect to the camera. On the other side, external parameters characterize the geometrical relation between the camera and the scene, or between different cameras. Particularly popular is the Direct Linear Transformation (DLT) algorithm, [99], where a 3-D calibration object with a grid of control points in known positions throughout the volume of interest is simultaneously recorded by all cameras. Some authors specifically investigated the effect on the system accuracy of changing the number and the 3-D configuration of the control points. It was established that the best accuracy is achieved when the control points are large in number and evenly distributed in the calibration volume. Recently the attention moved to the development of calibration procedures exploiting the epipolar constraint between a 3-D point and its 2-D projections on the target of two cameras. This approach, pioneered by Dapena and colleagues, [100], and further developed in the computer vision community, allowed to estimate the principal points of the cameras without the use of any additional device and allowed to calibrate on-line the internal and external parameters of an OSS only by surveying a rigid bar in motion inside the working volume. Such procedure closely resembles those implemented by BTS, Vicon, Motion Analysis, Qualisys, and Elite.

The goal of the cameras calibration is to determine the geometrical parameters [99, 101]:

- Internal (focal length, principal point coordinates and the distortion coefficients)

- External (position of the camera reference frame with respect to absolute reference system)

The calibration is performed with three subsequent transformations (2.13):

- First: a rigid transformation from the absolute coordinate system to the camera's coordinate system, which is placed in the center of projection.
- Second: a perspective projection from the tridimensional (3D) space to the bidimensional (2D) space of the camera.
- Third: a 2D affine transformation from the image coordinate system to the sensor's reference system.

Each camera can be described by the simple pin-hole model [102]. The pin-hole model is the perspective projection model used to transform the real 3D coordinates to 2D image coordinates. In this model all the rays coming from the scene must cross a small hole to impact with the image sensor. Real lenses do not have this linear behavior, so that the pin-hole model must be corrected with distortion corrective terms. The pin-hole model must be complemented with other distortion parameters that correct their ideal behavior to come close to the real behavior of the objective as much as possible.

The origin of camera reference system is placed in the center of projection, where the z-axis is the optical axis. The image plane (coordinates (u, v)) is placed at a distance from the center of projection equal to the focal length and perpendicular to the optical axis. The principal point (u_0, v_0) is determined by the intersection of the optical axis with the image plane. The image plane is usually placed in front of the projection center C to provide the image without inversion. An explanatory scheme of the pin-hole model is shown in 2.14.

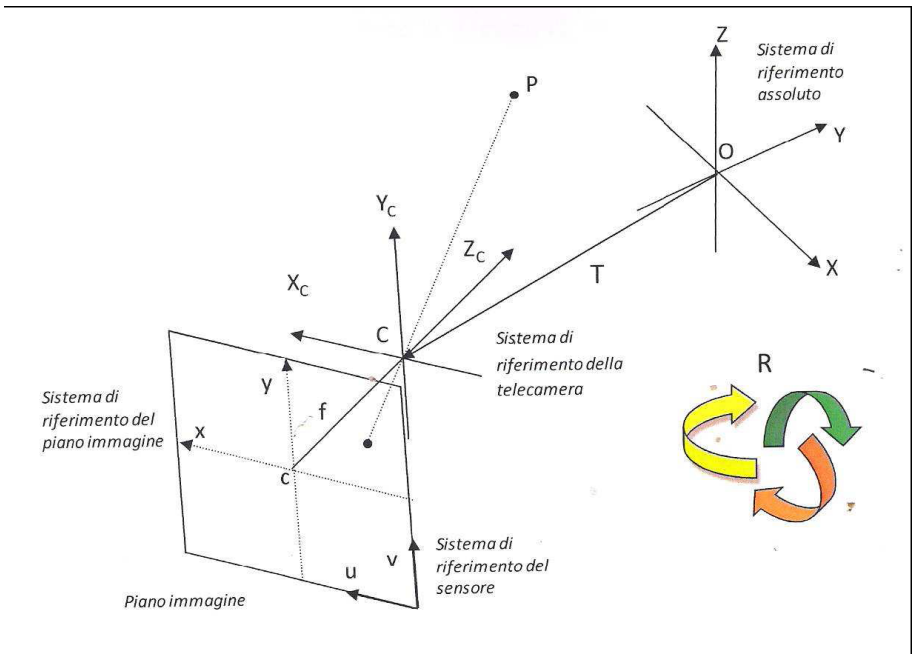

Figure 2.13: The point P projection on the image plane in the 3D space: 1) Rigid transformation from the absolute coordinate system to the camera's coordinate system, 2) perspective projection from the camera reference frame to the image plane frame, 3) 2D affine transformation from image plane frame to the reference system of the sensor.

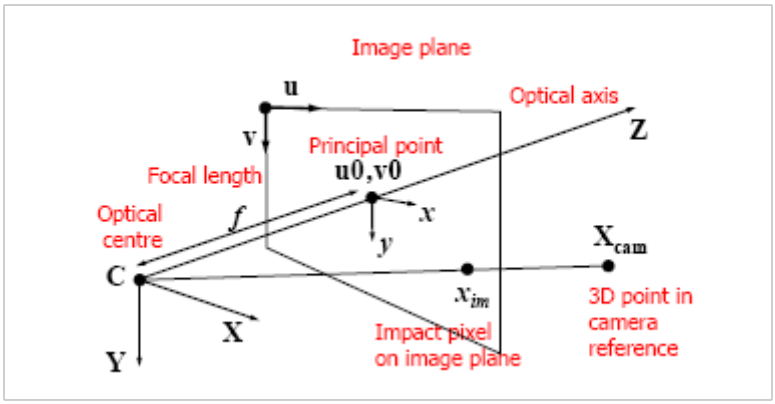

Figure 2.14: Explanatory diagram of the pin-hole model.

A scene point X_{cam} already given for the camera reference system [X Y Z], is projected using the pin-hole model onto the image plane at x_{im} with coordinates (x, y). This image plane values are obtained applying the equations of perspective projection for an objective of focal length f using equation 2.13.

$$\begin{bmatrix} x \\ y \end{bmatrix} = \frac{f}{Z} \begin{bmatrix} X \\ Y \end{bmatrix} \tag{2.13}$$

The pixel coordinates (u, v) of this plane image position are obtained using the horizontal and vertical size of pixels and referencing these values to the image sensor upper left origin, so that the value of the principal point (u_0, v_0) must be added. This transformation is expressed in 2.14.

$$\begin{aligned} u &= s_x \cdot x + u_0 \\ v &= s_y \cdot y + v_0 \end{aligned} \tag{2.14}$$

The three-dimensional point Xcam which has as impact pixel (u, v) is not unique. All the points over the straight line that connects the centre of projection C with the point X_{cam} initially considered are possible original points. The projection onto the pixel (u, v) of points $M(X, Y, Z)$ of that straight line is expressed in equation 2.15:

$$\lambda \begin{bmatrix} u \\ v \\ 1 \end{bmatrix} = \begin{bmatrix} f_x & 0 & u_0 \\ 0 & f_y & v_0 \\ 0 & 0 & 1 \end{bmatrix} \begin{bmatrix} X_{cam} \\ Y_{cam} \\ Z_{cam} \end{bmatrix} \tag{2.15}$$

where

$$\begin{aligned} f_x &= s_x \cdot f \\ f_y &= s_y \cdot f \end{aligned} \tag{2.16}$$

The *cam* sub-index for the (X, Y, Z) coordinates denotes that the point M is expressed in the camera reference system. In general the coordinates for objects of the scene are expressed on the world/object coordinate systems. Note that the centre of projection C, origin of the reference camera system, is initially unknown. The coordinates of a scene point M expressed for an external world/object reference system are given by (X_w, Y_w, Z_w). They must be transformed into the camera reference system in order to apply the projection equations of the pin-hole model. The matrix transformation between the external coordinate system to the camera reference system is expressed as a rotation/translation matrix, extrinsic matrix RT_{ext}. The transformation in homogeneous coordinates is shown in expression 2.17.

$$\begin{bmatrix} X_{cam} \\ Y_{cam} \\ Z_{cam} \\ 1 \end{bmatrix} = \begin{bmatrix} r_{11} & r_{12} & r_{13} & t_x \\ r_{21} & r_{22} & r_{23} & t_y \\ r_{31} & r_{32} & r_{33} & t_z \\ 0 & 0 & 0 & 1 \end{bmatrix} \begin{bmatrix} X_w \\ Y_w \\ Z_w \\ 1 \end{bmatrix} \tag{2.17}$$

The commonly used notation to express the equations of projection $\mathbf{P}$ for a point $M(X, Y, Z)W$ onto the image plane in a pixel of coordinates $m(u, v)$ is shown in 2.18:

$$m \approx \mathbf{P}M \tag{2.18}$$

where matrix $\mathbf{P}$ can be expressed as in equation 2.19:

$$\mathbf{P} = \begin{bmatrix} f_x & s & u_0 & 0 \\ 0 & f_y & v_0 & 0 \\ 0 & 0 & 1 & 0 \end{bmatrix} \begin{bmatrix} r_{11} & r_{12} & r_{13} & t_x \\ r_{21} & r_{22} & r_{23} & t_y \\ r_{31} & r_{32} & r_{33} & t_z \\ 0 & 0 & 0 & 1 \end{bmatrix} \tag{2.19}$$

The skew parameter s (take into account the non-orthogonality between x and y axis) is considered null for current CCD devices. Also note that perspective projection is always defined up to a scale factor λ. The pin-hole model does not consider the thickness of lenses. The pin-hole model lacks to consider the transformation between principal planes of a thick lens. Pin-hole model does not give valid Euclidean distances to scene objects but it is capable to model the image capture applying the perspective projection directly. Therefore the main limitation due to the use of pin-hole model is relative to the size of the hole. In fact, the hole is supposed to be very small so that the intensity of the beam passing through the hole is very low, then the photosensitive elements that are part of the image plane may not detect any beam. One of the possible siolution would be to increase the size of the hole by using a diaphragm and a focusing tool. This instrument causes a further distortion of the image. The distortions are divided into chromatic aberration (or distortions), that degrade image quality, and geometric distortions, that is to say they change the position of the contents in the image. The correction of distortions can be performed before the calibration or simultaneously, introducing some operators for the estimate of the distorsion. After determining the parameters for the correction of distortion, the system calibration can be performed. In order to calibrate the system, a set of control-'known' points placed within the volume of calibration should be available. There are different calibration methods, the most used is based on epipolar geometry. The methods based on epipolar geometry are based on the use of linear equations and do not require the knowledge of the points' space coordinates [103].

Tridimensional Reconstruction and Tracking

After calibrating the cameras can reconstruct the 3D points position. The 3D position of a point can be reconstructed if the point is seen at least by two cameras. The procedure which adopt images obtained from two cameras for the reconstruction is called triangulation. The triangulation method uses the coordinates of the projections in the image plane of a reference systems to get the 3D location in the space. If the system was perfect, the location reconstruction of the point would be the intersection of two lines, but because of the noise, the lines are skewed and then the point is reconstructed by applying the least-squares system of the following equations:

$$\left[\begin{array}{c} a_{111}X + a_{121}Y + a_{131}Z = a_{141} \\ a_{211}X + a_{221}Y + a_{231}Z = a_{241} \\ a_{112}X + a_{122}Y + a_{132}Z = a_{142} \\ a_{212}X + a_{222}Y + a_{232}Z = a_{242} \\ \cdots \\ a_{11k}X + a_{12k}Y + a_{13k}Z = a_{14k} \\ a_{21k}X + a_{22k}Y + a_{23k}Z = a_{24k} \end{array}\right] \tag{2.20}$$

where the indices a_{ijk} are given by using the collinearity equations for each camera k.

After the reconstruction of the 3D position of each point for each frame, the tracking is adopted to evaluate the trajectories [104, 105]. The tracking procedure is the main problem for the gait analysis. In order to evaluate the trajectory of each marker, two types of information can be used:

- The smoothness of the trajectory
- The 'a priori' knowledge of the subject's movements.

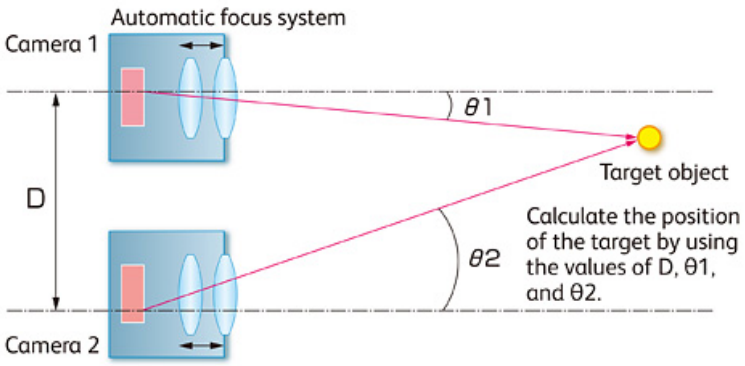

Figure 2.15: Example of 3D reconstruction by using the triangulation method.

In the first case recursive estimators like the Kalman filter can be used: this method can estimate the state of a dynamic system from a series of data with noise. This procedure is based on two steps:

1. a predictive step by which the exact position of the marker can be evaluated, according to the previous measurements, the dynamic model and the variance of the prediction itself.

2. an update step of the prediction.

In the second case, the a priori knowledge may vary greatly, therefore it is more difficult to implement algorithms suitable for different applications.

Digital Cameras

The optoelectronic systems are based on digital cameras which work in the visible light and near-infrared range. Digital cameras' sensors convert the detected light signal into an electrical signal. The most commonly used sensors are the CCD (Charge Coupled Device), the CMOS (Complementary Metal Oxide Semiconductor) or the lateral effect photodiode. CCDs typically

Figure 2.16: Example of SMART camera and illuminator (BTS Spa, Padova).

have a signal to noise ratio higher if compared to the CMOS. Each sensor can be made up by pixel linear arrays or pixel matrices, if each pixel can be identified by two coordinates (x, y) then it is defined as addressable. All the sensor's area (filling factor) is thought to capture the light and in the case of the motion capture system cameras the filling factor is very high. The sensors used for the automatic movement acquisition provide a spatial resolution up to 1.3 megapixels with a sample frequency up to 1kHz. Since CMOS is less sensitive than the CCDs to the infrared wavelengths, they rely on the visible light. If the CCDs cameras are adopted, it necessary to use an illuminator whichis positioned behind the focal plane so that the radiation does not affect the acquisition. These illuminators emit high power pulses in the infrared with a wavelength of 880 nm and they are digitally controlled. These pulses are used to find the position of the markers that can reflect infrared light. Then it's possible to obtain the positions of the markers placed on the anatomical landmarks at each time frame, in this way, thanks to the software, the recorded movements of the subject can be reconstructed.

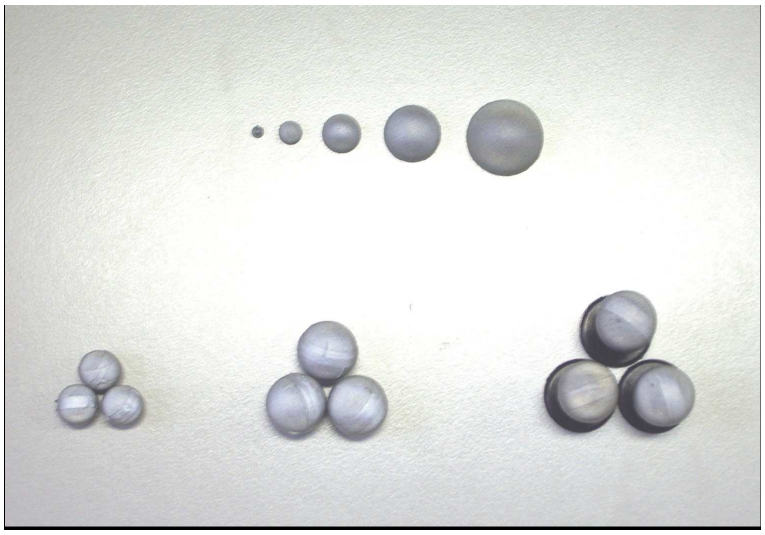

Figure 2.17: Passive reflective markers: hemispherical, spherical and spherical with flat base.

Markers

For the motion capture either active or passive markers can be used. Active markers consist of active LED (Light-Emitting Diodes) that generate a light signal, so there is no need for an external lighting device, however, they have to be powered and synchronized with cables, which become not handy and intrusive. Since using the LEDs there is the possibility to emit timed signal,there is no need for a data preprocessing to recognize the markers positions. A possible drawback of the active markers is that the emission angles are narrow so that the cameras' setup become a critical issue. On the other hand the passive markers consist of plastic material coated with reflective material that can reflects light emitted from an external lighting device.

Passive markers usually have a spherical shape, because it is the best geometric shape that improves the reflection of infrared rays, making these

markers clearly visible. By using also cameras equipped with optical filters, the passive markers are immediately recognized with respect to the scene. Compared to the use of the active markers, in this case it is necessary to apply a pre-processing step to identify and classify the markers. Both the types of markers are placed on precise anatomical landmarks, which will be adopted for the subsequent reconstruction of the movement of each anatomical segment [98].

Force Platforms

The force platforms are devices that can measure ground reaction forces during the walk. A system of forces can be replaced with an equivalent resultant force and a resultant torque, so that to derive the total force applied on a structure it is necessary to know the three force components and three component of the torque. The transducers used to measure the forces can be made of six or three components. The method adopted to measure the force is based on the variation of the sensors' electrical properties, the variation is caused by the mechanic deformation of the sensors' material and the deformation is directly proportional to the intensity of the measured forces. It is important that the material used to build the sensors has an elastic response appropriate for this purpose because the quality of the response can affect the quality of the transducer. The technologies applied to build the force transducers are based on strain gauges and piezoelectric crystals. A strain gauge converts its length variation into an electric signal by means of the variation of its electrical resistance. The highest sensitivity of the sensor is along its main direction, therefore in order to measure the force along different directions it is necessary, in the same platform, to use more transducers positioned in different directions. On the other hand the piezoelectric

Figure 2.18: Klistler dynamometric platform.

transducers exploit the properties of some crystals (the most common is the quartz) to generate a voltage when they are subjected to mechanical stress. They are extremely sensitive, but they are not suitable to measure static loads, since the stored charge is basically lost due to the mechanical stress.

During a gait analysis by means of the force platforms it is possible to measure the three components of the ground reaction force and the resulting torque reaction. Knowing the resultant force vector it is possible to evaluate the coordinates of the force vector's point of application through the equations:

$$\begin{aligned} x &= -hF_x - \frac{M_x}{F_z} \\ y &= -hF_y - \frac{M_y}{F_z} \end{aligned} \tag{2.21}$$

where h is the height of the surface with respect to the reference system x, y. These coordinates identify the point on which the resultant of the horizontal moments is equal to zero. The further moment is defined as free moment M_z. The force components added to the free moment are those transmitted to the human body. The point of application of force is called the center of pressure (COP) and it represents the centroid of the vertical force distribution on the plantar surface of the foot or the point location of the resultant ground reaction force vector in the plane of the ground at

Figure 2.19: Wireless FREEEMG electromyograph (BTS Spa, Padova).

which the ground reaction force vector is considered to apply [106], the COP is important to evaluate the moments of the joints [98].

Electromyography

The electromyography (EMG) is a necessary tool for measuring the electric potential of a muscle during its contraction. These potentials are generated by electrical depolarization of muscle fibers in response to an electrical impulse coming from a neuromuscular junction. There are two kinds of EMG in widespread use: surface EMG and intramuscular (needle and fine-wire) EMG. The needle electromyography involves the use of short or long needles inserted in the muscles in order to record their activity either during muscles relaxation or during muscles contraction. With the use of intramuscular EMG, the recorded activities reflect the potential of a single motor unit. The surface ENG is based on the use of surface electrodes, therefore the measured signal is the result of the activity of a group of motor units. With respect to the previous technique, the surface EMG provides comprehensive information and it avoid the possible risks caused by the insertion of needles.

Kinematics and Kinetics

The objective of segmental kinematics is the collection of numerical information that allows the reconstruction of a body, considered rigid or not, or bony segment in space in each sampled time instant during the execution of a motor task. For this purpose, two pieces of information are necessary: one relative to morphology and one to movement. The morphological description of a segment can be obtained by representing it as an ensemble of particles and providing the position vector of each relative to an orthogonal set of axes (local frame (LF)):

$$^{l}\mathbf{p} = \left[\begin{array}{ccc} ^{l}p_x & ^{l}py & ^{l}p_z \end{array} \right] \tag{2.22}$$

It follows logically that the more particles used, the more detailed the description will be 2.20.

If the body under analysis is considered deformable, then the vector $^{l}\mathbf{p}$ must be given for each particle and each sampled instant of time during the observation interval. However, as is often the case in human movement analysis, if the investigator is not interested in the deformations of the segment involved, but only in its global location in space, then this may be considered non-deformable in an absolute sense and represented as a rigid body. This entails enormous simplification since, under this hypothesis, the above mentioned particle position vectors are invariant with respect to time and-or boundary conditions and can, therefore, be measured only on one occasion and under the most favorable experimental conditions. Similar considerations apply to the inertial parameters (e.g., location of the center of mass, mass moments of inertia) of the segment involved.

The morphology of a segment may be represented with respect to any arbitrary frame, that is, with respect to any observer. Given a LF and

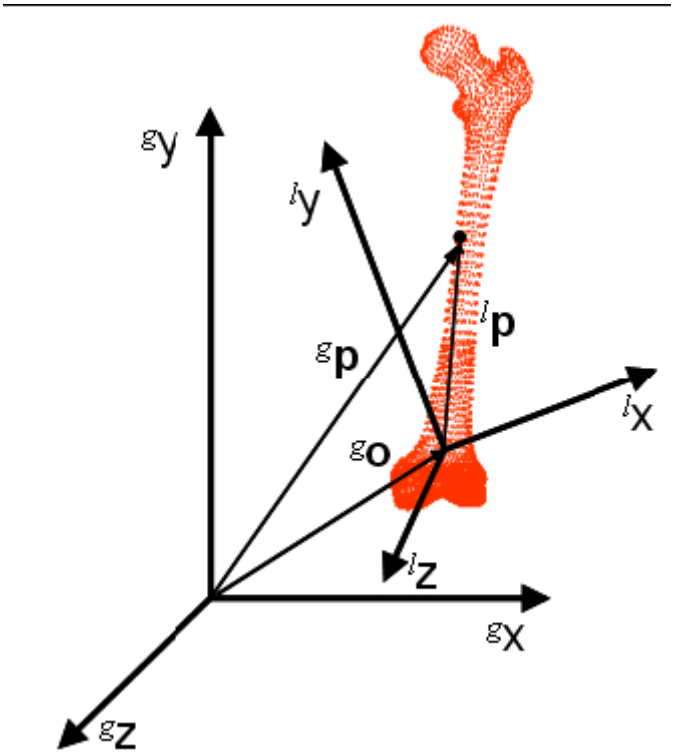

Figure 2.20: The position vector of a particle represented in a global $({}^{g}x,{}^{g}y,{}^{g}z)$ and a local $({}^{l}x,{}^{l}y,{}^{l}z)$ frame, indicated as gp and ${}^{l}p$, respectively.

another frame, which we refer to as the global frame (GF), it is possible to derive the position vectors of the particles of the segment under analysis defined in the latter frame (${}^{g}\mathbf{p}$) provided that those defined in the former (${}^{l}\mathbf{p}$) are given 2.20. This exercise is called vector or coordinate transformation and is obtained through the following equation :

$$ {}^{g}\mathbf{p} \;=\; {}^{l}\mathbf{R}_{l}^{l}\mathbf{p} + \mathbf{o} \tag{2.23} $$

where:

$$ {}^{g}\mathbf{R}_{l} = \begin{bmatrix} cos(\theta)_{x_g x_l} & cos(\theta)_{x_g y_l} & cos(\theta)_{x_g z_l} \\ cos(\theta)_{y_g x_l} & cos(\theta)_{y_g y_l} & cos(\theta)_{y_g z_l} \\ cos(\theta)_{z_g x_l} & cos(\theta)_{z_g y_l} & cos(\theta)_{z_g z_l} \end{bmatrix} \tag{2.24} $$

defines the orientation of the LF, relative to the GF frame and is referred to as the orientation matrix, and ${}^{g}\mathbf{o}$ is the position vector of the origin of the LF relative to the GF, and defines the position of the former relative to the latter. The column elements of the matrix in 2.24 are the direction cosines, or the unit vector components, defining the orientation of each LF axis relative to the global frame. With reference to these nine matrix elements, it is important to emphasize that they are not independent. In fact, taking into account their definition and the fact that the frame axes they define are mutually orthogonal and that triplets of them represent unit vectors, six scalar equations may be written that reduce the number of independent elements to three. In summary, three scalar independent quantities define the relative orientation, and three the relative position. The ensemble of position and orientation of any one frame relative to another, that is, of a rigid body relative to another, is referred to as pose. If the problem is representing the segment under analysis in virtual reality, given the invariant position vector of its particles relative to a local frame, then, by providing the computer with

the above-mentioned six quantities, it is possible to view the segment from any other global perspective. The mathematical tool illustrated above may be used to describe segment movement as well. In fact, if the pose of the LF is described in each sampled instant of time during movement relative to a GF by giving the six independent scalar quantities implied in ${}^{g}\mathbf{R}_{l}$ and ${}^{l}\mathbf{o}$ then the segment morphology (${}^{l}\mathbf{p}$) can be reconstructed in its instantaneous location (${}^{g}\mathbf{p}$) through equation 2.23. It is interesting to emphasize that this approach, based on the assumption of rigidity, allows the description of the pose of a body using only six numerical values for each sampled instant of time. To these values, the time invariant local coordinates of the particles used to represent the morphology must be added for virtual reality representation of the movement.

The description of the skeletal-system movement involves the definition of several set of axes that are either global or local.

Global frames

In a movement analysis laboratory, the following inertial, global, frames can be defined [107, 96] 2.21.

- Photogrammetric frame: This is the set of axes in which marker position coordinates are provided by the stereophotogrammetric system. These are arbitrarily defined relative to the calibration object or procedure used.

- Motor task frame: This frame is consistent with the analyzed motor task and sometimes describes its basic features. For instance, when locomotor acts are investigated, one axis of the frame indicates the mean direction of progression, possibly including the orientation of the floor (in case of non-level locomotion). According to the general recommendations from the International Society of Biomechanics [108], in human

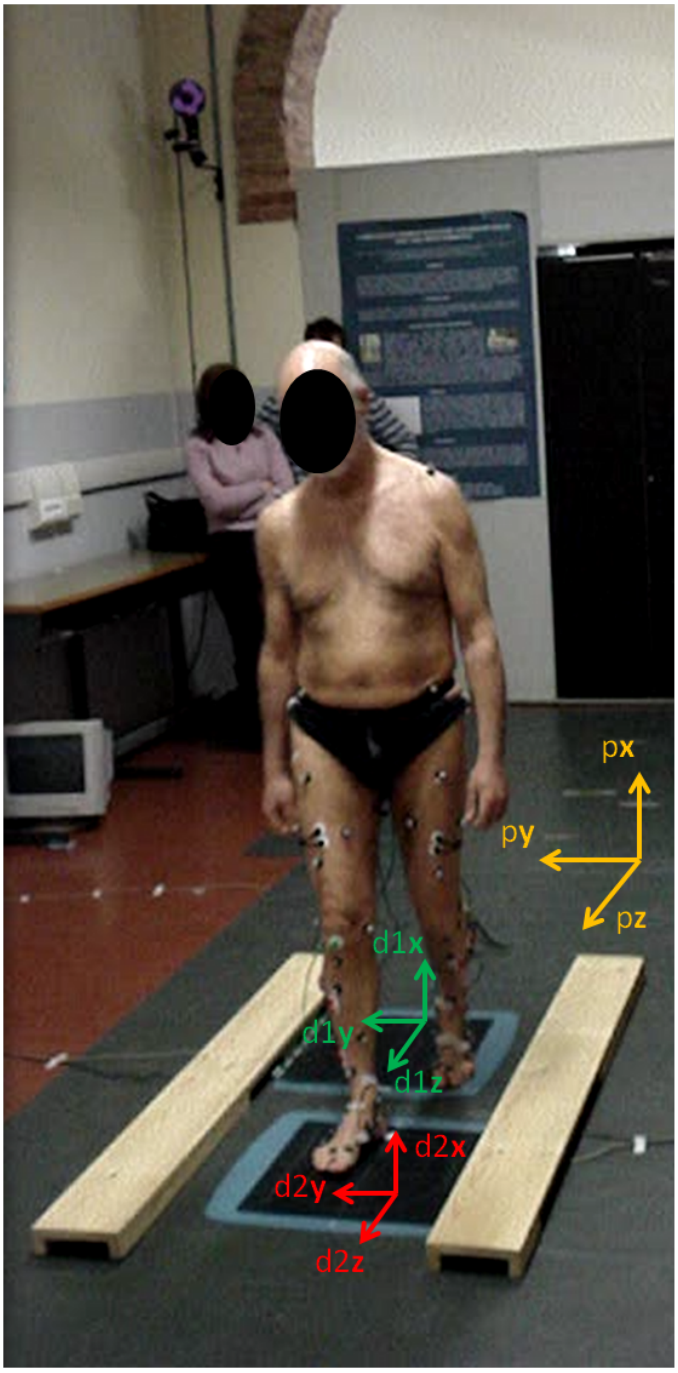

Figure 2.21: Example of a human movement analysis laboratory. Basic measurement instruments are depicted together with their systems of axes (p: photogrammetry; d: dynamometry). If level walking is analyzed, the motor task frame may coincide with the frame of one of the two force plates.

movement analysis orthogonal coordinate systems should have the X axis pointing forward in most locomotor tasks coinciding with the direction of progression, Y pointing vertically upwards, and Z pointing to the right.

- Dynamometer frame: This is the frame in which force and moment components are given by the instrument and is defined by the relevant calibration matrix.

- Plumb Line: This is a single axis and represents the orientation of the gravity line, usually assumed to point downward.

Within the same experiment, different mechanical quantities are measured with respect to different global frames. However, normally, their interpretation, or use as input to the mathematical models that allow for the estimation of non-measurable quantities, requires that all of them be represented in the same frame (primary global frame). The latter role is usually assumed by the motor task frame. Thus, a global frame calibration procedure must be carried out. This consists of the determination of the position vector and the orientation matrix of all secondary global frames involved relative to the primary global frame (${}^{pg}\mathbf{R}_{sg}, {}^{pg}\mathbf{o}$). This allows for the transformation of any vector given in the former frames into a vector in the primary frame 2.23. From an operative point of view, ad hoc experiments are carried out which allow for the determination of the position vectors of selected fiducial points in both the secondary and primary global frame. By using an adequate number (N) of these points and feeding their position vectors into equations having the same form of equation 2.23, where the secondary global frame takes the place of the local frame, the unknown orientation matrix and

position vector are estimated by the following equation:

$$^{pg}\mathbf{p}_k \;=\; ^{pg}\mathbf{R}^{sg}_{sg}\mathbf{p}_k +^{pg} \mathbf{o}k = 1, ..., N \tag{2.25}$$

For the sake of accuracy, this estimation counts on a redundant number of fiducial points and uses a least squares approach [96]. A typical example is the determination of the pose of the force plate frame relative to the photogrammetric frame by using a set of three or more markers located in known positions in the former frame [109].

Local frames

A generic local frame rigidly associated with a bony segment is referred to as technical frame (TF) [110, 107, 96, 108]. These frames are used to describe the location in space, either stationary or time-varying, of the segment under analysis 2.22.

- Morphology technical frame (MTF): This is the TF used in the course of the experiments that provide the segment morphology. It is defined by the technique and/or measuring equipment used and may be regarded as arbitrary.

- Marker cluster technical frame (CTF): This is the TF used to describe the movement of a segment and is reconstructed using the instantaneous position of at least three non-aligned superficial markers associated with the bony segment and tracked by a photogrammetric system (2.23). These markers, which are named technical markers, are positioned to comply with technical requirements such as visibility to a sufficient number of cameras and to minimize relative movement between them and underlying bone. Normally, their position has no repeatable reference to the morphology of the segment. For this same reason, the CTF has an arbitrary position and orientation with respect

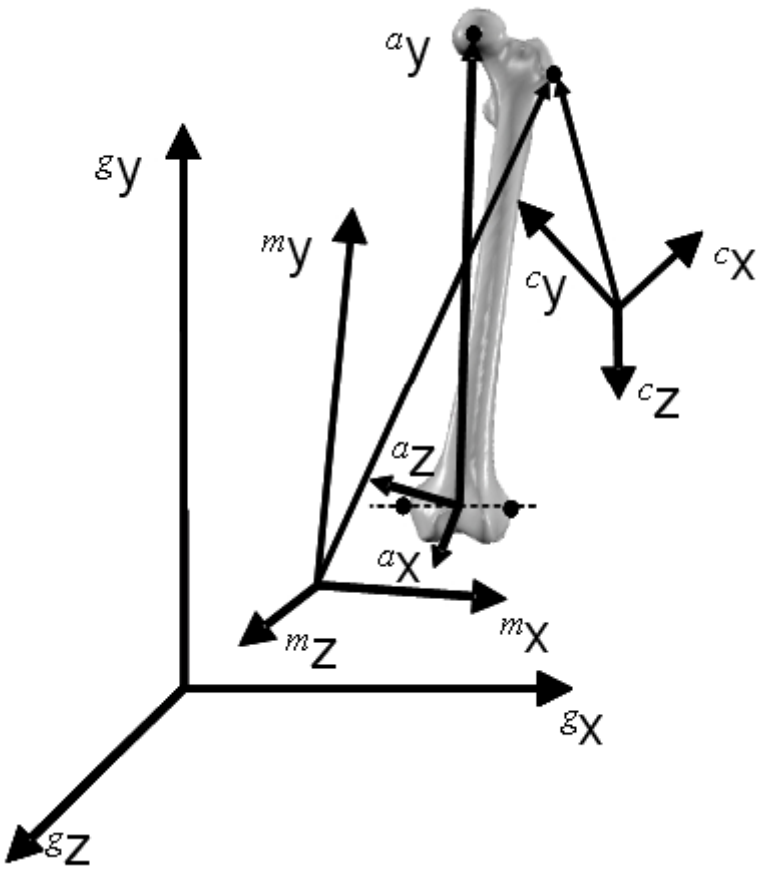

Figure 2.22: Morphological (${}^m\mathbf{X}$,${}^m\ \mathbf{Y}$,${}^m\,\mathbf{Z}$) and marker cluster (${}^c\mathbf{X}$,${}^c\ \mathbf{Y}$,${}^c\,\mathbf{Z}$) technical frames, and anatomical frame (${}^a\mathbf{X}$,${}^a\ \mathbf{Y}$,${}^a\,\mathbf{Z}$). The latter frame is defined as having the y axis joining the midpoint between the lateral and medial femoral epicondyles and with positive direction proximal, the z axis lies in the plane defined by the y axis and the center of the femoral head and points from left to right, the x axis is orthogonal to the yz plane with its positive direction forward [96].

to the bone which depend on both the location of the markers and the analytical procedure used to generate them [96]. In order to economize the number of markers, some authors construct some CTFs using virtual markers. These are points of a segment for which the location is determined, through some geometric rule, relative to the position of the technical markers in the relevant CTF. If a virtual marker, thus obtained, is supposed to be shared with an adjacent segment, then it may be used to construct the CTF of the latter segment. This is the case, for instance, when the two segments involved are hypothesized to be joined by a spherical hinge and the virtual marker is the center of rotation [111, 112] 2.23.

Normally, the instrumentation used to record morphology information is different from that used to reconstruct the segment movement, and the two procedures are separate both in time and location. Therefore, the two TFs referred to above are different (2.22). This circumstance raises a problem. In order to represent the segment in its instantaneous pose, both movement and morphology data must be given with reference to the same TF. Thus, a transformation of the position vectors given in the MTF into position vectors in the CTF, or vice versa, must be carried out (movement-morphology data registration). For this purpose an anatomical calibration procedure must be carried out 2.24. Similar to the global frame calibration procedure, the position vectors of a number of selected points belonging to the segment under analysis must be made available in both TFs involved (${}^{m}\mathbf{p}$ and ${}^{c}\mathbf{p}$ in 2.22). These points must coincide with anatomical landmarks (AL) so that they be identifiable in a repeatable fashion [113]. Superficial ALs, usually bony prominences, are used and identified by palpation, and

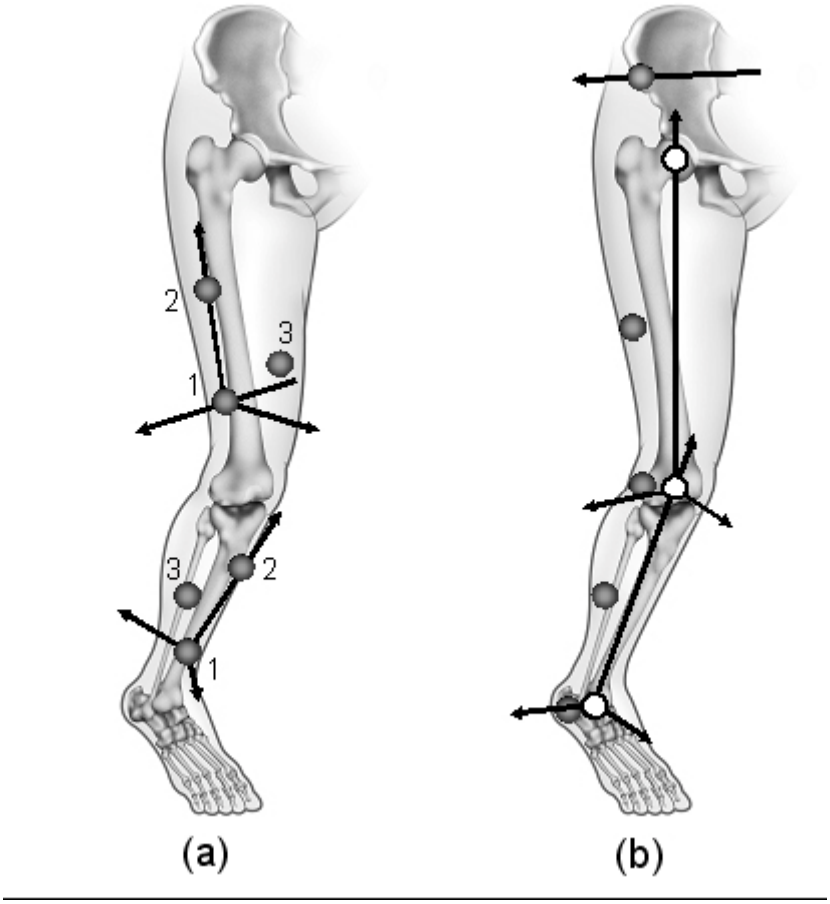

Figure 2.23: Examples of marker set and marker cluster technical frame. a) Three technical markers for each bony segment; the cluster technical frame is constructed using the following rule: $\mathbf{t}_j$ is the position vector of the origin, the z axis is oriented as $m_1 - m_2$, and the x axis as $(m_3 - m_2) \times (m_1 - m_2)$.

their position in the CTF is determined by locating markers on them (anatomical markers) and using stereophotogrammetry. These markers may be removed prior to tracking the movement under analysis, unless they are also made to play the role of technical markers (2.23). Internal AL positions are normally estimated using the location of superficial ALs and predictive models [111]. In the case of the centre of the femoral head, the fact that it can be considered to coincide with the center of rotation of the femur relative to the pelvis allows its location to be determined using movement data (functional approach [110]). The position of the ALs in the MTF is determined using a virtual palpation procedure. A possible alternative to the above-mentioned procedure consists of the determination of the position in the CTF of a highly redundant number of unlabeled points of sufficiently large portions of the bone under analysis [114].

- Anatomical frame: As opposed to the TFs, the location of which, relative to the underlying bony segment, is arbitrary and, as such, non repeatable, anatomical frames (AF) are defined specifically to meet the requirements of intra- and inter-subject repeatability. In addition, their planes normally approximate the frontal, transverse and sagittal anatomical planes. This is achieved by setting a geometric rule that constructs the AF using selected Als determined in the CTF through the anatomical calibration exercise illustrated above (2.24) [112, 108]. To this end, anatomical markers may also be placed in points that do not denote ALFs but lie on anatomical planes as identified by the operator [112, 113] (2.23). Alternatively, when the bone morphology is available, the AF can be defined using the intrinsic wealth of morphological information and first represented in the MTF and, then, in

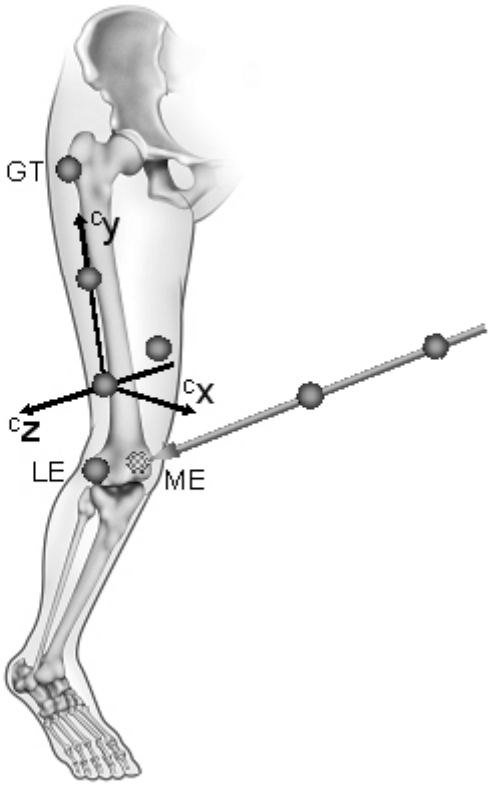

Figure 2.24: Some of them are calibrated using anatomical markers, others using a wand which carries a cluster of markers. Prior to recording, the end point of the wand, the position of which relative to the cluster of markers is accurately known, is made to coincide with the target anatomical landmark.

the CTF through the registration procedure illustrated above. Following the suggestion made in Cappozzo et al. [107], some authors refer to the general approach to human movement reconstruction presented previously as CAST (Calibrated Anatomical System Technique).

2.3.4 Kinematic of gait analysis

The normal locomotion requires the coordination of the neurological and the musculoskeletal systems to convert the essentially vertical moment of the lower limbs into a smooth forward movement of head and trunk. Many disorders of the musculoskeletal and nervous systems result in a significant interference with gait which make it difficult to participate in normal human activities. One of the basic purpose of gait analysis is to define these difficulties and to suggest remedial intervention. Another goal of gait analysis is to monitor the movement of the patient and to quantitatively measure parameters of gait that are fundamental for the evaluation of the patient's impairments and limited functionality. The use of this innovative technology and of advanced systems can help the traditional methods providing additional support for the optimal choice of rehabilitation programs. Gait analysis may also evaluate the effectiveness of rehabilitation plans during the recovery of the patient, indeed gait analysis can be suitable for this purpose especially for the following reasons:

- Non-invasivity
- Gait analysis can be performed more than once during a short period of time
- Gait analysis provides quantitative information

- Gait analysis obtained data are three-dimensional
- Possibility for multifactorial analysis: kinematic, kinetic and muscle activation data can be simultaneously acquired.

Human gait is characterized by a cyclic lower limbs and trunk motor activity patterns, indeed walking involves repetitious patterns of movement resulting in each foot periodically moving from one position of support to the next. These movements are cyclical in nature and occur over and over again step after step, so during gait, the musculoskeletal system performs special tasks which allow the progression of the subject:

- It generates impulsive force
- It maintains the stability of the upper body
- It helps in the shock absorption during the first impact with the ground

Hence, when describing human gait it is conventional to do this in terms of gait cycle. Because the movement of floor contact is the most readily defined event in the sequence of movements that is walking, this action is conventionally chosen to mark the beginning of the gait cycle. A complete gait cycle is defined as the interval of time between two successive initial contacts of the same foot (stride) and it represents the reference time interval in which all the biomechanical and muscular activity events can be described (2.25).

The gait cycle is divided into two major phases: the *stance phase* (stance) and *swing phase* (swing). The stance phase is defined as the period of time when the foot is on contact with the ground, it begins with the initial contact, which in normal gait is with the heel and ends at toe off, it usually represents about the 60% of the whole gait cycle. The swing phase is defined as the

period of time when the foot is not in contact with the ground. It occurs from toe off until the foot hits the gound again, this interval is equal to the remaining 40% of the whole gait cycle (2.25). If we define the period of time for a complete gait cycle as 100%, then it can be divided into eight different phases occurring in specific percentage of the cycle [10]:

1. **Initial Contact** (0–2% of the gait cycle): it occurs at the beginning of the gait cycle when heel touches the ground.

2. **Load Response** (0–10%): it is the first period of double support, is defined as a deceleration period during which the shock of the initial impact is absorbed by the contact with the ground and body weight is transferred from one limb to the other.

3. **Mid Stance** (10–30%): it is a period of body progression over a stable foot, the stability of the lower limb is an important feature of this phase, it ends when the body weight is aligned over the forefoot.

4. **Terminal stance** (30–50%): it begins with heel rise and it ends with the initial contact of the contralateral limb, during this phase the body weight is progressed beyond the suporting foot.

5. **Pre swing** (50–60%): it is the last period of the stance phase, corresponding to the second phase of double support. It begins with the initial contact of the contralateral foot, during this phase the limb moves from a position of general extension into flexion and although a stance phase, it is functionally important for limb progression by preparing the limb for swing. It ends with the toe off.

6. **Initial swing** (60–73%): it is the first period of the swing phase. In this phase the foot is lifted and the limb moves forward.

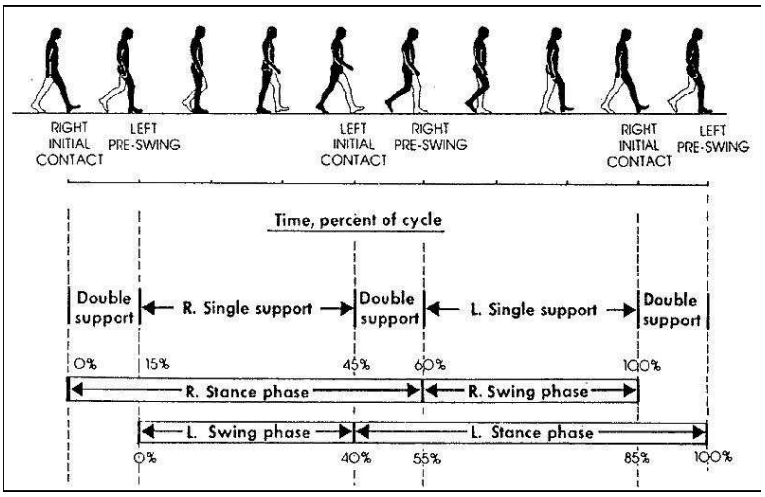

Figure 2.25: The gait cycle [115].

7. **Mid swing** (73–87%): it includes the progression of the limb, it ends when the swinging limb is forward and the tibia is vertical.

8. **Terminal swing** (87-100%): it is the final phase of the gait cycle and is a period of deceleration and preparation for the next ground contact.

Further characterization of human walking can be done with distance or spatial measurements such as step length and stride length and when these are combined with temporal parameters such as walking velocity, cadence can also be defined. Among the major space-time parameters we can define [10]:

- **Step length**: it is defined as the longitudinal distance between the two feet generally expressed in meters (m). It is the distance from a point of contact of one foot with the ground to the following occurrence of the same point of contact of the other foot with the ground(as for example the heel contact). In normal walking the right step is defined as the distance measured from heel strike of the left foot to the heel strike

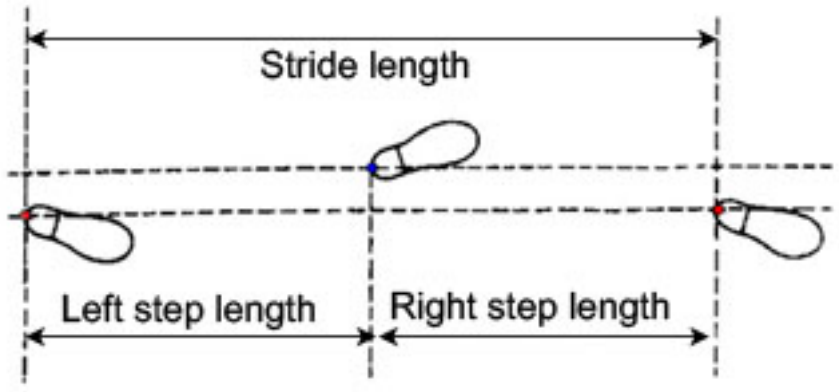

Figure 2.26: Spatial parameters of the step [10].

of the right foot. Conversely, the left step is defined as the distance measured from the hell strike of the right foot to the same event of the left foot (2.26).

- **Stride length**: it is the distance covered during a complete gait cycle and represents the sum of the right and the left step lengths.
- **Step width**: it is the mediolateral distance between the feet which is typically measured from the ankle joint center.
- **Cadence**: it is the number of steps per unit of time (usually a minute)
- **Walking velocity**: it is expressed as a distance over time, usually m/s.

2.3.5 Gait Analysis Protocols

A protocol is the scheme that defines the acquisition, the kinematic and dynamic data processing by means of a specific marker set and known mathematical conventions. It ensures the standardization of the acquisition set up

and the repeatability of the measurements. A lot of different protocols have been implemented for the quantitative gait analysis, the most widely used and important protocols are: the Davis–Helen Hayes protocol, the CAST protocol, the IORgait protocol, the SAFLo and the LAMB protocol.

Davis Helen Hayes Protocol

The first phase of the Davis protocol [111] relies on the measure of the subject's anthropometric parameters, such as:

- Body Weight
- Height
- Length of the tibia
- Distance between lateral and medial knee's femoral epicondyles
- Distance between the lateral and medial ankle's malleolus
- Thickness of the pelvis

A detailed description of all the anthropometric parameters and how to measure them is provided in figure **??**:

Then the protocol consists on positioning the marker set directly on the skin, on some specific anatomical landmarks, in particular 2.1:

The placement of the marker set is optimal because all the markers are placed on the external sides of the body segments (so that they become highly visible), but in case of rapid movements of the subject, the wands may vibrate and move, causing problems int he reconstruction of the gait. The protocol consists of a static acquisition, also known as the calibration of the subject: the different angles of two adjacent segments are acquired as a

Table 2.1: Marker Set of Davis–Helen Hayes Protocol

Marker Placement		
Body Segment	**Label**	**Name**
Trunk	RS	Right Jugular Notch where the clavicles meet the sternum
	LS	Left Jugular Notch where the clavicles meet the sternum
	N	Spinous Process of the 6th Cervical Vertebrae
Pelvis	R	Right Anterior Superior Iliac Spine
	B	Left Anterior Superior Iliac Spine
	H	Sacrum
Femur	R-LH	Right and Left Great Trochanter
	R-LF	Right and Left Femoris Wand
	R-LK	Right and Left Lateral Epicondyle of the knee
Tibia and Fibula	R-LP	Right and Left head of the Fibula
	R-LB	Right and Left Tibia Wand
	R-LA	Right and Left lateral malleolus of the ankle
Foot	R-LT	Right and Left Second Metatarsal Head
	R-LQ	Right and Left Calcaneus

Parameter	Description
Body mass	Measure (on a scale accurate to 0.01 kg) the mass of subject with all clothes except underwear removed
ASIS breadth	With a beam caliper, measure the horizontal distance between the anterior superior iliac spines
Thigh length	With a beam caliper, measure the vertical distance between the superior point of the greater trochanter of the femur and the superior margin of the lateral tibia
Midthigh circumference	With a tape perpendicular to the long axis of the leg and at a level midway between the trochanteric and tibial landmarks, measure the circumference of the thigh
Calf length	With a sliding caliper, measure the vertical distance between the superior margin of the lateral tibia and the lateral malleo lus
Calf circumference	With a tape perpendicular to the long axis of the lower leg, measure the maximum circumference of the calf
Knee diameter	With a spreading caliper, measure the maximum breadth of the knee across the femoral epicondyles
Foot length	With a beam caliper, measure the distance from the posterior margin of the heel to the tip of the longest toe
Malleolus height	With the subject standing, use a sliding caliper to measure the vertical distance from the standing surface to the lateral malleolus
Malleolus width	With a sliding caliper, measure the maximum distance between the medial and lateral malleoli
Foot breadth	With a beam caliper, measure the breadth across the distal ends of metatarsals I and V

Figure 2.27: Description of anthropometric parameters and how to measure them [116].

reference angle. The calibration is performed while the subject is standing in an upright position and it lasts for a few seconds. In this way the position of all markers placed on the body is acquired and with the help of the anthropometric measures the joints' centers of rotation can be estimated. When the static acquisition is completed, the second step is the dynamic acquisition: the subject is asked to walk at normal speed from a decided point. Thanks to the anthropometric measurements both the masses and the inertial moments of the body segments can be evaluated, on the other hand the relative positioning of the body segments, the joint angles, the velocities and the ac-

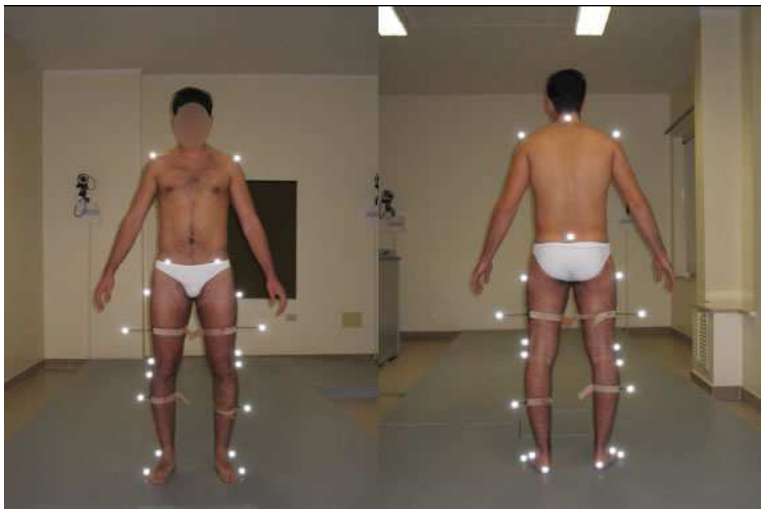

Figure 2.28: Davis protocol marker set [111].

celerations can be obtained by means of the markers' trajectories, which are reconstructed with the motion capture system (see figure: **??**). Once again based on the equations which rely on the anthropometric measurements the position of the joints' centers of rotation can be evaluated.

The Calibrated Anatomical System Technique - C.A.S.T. Protocol

The first step for the joints kinematic reconstruction, as mentioned, implies the definition of a technical frame for each body segment, which can be defined from the markers positions in the laboratory's absolute reference system. Capozzo et al. [107] have shown that the reference systems because of instrumental and experimental errors and of the artifacts are the result of an estimation. This reference system might coincide with the anatomical system and can be determined from the position of three markers, belonging to a cluster, which are not aligned, placed on the surface of a body's segment. This protocol ([107]) plans to place the clusters of markers in areas with limited tissue movements, in order to minimize the soft tissue artifacts.

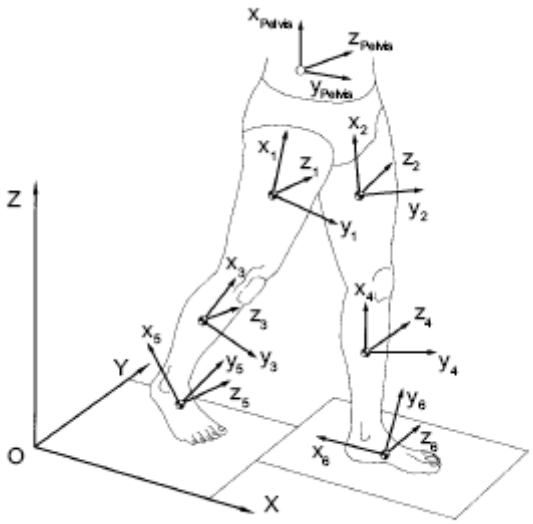

Figure 2.29: The segment reference frames (xyz) embedded at the centers of gravity of each segment, they are used to compute the joints angles and frames of reference for the joint moment reactions. [116].

The next step consists of the identification of anatomical landmarks without the application of markers in their correspondence, but reconstructing their position with the help of the technical frames previously defined. This procedure is defined as anatomical calibration. There are two different ways to perform the anatomical calibration:

1. The first method is to place a marker on the bony prominence and to determine the coordinates with respect to a the technical frame, using the positions of the marker clusters (see 2.30). This procedure requires the marker to be placed on the anatomical landmarks and the marker cluster to be seen by at least by two cameras. This procedure is applied for all the anatomical landmarks. The markers used to identify the anatomical landmarks are removed before the performance of the

the movement.

2. The second method uses a rigid wand with two markers placed at a known distance from the tip, the latter is placed on the anatomical landmark which has to be calibrated. Taking advantage of the distance between the markers and the tip of the wand, the position of the anatomical landmark of interest can be reconstructed with respect to the technical reference (see 2.31). For this methodology it is necessary that both the markers of the wand and those belonging to the cluster of interest are visible from at least two cameras. This method is more feasible than the first especially when the landmarks are in such positions difficult to be seen.

The IORgait Protocol

Comparing the first two protocols, it is worthy to notice that for the Davis protocol the set up of the patient is easier and faster if compared to the C.A.S.T. protocol. However, the C.A.S.T. protocol provides more accurate results. A new protocol has been introduced ([118, 119]) to find a trade off between reducing the time required for the set up of the subject and both the accuracy and the reliability of results. This protocol identifies the anatomical landmarks both by placing the markers directly on the landmarks and with the anatomical calibration.

The marker set consists of:

The Davis protocol wands have been replaced by the anatomical calibration which is simpler if the movements performed by the patient are fast. This protocol uses the Bryan–Cardan kinematic joint angles convention, in particular the *Grood&Suntay* convention, that ensures consistency with the

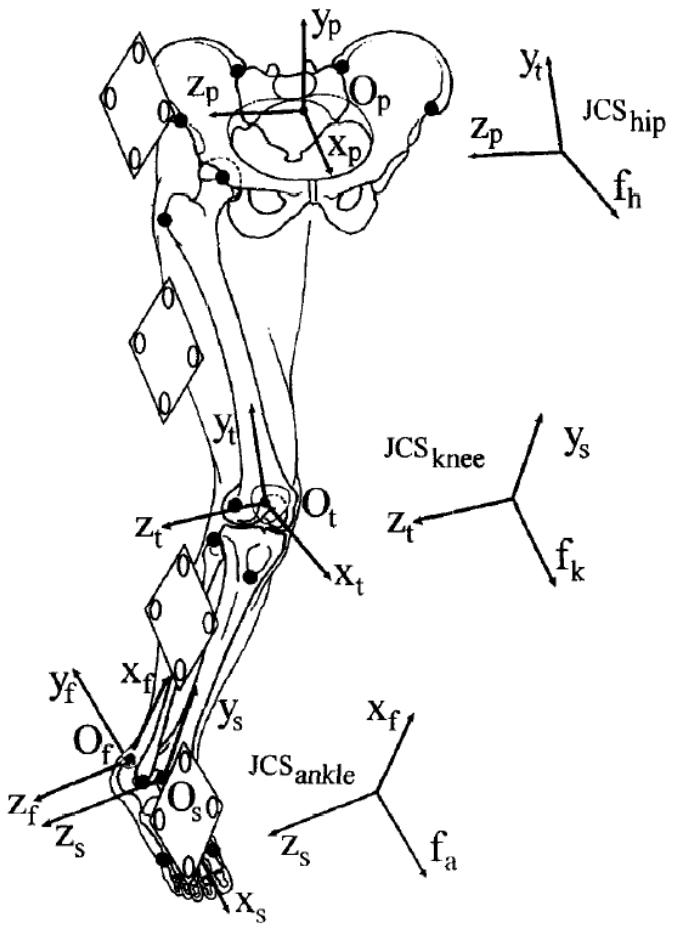

Figure 2.30: C.A.S.T. Protocol: Configuration of the collected plate-mounted markers (o) and of some of the reconstructed anatomical landmarks (•). Pelvic (p), thigh (t), shank (s) and foot (f) anatomical coordinate systems of axes are also shown [117].

Table 2.2: Marker Set of the C.A.S.T. Protocol

Marker Placement		
Body Segment	**Label**	**Name**
Pelvis	ASIS	Anterior Superior Iliac Spine
	PSIS	Posterior Superior Iliac Spine
	AC	Center of the Acetabulum
Femur	FH	Center of the Femural Head
	GT	Prominence of the Great Trochanter External Surface
	LE	Lateral Epicondyle
	ME	Medial Epicondyle
	LP	Anterolateral apex of patellar surface ridge
	MP	Anteromedial apex of patellar surface ridge
	LC	Most distal point of the lateral condyle
	MC	Most distal point of the medial condyle
Tibia and Fibula	IE	Intercondyle Eminence
	TT	Prominence of the Tibial Tuberosity
	HF	Apex of the Head of the Fibula
	MM	Distal Apex of the medial malleolus
	LM	Distal Apex of the lateral malleolus
	MMP	Most Medial point of the ridge of the medial Tibial Plateau
	MLP	Most Lateral point of the ridge of the medial Tibial Plateau
Foot	CA	Upper Ridge of the Calcaneous Posterior Surface
	FM	Dorsal Aspect of the First Metatarsal Head
	SM	Dorsal Aspect of the Second Metatarsal Head
	VM	Dorsal Aspect of the Fifth Metatarsal Head

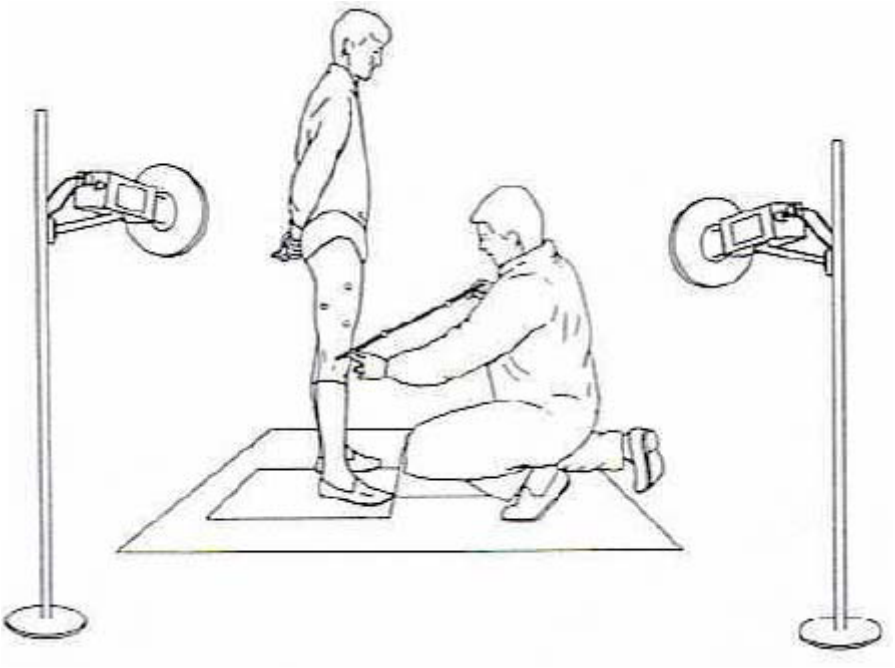

Figure 2.31: C.A.S.T. Protocol: anatomical landmarks calibration.

physiological and clinical terminology. The marker calibration is performed with a static acquisition of the patient, while the kinematic, the velocities and accelerations are obtained from the a dynamic acquisitions. This protocol is widely used for the gait analysis because it is very easy to use if compared with the first two protocols, and it has been shown that it has high accuracy [118].

The SAFLo Protocol

The SAFLo Protocol [120] is an anatomical protocol, as it requires the markers to be placed directly on the anatomical landmarks of the subject. Before the acquisition, the following anthropometric measures need to be collected, in order to reconstruct the three-dimensional model of the subject's body.

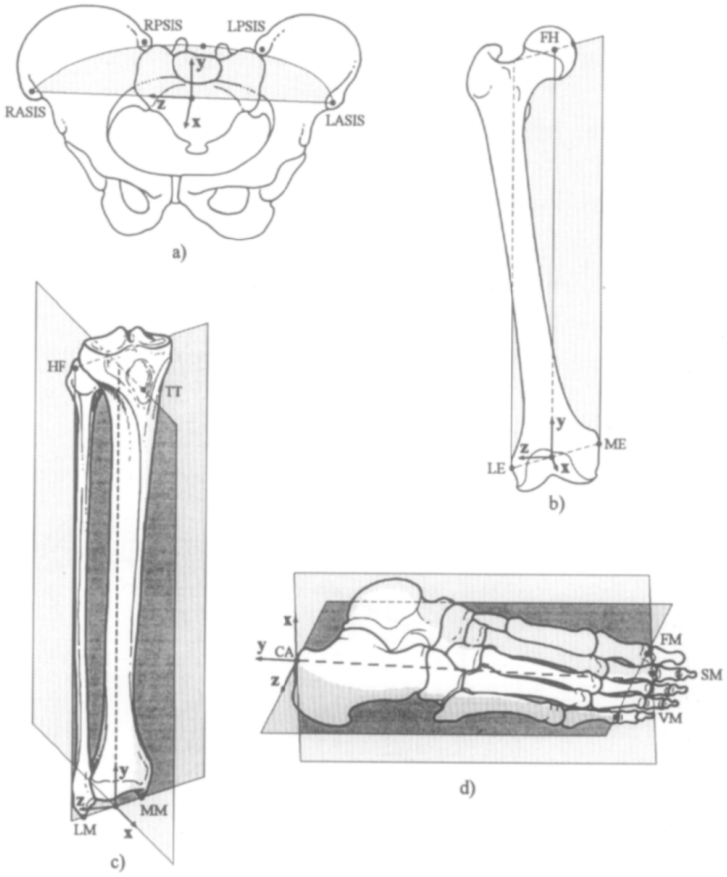

Figure 2.32: CAST protocol: bone embedded anatomical frames definition and orientation. [107].

- Height
- Body Weight
- Femur Length: the distance between the greater trochanter and the lateral femoral epicondyle
- Leg Length: the distance between the lateral femoral epicondyle and the lateral malleolus
- Foot Legth: the distance between the calcaneus and the big toe

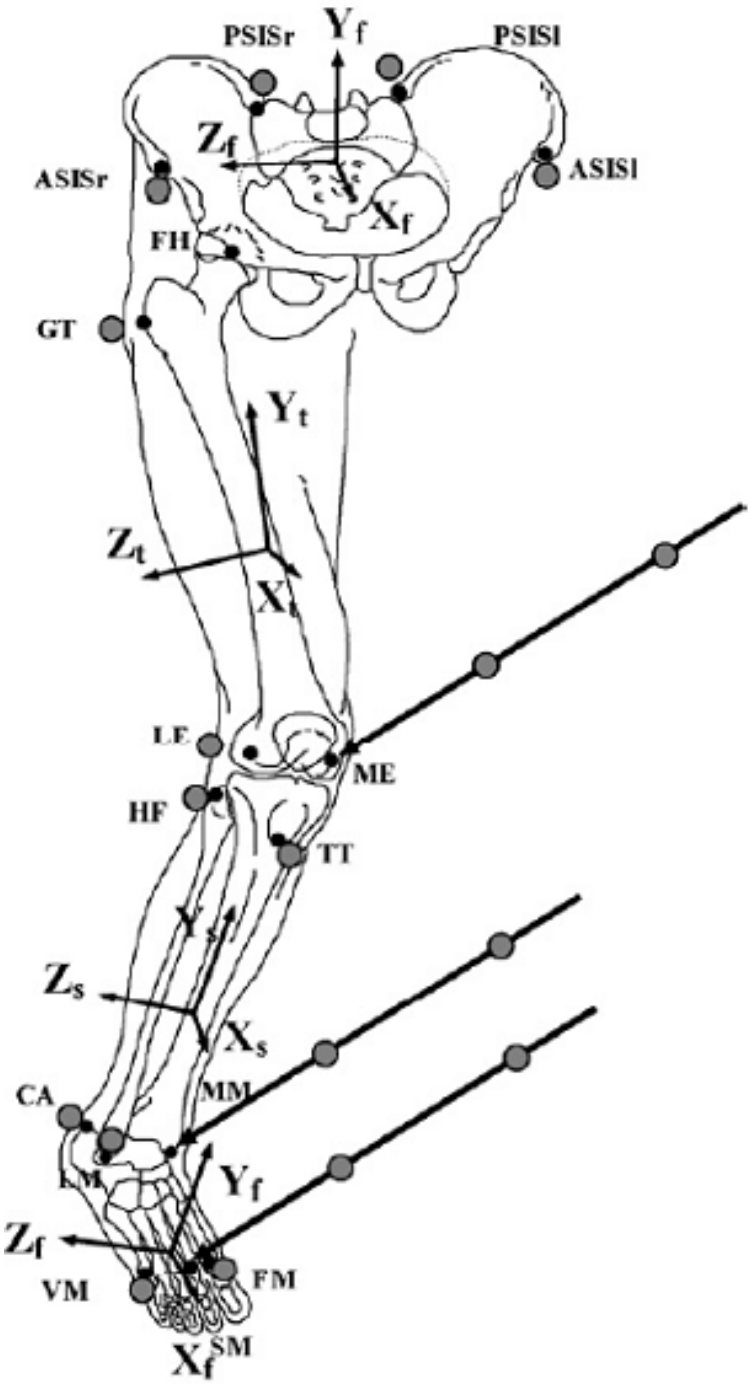

Figure 2.33: IORgait protocol: Markers position and calibration of anatomical landmarks [118].

Table 2.3: Marker Set of the Leadini's Protocol

Marker Placement		
Body Segment	**Label**	**Name**
Pelvis	RASIS	Right Anterior Superior Iliac Spine
	LASIS	LEft Anterior Superior Iliac Spine
	RPSIS	Right Posterior Superior Iliac Spine
	LPSIS	Left Posterior Superior Iliac Spine
Femur	GT	Prominence of the Great Trochanter External Surface
	LE	Lateral Epicondyle
Tibia and Fibula	HF	Apex of the Head of the Fibula
	TT	Prominence of the Tibial Tuberosity
	LM	Distal Apex of the lateral malleolus
Foot	CA	Upper Ridge of the Calcaneous Posterior Surface
	FM	Dorsal Aspect of the First Metatarsal Head
	VM	Dorsal Aspect of the Fifth Metatarsal Head

- Pelvis Width (PW): the distance between the two anterior superior iliac spines
- Pelvis Height (PH): the distance between the line between the two posterior superior iliac spines and the horizontal plane on which the subject is seated.
- VD: the vertical distance between the posterior iliac spines and the posterior iliac crests
- Distance between the lateral and medial epicondyles of the knee
- Distance between the lateral and medial malleolus of the ankle

- Distance between the first and the fifth metatarsal heads
- Distance between two hip joint centers (HZ)
- Distance between the midpoint of the hip joint center and the medial point of the iliac crest (HY)

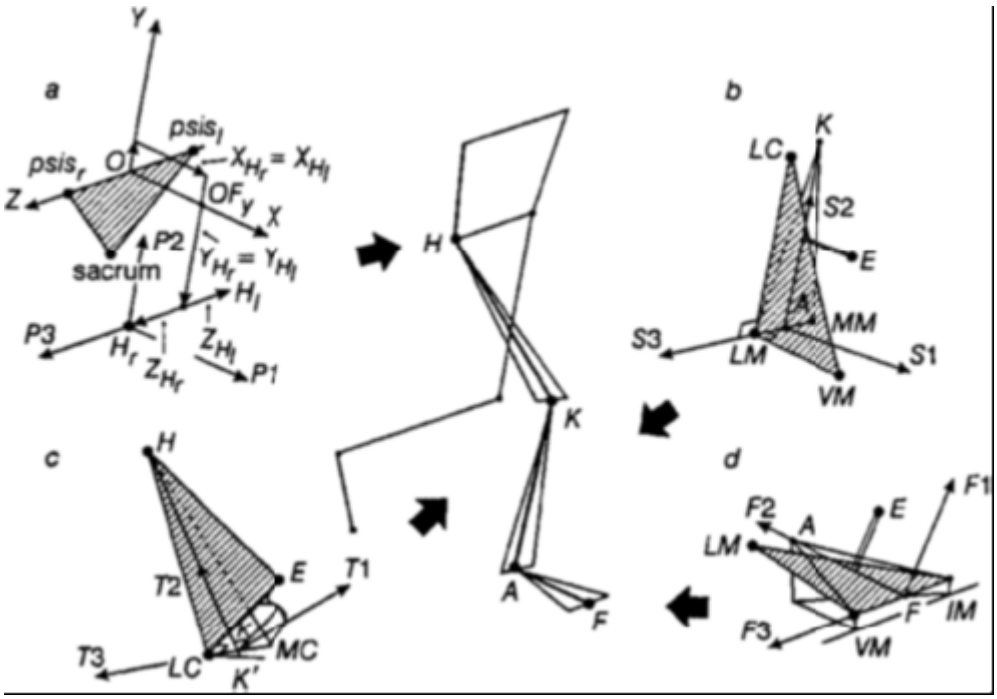

Figure 2.34: The SAFLo protocol: Pelvis anatomical frame and hip joint coordinate system (a) and knee anatomical reference frame (b) [120].

In addition to the markers placed directly on the skin there are also markers placed on additional wands. These markers are defined as extended markers. The rods are positioned on the thigh, leg and foot 2.4).

The LAMB Protocol

This new protocol [121, 122] was designed to study children gait and posture, both as regards normal and neurological subjects. This protocol took

Table 2.4: Marker Set of the SAFLo Protocol
Marker Placement

Body Segment	Description
Knee	The wand is connected to the lateral and medial condyle. The additional marker is perpendicular to the intercondylar line towards the lateral condyle
Tibia	The additional marker is supported by a wand connected to the anterior surface of the tibia
Foot	The additional marker is placed on the metatarsal area of the forefoot

advantage of the approaches including the anatomical, functional and calibration minimizing the operational constraints that may be caused by the anthropometric measures of the children and at the same time ensuring, as a result, a set of kinematic parameters of clinical significance. The protocol was then extensively used for adults, thus confirming its feasibility and results. The body is modeled as a set of 16 segments, 7 of which belong to the locomotor system (pelvis, thighs, legs and feet) and are identified by at least three points each (the third point considered for the thigh is the hip joint center, which can be estimated by using the pelvis).

The LAMB protocol takes advantage of some aspects of the other protocols (SAFLo and C.A.S.T.) as regards the placement of the markers set. The markers placed on the lateral and on the medial epicondyles are included in a cluster located above the femoral condyle, as required by the SAFLo Protocol. After the static acquisition the markers placed on the medial malleolus can be removed in order not to prevent the subject to walk normally. As for the C.A.S.T. a cluster of four marker are placed on each body segment so

that they can be used for the calibration of some anatomical landmarks.

The protocol consists of 60 markers placed as follows: 22 markers on each leg, 5 on the pelvis and 11 on the trunk. In detail, this protocol requires the placement of anatomical markers on: the zygomatic process of temporal bone, the spinous process of vertebrae C7 and T10, the scapular acromion, the lateral humeral epicondyle, the distal ulnar tuberosity, the medial PSIS, the ASIS, the greater trochanter, the medial and lateral femoral condyles, the head of the fibula, the medial and lateral malleolus, the first and the fifth metatarsal heads, the distal Achilles tendon insertion, and the dorsal aspect of the big toe.

The following markers are calibrated by means of the wand:

- Greater Trochanter
- Medial and Lateral epicondyles
- Medial and Lateral malleolus
- Tibial Tuberosity

All the other anatomical landmarks are calibrated using the corresponding markers as a reference, the calibration is performed during the static acquisition before the postural analysis. The use of mathematical models, independent from the absolute reference system, allows the reconstruction of calibrated points, the identification of the reference system of the pelvis, the estimation of the hip joint center, the identification of the reference system of the lower limbs and the joints centers, the evaluation of the joints angles and moments, of the muscle geometry, of the position of the COM and the work; it allows, in addition, the use of force platforms positioned to the ground according to a preferred direction. The marker-set, which allows

three-dimensional kinematic analysis, does not require the use of external devices such as wands or plates, reducing the marker setup for the subject. The positioning of the marker set limits the risk of skin effect and artifacts and it avoids the need for anthropometric measurements. In addition the anatomical calibration shortens the setup for the subject.

Figure 2.35: The LAMB protocol marker set [121].

Chapter 3

fMRI and Gait Analysis

3.1 Participants Recruitment

A healthy control subject (CS) (45 years old, male, BMI 22, right-handed) was enrolled to evaluate the feasibility of different motor tasks as clinical protocols. Four hemiparetic post-stroke subjects (SP) were recruited. All the patients (mean age 51 ± 6 years old, 3 males and 1 female, mean BMI 27 ± 2, right-handed) suffered from a chronic hemiparesis due to hemorrhagic stroke, which caused a left lenticulocapsular lesion for patients SP1, SP3, SP4 and a right one for patient SP2. fMRI acquisitions were performed before (T0 and T1 as a repeatability test, to check the reliability of the collected data), after electromyography (EMG) biofeedback rehabilitation (BFB) (T2) and after three months for the follow up (T3). He underwent task oriented BFB consisting of a total of 15 rehabilitation sessions divided in three session every week of 45 minutes each

3.2 fMRI Instrumental Assessment

Four different sessions of acquisitions were performed:

1. Time T0: Post-stroke patients underwent a clinical, MRI and fMRI evaluation to get a general functional clinical picture, to assess the extent of the ictal injury and to analyze brain activity at the starting stage, i.e. pre-rehabilitation treatment.

2. Time T1: 2 months after T0, patients underwent a clinical and a MRI retest to assess the stabilization of the functional clinical picture and to ensure the absence of new ictal events; moreover the fMRI and the instrumental gait analysis were performed. Patients then underwent a rehabilitation program aimed at improving the global ankle joint functionality during gait.

3. Time T2/T3: Patients were asked to come back for further assessments within 1 week of the end of rehabilitation (T2) and after 3 months of follow-up (T3) after the initial assessment.

The T2 and T3 assessments will include the same tests performed at T1.

All assessments and rehabilitation sessions were held at the IRCCS S. Maria Nascente Don Carlo Gnocchi Foundation in Milan at the presence of medical staff, physiotherapists and laboratory technicians involved in the study.

The healthy subject underwent just an fMRI analysis, in order to determine the normative brain activation areas related to the movements of the ankle joint.

All fMRI data were collected with a 1.5 T Siemens Magnetom Avanto scanner (Erlangen, Germany). Anatomic registration was acquired with a

T1-weighted inversion recovery sequence with repetition time (TR) = 1900 ms; echo time (TE) = 3.37 ms; T1= 1100 ms; flip angle =15 ° ; 176 slices −1 mm thick; matrix 256 × 192; field of view (FOV) = 256 × 192 mm. For functional imaging sessions an echo-planar imaging (EPI) $T2^*$-weighted sequence was used: TR = 2500 ms, TE = 50 ms; matrix 64 × 64; FOV = 250 × 250 mm; voxel size = 3.9×3.9×5 mm. Subjects were asked to perform a blocked design for two different tasks: active (A) and passive (B) ankle dorsi/plantarflexion movements.

Task A consisted in the active movement of the ankle (dorsiflexion and plantarflexion of about 15 ° with a frequency of 0.5 Hz), while task B consisted in performing the same passive movement (the patient was helped by an operator). In both cases, the patient's foot was supported by a pillow (or by another device) in order to enable the voluntary movement of ankle flexion trying to avoid the help of the leg which was blocked by a brace to minimize the use/help of the knee.

The specific motor paradigm consisted of six 30 second periods of task B each one followed by 30 seconds of rest and then six periods of task A (again followed by rest blocks), first for the unaffected ankle and afterwards for the paretic side (see figure 3.1). Each task-block start-stop event was based on acoustic signal. Each functional acquisition included 144 volumes of 25 images, for a total of 3600 scans. Subjects were trained to perform the tasks before the examination; an operator was close to the patient for safety reasons and in order to check that the tasks was performed correctly.

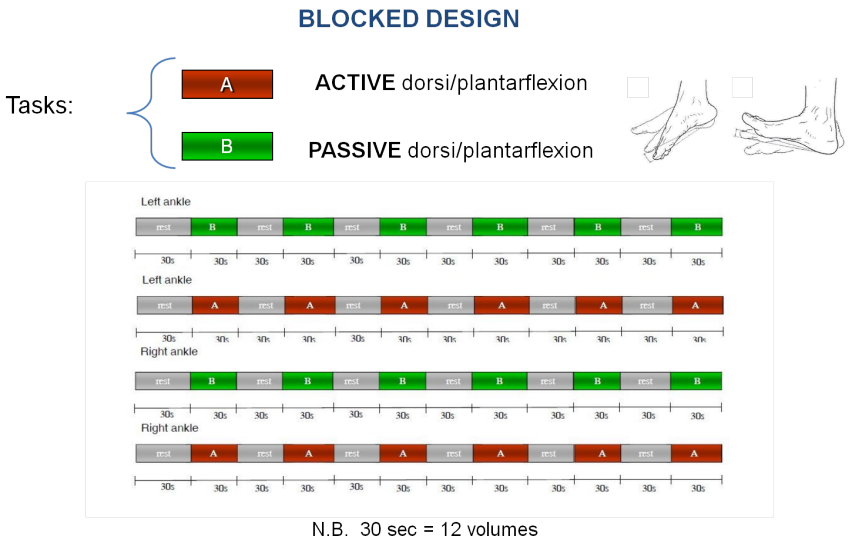

Figure 3.1: Block experimental design used during the fMRI acquisitions.

3.3 Clinical Assessment

All the post-stroke patients underwent the clinical evaluation, which included the use of the internationally accepted scales of impairment and disability such as the Modified Minimental Test (MMT) to assess the attention deficit, the Timed walking test (TW) to assess the ability to walk at least for 10 meters, the Timed Up and Go (TUG) and the Berg Balance Scale (BBS) to evaluate the static and dynamic balance.

3.3.1 Training Procedures

Patients then underwent a rehabilitation program aimed at improving the global ankle joint functionality during gait. In particular, an auditory biofeedback tool based on the electromyographic (EMG) signal was used; the biofeedback device was SATEM Mygotron (SATEM srl, Roma, Italy).

The device was applied to the gastrocnemius lateralis, in order to increase

the ankle joint power production during the push-off phase of the gait cycle. The rehabilitation treatment included 15 BFB sessions, 3 per week, of 45 minutes each [15].

EMG-rectified and 100-ms averaged data were recorded at 150 Hz, band-pass filtered at 20 to 950 Hz, and then amplified with a gain of 40,000 (50 $\mu Vrms$ range).

A rehabilitation protocol was designed following the theorem of motor control learning [123]. The goal was to improve functional gait; thus, feedback was delivered during walk over ground. EMG BFB was applied to the gastrocnemius lateralis. EMG was recorded and presented as an analogical audio signal to the patient; an auditory feedback tone was used to indicate whether push-off power met the target.

The therapeutic sessions were divided into 4 phases. The aims of these phases were to improve gait performance, to increase patient's auto error detection, and to transfer acquired skills during biofeedback condition to a context in which the feedback was no longer available [14, 15]. The treatment phases were identified according to Jonsdottir et al., 2007 [14].

The patients underwent 2 or 3 treatment sessions a week, of 45 minutes each. During the first phase (first five treatments), the exercise was constant: the patients were free to walk at a comfortable speed and were trained with uninterrupted BFB-EMG and verbal directions. The patients were carefully taught about how to properly raise the heel to allow the knee bending while pushing the forefoot on the ground. During the second phase (treatments 6-10) a variable exercises pattern was adopted (as for example: changing the step length or the speed), the BFB EMG was kept constant, but the verbal directions were reduced. In the third phase (treatments 11-15) again a variable exercises pattern was adopted (such as during the 2nd phase, this

time changing the nature of the ground on which the patients walked), the patients were let to detect their own errors, providing them with the BFB-EMG only occasionally. In the fourth and last phase, the BFB-EMG was mostly omitted, while the exercise varied as during the 2nd and the 3rd phase. All rehabilitation sessions were held at the Neuromotor Rehabilitation Gym of the the IRCCS S. Maria Nascente Don Carlo Gnocchi Foundation in Milan at the presence of medical staff and physiotherapists.

3.4 Gait Analysis Instrumental Assessment

Kinematic and dynamic gait analysis was performed by means of an integrated motion analysis system with ground reaction force plates and a surface electromyography was used in order to evaluate the patterns of muscles' activation. A 9 cameras motion capture system Elite (200 Hz, BTS, Milan, Italy), was used together with a Kistler force plate (Winterthur, Switzerland, 1000 Hz) in order to perform the instrumental assessment of gait analysis. EMG recordings were made with an electromyographic 8-channel wireless device (Aurion, Milan) at 1000 Hz; he 3 devices were synchronized.

The 9 infrared cameras motion capture system detected the spatial position of 40 markers placed on the anatomical landmarks placed according to a modified version of the LAMB protocol described in chapter 1; to evaluate the three dimensional kinematics of the lower limbs [124]. In detail, this protocol requires the placement of anatomical markers: the zygomatic process of temporal bone, the spinous process of vertebrae C7 and T10, the scapular acromion, the lateral humeral epicondyle, the distal ulnar tuberosity, the medial PSIS, the ASIS, the greater trochanter, the medial and lateral femoral condyles, the head of the fibula, the medial and lateral malleolus,

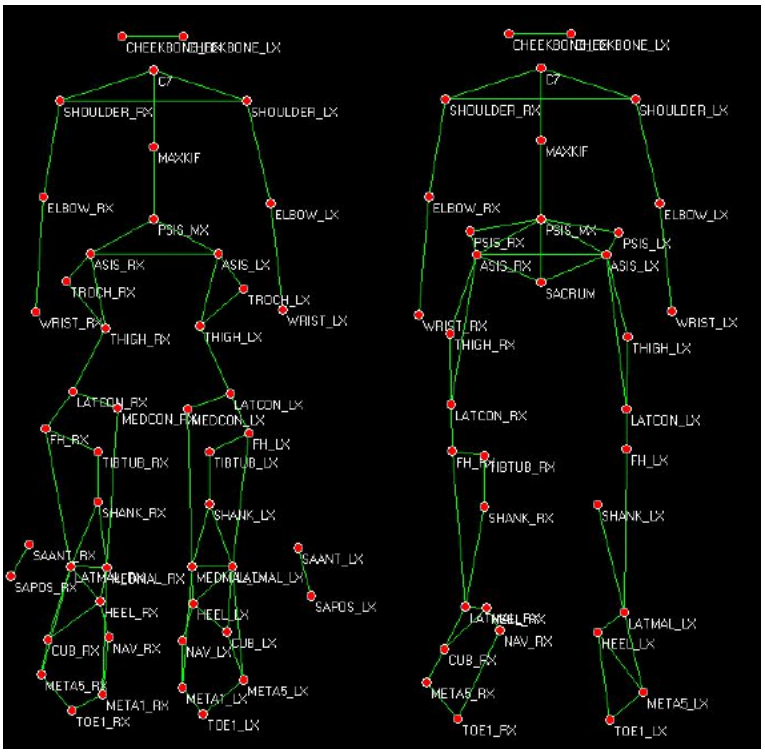

Figure 3.2: The modified LAMB marker-set used for the static (on the left) and the dynamic (on the right) gait acquisitions.

the first and the fifth metatarsal heads, the distal Achilles tendon insertion, and the dorsal aspect of the big toe.

As can be seen from Figure3.2, the original LAMB protocol was modified in this study to allow a more detailed assessment of the sub-talar and ankle joints kinematic during the gait. A total of 40 markers were used. Additional markers were placed on the navicular bone, the cuboid, and the tuberosity of the tibia, then extra 4 markers (two for each side) were placed in correspondence to the medial point between the tibia and the femur. Sometimes due to the functional limitations of the subject (when for example the paretic upper limb obscured the ASIS) or to subject-specific issues, extra markers (placed on the PSIS and /or on the sacrum) were used to identify

the reference system of the pelvis.

AS regards the EMG recordings, 16 surface electrodes were placed on 16 muscles (8 for each lower limb) to collect the EMG signal. The electrode placement followed the European recommendations of the surface electromyography-SENIAM. The electrodes were placed in correspondence of the following muscles, after having properly cleaned the skin: tibialis anterior, soleus, lateral gastrocnemius, peroneus long, rectus femoris, vastus lateralis, biceps femoris, and semimembranosus.

A first static acquisition, with the subject standing and looking towards the horizon, allowed the calibration of some markers which were finally removed as they represented an obstacle for the gait of the patients, these markers were those placed on: the greater trochanter, the medial condyle, the first metatarsal head, and the medial malleolus. Gait analysis was then conducted on an 8-m walkway; each subject was asked to walk at both a self-selected and a fast speed; data of several barefoot gait trials were collected. The patients underwent two different types of dynamic tests: the first was represented by a walk at self-selected speed, which is to say the most comfortable speed for the patient (hereinafter denoted by SS, self selected). For the second dynamic tests the subjects were asked to increase the walking speed in order to achieve the maximum possible speed (hereinafter denoted by F, fast). The dynamic acquisitions were taken into consideration only if the patients stepped completely at least one of two platforms with a single foot, as exemplified in Figure 3.3.

To ensure statistical significance, at least three gaits on each side and for each test (i.e. three cycles of step with right foot stepped on the platform, three with the left foot; then at least six at SS-speed and six at F-speed). In some cases, however, the testes were not completed either because the

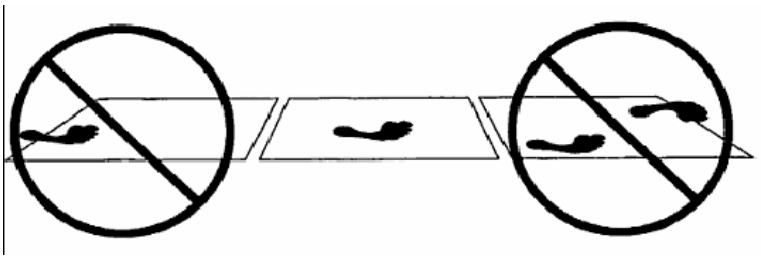

Figure 3.3: Example of a proper contact of the foot on the force platform, on the left side example of a partial contact, on the right example of a multiple contact: both the last two examples were discarded from the analysis.

subject was not able to make a sufficient number of correct steps, or the patient was not able to further repeat the tests because of fatigue issues which could significantly modify the patients performance, so that the data would not have been reliable. After the gait acquisition all the markers and the EMG electrodes except for those placed in correspondence to the lateral gastrocnemius muscle, the soleus and the tibialis anterior. After the subject was asked to lay on a bed, a minute of EMG activity in resting state was recorded, this in order to have a reference baseline signal. After that, the fMRI blocked design was performed on the paretic limb (see prevoius section): the subject was relaxed, with knees slightly bent and immobilized. Six 30 seconds blocks of rest were switched with six 30 seconds blocks of the extension / plantar flexion task, making movements before passively, and then actively. These acquisitions allowed to correlate directly the activity of the muscles involved in the same motor act performed during the fMRI.

3.5 Statistical Analysis

3.5.1 fMRI Data Analysis

fMRI data were analysed using $SPM8$ software (Wellcome Department of Cognitive Neurology, Institute of Neurology, University College London, London, UK) according to procedure described the chapter 2.2.

Images were corrected for movement, then coregistered, normalized on a stereotaxic atlas and spatially smoothed using a Gaussian kernel of $8 \times 8 \times 8$ mm. Univariate general linear model (GLM) approach [125, 126] was after applied assuming a canonical hemodynamic response function. On the basis of GLM results, the t-contrast maps were calculated, and the activation areas were obtained using a t-test. A value of $p < 0.05$ (corrected for multiple comparisons, Family Wise Error, based on the random field theory (RFT), which provides a way of adjusting the P-values that takes into account the fact that neighboring sensors are not independent, by virtue of continuity in the original data) was defined as the significance threshold (minimum size: 15 $voxels$).

First images were corrected for movement: the realignment process (SPM 'realign' function) was performed in order to correct for the functional movements of the head caused by physiological causes such as the breathing and the heartbeat, or caused by fatigue and stress related to the task. The latter reason is the main cause inthis specific case. In fact the subjects were asked to perform ankle dorsi-plantarflexion and although the attempt to immobilize the head from the rest of the body, such tasks inevitably affected the head movements, especially as a result of the motor disorders that affected the patients movement patterns: the more the patient was impaired, the more the head moved. The correction of head motion was a critical step,

since it is the cause the main error during fMRI data analysis. The SPM realignment of the acquired time series images was performed with the least squares approach and 6 rigid spatial transformations (6 parameters). The acquired 144 images were aligned to the first acquired image, the 'reference' images, as the first image position was not affected by head motions. The realignment was performed in order to match the remaining images to the orientation of the 'reference' one.

After the correction for the head movements and the images realignment, the anatomical coregistration (SPM 'coregister' function) was performed in order to exploit the high resolution of the anatomical images and to identify the different functional structures in the fMRI images.

In order to compare each functional images related to the different subjects, it was necessary to match the fMRI images to a reference model of the brain; this step is called the normalization step: the images were normalized to a common reference atlas. The SPM 'normalise' function required a 'source image' which is warped in order to match with the 'template image'; the anatomical image was used as the reference, and the MNI space provided in SPM was used as the template. Once the distortion was evaluated, all the functional images were warped according to the same evaluated distortion.

The normalization was performed to compensate for morphological differences between the brain and the template source: the algorithm minimized the sum of squared differences between the image to be normalized and a linear combination of the template images. To reach the global optimum, i.e. to get an estimate of the spatial transformation which was not affected by bias, it was necessary that the image contrasts between the template and the reference images were similar. The first step was to evaluate the 12 parameters of the optimum transformation. The normalization was initially performed

by matching the whole skull (including the scalp) with the template image, and then considering only the brain volume. Then the nonlinear deformation necessary to obtain a perfect correspondence between the reference the template images were estimated. The acquired 144 fMRI images were made up of 25 slices of 64x64 pixels and 5mm thick were fitted to the size of the Template volume, i.e. they were converted into 91 slices of 109x91 pixels images. Finally a spatial smoothing was performed in order to increase the SNR by reducing the noise thanks to the high-pass filter but at the same time the spatial resolution got worse, because the value of each voxel was evaluated as a weighted average of the adjacent voxels values. The SPM 'smooth' function used a Gaussian filter, the size of its normal kernel was specified and expressed in millimeters as the full width half maximum (FWHM): a value of $8x8x8mm$ was adopted, which was found to be a good compromise.

The statistical analysis of fMRI data used the General Linear Model approach (see section 2.2), the model assumes that the signals from different voxels are independent. First the design matrix was defined, then the GLM parameters were estimated. Finally the contrast vector was defined and a t-tests was performed to get the Statistical Parametric Maps (SPM) which described the voxels activated during the tasks examined, with an established statistical significance.

The design matrix described the experimental design and specified the hypotheses to be tested: it consisted of a number of rows equal to the number of scans and a column for each variable β to estimate . The experimental design was defined to specify the sequence and length of the 'task–rest' blocks. In this study the sequence was: 12:24:144, i.e. the first task block began after volume number 12, 24 volumes divided the two different task blocks, the last task block ended with volume number 144. The duration of each task or

rest block was 12 scans. In order to obtain the design matrix a model of hemodynamic response to HDR was specified in addition to the experimental design. The Canonical Hemodynamic Response Function (HRF) with time and dispersion derivate was chosen. The reason of this choice was because this model allowed a greater number of degrees of freedom for the description of the shape and timing course of the hemodynamic response with respect to the simple Canonical model.

The design matrix was then calculated by SPM as a convolution between the experimental design and the HDR, the matrix consisted of 144 rows and 4 columns, where the first column represented the Canonical function, the second the time derivative (Temporal), the third to the spatial derivative (Dispersion), and the last column, a constant value, referred to the baseline function, which is to say corresponding to a rest phase (rest).

The second phase of the statistical β parameter estimation of the described GLM model. The adopted estimation method was the Restricted Maximum Likelihood (REML). At this stage SPM generated four β images one for each β parameter, containing the estimated values, another image (called ResMS.img) was created to describe the variance of the estimation error, a further one (called mask.img) reported which voxels were included in the analysis, and a final image ($con_0001.img$) specified for each voxel the value of the evaluated t-contrast. During the final stage of the statistical analysis the contrast vector was specified in order to perform the statistical test and to get the Statistical Parametric Maps. In particular, in this case, the t-contrast vector was equal to [1000]: this because we considered only the first parameter of the β vector, that is to say the values corresponding to the Canonical HDF. This parameter was chose because the areas that are evaluated as active considering only the first term (Canonical) are the

same as the results obtained considering all the parameters, in addition, the activation areas obtained taking into account only the derivative terms, are really difficult to functionally and physiologically interpret.

The FWE correction was adopted and the p-value was chosen equal to 0.05. Finally, to get the Statistical Parametric Maps avoiding the presence of scattered activation of single voxels, the number of contiguous voxels that had to be simultaneously active in order to label the area as active (the so called 'extents threshold'), was set to 15 voxels.

fMRI Quantitative Indices

The fMRI images after being processed through the pre-processing steps described above were used to get the Statistical Parametric Maps using the GLM method.

Then the pre-processed FMRI images were used for a further data analysis which was not subject to the limitations identified by the GLM method and which could be considered robust and standardized, thus allowing to identify the quantitative indices which both described the neural activity and the enclosed clinical–physiological meaning. An ad-hoc routine was implemented in Matlab Version 7.10 (R2010a). Unlike the previous statistical analysis, we analyzed each of the voxels making up the volume, but grouped into different Regions Of Interests (ROIs). The interest moved from the detailed localization of the brain into the different areas of the brain, this because one of the purposes of this study was to identify the brain activation areas during the block design of different tasks and to quantify the changing of the activation signal over the time and over different subjects, so the purpose was not the morphologically accurate identification of the activation areas. Moreover, contiguous voxels are surely correlated and the different

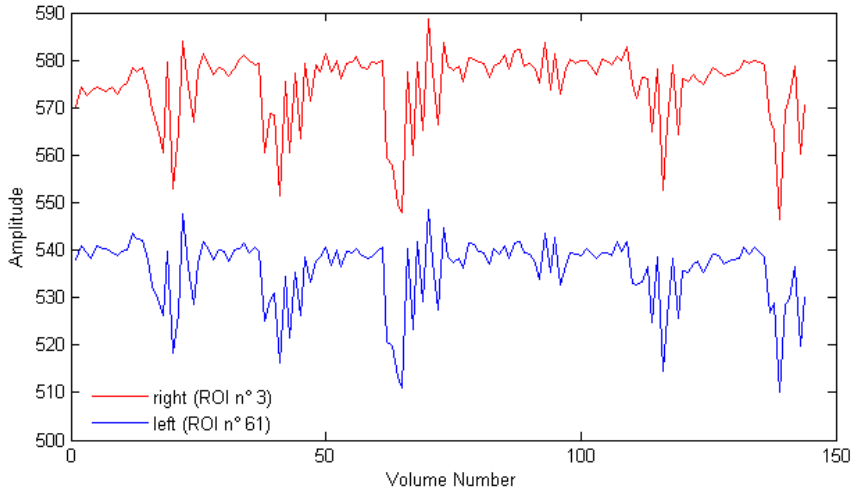

Figure 3.4: Example of average signal detected in ROI number 3: in red the right hemisphere and in blue the left hemisphere.

pre-processing stages increased mutual dependence, so by means of the post-processing a detailed 'voxel by voxel' analysis lost its significance. In order to evaluate the quantitative indices, as the functional images had been normalized to MNI space, the entire brain volume was divided with the help of a new template into 116 anatomical ROIs (see Table 3.1). Then the right and the left hemispheres were symmetrically divided so that each hemisphere was then partitioned into 58 corresponding ROIs. This partition was applied to all the functional images acquired.

For each ROI we obtained the time series of the average signals for the different voxels which the ROI was made up of. An example is shown in Figure 3.4: in red the trend of average signal of the third ROI of the right hemisphere, in blue of the left hemisphere.

For each pair of corresponding ROIs (i.e. the i-th ROI of the right hemisphere, with the i-th ROI of the left hemisphere) the differences indices of the average signal of the two time series were evaluated: the average differences

Table 3.1: Description and number of the considered ROIs.

ROI Name	Right Emisphere ROI number	Left Emisphere ROI number
Frontal Pole	1	59
Insular Cortex	2	60
Superior Frontal Gyrus	3	61
Middle Frontal Gyrus	4	62
Inferior Frontal Gyrus Pars	5	63
Inferior Frontal Gyrus Pars	6	64
Precentral Gyrus	7	65
Temporal Pole	8	66
Superior Anterior Temporal Gyrus	9	67
Superior Posterior Temporal Gyrus	10	68
Middle Anterior Temporal Gyrus	11	69
Middle Posterior Temporal Gyrus	12	70
Middle Temporooccipital Temporal Gyrus	13	71
Inferior Anterior Temporal Gyrus	14	72
Inferior Posterior Temporal Gyrus	15	73
Inferior Temporooccipital Temporal Gyrus	16	74
Postcentral Gyrus	17	75
Superior Parietal Lobule	18	76
Supramarginal Gyrus– Anterior Division	19	77
Supramarginal Gyrus– Posterior Division	20	78
Angula Gyrus	21	79
Lateral Occipital Superior Cortex	22	80
Lateral Occipital Inferior Cortex	23	81
Intracalcarine Cortex	24	82
Frontal Medial Cortex	25	83
Lobule Motor Cortex	26	84
Subcallosal Cortex	27	85
Paracingulate Gyrus	28	86
Cingulate Gyrus–Anterior Division	29	87
Cingulate Gyrus Posterior Division	30	88
Precuneous Cortex	31	89
Cuneal Cortex	32	90
Frontal Orbital Cortex	33	91
Parahippocampal Gyrus–Anterior Division	34	92
Parahippocampal Gyrus–Posterior Division	35	93
Lingual Gyrus	36	94
Temporl Anterior Fusiform Cortex	37	95
Temporl Posterior Fusiform Cortex	38	96
Temporl Occipital Fusiform Cortex	39	97
Occipital Fusiform Cortex	40	98
Frontal Operculum Cortex	41	99
Central Operculum Cortex	42	100
Parietal Operculum Cortex	43	101
Planum Polare Cortex	44	102
Heschl's Gyrus	45	103
Planum Temporale	46	104
Supracalcarine Cortex	47	105
Occipital Pole	48	106
Lateral Ventrical	49	107
Thalamus	50	108
Caudate	51	109
Putamen	52	110
Pallidum	53	111
Brain-Stem	54	112
Hippocampus	55	113
Amygdala	56	114
Accumbens	57	115
Cerebellum	58	116

between the time average of the contralateral (with respect to the moving limb) hemisphere ROI signal and the ipsilateral hemisphere ROI signal were evaluated. As for example in the case of right limb movement, the time average of the difference between the average signal of the left hemisphere and the average signal of the right hemisphere was evaluated, conversely for the left limb movement. This choice was made based on the evidence that the movement of a limb is controlled by the contralateral hemisphere. Using this value, a positive value of the average difference between the average signal of the corresponding ROIs meant that the hemisphere contralateral to the movement was actually more active than the ipsilateral one, and conversely if the difference was negative. In conclusion, for each patient, for each of the four sessions (i.e. the four sequences of 'rest–task' blocks), and for each of the 58 ROIs divided the whole brain volume, two different indices were evaluated. Starting from the evaluation of these differences, three indices which could allow to describe and quantify the neural activity and the recovery after the rehabilitation treatment were used. The first one (defined as '$diffPost - Pre$'), represented the change in the hemisphere differences detected before and after the rehabilitation treatment, so that a negative value meant that the difference signal between the two hemispheres got worse (higher), conversely a positive value highlighted an improvement. An improvement meant that after the rehabilitation treatment a greater interest of the contralateral side to the movement was observed, in fact, based on the literature, the contralateral hemisphere to the limb which was performing the task was expected to be more active than the ipsilateral hemisphere. On the other hand if the ipsilateral hemisphere to the movement was recruited more than the other, it marked a pathological behavior. Therefore, if therapy was not able to restore a 'normal' condition, it could not be defined

as a beneficial treatment as regards the neural activity. The second index was based on the evaluation of the percentage change in the difference signal between the two hemispheres of the paretic limb movement and the the healthy limb, which was expected to be close to zero if the brain is assumed to work in a symmetric way during the tasks. So the second index (referred as '$diffPost - PreCL - IL$', was then evaluated as the change in time of the variation of the difference between the neural response to the movement of the two limbs: a negative value meant an improving effect of the therapy on the patients recovery. The third index (referred as '$diffA - P$', was representative of the change in the difference of the signal between the two hemispheres, between the active and passive task. A positive value could show which of the ROIs were actually involved during the active movement. However as it will be discussed later, this index was found difficult to interpret. A more detailed discussion will be provided together with the results for the subjects analyzed in this thesis in section 3.6.

3.5.2 Gait Data Analysis

After obtaining data by using the SMART software Capture, which allowed to synchronously acquire signals from the system optoelectronic, the force platforms and the electromyography, we proceeded to the data processing.The first step is the use of SMART Tracker for labeling the markers detected and for the correction of the automatic tracking. The files related to the gait acquisitions were analyzed using the LAMBEVED software, which is basically used for the recognition and extraction of the gait cycles which have to be considered. A graphical interface allows the frame by frame visualization of the gait data contained in the TDF files, representing the 3D positions of the markers, of the platforms and of the resultant force vector

of the platforms. It is possible to manually detect the timing of the main stride-step events: the heel strike (initial contact) and the toe off for each of the feet.

The tracked TDF files of the static and dynamic acquisitions and the files containing information evaluated with LAMBEVED, were used by a program developed in Matlab Version 7.10 (R2010a) which, after applying filtering and interpolation, automatically recognized the LAMB different markers provided by the adopted protocol, evaluated the anatomical reference systems and the kinematic variables in accordance with the conventions provided. The forces, the joints moments and powers are estimated through the inverse dynamics model using the kinematic and the forces platforms data. LAMBEVED then evaluated the average of the values obtained from several repetitions of the same task (i.e., walking at SS-speed for the right side, walking at F-speed for the left side, etc.). Finally, a table summarizing all the evaluated parameters and a file containing the Graphical Display of time course of all the main kinematic and kinetic data compared with the normative bands were provided. For all the parameters the normative bands were obtained from a population of healthy subjects, for a wide range of different walking speeds.

The following gait variables were evaluated: space-time parameters (speed, cadence, stride and step length), three-dimensional kinetic and kinematics variables of the hip, pelvis and ankle, the power peak of the ankle in terms of absolute value and of timing of onset, the positive and negative work of the ankle and the hip, and EMG activity. General parameters like velocity, frequency, stride length, and step length were normalized with respect to the patient's height (h).

More in detail the parameters taken into consideration were:

- General information, such as: age (Age, sex (Sex), height (BH [cm]), weight (BW [Kg]), FootOnPlat (the platform number stepped by the foot);
- Spatial and temporal information of the different gait phases, such as:
  - Walking Speed (speed) and cadence (cadence [steps / min]);
  - Step Length (StepLength, i.e. a single step), and Stride Length (StrideLength, i.e. the whole gait cycle);
  - Time duration of double support (DoubleSupTime [% gait cycle]), duration of the stride phase (StrideTime [% gait cycle]), of the Stance phases, or support (StanceTime [% gait cycle]), and of Swing phase(Swingtime [% gait cycle]);
  - Speed of the swing phase (SwingVel).

  As regards all these parameters is indicated both their raw value (Raw) and the normalized (Nor). The normalization is calculated with respect to: the height (BH), the walking speed ([% BH/s]) and the stride length [stride length/BH]; or with respect to a percentage of the gait cycle, the temporal durations and lengths ([% of the gait cycle or stride length]).
- Information on the ankle:
  - Peak power produced by the ankle (AnklePowerPeak [W/kg]);
  - Ankle Positive work (AnklePositiveWork [J / kg]) and Ankle Negative work (AnkleNegativeWork [J / kg]);
  - Power developed during hell strike for the ipsilateral foot (AnklePowerPeakFromOmoLateralHS [AnklePowerPeak%]) and contralateral foot (AnklePowerPeakFromControLateralHS [AnklePowerPeak%]);

  - Temporal delay between the heel strike of the ipsilateral foot (AnklePowerOnsetFromOmoLateralHS [% gait cycle]) and contralateral foot (AnklePowerOnsetFromControLateralHS [% gait cycle]) from the ankle peak power onset;

- Information about the knee:

  - Time interval between ipsilateral foot hell strike (KneeFlexionOnsetFromOmoLateralHS [s]) or contralateral foot hell strike (KneeFlexionOnsetFromControLateralHS [s]) and the beginning of the knee flexion;
  - Maximum knee flexion (KneeFlexionPeak [deg]);
  - Value of knee flexion in correspondence to the ankle power peak (KneeFlexionAtAnklePowerPeak [deg]);

- Information about the hip:

  - Maximum Hip flexion (HipFlexionPeak [deg]) and extension (HipExtensionPeak [deg]);
  - Hip moment in the frontal plane during the contralateral foot toe-off phase (HipFrontalMomentAtControLateralTO [Nm/kg]);
  - Hip Peak power (HipPowerPeak [W/kg]);
  - Hip Positive work (HipPositiveWork [J/kg]) and Negative work (HipNegativeWork [J/kg])

- Pelvis Rotation (PelvisRotatio [deg]) and elevation (PelvisElevation [deg]) in correspondence to the heel strike (HS) and the toe off (TO), of the ipsilateral foot (Ipsilateral) and contralateral foot (contralateral):

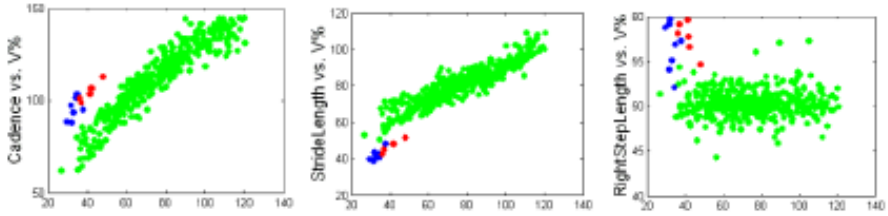

Figure 3.5: Example of graphical representation of two correct types of steps.

PelvisRotationAtOmoLateralHS, PelvisRotationAtOmoLateralTO, PelvisRotationAtControLateralHS, PelvisRotationAtControLateralTO, PelvisElevationAtOmoLateralHS, PelvisElevationAtOmoLateralTO, PelvisElevationAtControLateralHS, PelvisElevationAtControLateralTO.

As mentioned, in addition to the values of these parameters, the software developed in Matlab Version 7.10 (R2010a) also provided a report containing the graphical display of time course of all the main kinematic and kinetic and EMG data compared to the normative bands. As an example, here are the graphs of a report:

In the three graphs in figure 3.5 the values for the right side are in blue, those for the left side are in red, green values represent the normative bands. From left to right the graphs represent respectively the cadence (cadence), the stride length (StrideLength) and the right step length (y-axis), compared to the walking speed (x-axis). It can be noticed as the normal values are available for a wide range of different speeds. In this case considering a given speed, the subject for both the right side and left side, showed an higher cadence and a lower stride length (StrideLenght) if compared with the normative bands.

In figure 3.6 on the left the antero-posterior velocity of the center of mass (COM forward speed) is shown, in the center the vertical position of

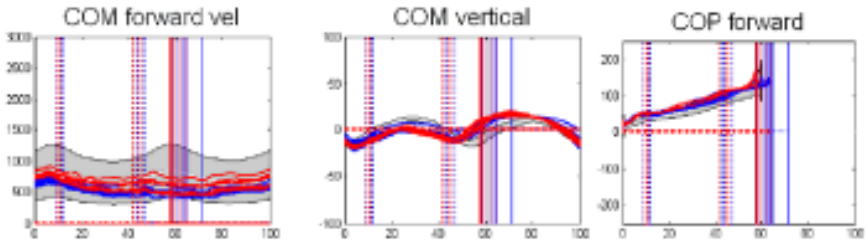

Figure 3.6: Example of graphical representation of the COM and COP.

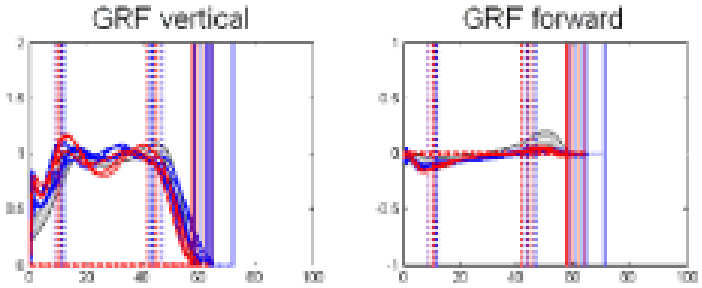

Figure 3.7: Example of graphical representation of the ground reaction forces.

the center of mass (vertical COM) is displayed, on the right the antero-posterior pattern of the center of pressure (COP forward) is shown. In all the graphs the x-axis is representative of the percentage of the phase of gait cycle, the vertical lines mark the different events of the gait cycle. The blue lines represent the right side, while the red ones represent the left side. Normative bands are shown in gray

Information about the ground reaction forces measured with the force platforms are also reported (figure 3.7): on the left the vertical ground reaction forces (GFR vertical), on the right the longitudinal ground reaction forces (forward GRF);

The trunk kinematics is shown in the following three graphs (figure 3.8): on the left the flexion-extension angle(TRUNK SAG), in the center the ab-

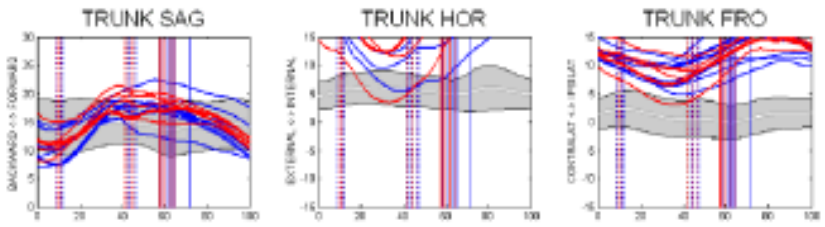

Figure 3.8: Example of Trunk kinematics.

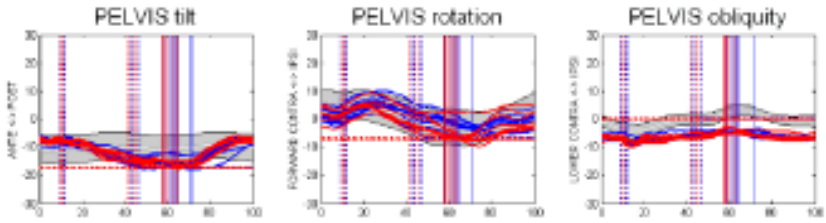

Figure 3.9: Example of Pelvis kinematics.

adduction angle (TRUNK HOR), on the right the intra-extra rotation angle (TRUNK FRO);

The pelvis kinematic pattern is shown in the following three graphs (figure 3.9): on the left the anterior-posterior tilt (tilt PELVIS), in the center the intra-extra rotation (PELVIS rotation), on the right the medio-lateral tilt (obliquity PELVIS);

In figure 3.10 the inclination of the thigh (Thigh inclination) and of the shanks (SHANK inclination) are reported;

The foot, figure inclination (FOOT inclination) is shown on the left and the foot rotation is shown on the right (FOOT rotation) of figure 3.11 ;

The hip joint kinematics is represented in figure 3.12: on the left the adduction angle(HIP adduction), in the center the rotation angle (HIP rotation) and on the right the flexion-extension angle (HIP fLX);

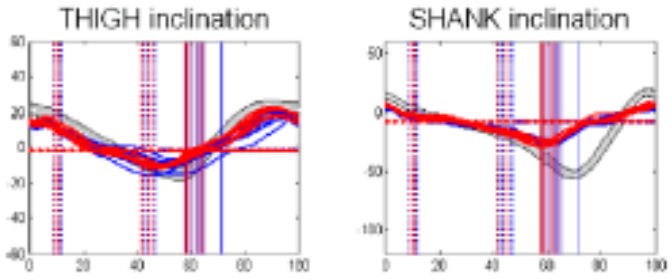

Figure 3.10: Example of Thigh and Shank inclination.

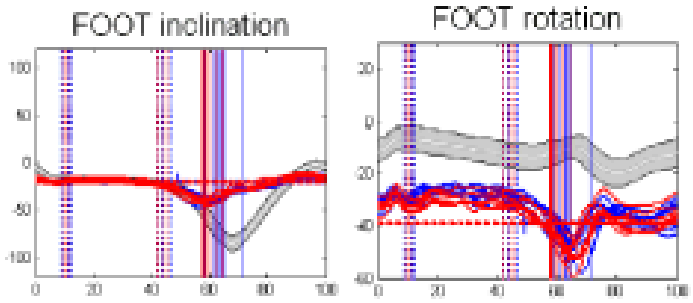

Figure 3.11: Example of foot inclination and rotation.

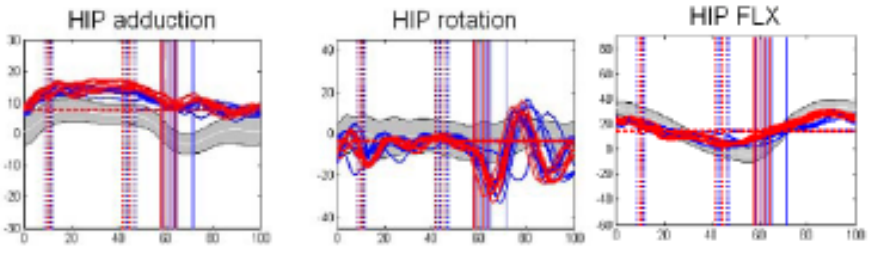

Figure 3.12: Example of Hip kinematics.

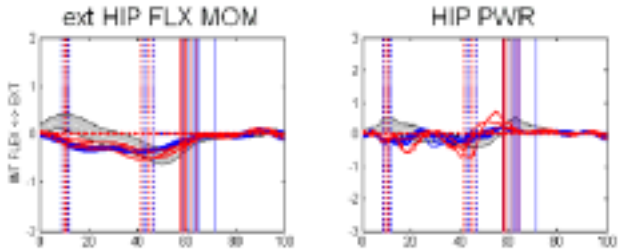

Figure 3.13: Example of Hip kinetics.

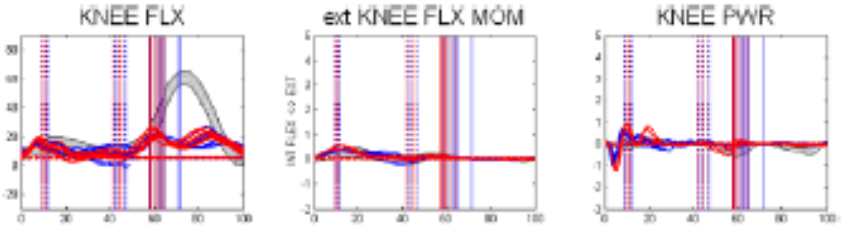

Figure 3.14: Example of Knee kinematics.

In figure 3.13 the hip external flexion moment (FLX ext HIP MOM), on left, and on the right the hip power (HIP PWR) are shown;

The knee kinematic pattern is shown as follows: on the left (figure 3.14) the knee flexion-extension (KNEE FLEX), in the center the external knee flexion moment (FLEX KNEE ext MOM), on the right the knee power (PWR KNEE);

As for the knee, the figure 3.15 shows the ankle dorsiflexion (DORSIFLEX ANKLE) on the left, at the ankle external dorsiflexion moment (ext ANKLE DORSIFLEX MOM) and the ankle power (ANKLE PWR).

In the last part of the report (figure 3.16), the EMG activity of the eight muscles are reported.

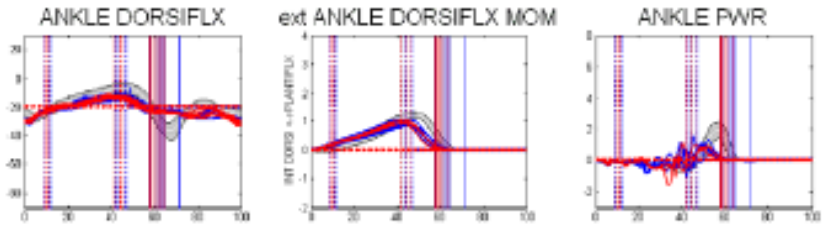

Figure 3.15: Example of Ankle kinematics and kinetics.

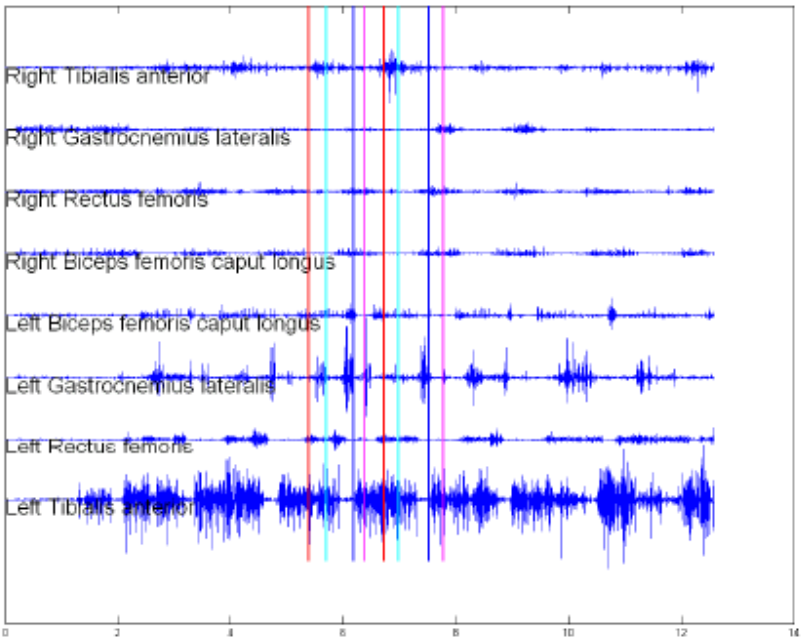

Figure 3.16: Example of EMG activity of the eight muscles.

Gait Analysis Quantitative Indices

The analysis focused on the most representative parameters: the Speed Raw (referred as Speed), the Cadence Raw (referred as Cadence), the Stride Length, the Ankle Power Peak, the Ankle Positive Work, the Ankle Negative Work, and the Ankle Power Peak From Contro Lateral Heel Strike. All these parameters were considered for both the affected and for the unaffected side, both for Walk at self selected speed (SS) and at fast speed (F). In total, for each acquisition, 28 parameters were considered (7 for each of the four combinations of speed and side). The choice of the effectiveness of these parameters was demonstrated in previous studies ([127, 15]). All the hemiparetic subjects showed, at normal speed, an higher cadence and a smaller step length if compared to those of the control subjects walking at the same speed; it is worthy to notice that the gap became smaller as the the free walking speed became closer to the non-pathological (faster) speed. Similarly, the power produced by the ankle plantar-flexor muscles was greatly reduced. During the fast walking, instead, while the cadence and stride length values were shown to be comparable with the non-pathological values, the ankle positive work turned out to be still below the normative bands. On the other hand the hip positive worked was back in the normal range in case of the free speed walking, while it increased a lot with the fast walking. It indicated that, in order to increase the speed, the majority of the patients adopted different strategies with respect to the healthy subjects: the limited ability to express power by means of the ankle joint was bypassed by an abnormal increase of the hip positive work, the hip represented therefore an important source to control and to modulate the speed in post-stroke patients. In hemiparetic patients was also observed a difficulty in correctly modulating the ankle power at different speeds, because if during the free speed walking the timing of

the ankle peak power is in a not pathological vales range, when the speed increased half of the patients showed a delayed onset, while a 10% of the patients showed an earlier onset. The latter observation could justify the interest for the AnklePowerOnsetFromControLateralHS parameter: a lower value means that the onset of the ankle power is earler than the normative range, while an higher value means a delay of the onset (later than it usually happens during a gait cycle). A small difference between this value in the normal speed walking and at an higher speeds means that the early onset is reduced if compared to a non-pathological condition.

In [14] was observed how biofeedback was able to increase the ankle power peak, together with a significant increase in walking speed, stride length and cadence. This result is in agreement with Colborne et al. ([5]): they observed an increased push-off impulse together with changes in gait speed and stride length. It was also noticed that the onset of the push-off power peak was delayed in time with the BFB treatment, while the power peak is earlier considering the hell strike for the non-paretic limb, thus showing that mostly of the power produced by the plantarflexors might have been used for the body progression, causing a faster walk and an increased stride length.

The second reason for the parameters choice was that they may be directly related to the fMRI data, which were related to the dorsi-plantarflexion. Therefore for this reason we considered beside the walking speed and cadence, the power, the work and timing related only to the ankle, not even, for example, for the hip as suggested in ([127]). It is worthy to notice that in healthy subjects ankle plantar-dorsiflexion produces about 80% of total energy required during the gait ([12]), while patients with hemiparesis tend to have a reduction of the ankle power peak during the push-off phase in addition to a reduction of the walking speed ([13]).

So all the cited parameters were calculated for walking at Self Selected speed (SS) fast (F), both for the limb contralateral to the lesion (CL) for the ipsilateral (IL), both before (Pre) and after (Post) treatment.

As stated above, the first gait improvement of the post-stroke patient is an increased speed. Associated with the increased speed (Speed), the other parameters show a 'trend towards normality', which is to say the parameters values vary directly in relation to the speed increment. In particular:

- the values of the Cadence, the StrideLength, the AnklePowerPeak, and the AnklePositiveWork increase;
- the values of the AnklePowerOnsetFromControLateralHS, and the AnkleNegativeWork decrease;

These 'normal trend' was described in the literature. The numerical quantification used in this thesis is derived from the normative bands obtained with the data of 10 normal subjects (mean age: 34 ± 12 years old, mean BMI 24 ± 5 Kg/m^2) evaluated at the SAFLo Laboratory of the IRCCS S. Maria Nascente Don Carlo Gnocchi Foundation in Milan, where the gait analysis was performed. In particular, the specific features and values of the walking at normal and fast speed were taken into account.

For each gait parameter, the difference between the value of the analyzed patient walking and the corresponding value of the normative bands was estimated. This difference was evaluated as a percentage with respect to the normative band. This allowed a comparison between the different gait parameters, in this way the parameters which differed more from the normative bands and those which were mostly influenced by the treatment could be highlighted. If the evaluated difference was negative, it meant that the patient's gait parameter had a lower value than the normative one, vice

versa when the evaluated difference was positive, it meant that the patient's gait parameter had an higher value than the normative one.

Starting from the evaluated difference values, three different indices were estimated in order to assess the effects of the EMG BFB treatment on the patients motor recovery.

The first index, referred as '$varPre-Post$', was evaluated as the change of the percentage differences between the pre (Pre) and post (Post) conditions. The rehabilitation treatment, improving the motor performance, should reduce the difference: this was represented by a negative value of the '$varPre-Post$' index, thus because the patient data should be closer to the normative bands after the BFB rehabilitation treatment that before. The change among the different parameters could be not consistent, this because either some parameters could improve and some others could get worse, or some improvement could be more related to some parameters than to others. This trend could show either that the EMG BFB treatment was more effective for some neuro-motor patterns associated with the gait, or simply that this therapy allowed a faster recovery of the most damaged gait parameters.

The second and third indices are the most meaningful indices, they were related to the specific pathology and to the experimental set up which involved walking at normal and fast speed. The second index was based on the estimation of the percentage differences ($diffF-SS$) between the value of each parameter evaluated for the maximum walking speed (F) and for the walk at normal speed (SS). A positive value meant that the patients' fast speed gait differed more than the normal speed gait if compared to the normative bands. The second index, referred as '$vardiffF-SSPost-Pre$', was calculated as the percentage difference between the absolute values of $diffF-SS$ measured before treatment (Pre) and post treatment (Post). A

positive value of this index meant that after therapy the difference between the gait parameters' changes between the N and F walking with respect to the normative bands increased. The third index was based on the evaluation ot the percentage changes ($diffIL - CL$) between the value of each parameter relative to the ipsilateral (IL) and the contralateral (CL) side to the lesion. A negative value of $diffIL - CL$, meant that the patients' gait differed from the normal reference mostly for the CL limb rather than the IL limb.

The third index, referred as '$vardiffIL-CLPost-Pre$', was evaluated as the percentage difference between the absolute values of $diffIL - CL$ measured before treatment (Pre) and after treatment (Post). The treatment should decrease the gap between the affected and the unaffected side and this should be confirmed by a negative value of the $vardiffIL - CLPost - Pre$ index, it is worthy to notice that during the rehabilitation treatment the unaffected limb could also modify the motor pattern as to compensate for the affected limb's deficit, so a positive value of the $vardiffIL - CLPost - Pre$ index could be justified by this reason. A more detailed discussion of the meanings of these indices will be discussed together with the results in chapters 3.6 and 3.7.

3.5.3 Correlation Analysis

The last goal of this study is to evaluate whether the EMG BFB improved the patient overall status. In particular, we wanted to determine if any improvements could be attributed to either a peripheral or central nervous system recovery, and to understand the relationship between them. We both performed a qualitative correlation analysis using categorical variables and a quantitative correlation analysis based on the evaluated fMRI and gait

analysis indices.

Categorical Variables Correlation

Analysis of correlation was performed using R Statistic software ([128]) first considering categorical variables (*hetcor* function). For instance agreement and disagreement with respect to the improvement of the following variables has been identified: velocity, cadence, stride length, ankle-related power onset timing, power peak timing, power peak value, positive and negative work in both conditions of normal and fast speed walking, and normal (primary motor area: MI), diffuse or no brain activation, for both active and passive ADP movements on both sides. With both the brain activity and gait analysis data, we were interested in examining the relationship between the results obtained with the functional magnetic resonance imaging and those obtained from the gait analysis, that is to say we wanted to perform a correlation analysis between the most meaningful variables considered for this study. The correlation analysis was performed using the$R$ software an environment developed specifically for the statistical data analysis. More in detail the following package was used:

- Polycore: this is a package that contains functions to evaluate different kinds of correlation (polychoric, polyserial, etc.). For our analysis the Heterogeneous Correlation Matrix (*hetcor* function) was adopted. *Hetcor* provided the heterogeneous Correlation matrix, consisting of the Pearson Correlation between numerical variables, the Polyserial Correlation between numerical and ordinal variables and the Polychoric Correlation between ordinal variables. The correlation analysis was performed between the following data matrix in order to correlate the following variables related to fMRI and gait analysis (see Table 3.2).

Then the correlation analysis was performed by using categorical variables in terms of 'agreement' or 'disagreement' related to the variables–conditions of listed in Table 3.2. Two different types of correlation were performed: the first type considered both the fMRI and gait analysis data together, while for the second only either the fMRI or the gait analysis data were taken into account in order to correlate separately categorical variables relating to the first or to the second analysis. Correlation analysis were performed between:

- Pre and Post fMRI and gait analysis categorical variables for both the affected and non affected sides.
- Pre and Post fMRI categorical variables for both the affected and non affected sides.
- Pre and Post gait analysis categorical variables for both the affected and non affected sides.
- Pre and Post fMRI and gait analysis categorical variables for the affected side.
- Pre and Post fMRI categorical variables for the affected side.
- Pre and Post gait analysis categorical variables for the affected side.
- Pre and Post fMRI and gait analysis categorical variables for the non affected side.
- Pre and Post fMRI categorical variables for the non affected side.
- Pre and Post gait analysis categorical variables for the non affected side.

Table 3.2: Description of the Categorical Variables adopted for the qualitative correlation analysis.

Categorical Variables	Pre Treatment (Agree or Disagree)	Post treatment (Agree or Disagree)
Task A		
M1 Activation		
Increased M1 Activation		
Increased M1 Activation Size		
Cerebellum Activation		
Increased Cerebellum Activation		
Increased Cerebellum Activation Size		
No Activation Changes		
Task B		
M1 Activation		
Increased M1 Activation		
Increased M1 Activation Size		
Cerebellum Activation		
Increased Cerebellum Activation		
Increased Cerebellum Activation Size		
No Activation Changes		
Fast Speed		
Increased Raw Speed		
Increased Normalized Speed		
Increased Normalized Cadence		
Increased Ankle Power Peak		
Increased Ankle Positive Work		
Increased Ankle Negative Work		
Ankle Power Onset From Omolateral in normative bands		
Self Selected Speed		
Increased Raw Speed		
Increased Normalized Speed		
Increased Normalized Cadence		
Increased Ankle Power Peak		
Increased Ankle Negative Work		
Ankle Power Onset From Omolateral in normative bands		

Quantitative Correlation

In order to perform the quantitative correlation analysis, comparable indices for the fMRI and the gait analysis were identified. Therefore the first indices (i.e. fMRI '$diffPost-Pre$' index and gait '$varPre-Post$' index) were chosen. Indeed both the chosen indices expressed a percentage of improvement or worsening of the parameters they referred to. Moreover the correlation between different experimental conditions was performed in order to justify their acquisition. Indeed if the results obtained from the different tasks statistically did not show strong correlation, on the other hand the information they gave was related to different features associated both to the movement and to the recovery of the impaired functions. In more details for each subject the following correlation analysis were performed:

- As regards the gait analysis, we evaluated the correlation between the improvement–deterioration of all the parameters related to:
  - The Healthy and Paretic limb;
  - The walking at Self Selected and Fast speed;
  - The Healthy and Paretic limb only for the walking at Self Selected speed;
  - The Healthy and Paretic limb only for the walking at Fast speed;
  - The walking at Self Selected and Fast speed for the limb contralateral to the lesion;
  - The walking at Self Selected and Fast speed for the limb ipsilateral to the lesion.
- As regards the the fMRI analysis, we evaluated the correlation between the improvement –deterioration of all parameters related to:

- The Healthy and Paretic limb;
- The Passive and the Active task;
- The Healthy and Paretic limb for the Passive Task;
- The Healthy and Paretic limb for the Active Task;
- The Passive and the Active task for the limb contralateral to the lesion;
- The Passive and the Active task for the limb ipsilateral to the lesion.

Therefore Pearson correlation coefficients (Matlab Version 7.10 (R2010a) *corr* function) were evaluated between the results obtained from different task conditions, and between the results obtained from different subjects. Moreover a Wilcoxon Rank Sum Test (Wilcoxon-Mann-Whitney test, Matlab Version 7.10 (R2010a) *ranksum* function) was performed between the fMRI data and the gait analysis indices in order to test if the indices derived from fMRI and the gait analysis gave the same information about the outcomes after the EMG BFB rehabilitation treatment.

Low correlation indices suggested that the experimental protocol was suitable for the study because different sessions provided different information. Specifically for each of the subjects the Pearson correlation between the chosen parameters related to the motor performance and those related to the neural activation were evaluated. This aimed at determining whether the rehabilitation treatment induced a comparable recovery for the different subjects and whether the same information could be observed from either the gait or the fMRI data. Finally by means of the Wilcoxon Rank Sum Test agreement between the changes induced by the therapy on the motor outcomes and the changes related to the neural activation patterns was eval-

uated.

3.6 Results

3.6.1 fMRI Results

The activation maps related to the task A and B pre and post EMG BFB treatment are reported below for both the control subject and the patients.

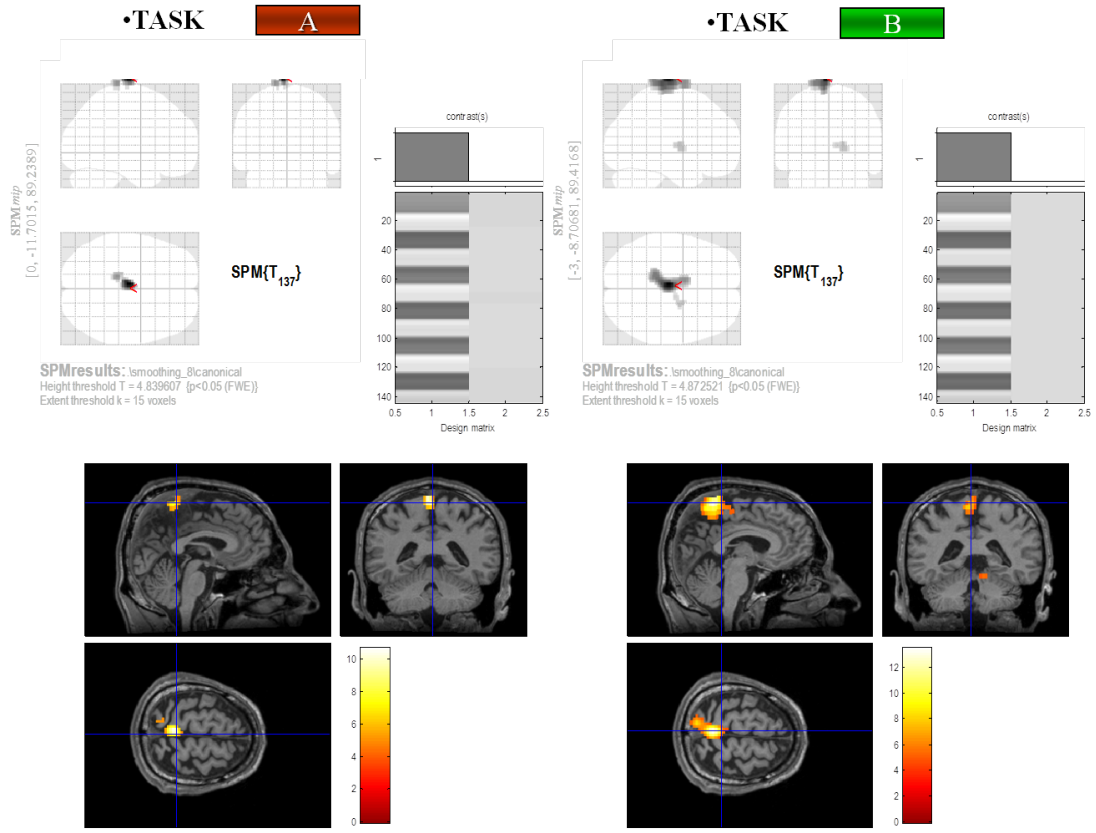

Figure 3.17: Brain activation of the Control Subject for both task A (on the left) and task B (on the right).

Concerning the task A, individual activation conjunction maps revealed activation of the right primary motor area (MI) for the control subject, and for the task B the same brain activation areas, apparently with greater activation, were revealed.

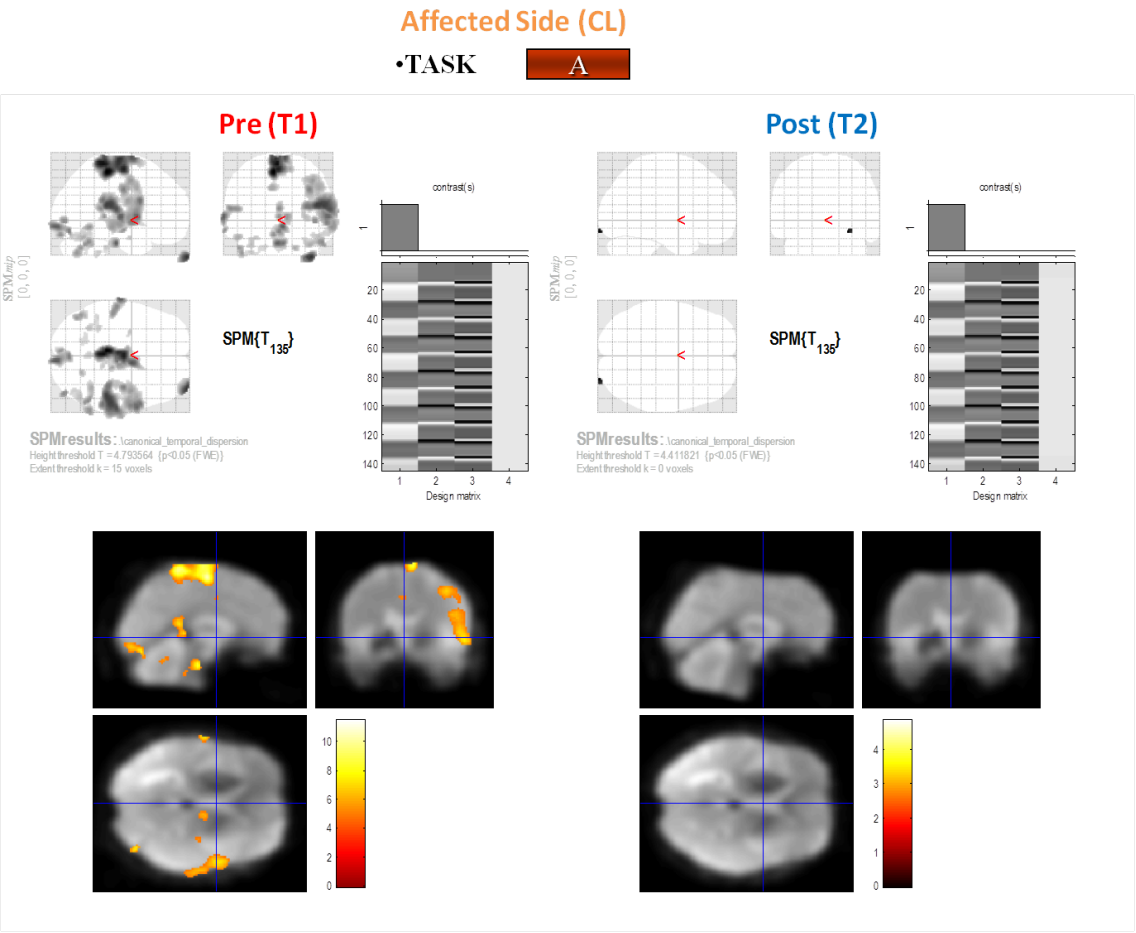

Figure 3.18: SP1: Brain activation during task A of the contralateral limb for the Pre(on the the left) and Post (on the right) treatment.

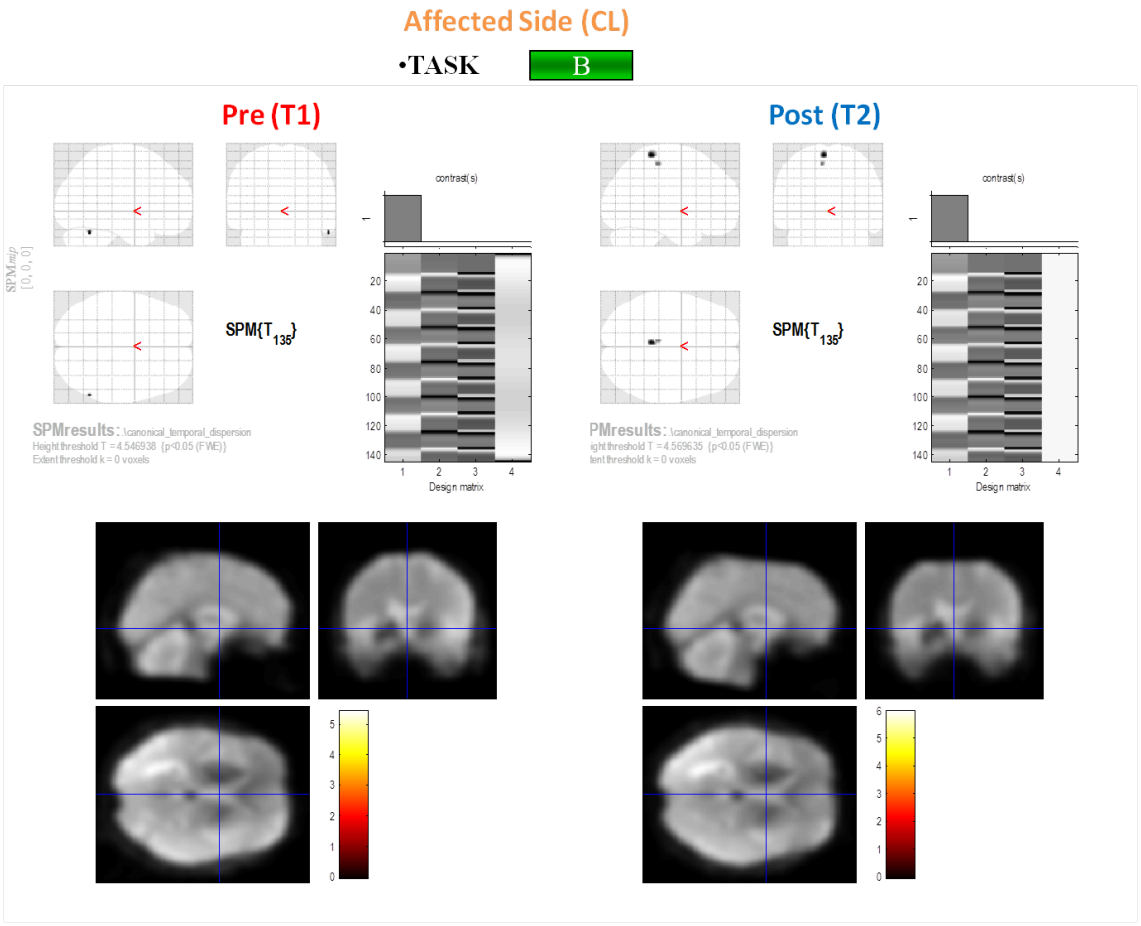

Figure 3.19: SP1: Brain activation during task B of the contralateral limb for the Pre(on the the left) and Post (on the right) treatment.

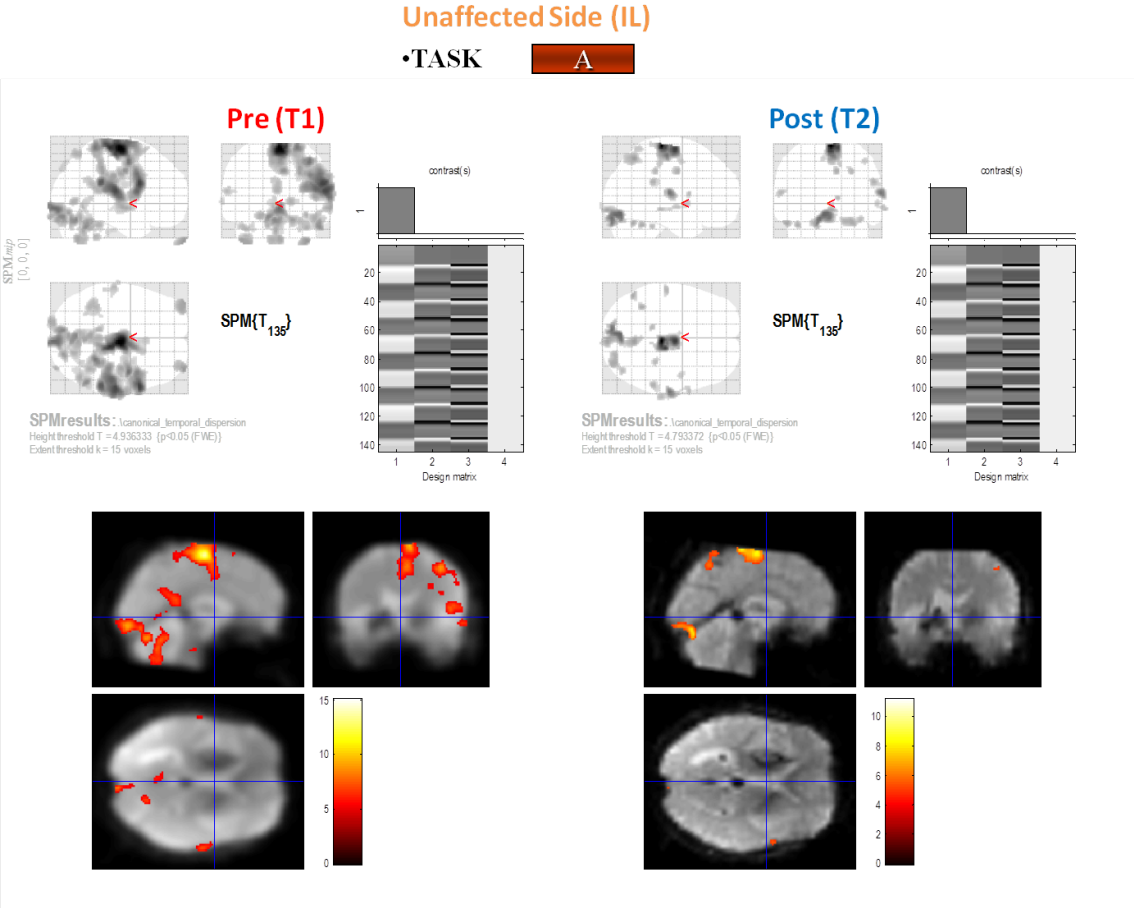

Figure 3.20: SP1: Brain activation during task A of the ipsilateral limb for the Pre(on the the left) and Post (on the right) treatment.

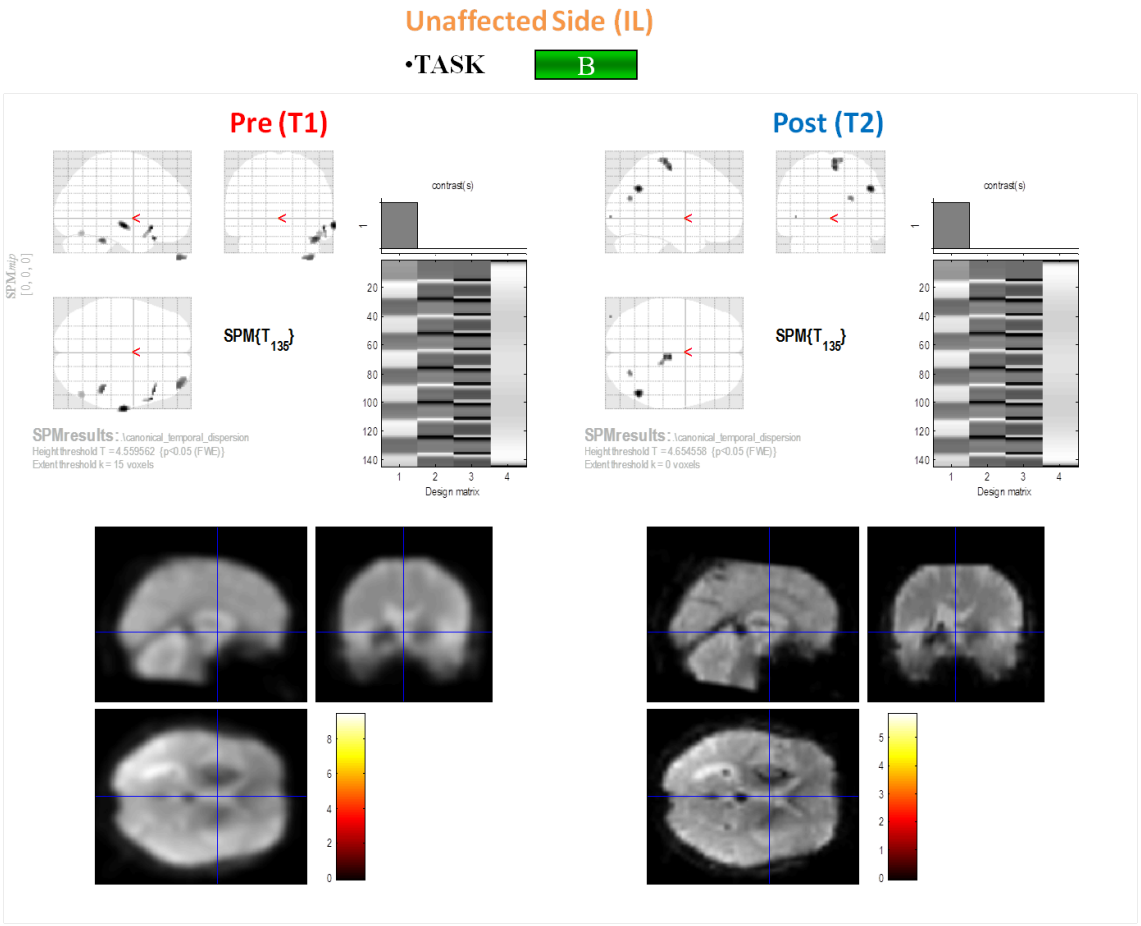

Figure 3.21: SP1: Brain activation during task B of the ipsilateral limb for the Pre(on the the left) and Post (on the right) treatment.

As regards the task A at time T1 a scattered activation of the right primary motor area (MI), the premotor cortex, the right motor cortex, the visual area and the cerebellum both for the contralateral and ipsilateral side was found; at time T2 no activation was shown for the CL side, while a more confined activation of the MI and of the cerebellum. For the task B at T1 no activation was found for the CL side, while the activation of the cerebellum was revealed for the IL side. Considering the results at T2 for both the CL and IL sides the MI was found to be active.

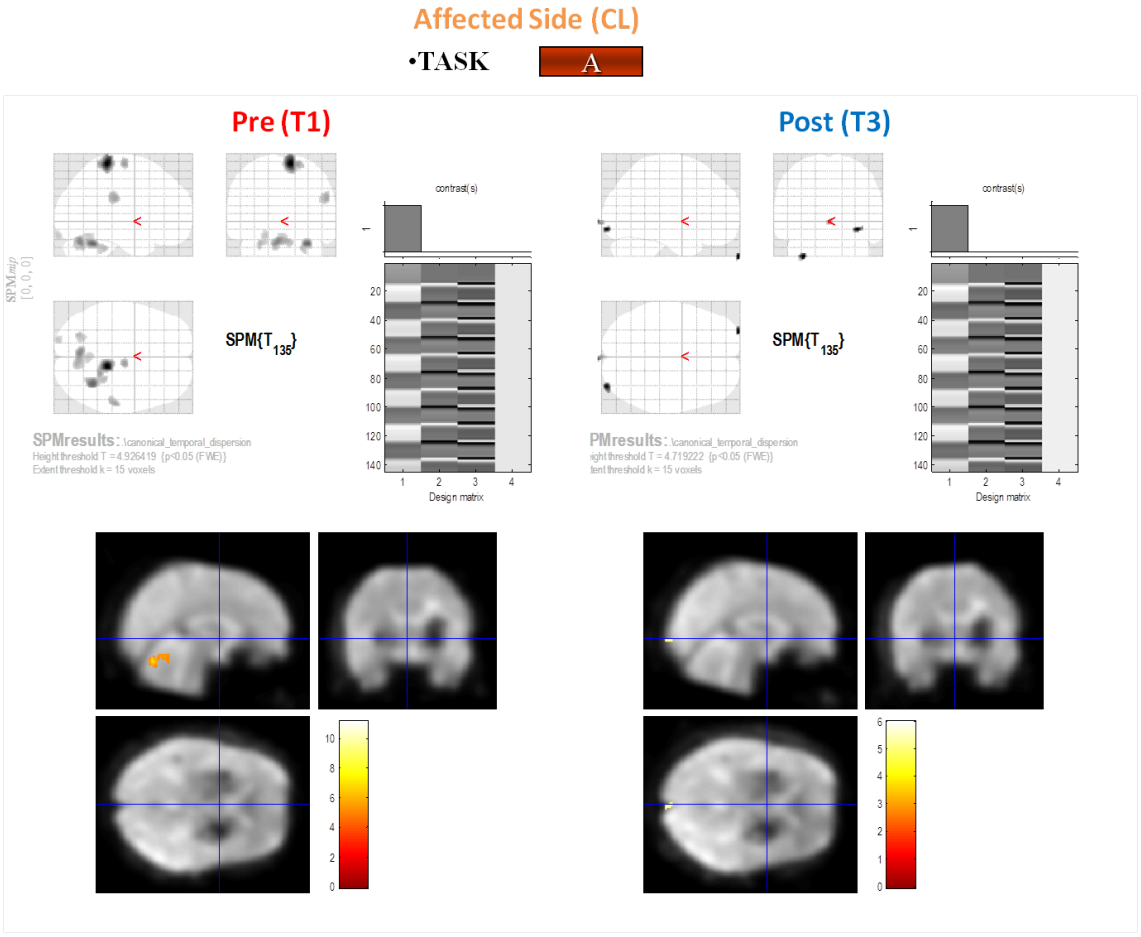

Figure 3.22: SP2: Brain activation during task A of the contralateral limb for the Pre(on the the left) and Post (on the right) treatment.

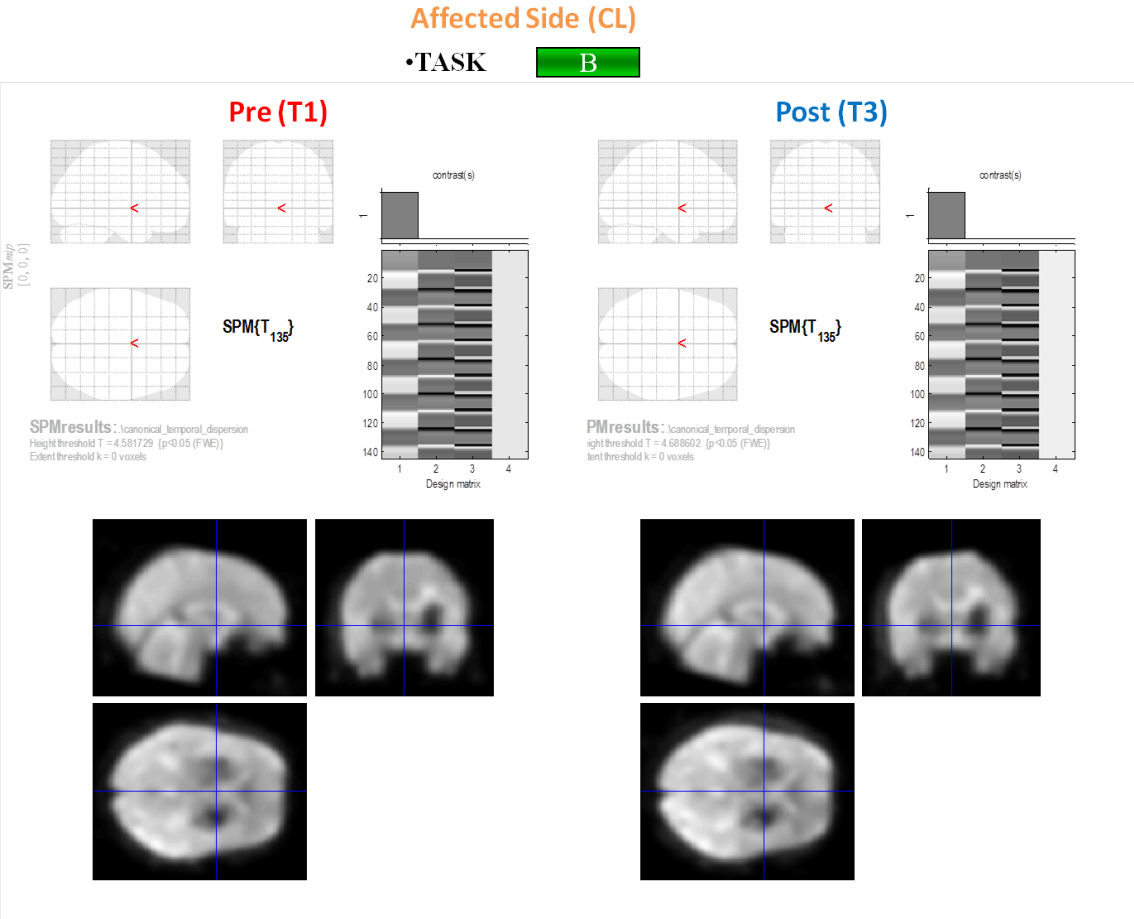

Figure 3.23: SP2: Brain activation during task B of the contralateral limb for the Pre(on the the left) and Post (on the right) treatment.

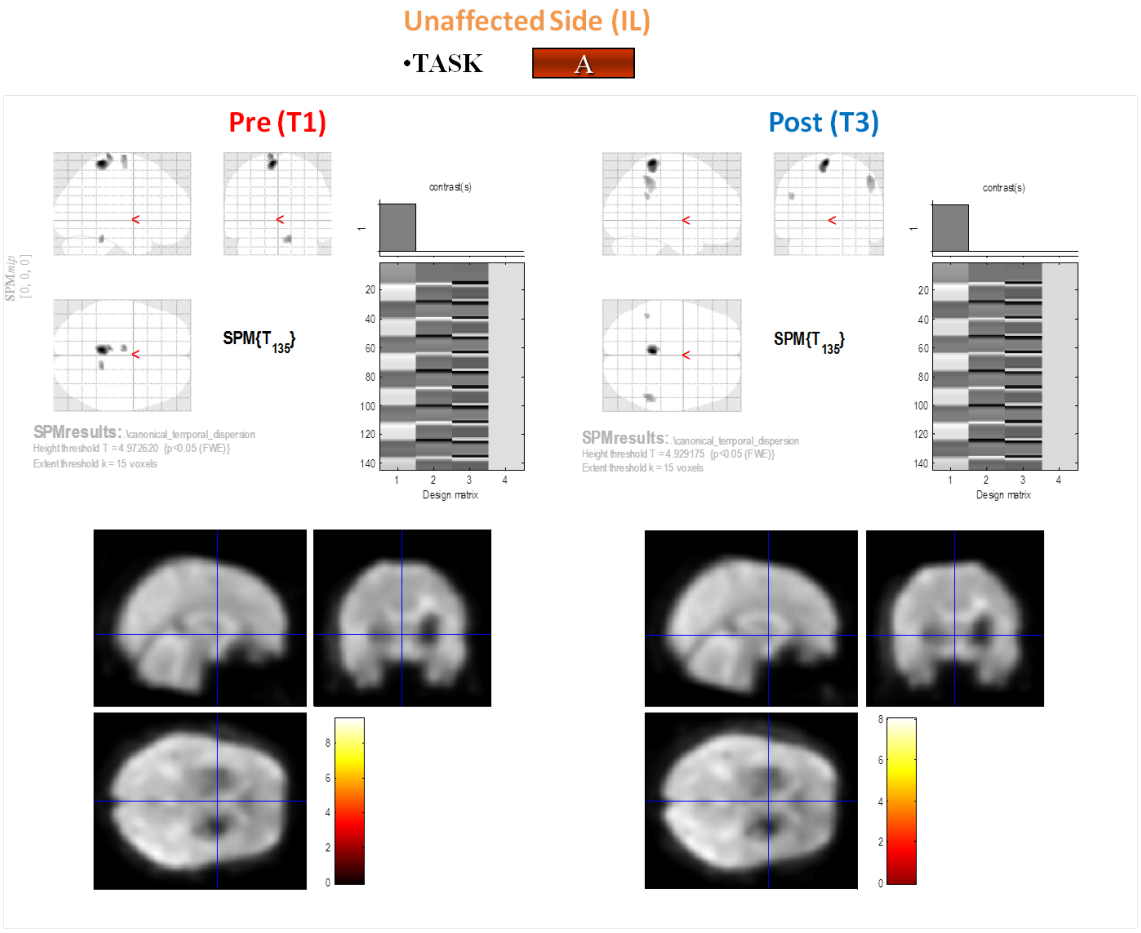

Figure 3.24: SP2: Brain activation during task A of the ipsilateral limb for the Pre(on the the left) and Post (on the right) treatment.

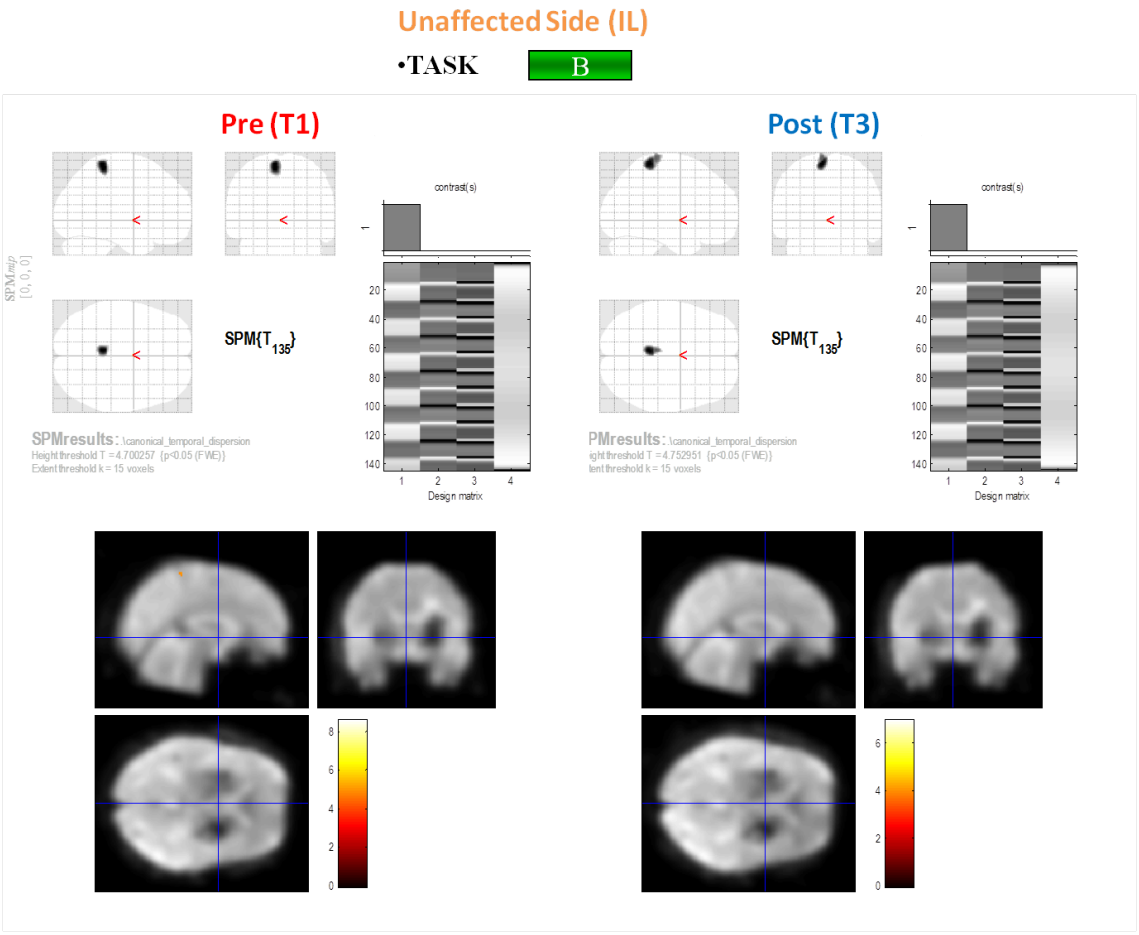

Figure 3.25: SP2: Brain activation during task B of the ipsilateral limb for the Pre(on the the left) and Post (on the right) treatment.

Concerning the active task, at time T1, the activation of the MI area, of the premotor cortex for both the sides was found, in addition for the contralateral side the cerebellum was shown to be active; while considering time T3 the activation of the cerebellum for the CL side, and a confined activation of MI, of the visual area, and of the right motor cortex for the IL side were observed. During the task B no activation was found for the CL side for both T1 and T3, meanwhile the activation of MI together with the premotor cortex and the cerebellum was revealed for the IL side at time T1, while an increased activation of MI and of the right motor cortex was found at time T3.

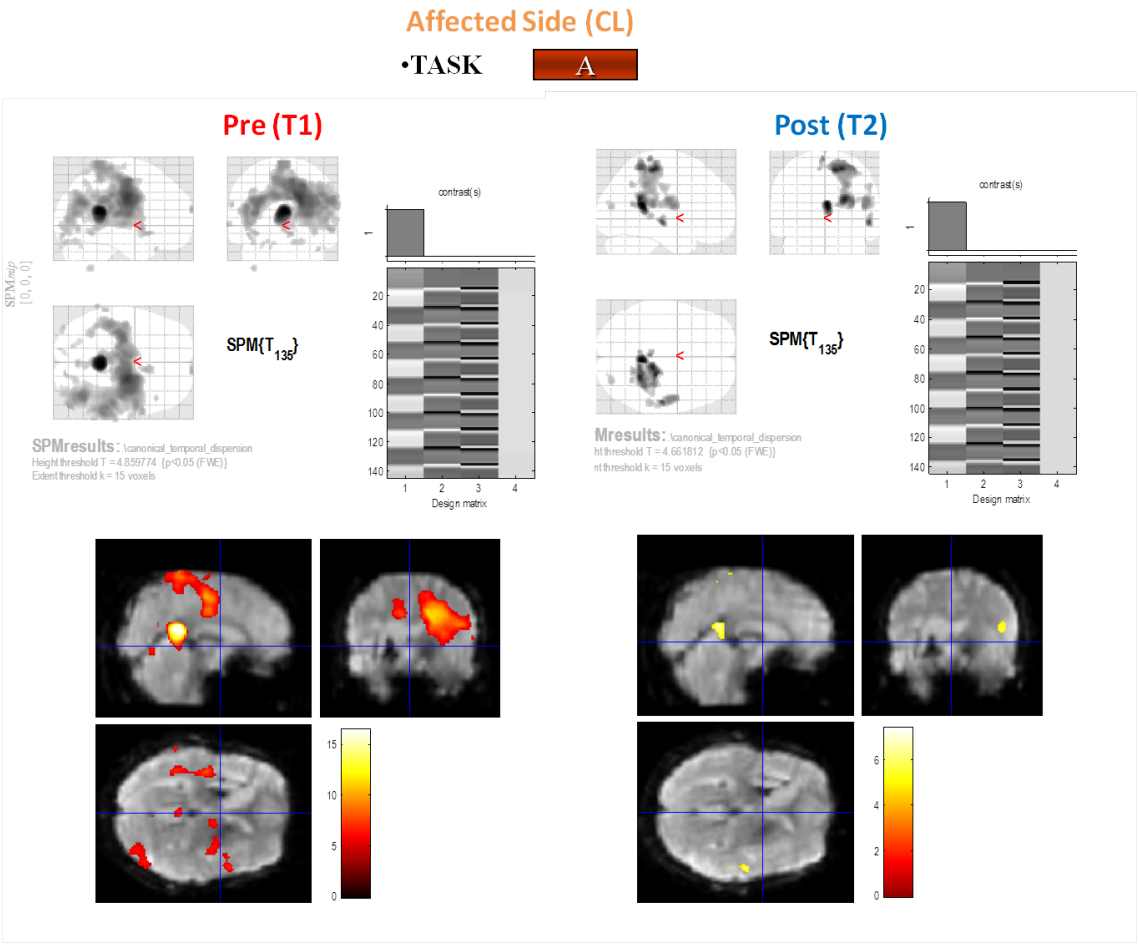

Figure 3.26: SP3: Brain activation during task A of the contralateral limb for the Pre(on the the left) and Post (on the right) treatment.

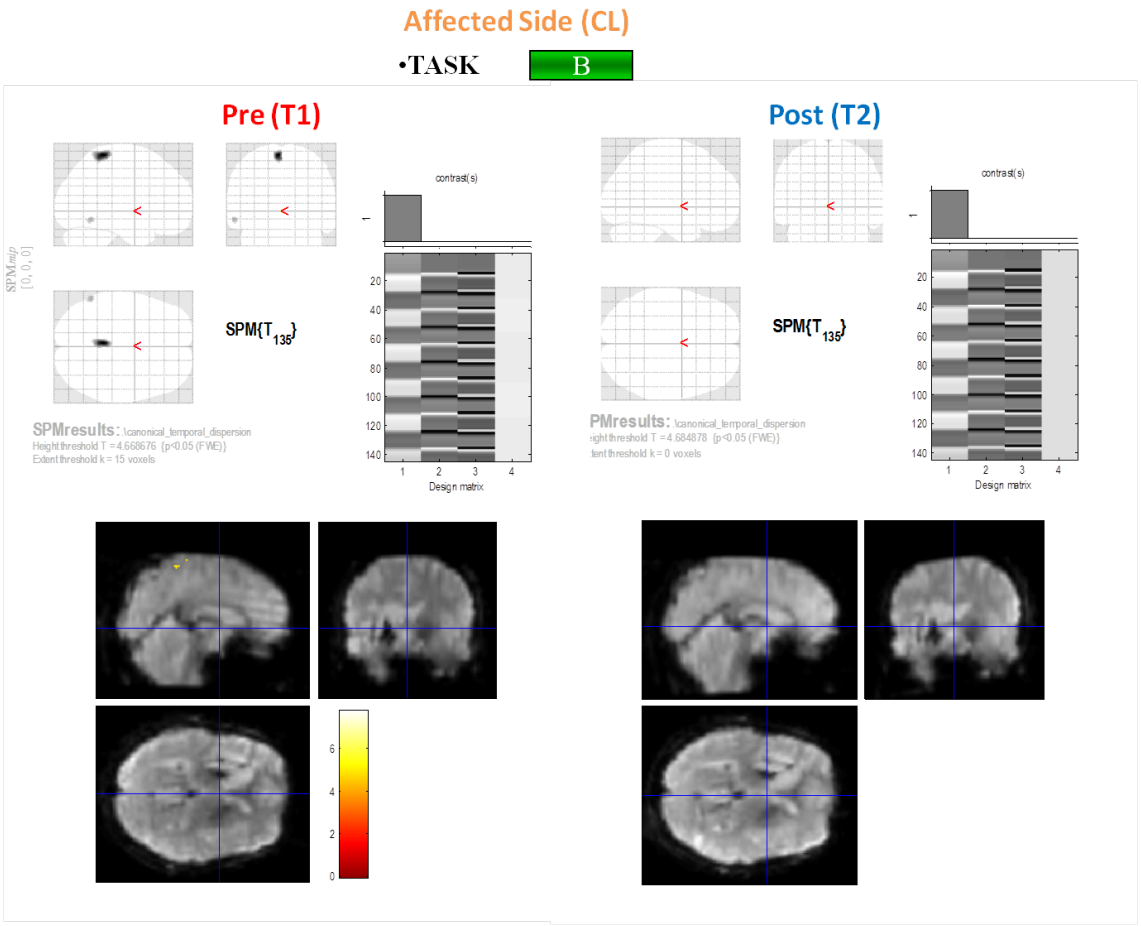

Figure 3.27: SP3: Brain activation during task B of the contralateral limb for the Pre(on the the left) and Post (on the right) treatment.

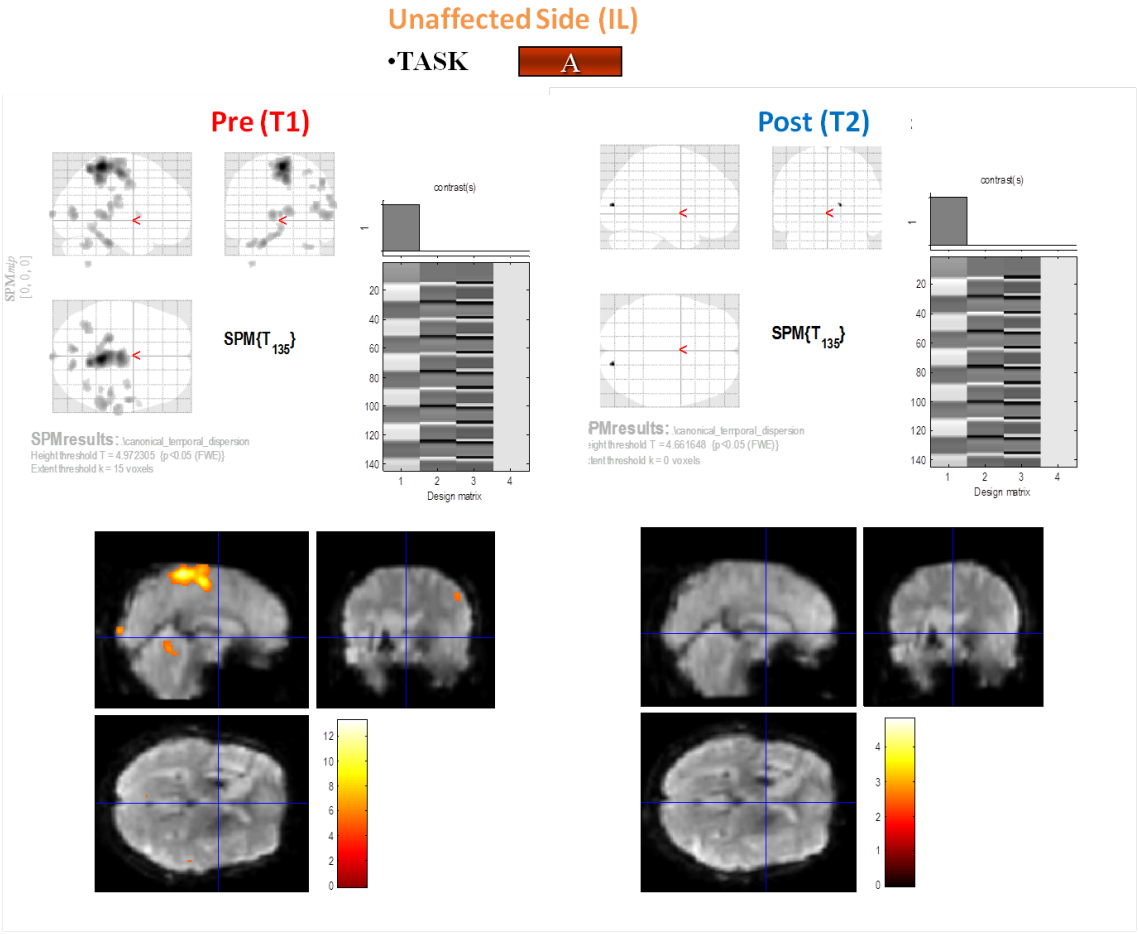

Figure 3.28: SP3: Brain activation during task A of the ipsilateral limb for the Pre(on the the left) and Post (on the right) treatment.

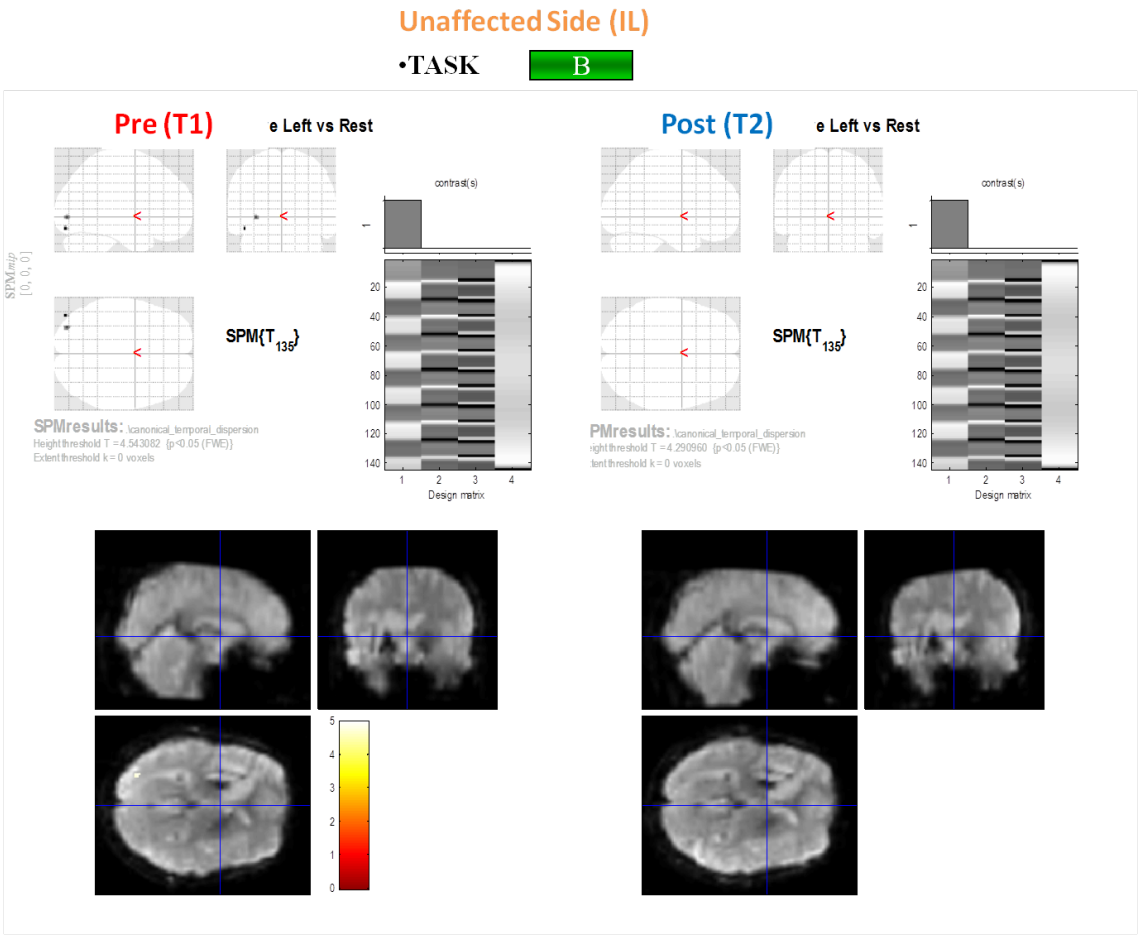

Figure 3.29: SP3: Brain activation during task B of the ipsilateral limb for the Pre(on the the left) and Post (on the right) treatment.

As regards the task A at time T1 a scattered activation of the primary motor area (MI), the premotor cortex, the right motor cortex, and the cerebellum both for the contralateral and ipsilateral side was found, more pronounced for the CL side; at time T2 no activation was shown for the IL side, while a more confined activation of the right MI, of the visual area and of the right motor cortex was found for the IL side. For the task B no activation was found for the IL side at both T1 and T2, meanwhile the activation of the MI was revealed for the CL side at time T1, while no activation as found at time T2.

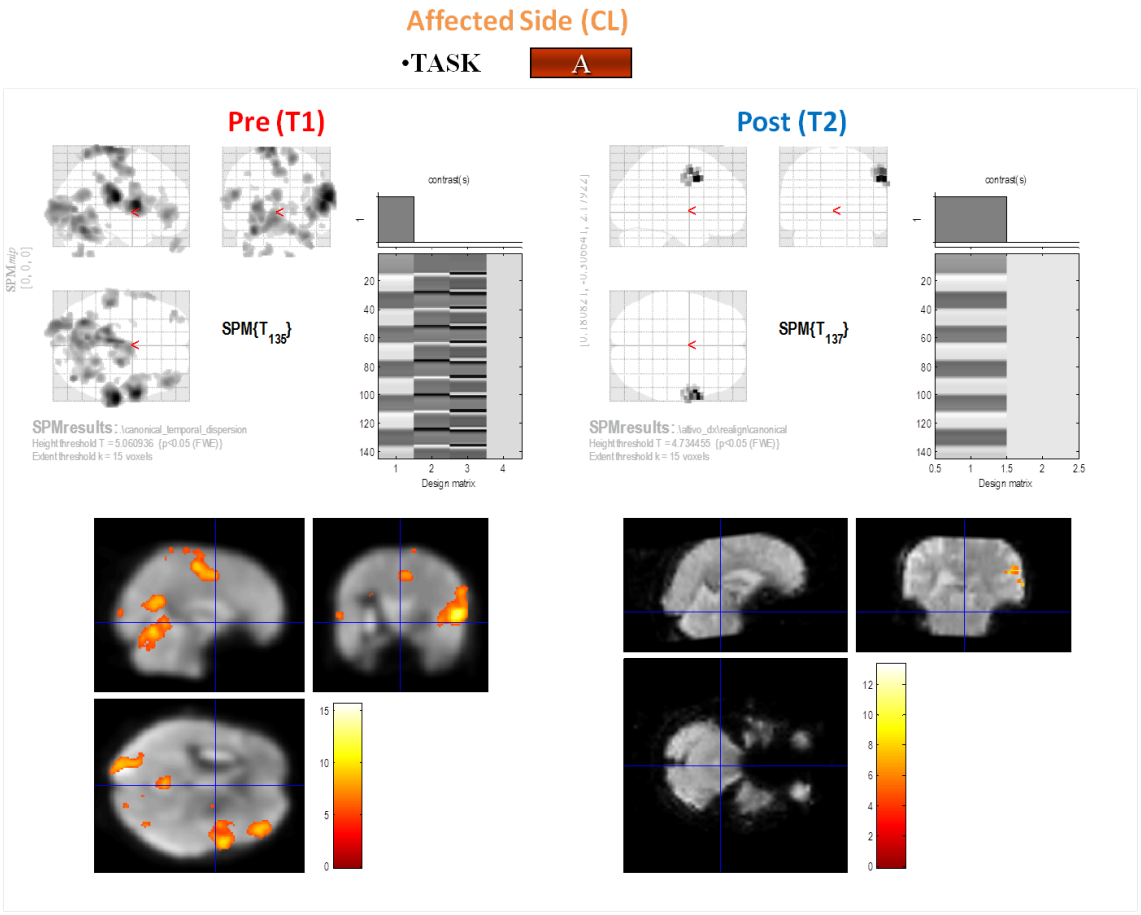

Figure 3.30: SP4: Brain activation during task A of the contralateral limb for the Pre(on the the left) and Post (on the right) treatment.

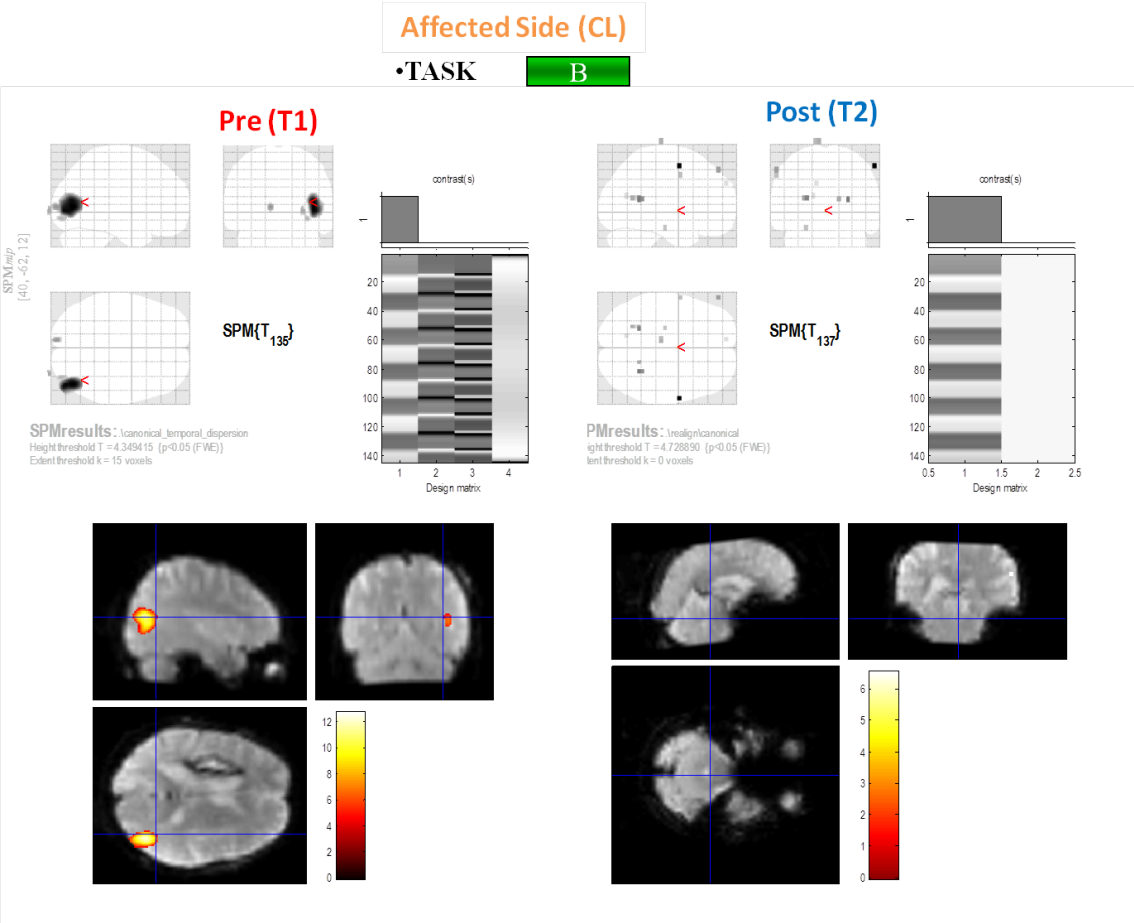

Figure 3.31: SP4: Brain activation during task B of the contralateral limb for the Pre(on the the left) and Post (on the right) treatment.

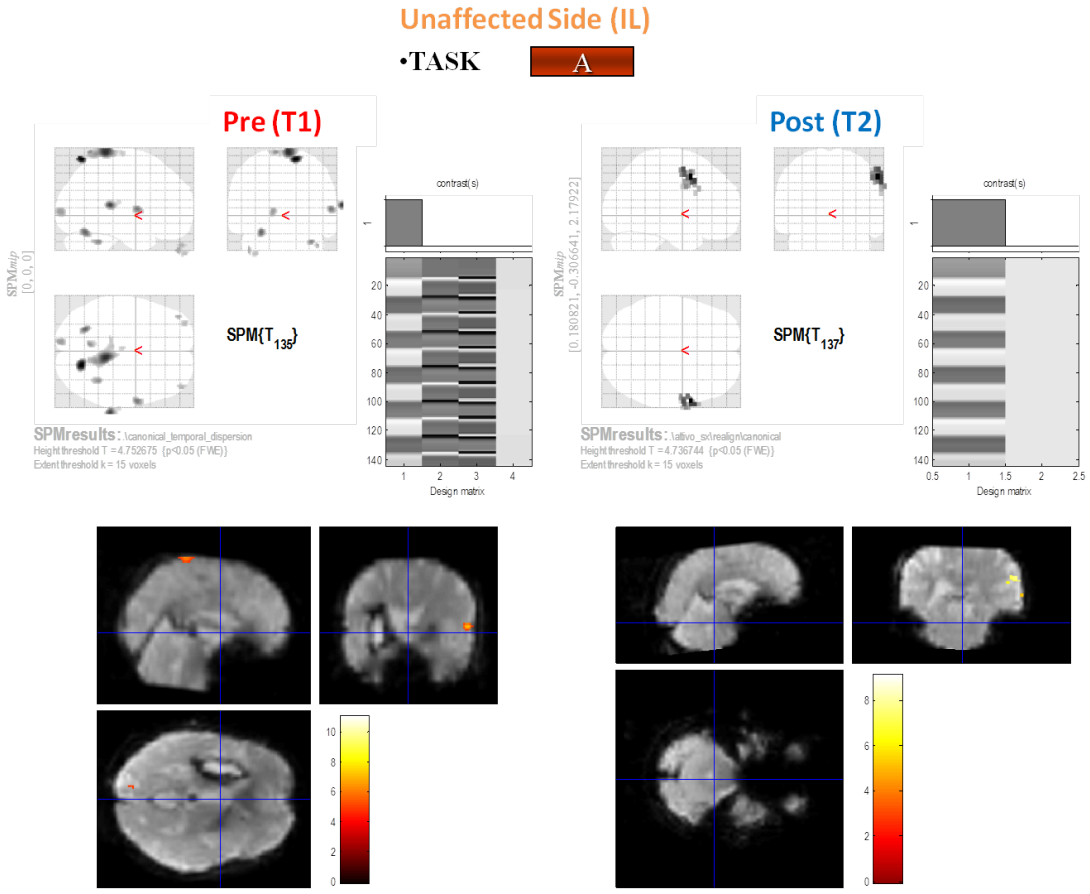

Figure 3.32: SP4: Brain activation during task A of the ipsilateral limb for the Pre(on the the left) and Post (on the right) treatment.

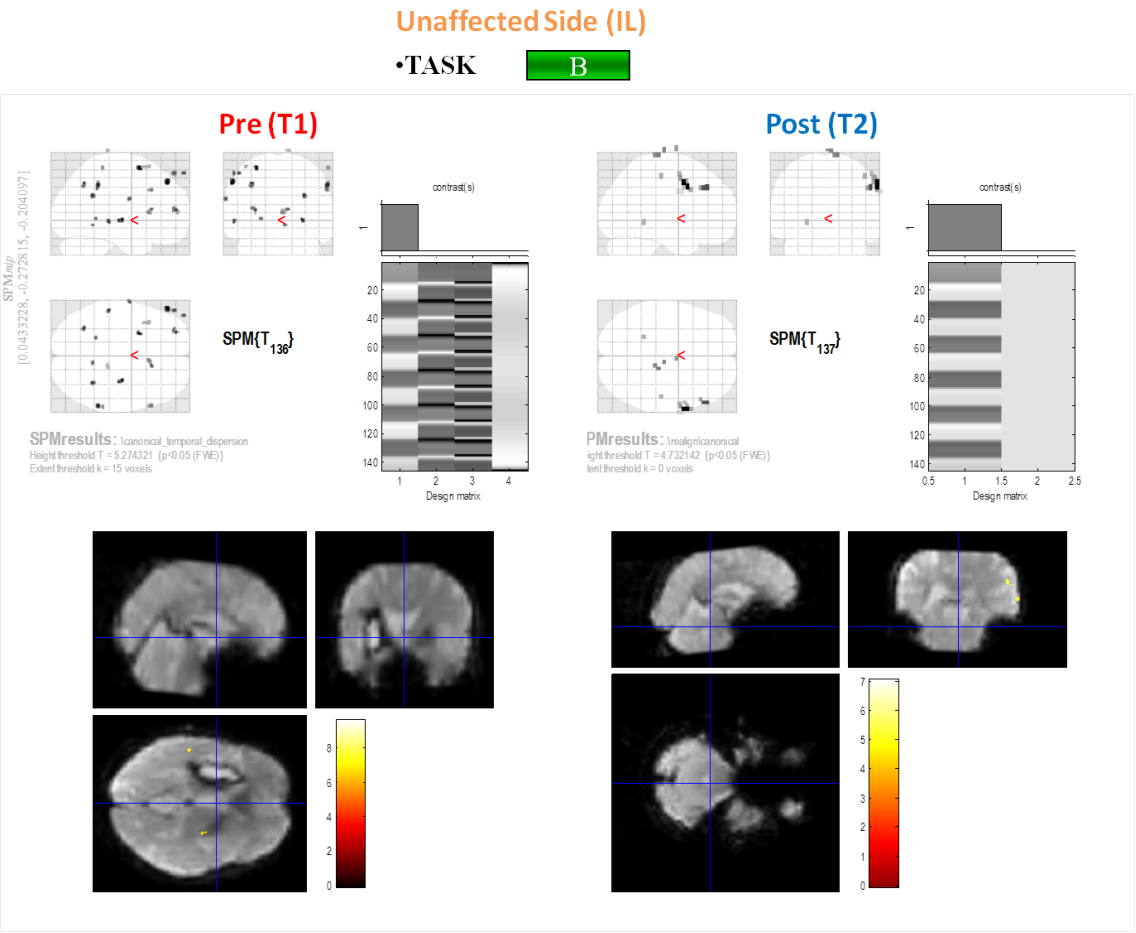

Figure 3.33: SP4: Brain activation during task B of the ipsilateral limb for the Pre(on the the left) and Post (on the right) treatment.

During task A at time T1 a scattered activation of the primary motor area (MI), the premotor cortex, the right motor cortex, the visual area and the cerebellum for the contralateral side was found, a more confined activation of MI and of the cerebellum was observed for the IL side; at time T2 a defined activation iof the right motor cortex was revealed for both the sides. As regards task B at time T1, considering the affected-CL side, the SP4 showed a confined activation of the cerebellum and no activation at time T2. Besides, focusing on the unaffected-IL side, basically no active area was noticed at time T1, and a limited activation of MI and of the right motor cortex was found at time T2.

As shown before sometimes no activation area was found to be active using the GLM method, so trying to determine the cause the raw signal was investigated. More in details the motor area M1 was identified on the normalized images. The choice of the MI area was chosen because it was supposed to be the most involved during the execution of the ankle movement. The average signal across all voxels of the M1 area, for both the hemispheres left and right, over the time was evaluated. An example of the outcome is shown in figure 3.34

In such a case where the signals recorded during active movement had an irregular pattern, the presence of a drift was found, and the amplitudes during the task varied greatly, a GLM statistical test for such a signal might fail, as the hypothesis were not verified. The reason why the signal was found irregular in several cases could be due to the way the task was performed. Indeed, the post-stroke patient typically is not able to accurately perform the ankle dorsi-plantarflexion. In particular, despite being partially immobilized and thought by the staff before the the acquisition, the subject often was not able not to keep still and not to move the rest of the body (i.e. the leg,

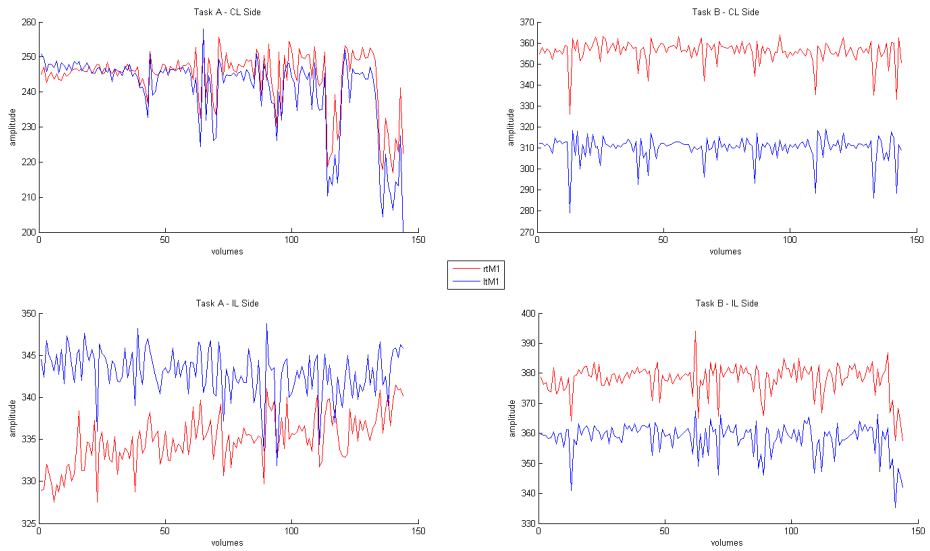

Figure 3.34: Example of the mean signal for area M1 during the four experimental conditions: in red the right hemisphere data, in blue the left hemisphere data.

the thigh, and the upper limbs) but the ankle, thus as a compensation strategy adopted by the patient to bypass his functional limitations. In addition, these movements could be very heterogeneous and variable among different acquired blocks of tasks. This could explain why the GLM test sometimes seemed to fail mainly for the active movements involving the paretic-CL limb. However, also the signals detected during the passive task could be influenced by an improper execution of the movement. Indeed, especially if the paretic limb, the subject tended to resist instead of follow the movement imposed by the operator. A final limitation that could affect the detected signal is that the post-stroke patients could not meet the timing of the task: typically during the task A the subjects had a lower frequency which was not constant for the 30 seconds duration of the block, and this was due mainly to the mus-

cles fatigue. Task A was shown to be less homogeneous than task B, and it was characterized by not constant acceleration and deceleration. The reasons mentioned above could be an explanation for the results obtained: a different signal from that estimated by the convolution of the hemodynamic response with the experimental design, could cause the GLM model to estimate wrong parameters.

All the fMRI indices were evaluated for four out of 58 brain areas which represented the ROI that, according to the literature, should be the most involved during the execution of a motor task. More precisely the motor area (corresponding to ROI 26–84), the premotor area (corresponding to ROI 7–65), the sensory-motor area (corresponding to ROI 17–75) and the cerebellum (corresponding to ROI 58–116) were considered. The three indices (diff Post–Pre, diff Post–Pre CL–IL, diff A–P) evaluated for each subject (except for SP4 as the coregistration step could not be performed), side and task are shown in the tables below. The third index (diff A–P) could be evaluated also for the control subject.

Table 3.3: SP1: First Index: diff Post-Pre, values are expressed in percentage [%]

diff Post–Pre Index	**CL side–Task A**	**CL side–Task B**	**IL side–Task A**	**IL side–Task B**
Premotor Area	30.7	31.5	-24.7	-2.7
Sensory Motor Area	24.1	17.1	-5	7.1
Motor Area	-97.5	-32.7	89.1	72.3
Cerebellum	74.6	-9.09	1342	109.5

SP1 showed negative differences between the two hemispheres during both the active and passive tasks of the paretic limb as regards the motor, premotor, and sensory-motor areas, which is a pathological symptom. These differences became positive for the ipsilateral side, thus indicating a normal control. This was observed both before and after the rehabilitation program, although some changes appeared. Specifically for the paretic limb the first index had a positive value for the pre-motor and sensory-motor area during the movement of the contralateral side, showing a recovery of the neural activity. In contrast, the motor area activation seemed more compromised after the therapy. Finally, the cerebellum showed different behaviors: the motor area showed a worsening concerning the passive task, while an improvement

during the active task. As the of the cerebellum allows the adaptation of the motor pattern to the different external conditions, the value assumed during the active task seemed to be really relevant. Looking at the ipsilateral side, no significant changes were found, while as regards the contralateral side the activation of both the cerebellum and of the motor area improved.

Table 3.4: SP2: First Index: diff Post-Pre, values are expressed in percentage [%]

diff Post–Pre Index	**CL side– Task A**	**CL side–Task B**	**IL side–Task A**	**IL side–Task B**
Premotor Area	-253.5	-109.7	84	110.7
Sensory Motor Area	-143.8	-94.8	75.2	101
Motor Area	-87.2	-8.1	-0.8	7.1
Cerebellum	-251.5	-136.3	182.3	206

Before the EMG BFB treatment SP2 showed a pathological activation (with negative differences between the CL an IL hemisphere) of the premotor and sensory-motor areas related to the CL side task and of the motor area and the cerebellum in the case of the IL limb. After the rehabilitation protocol, the subject seemed to decrease the activation of all the areas considering the paretic limb. The activations detected during the unaffected side movement, however, showed good improvements. These results show a modified neurological picture after the EMG BFB treatment with a greater involvement of the healthy hemisphere.

Table 3.5: SP3: First Index: diff Post-Pre, values are expressed in percentage [%]

diff Post–Pre Index	**CL side– Task A**	**CL side–Task B**	**IL side–Task A**	**IL side–Task B**
Premotor Area	-392	-375.4	366.6	523.2
Sensory Motor Area	-890.6	-723.2	1078	1058
Motor Area	-27	-24	26	245
Cerebellum	2354	353.6	-427.2	-1300

Before the treatment SP3 had an apparently correct activation when moving the paretic limb, in the sense the hemisphere contralateral to the movement was more activated than the other. After the therapy, the neurological picture appeared changed: the activity of the pre-motor, sensory-motor and motor areas showed abnormal activation during the execution of the paretic limb task, while showed normal results considering the performance of the unaffected side. So also SP3 changed the neurological picture after treatment.

Table 3.6: SP1: Second Index: diff Post-Pre CL-IL, values are expressed in percentage [%]

diff Post–Pre CL–IL Index	**Task A**	**Task B**
Premotor Area	-10.1	-45.5
Sensory Motor Area	-20.3	-31.9
Motor Area	6.9	-31.1
Cerebellum	-135.9	8.5

SP1 showed a decrease of the second index for all the ROIs, except for an increase of the motor area for task A and the cerebellum for the task B. Such results are in agreement with the first index results: a neurological recovery occurred. The values of this index are more significant in case of the passive movement, showing a trend towards a normal brain activation.

Table 3.7: SP2: Second Index: diff Post-Pre CL-IL, values are expressed in percentage [%]

diff Post–Pre CL–IL Index	**Task A**	**Task B**
Premotor Area	-1.2	0.5
Sensory Motor Area	1.7	2.9
Motor Area	23.6	-1.3
Cerebellum	-56.8	35.8

The index did not change during the passive tasks, but for the motor area. Even for the active task a great improvement with regard to the cerebellum activation was observed. It is interesting to highlight the difference in the time evolution of the cerebellum activity.

Table 3.8: SP3: Second Index: diff Post-Pre CL-IL, values are expressed in percentage [%]

diff Post–Pre CL–IL Index	**Task A**	**Task B**
Premotor Area	-4.7	-9.4
Sensory Motor Area	-20.9	-33.6
Motor Area	1.2	22.3
Cerebellum	-60.2	-282.9

In this case the index was negative for all the considered ROIs and for both the tasks with the only exception of the motor area, especially for the passive task. the second index showed an overall improvement.

Table 3.9: Control Subject: Third Index: diff A-P, values are expressed in percentage [%]

diff A–P Index	**Right Side**
Premotor Area	-4.1
Sensory Motor Area	-28.6
Motor Area	-14.4
Cerebellum	13.1

The results showed that only the cerebellum activity of the contralateral hemisphere increased during task A. A threshold of the absolute value of this index could be considered as an activation index: the problem would be to identify a reliable threshold of change, indicating which areas could be considered as active. Given only one control subject, which cannot be

considered as statistically significant, and given the small changes evaluated, this index will not be considered to assess the neural recovery.

Table 3.10: SP1: Third Index: diff A-P, values are expressed in percentage [%]

diff A–P Index	**CL Side – Pre**	**CL Side – Post**	**IL Side – Pre**	**IL Side – Post**
Premotor Area	4.4	5.5	27.1	-1.7
Sensory Motor Area	1.8	-6.8	17.7	4.4
Motor Area	12.7	67.8	-1	8.7
Cerebellum	-45.1	-92.7	-83.3	14.7

Significant changes were found especially with regard to the motor area, but only during the paretic limb movement, and to the cerebellum.

Table 3.11: SP2: Third Index: diff A-P, values are expressed in percentage [%]

diff A–P Index	**CL Side – Pre**	**CL Side – Post**	**IL Side – Pre**	**IL Side – Post**
Premotor Area	21.1	-33.1	12	-2.2
Sensory Motor Area	3.3	-21	8.3	-5.6
Motor Area	35.2	-81.2	-6.6	-15.6
Cerebellum	-46.4	20.3	-44.2	11.9

Again a significant change was observed for the activation of the motor area, but mainly associated with the paretic limb movements, and of the cerebellum. In addition the premotor area showed high values and with opposite sign between the Pre and Post treatment.

SB3 showed higher changes than those found for the other subjects, the cerebellum showed an heterogeneous pattern.

Table 3.12: SP: Third Index: diff A-P, values are expressed in percentage [%]

diff A–P Index	CL Side – Pre	CL Side – Post	IL Side – Pre	IL Side – Post
Premotor Area	-23.4	20.8	4.4	-28.4
Sensory Motor Area	-27.6	12.9	24.8	-23.5
Motor Area	-21	53.5	-12.3	-75.9
Cerebellum	-70.7	58.7	-396.3	-86.8

Table 3.13: Description of the gait analysis and fMRI available data for the recruited stoke patients (n.a.= Not Available).

SP	T0	T1	T2	T3
SP1	gait analysis and fMRI	gait analysis and fMRI	gait analysis and fMRI	n.a.
SP2	n.a.	gait analysis and fMRI	n.a.	gait analysis and fMRI
SP3	n.a.	gait analysis and fMRI	gait analysis and fMRI	n.a.
SP4	gait analysis and fMRI	gait analysis and fMRI	gait analysis and fMRI	n.a.

3.6.2 Gait Analysis Results

In this thesis four subjects were evaluated. The small cohort of the sample was mainly due to two factors: first because the total duration of a complete evaluation of a single subject required about 8 months, and second because the patients needed to meet the specific inclusion and exclusion criteria. In addition not all the subjects could perform all the acquisitions established by the experimental protocol (i.e. T0, T1, T2 and T3). In particular Table 3.13 reports a summary of the available data.

So for each of the patients involved in the study only the analysis performed before treatment (Pre: either T0 or T1) could be compared with those performed after treatment (Post: either T2 or T3). The missing data of either T0 or T1 for some subjects was not a limitation of this study: indeed all the recruited patients suffered from a chronic hemiparesis and they did not undergo rehabilitation therapy between T0 and T1; evidence in literature led

to suppose that, in this case, very likely no significant changes of neural had occurred and consequently the fMRI studies could be considered repeatable. The comparison between subjects could be influenced by the fact that for some SP time T2 and for some other SP time T3 were considered as post-therapy because in this way it was not possible to assess whether any motor learning had been maintained over time. As regards SP1 and SP4 the T1 data were considered as Pre-treatment because as the subject underwent to a previous test, during T1 the subject was thought to be less influenced by the experimental protocol. In addition for SP3 and SP4 (the first recruited patients) only the gait analysis parameters related to the paretic side were available. This because originally the experimental protocol required the analysis of the paretic side only, and later it was modified, extending it also to the unaffected limb. This because often in hemiparetic patients changes in gait patterns even related the unaffected side could occur as a compensative strategy to the paretic side. As a result the effects of the rehabilitation treatment could involve even the unaffected limb, it was therefore worthy to evaluate and quantify the relationship between the consequences of the EMG BFB protocol on both the affected and the unaffected limb. Based on these considerations we decided to evaluate also the kinematic and kinetic parameters and for the unaffected side, the comparison between the two sides' data turned out as an index for the assessment of the motor recovery. The CS for this study underwent a single fMRI session. The CS did not performed gait analysis, so we could not correlate the fMRI indices with the gait parameters. In addition, fMRI data were available only for one side, the right one.

Gait analysis data obtained were evaluated as described in section 3.4 to get the kinetic and kinematic data. The results were shown in a summary table and report consisting of the patients' graphics of the kinetic and kine-

matic variables compared to the normative bands. For each subject, the reports and the graphics of the parameters evaluated for both the Pre and Post evaluations are reported. As regards the reports in blue are displayed the data of the right side, in red of the left side, and in gray or green of the normative bands.

The normative bands mean values for both the walking at SS and F speed considered to evaluate the gait indices are shown in table 3.14.

Table 3.14: Normative bands mean values for the gait analysis.

Parameters	**Self Selected Speed**	**Fast Speed**
Speed [m/s]	1.04	1.49
Cadence [Steps/min]	49.9	61.18
Stride Length	73.29	86.82
Ankle Power Peak [W/Kg]	2.42	3.24
Ankle Positive Work [J/Kg]	0.30	0.33
Ankle Negative Work [J/Kg]	-0.70	-0.04
Ankle Power Onset From Contralateral HS [% of the Gait Cycle]	16.02	13.19

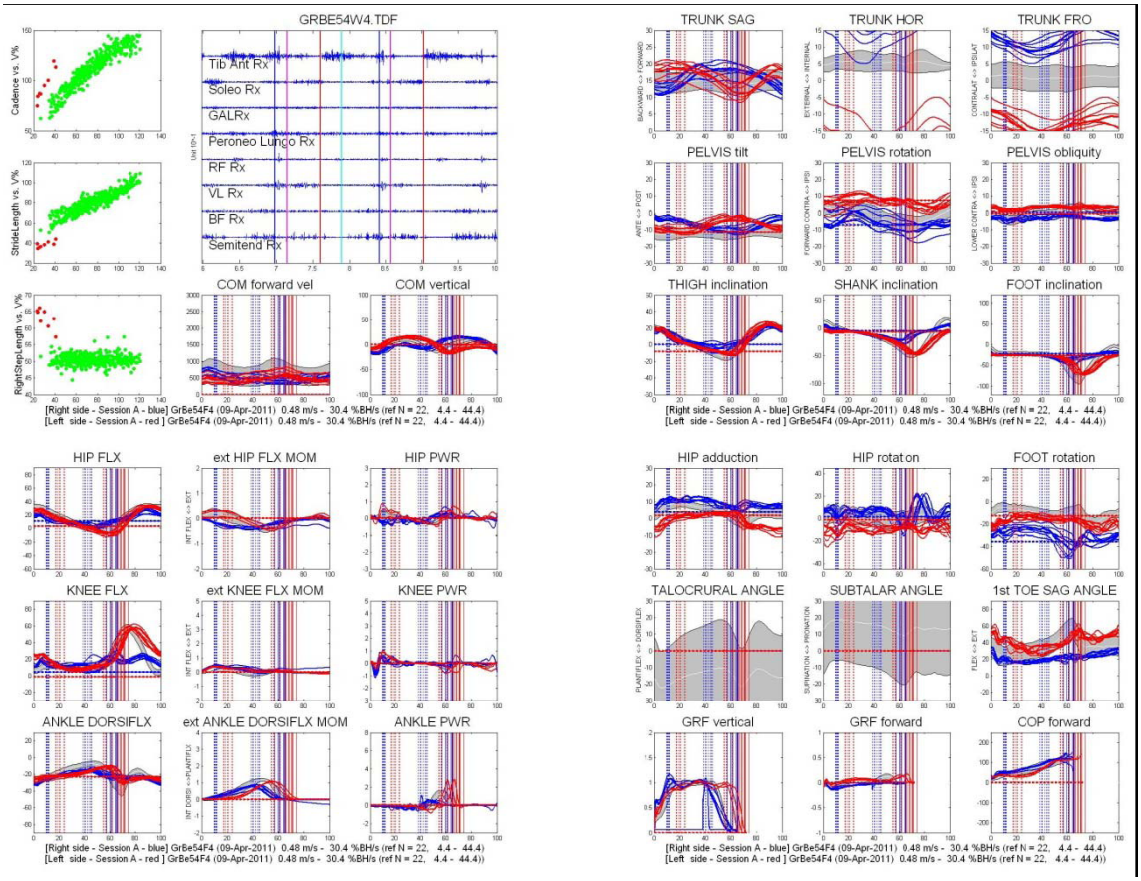

Figure 3.35: SP1: Pre–treatment Report (T1).

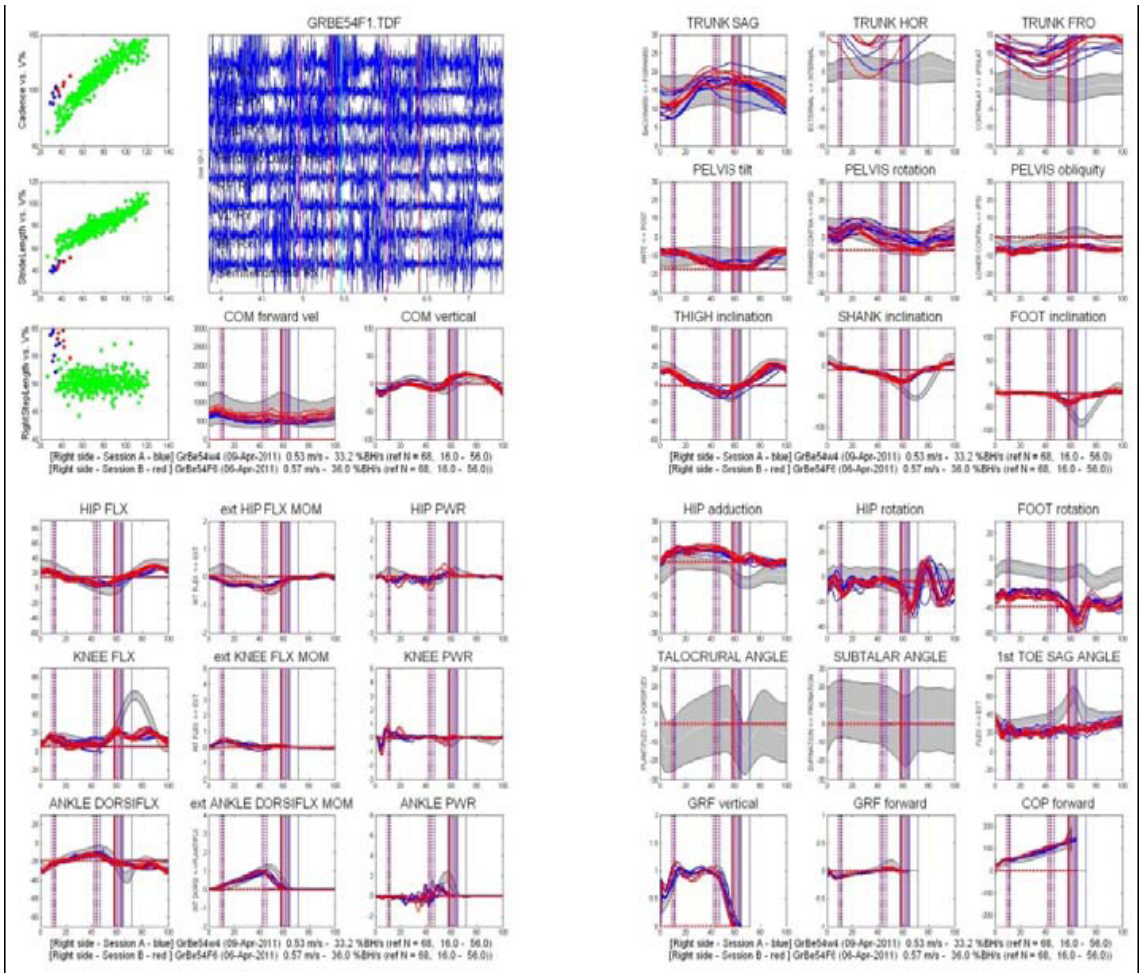

Figure 3.36: SP1: Post–treatment Report (T2).

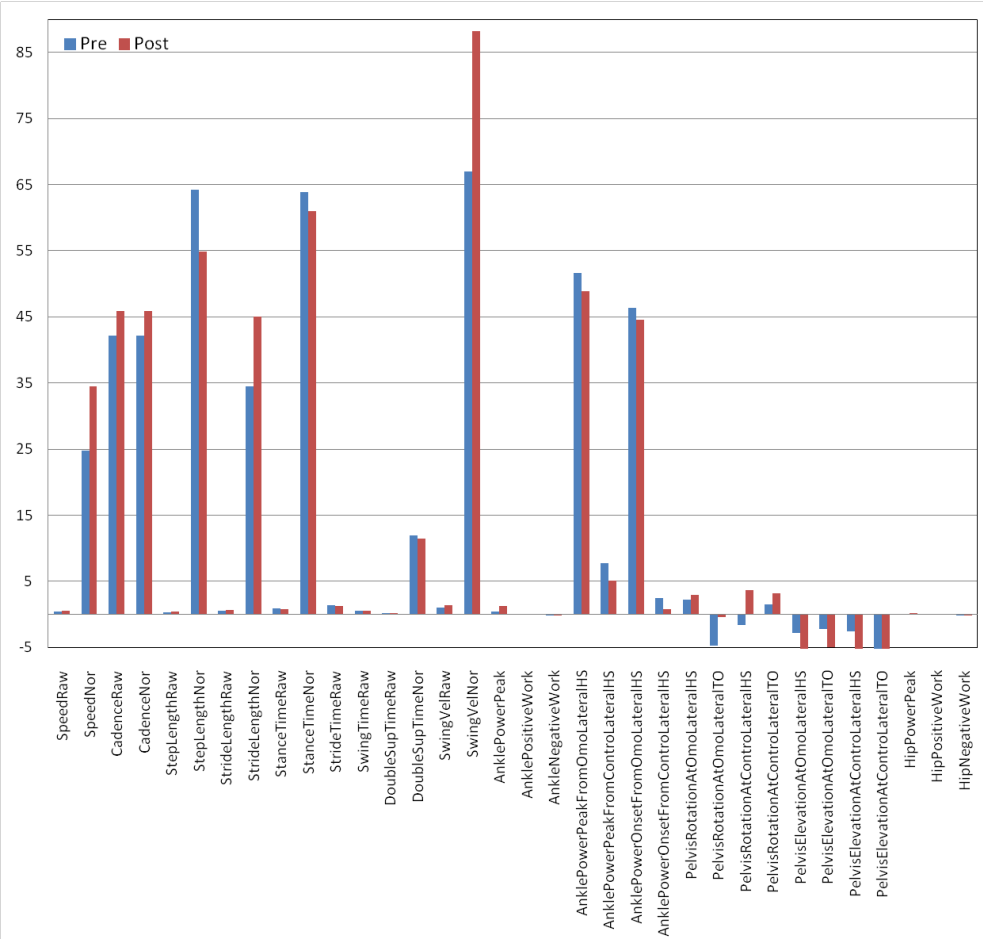

Figure 3.37: SP1: Contralateral Side Parameters – Self Selected Speed – T1 vs T2.

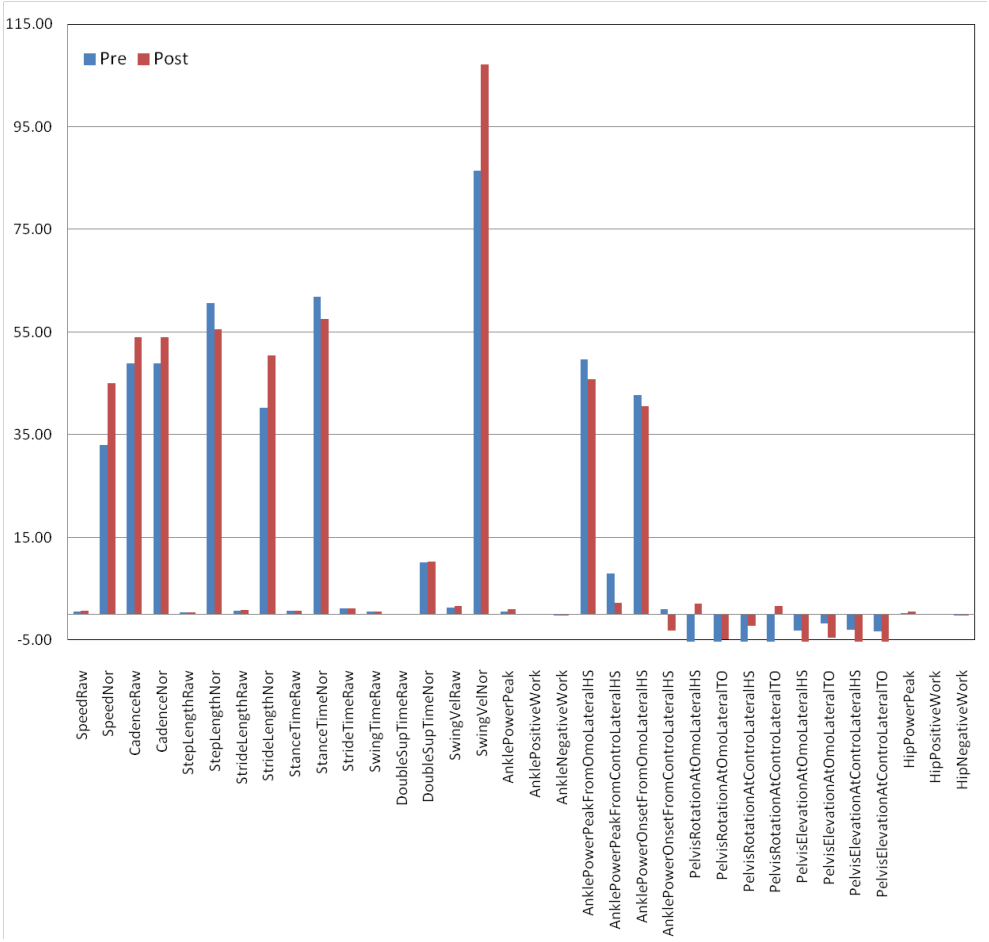

Figure 3.38: SP1: Contralateral Side Parameters – Fast Speed – T1 vs T2.

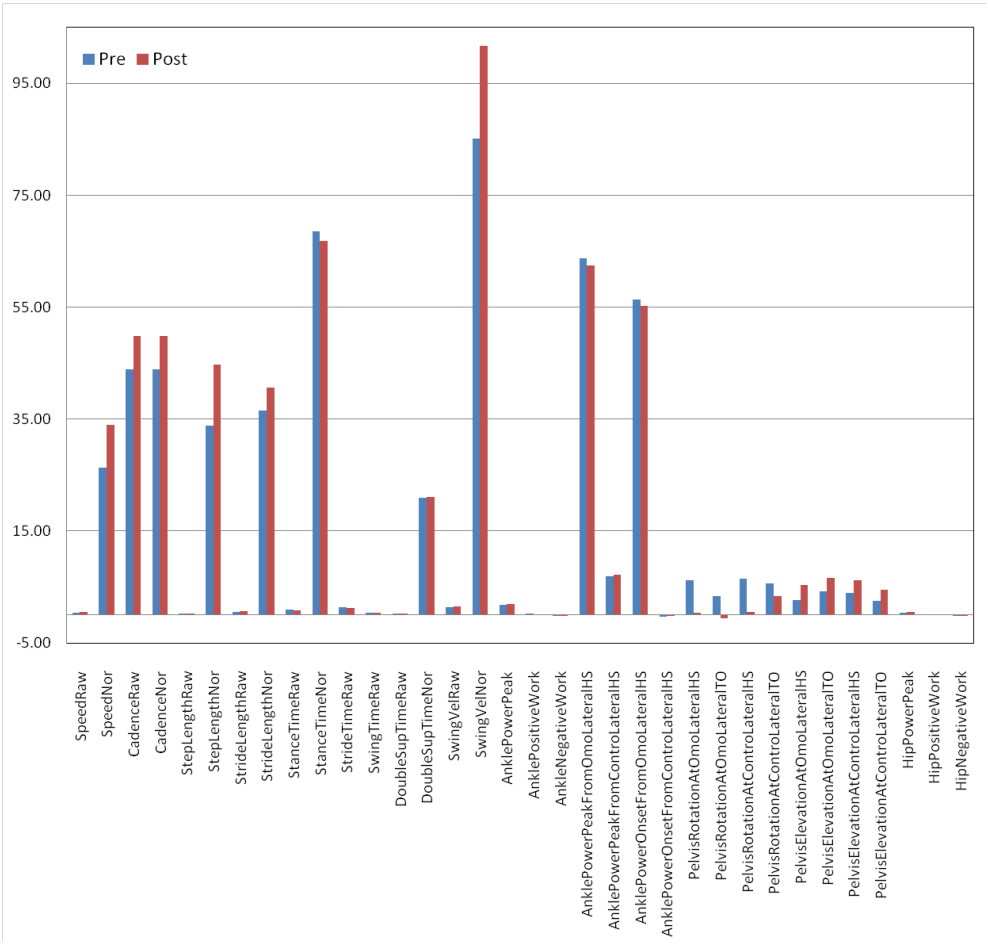

Figure 3.39: SP1: Ipsilateral Side Parameters – Self Selected Speed – T1 vs T2.

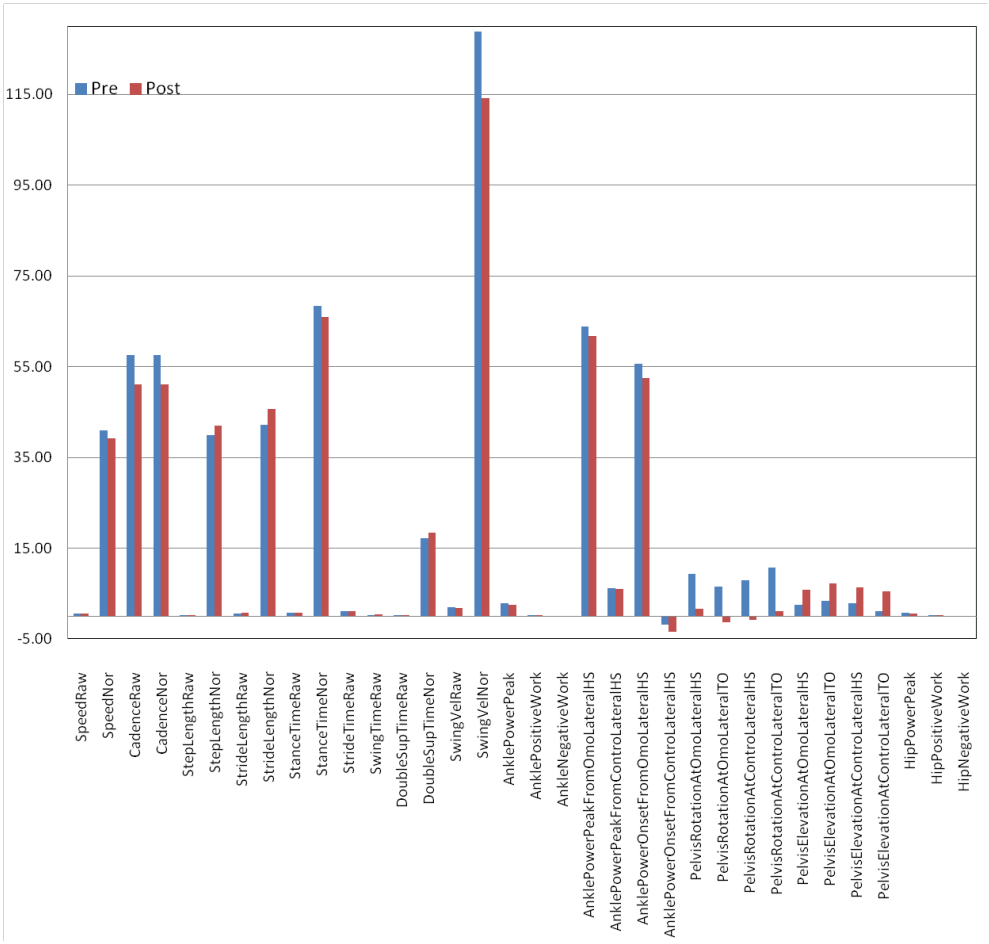

Figure 3.40: SP1: Ipsilateral Side Parameters – Fast Speed – T1 vs T2.

The gait report and results were confirmed by the evaluated parameters. As regards the IL side at F speed the speed was lower than the normative values and did not change over time, an increased Stride Length and a decreased Cadence were found, while for the other tests the speed the Stride Length and the Cadence increased. The Ankle Power Peak was lower than the normative bands and an early onset was found over time.

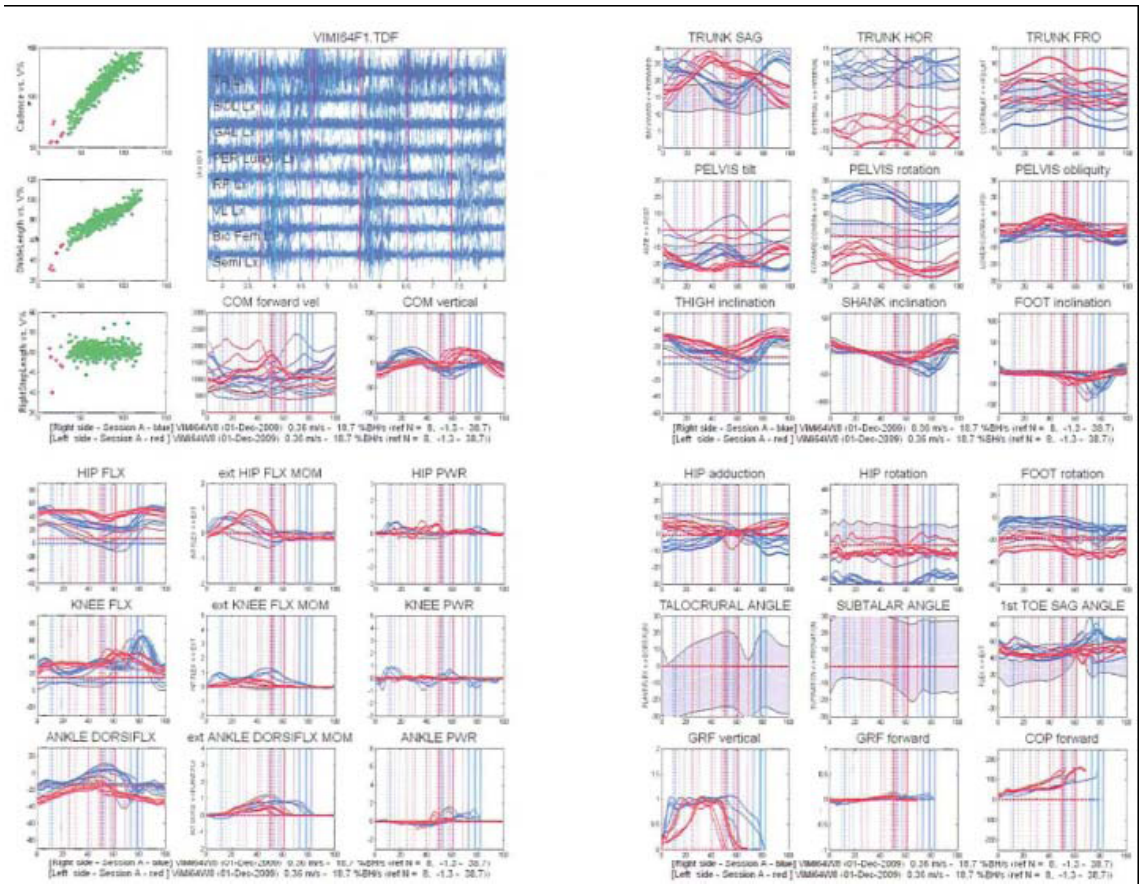

Figure 3.41: SP2: Pre–treatment Report (T1).

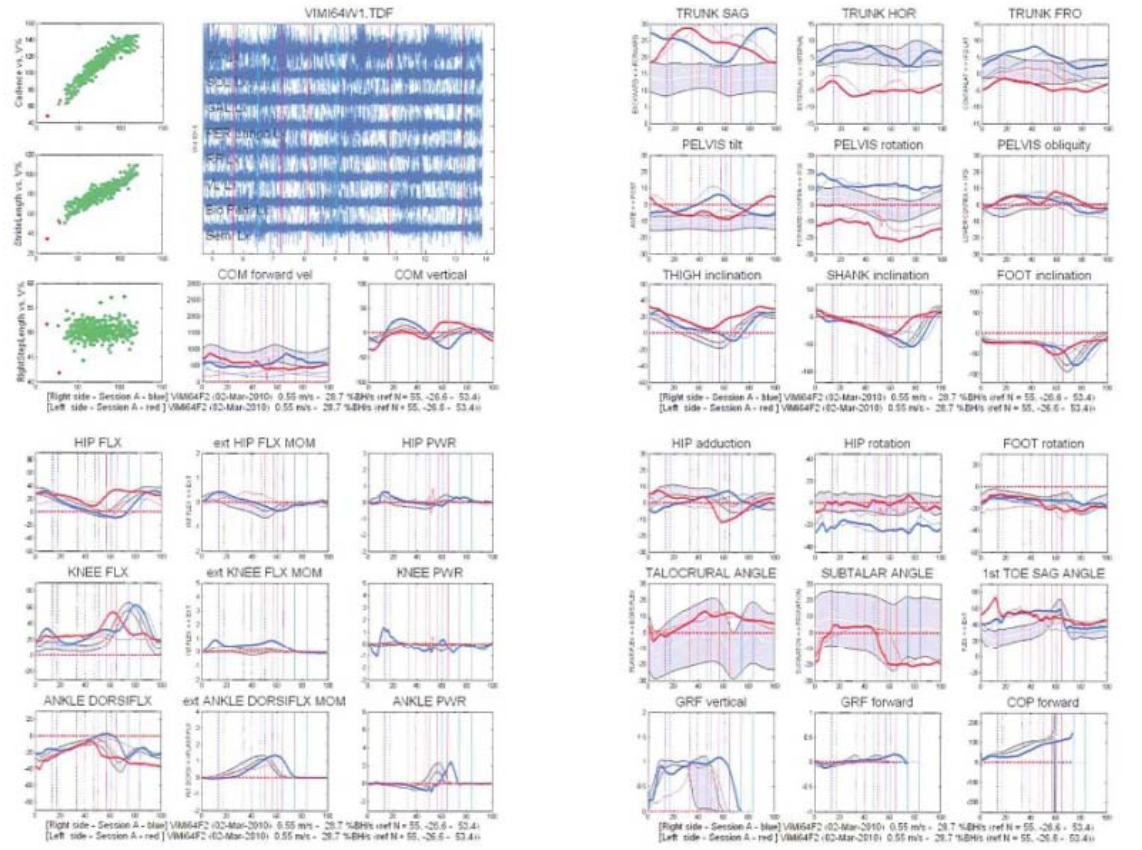

Figure 3.42: SP2: Post–treatment Report (T3).

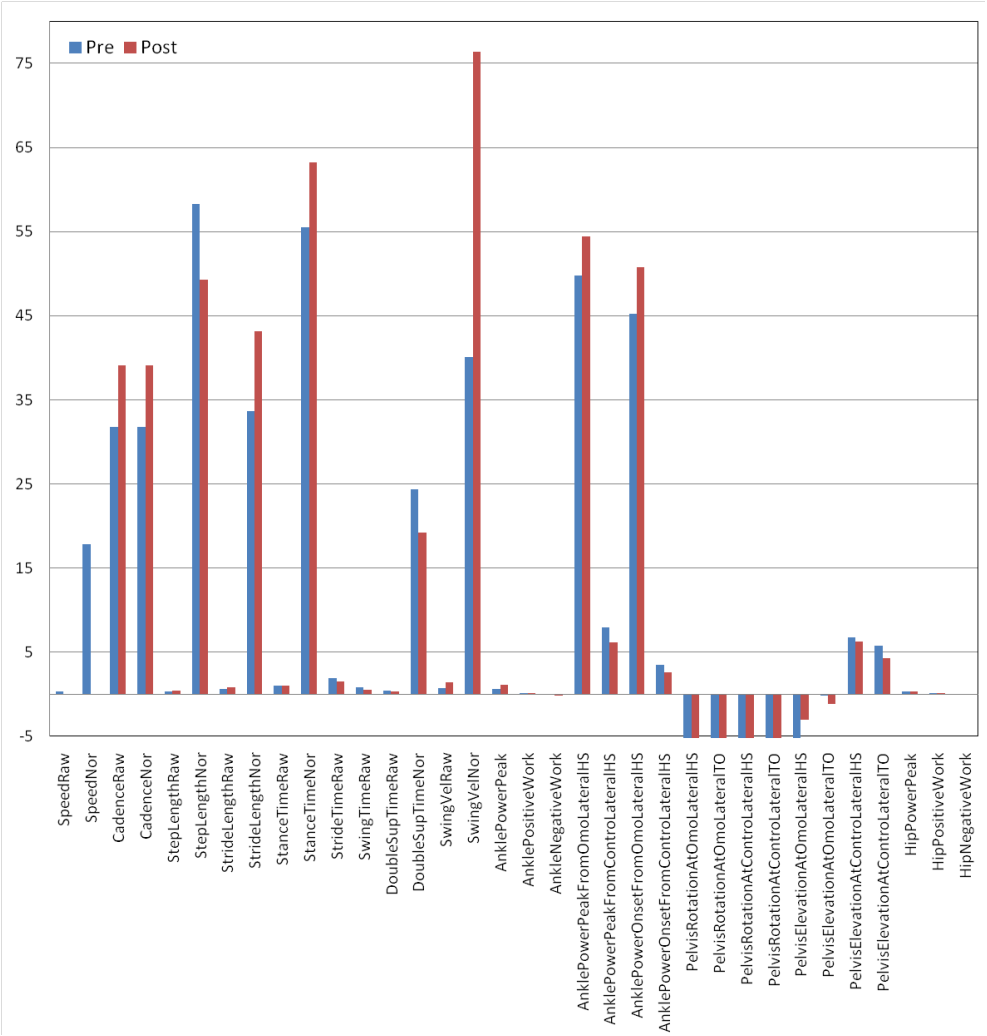

Figure 3.43: SP2: Contralateral Side Parameters –Self Selected Speed – T1 vs T3.

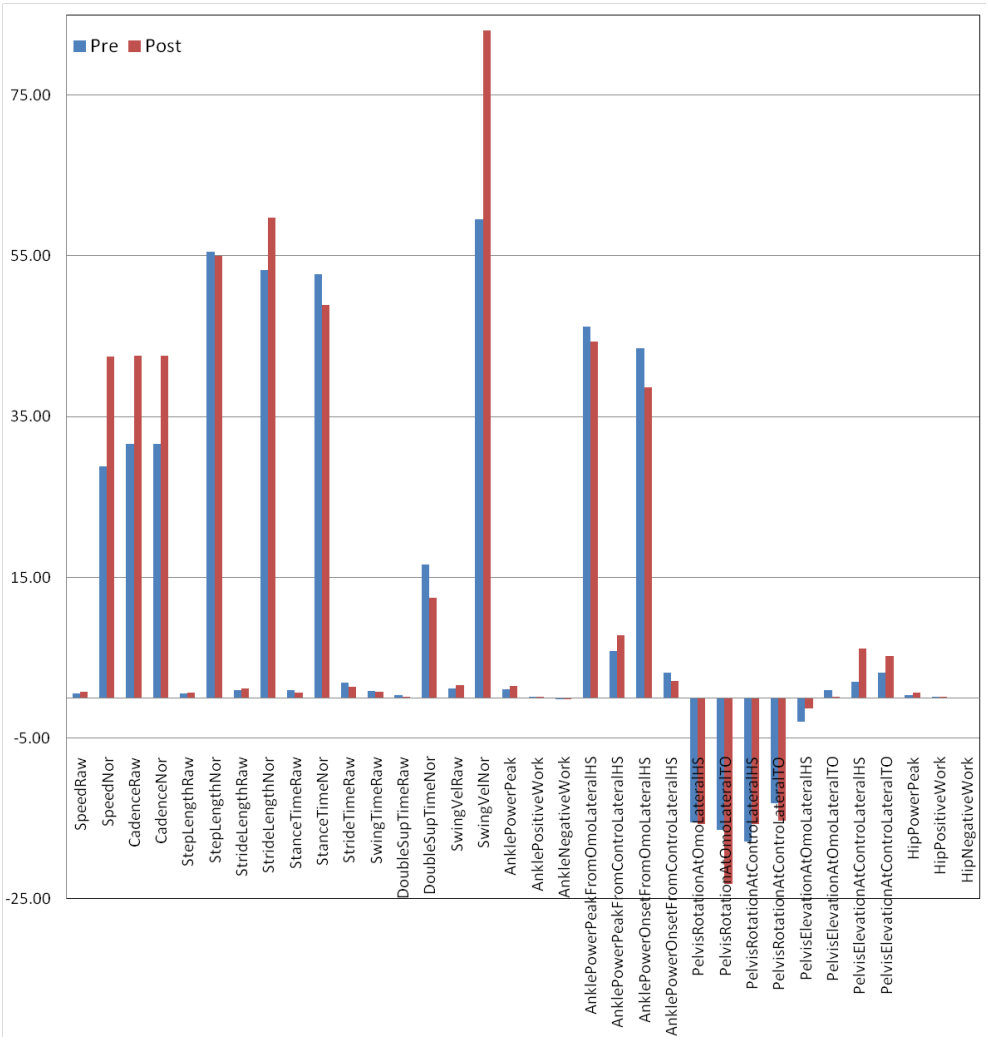

Figure 3.44: SP2: Contralateral Side Parameters – Fast Speed – T1 vs T3.

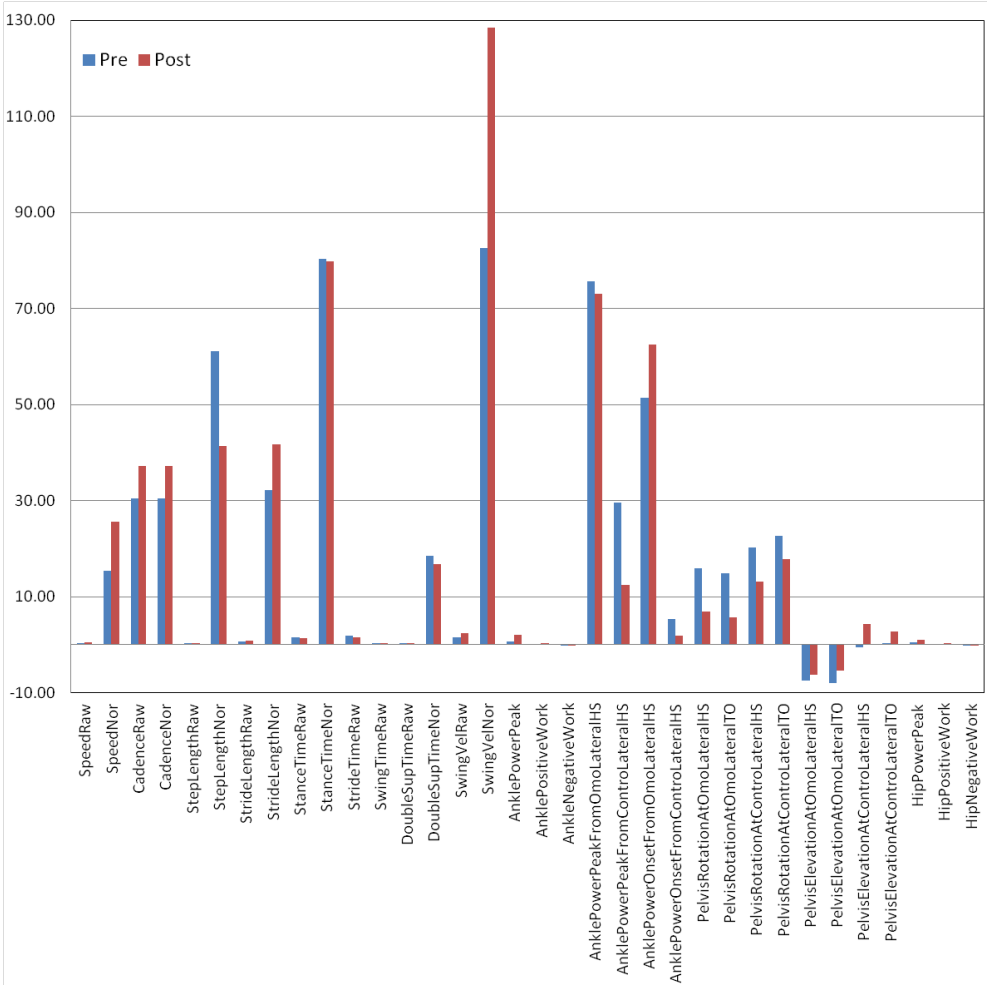

Figure 3.45: SP2: Ipsilateral Side Parameters – Self Selected Speed – T1 vs T3.

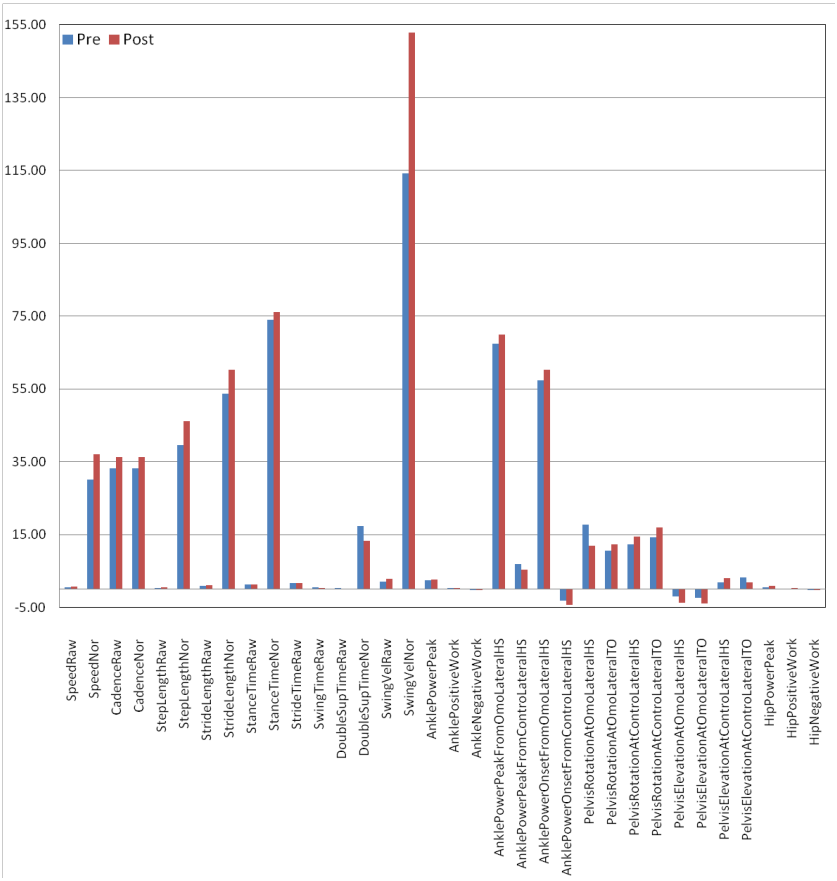

Figure 3.46: SP2: Ipsilateral Side Parameters – Fast Speed – T1 vs T3.

SP2 showed increased cadence and Stride Length even though they are lower than the normative values. In addition, the ankle power peak greatly increased, the onset slightly improved even if a still early onset was found.

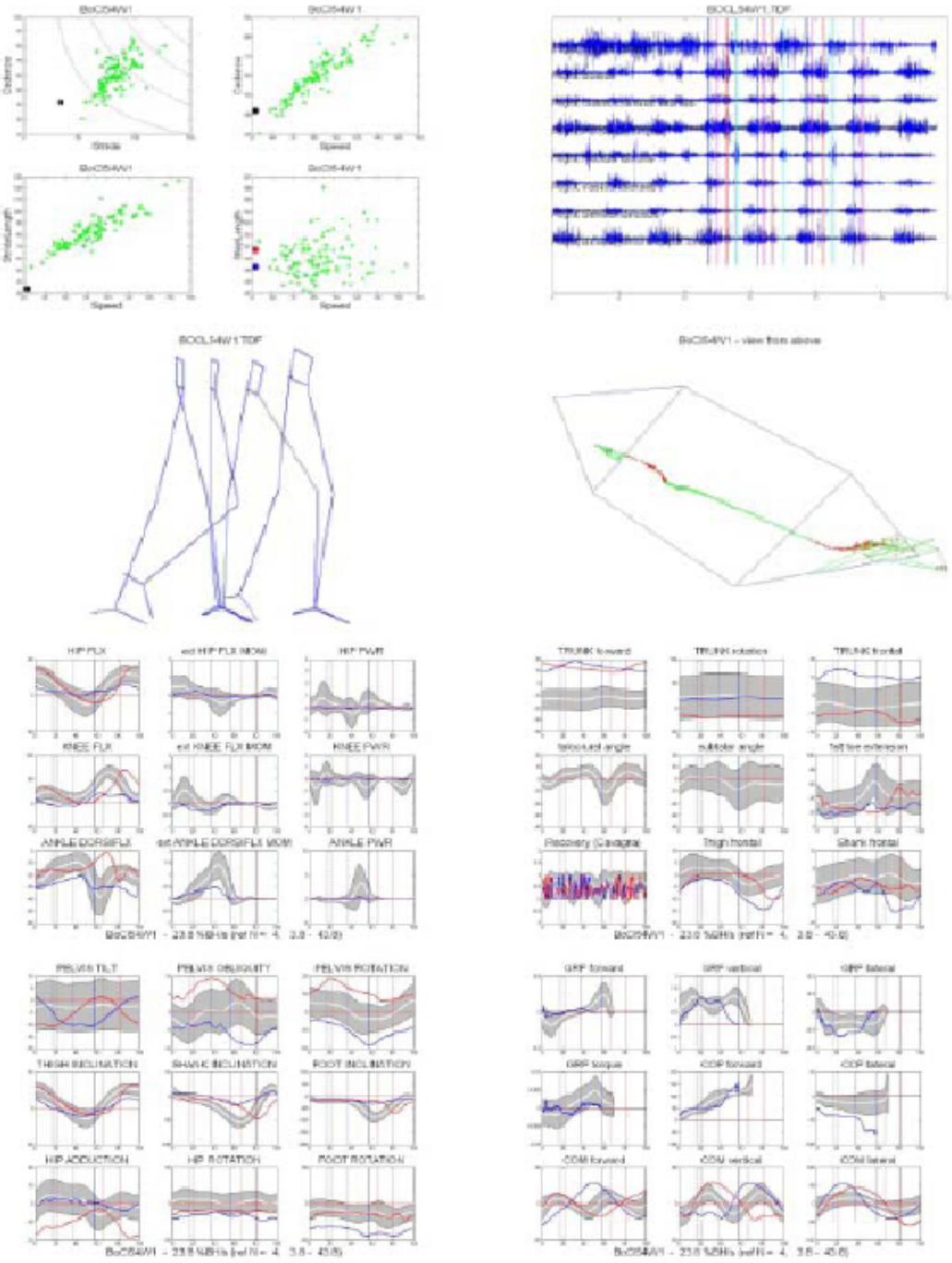

Figure 3.47: SP3: Pre–treatment Report (T1).

SP3 like SP1 showed a decrease in almost all the parameters for the post treatment, mostly for the walking at F speed, except for the Stride Length. So the Pre therapy overall picture did not seem to change after the treatment.

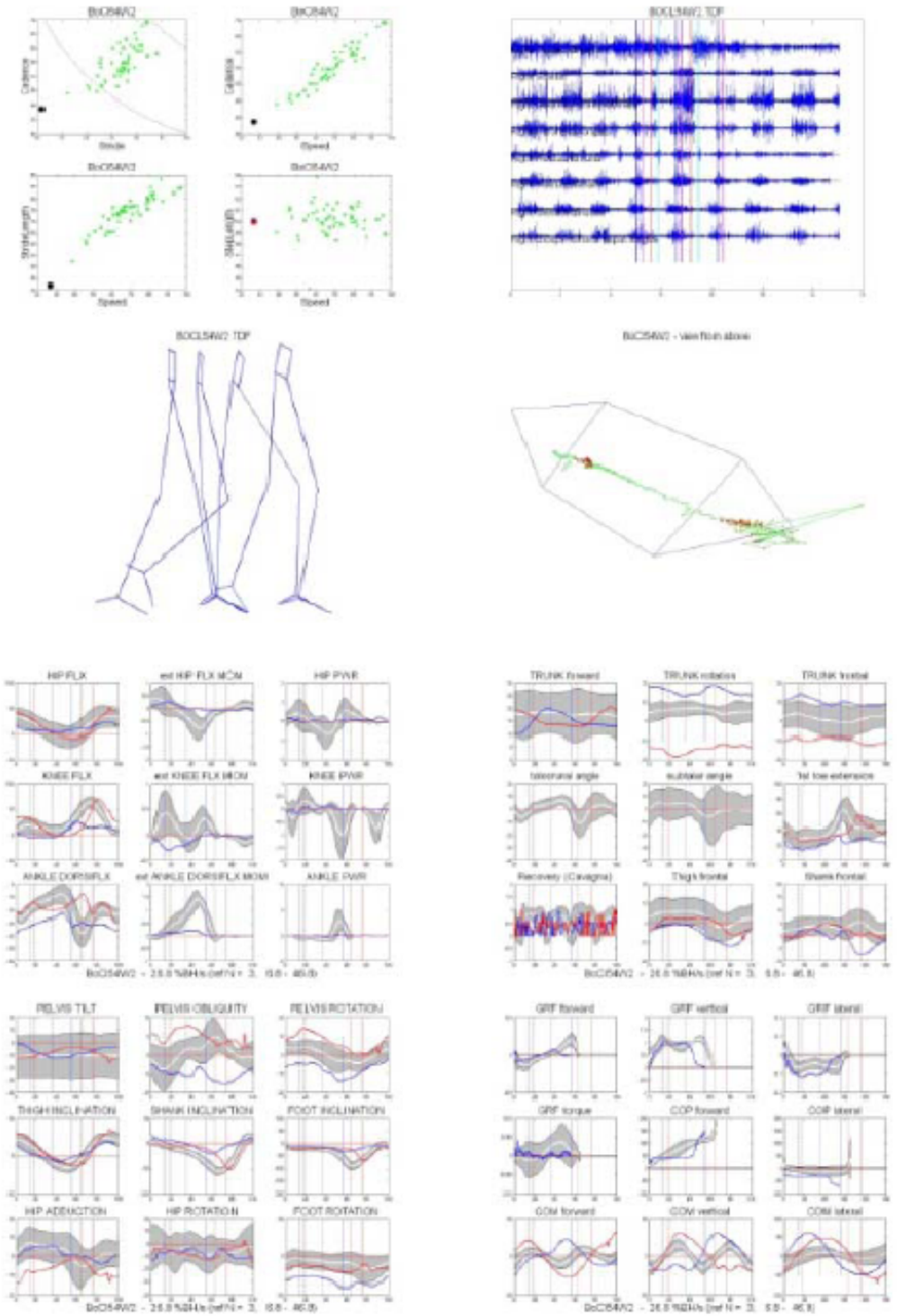

Figure 3.48: SP3: Post–treatment Report (T2).

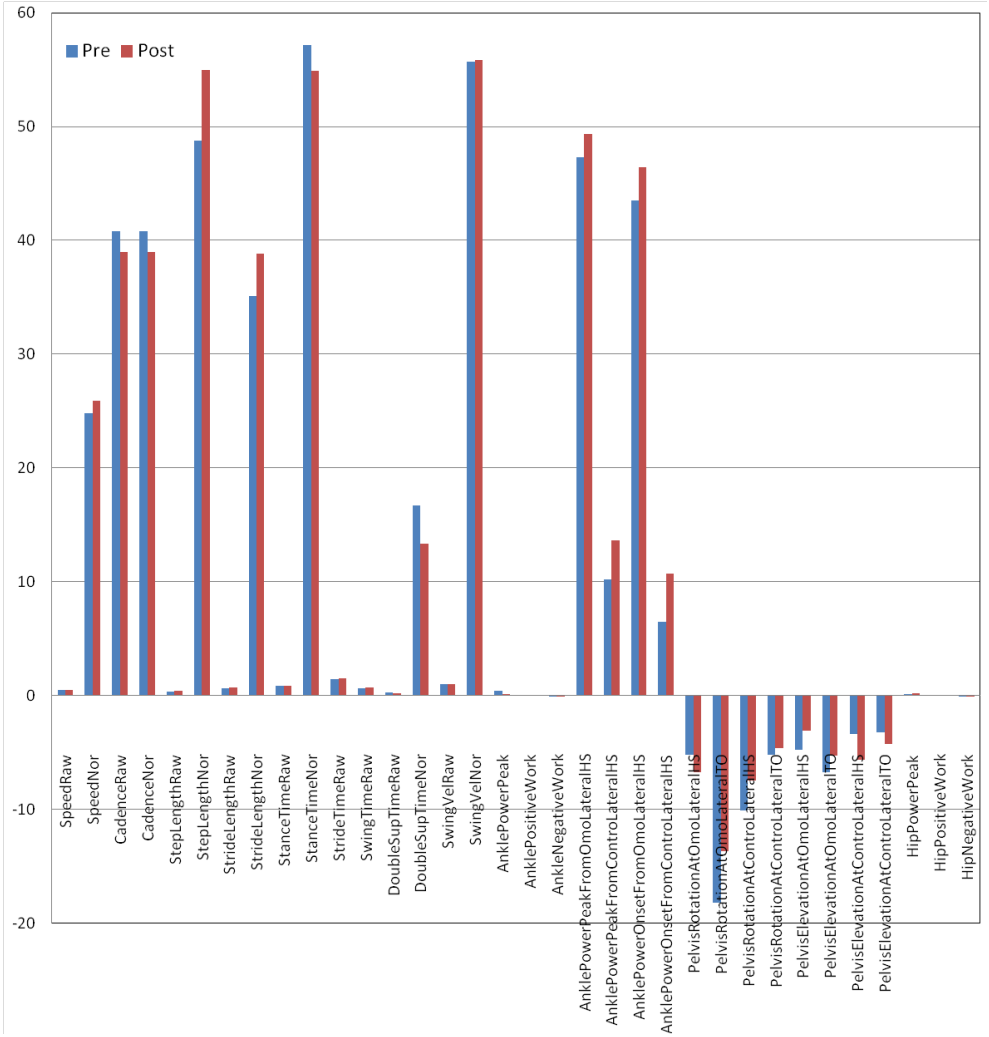

Figure 3.49: SP3: Contralateral Side Parameters – Self Selected Speed – T1 vs T2.

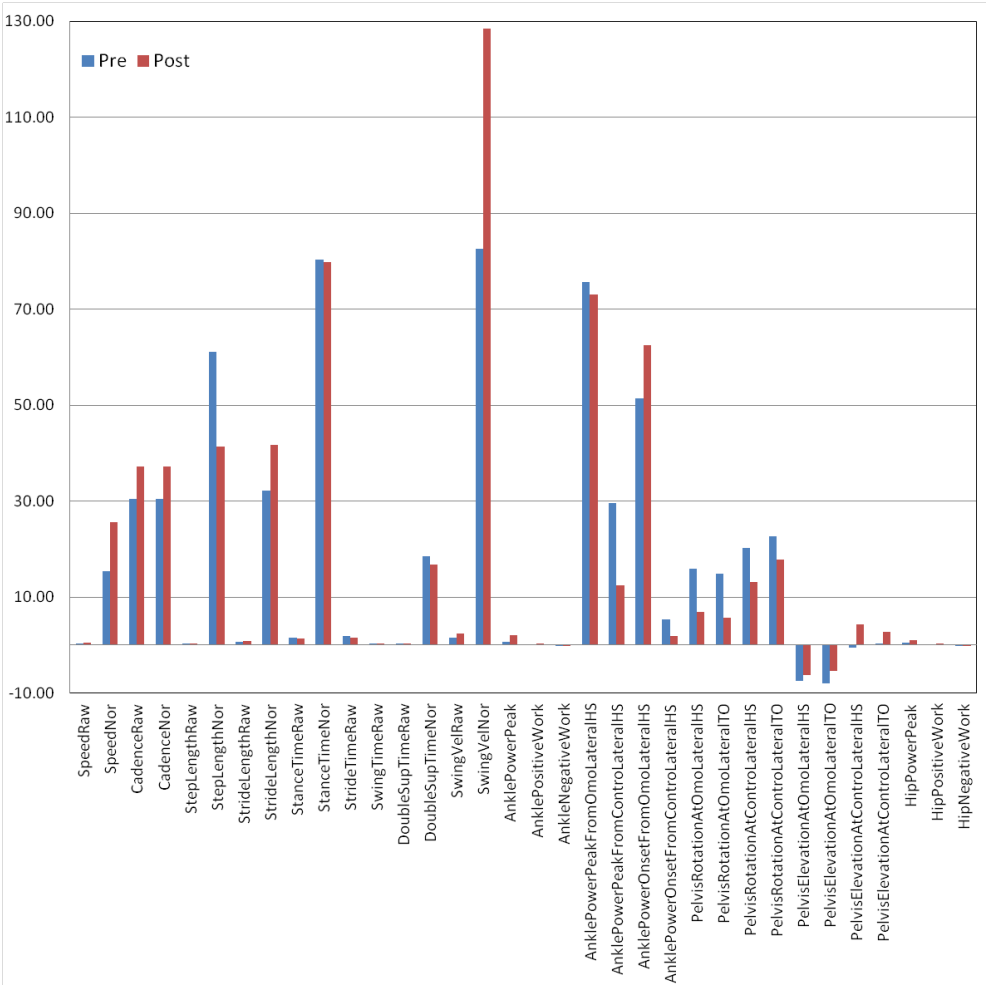

Figure 3.50: SP3: Contralateral Side Parameters - Fast Speed – T1 vs T2.

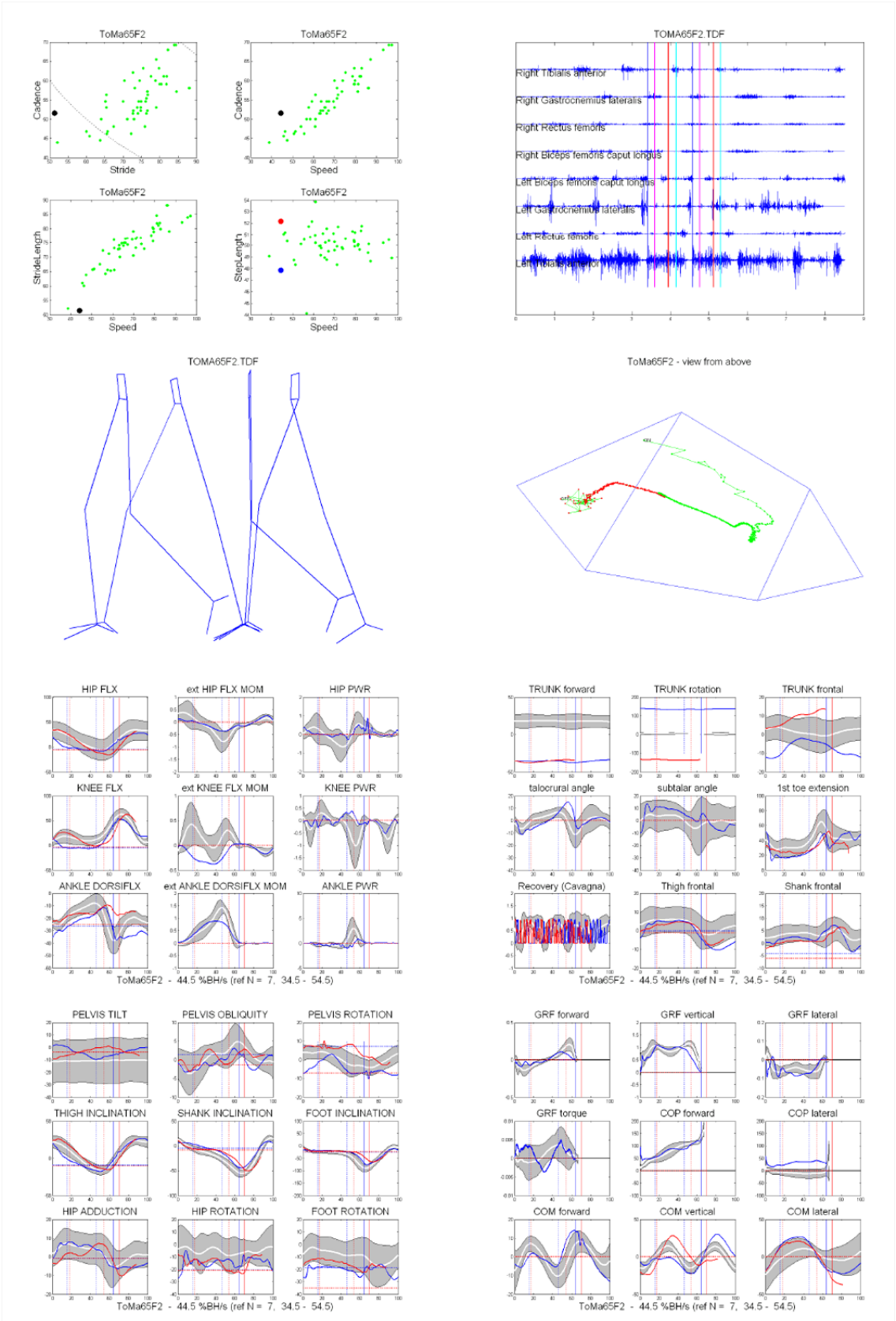

Figure 3.51: SP4: Pre–treatment Report (T1).

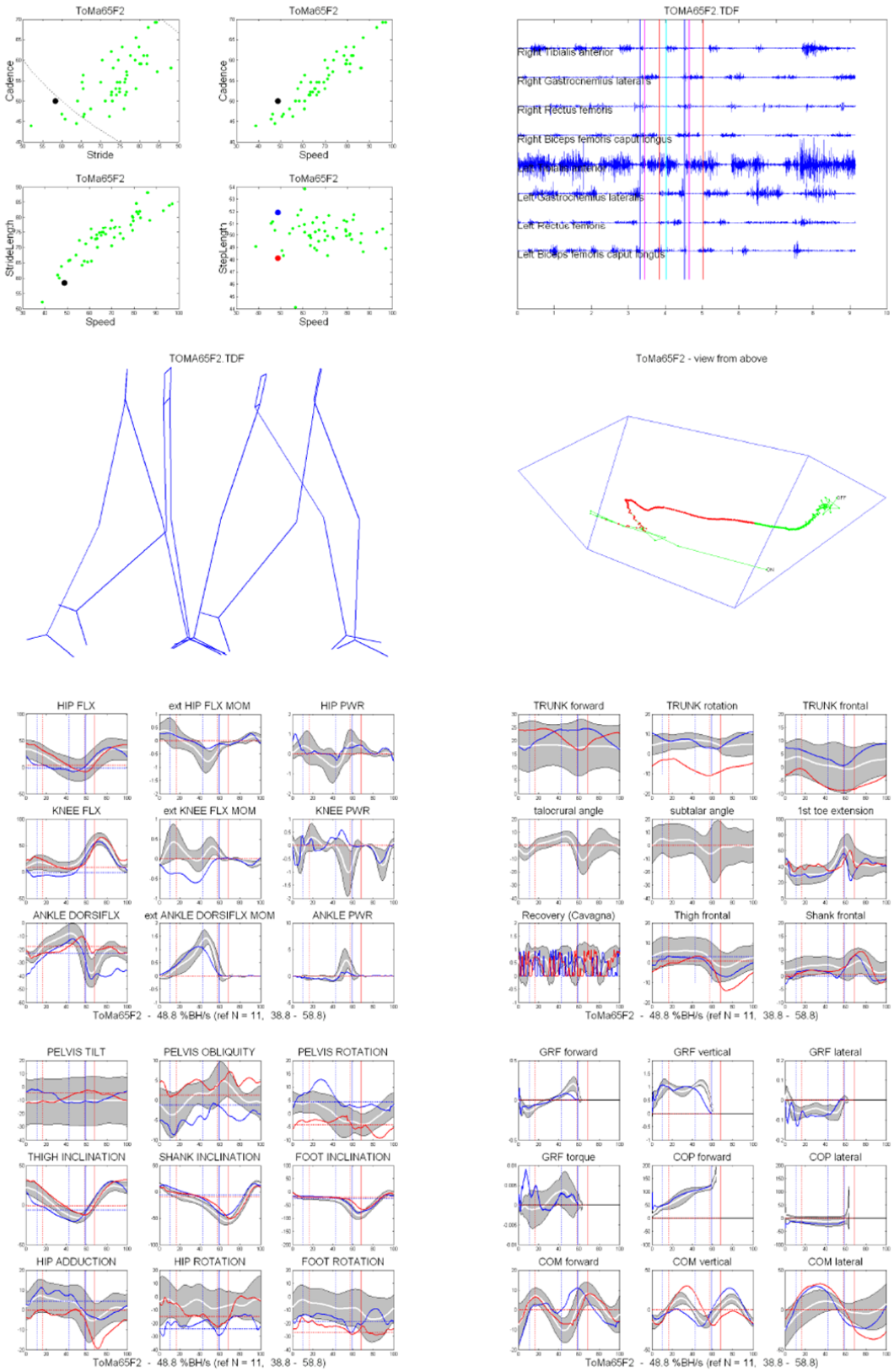

Figure 3.52: SP4: Post–treatment Report (T2).

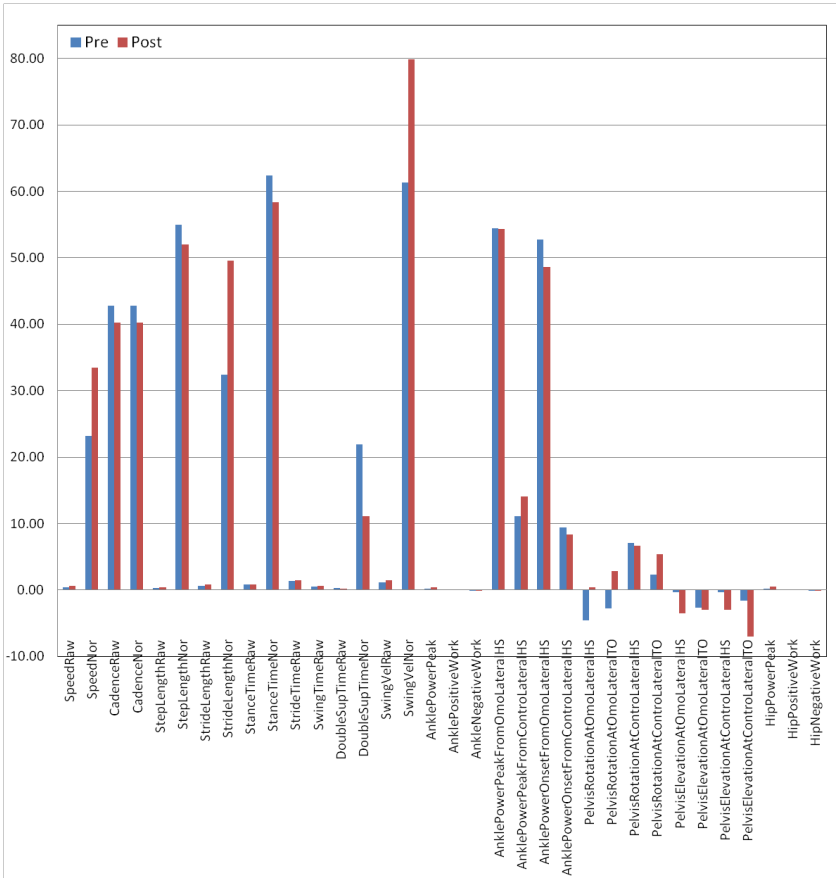

Figure 3.53: SP4: Contralateral Side Parameters – Self Selected Speed - T1 vs T2.

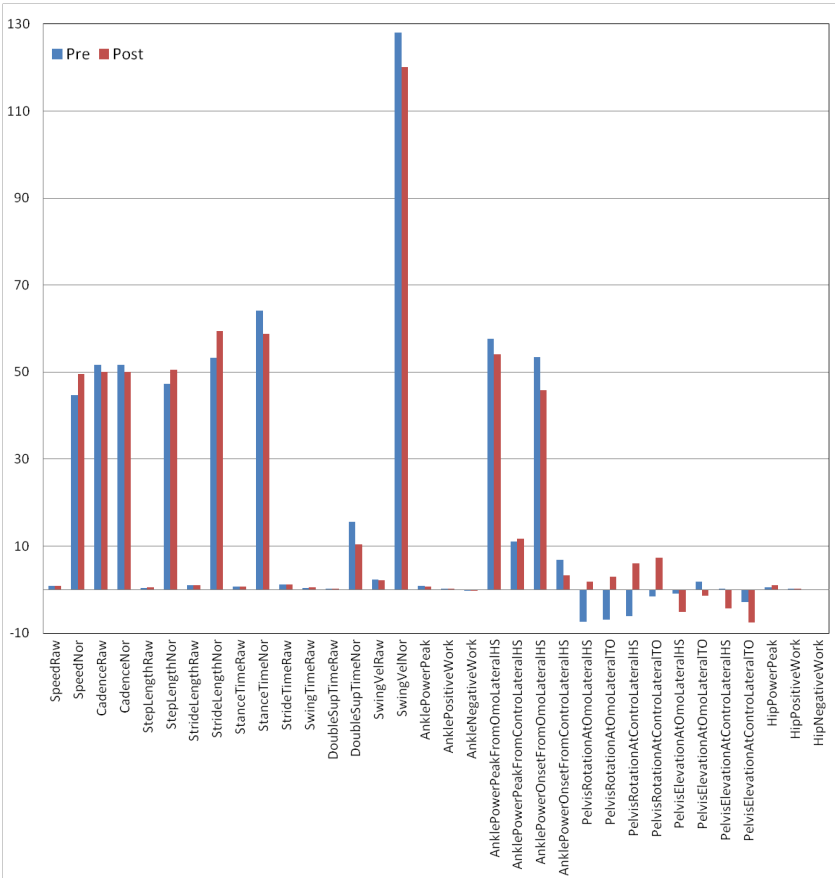

Figure 3.54: SP4: Contralateral Side Parameters – T1 vs T2.

As regards SP4 for the Post treatment an increased Stride Length and a decreased Cadence were found for both the walking speed. The Ankle Power Peak greatly increased and the onset did not change its timing over time.

The three indices (var Post–Pre, var diff F–SS Post–Pre, var diff IL–CL Post–Pre (see 3.5)) evaluated for each subject and side are shown in the tables below:

Table 3.15: SP1: First Index: var Post-Pre, values are expressed in percentage [%]

var Post–Pre Index	**CL–SS Speed**	**IL–SS Speed**	**CL–F Speed**	**IL–F Speed**
Speed	-14.79	-11.57	-12.75	2.24
Cadence	-7.61	-11.73	-8.52	10.65
Stride Length	-14.40	-5.59	-11.68	-4.04
Ankle Power Peak	-36.17	-3.53	-13.08	12.31
Ankle Positive Work	-24.14	15.58	-11.06	-2.94
Ankle Negative Work	49.41	24.94	95.58	114.70
Ankle Power Onset From Contralateral HS	-15.24	2.13	-31.25	-11.06

The results revealed that, for both the walking at SS and F speed, the absolute value of the Ankle Negative Work increased over time, that is to say the energy absorbed by the ankle increased. As regards the unaffected side only the speed, the ankle power peak and the ankle negative work increased so the overall picture seemed not to improve, this was probably less significant as it could be caused by the natural variability between different steps, especially considering that the Speed did not change between Pre and Post treatment (a relative small decrease was found). All the rest of the parameters showed an improvement over time (negative values), mostly for the walking at SS speed, so for SP1 the EMG BFB treatment seemed to be effective and it improved both the power produced by the ankle and its timing.

In agreement with SP1, SP2 showed more evident improvements for

Table 3.16: SP2: First Index: var Post-Pre, values are expressed in percentage [%]

var Post–Pre Index	CL–SS Speed [%]	IL–SS Speed	CL–F Speed	IL–F Speed
Speed	n.a.	-19.29	-17.45	-8.72
Cadence	-14.71	-13.57	-17.80	-5.25
Stride Length	-12.95	-13.02	-7.49	-7.64
Ankle Power Peak	-19.10	-61.63	-12.18	-9.22
Ankle Positive Work	-15.69	-29.10	0.30	27.29
Ankle Negative Work	72	169.41	-161.93	150.68
Ankle Power Onset From Contralateral HS	-7.76	-31.84	-7.82	-9.06

the unaffected side as regards the walking at SS and for the affected limb as regards the F speed. All the parameters improved except for the Ankle Negative Work, as the energy absorbed by the ankle resulted higher than the normative band.

Table 3.17: SP3: First Index: var Post-Pre, values are expressed in percentage [%]

var Post–Pre Index	CL–SS Speed [%]	IL–SS Speed	CL–F Speed	IL–F Speed
Speed	-1.93	n.a.	0.67	n.a.
Cadence	3.73	n.a.	8.53	n.a.
Stride Length	-5.08	n.a.	-5.31	n.a.
Ankle Power Peak	11.16	n.a.	5.52	n.a.
Ankle Positive Work	9.01	n.a.	-9.56	n.a.
Ankle Negative Work	26.82	n.a.	26.99	n.a.
Ankle Power Onset From Contralateral HS	39.15	n.a.	85.52	n.a.

The results did not showed a real improvement of the gait parameters for the contralateral side. The Speed did not change, while the Stride Length increased, thus to balance the decrease of the Cadence value: in order to maintain the same speed as the subject walked with longer steps, but with a lower cadence, this could be reflected in the modified walking strategy with the early onset of the ankle power peak. The positive work seemed to increase

improved for the walking at F speed.

Table 3.18: SP4: First Index: var Post-Pre, values are expressed in percentage [%]

var Post–Pre Index	CL–SS Speed [%]	IL–SS Speed	CL–F Speed	IL–F Speed
Speed	-17.36	n.a.	-6.04	n.a.
Cadence	4.95	n.a.	2.81	n.a.
Stride Length	-23.43	n.a.	-7.15	n.a.
Ankle Power Peak	-9.92	n.a.	0.93	n.a.
Ankle Positive Work	-10.01	n.a.	-8.96	n.a.
Ankle Negative Work	-16.47	n.a.	89.96	n.a.
Ankle Power Onset From Contralateral HS	-9.30	n.a.	-26.80	n.a.

All the parameters showed an improvement except for the ankle negative work at F speed. The EMG BFB seemed to have a positive effect over time especially for the parameters of the walking at SS speed. The cadence value slightly decreased for both the walking speed.

Table 3.19: SP1: Second Index: var diff F–SS Post–Pre, values are expressed in percentage [%]

var diff F–SS Post–Pre Index	CL	IL
Speed	2.04	7.57
Cadence	-0.91	10.39
Stride Length	2.72	1.56
Ankle Power Peak	22.78	-5.74
Ankle Positive Work	2.19	-9.77
Ankle Negative Work	46.17	89.76
Ankle Power Onset From Contralateral HS	16.02	13.19

In agreement with the first index results, more significant improvements were observed for the walking at SS speed. The patient seemed to perform a more proper gait as regards the SS speed, some limitations were still present during the F speed walking. This could show how the EMG BFB therapy could be more effective for the recovery of the walking at SS speed.

Table 3.20: SP2: Second Index: var diff F–SS Post–Pre, values are expressed in percentage [%]

var diff F–SS Post–Pre Index	**CL**	**IL**
Speed	n.a.	-10.01
Cadence	-3.09	8.32
Stride Length	-5.46	-5.38
Ankle Power Peak	-6.03	-47.56
Ankle Positive Work	-6.33	-28.63
Ankle Negative Work	-233.93	-18.73
Ankle Power Onset From Contralateral HS	0.14	-22.79

With regard to the contralateral side the index showed negative values or slightly positive in the case of the AnkleNegativeWork; the Ankle Negative Work showed the higher changes. In fact, the difference between the values of the ankle negative work and the normative bands for the two walking speeds appeared to decrease after the treatment. The index values for the ipsilateral side showed negative values, so the results suggested that the recovery process was more consistent between the two analyzed walking, confirming the first index trend.

Table 3.21: SP3: Second Index: var diff F–SS Post–Pre, values are expressed in percentage [%]

var diff F–SS Post–Pre Index	**CL**	**IL**
Speed	2.60	n.a.
Cadence	4.80	n.a.
Stride Length	0.23	n.a.
Ankle Power Peak	-5.64	n.a.
Ankle Positive Work	-0.96	n.a.
Ankle Negative Work	-0.16	n.a.
Ankle Power Onset From Contralateral HS	46.38	n.a.

The second index suggested that the EMG BFB therapy did not highly change the walk. Only as regards the Ankle Power Onset showed the differ-

ence observed between the two walking speeds increased after the treatment.

Table 3.22: SP4: Second Index: var diff F–SS Post–Pre, values are expressed in percentage [%]

var diff F–SS Post–Pre Index	CL	IL
Speed	-11.32	n.a.
Cadence	-0.10	n.a.
Stride Length	-16.28	n.a.
Ankle Power Peak	-10.85	n.a.
Ankle Positive Work	-1.05	n.a.
Ankle Negative Work	106.43	n.a.
Ankle Power Onset From Contralateral HS	17.50	n.a.

SP4 showed negative values (or close to zero) for all the parameters except for the Ankle Power Onset and the cadence (in agreement with the first index results), thus suggesting a good recovery for both the SS and F speed walking.

Table 3.23: SP1: Third Index: var diff OL–CL Post–Pre, values are expressed in percentage [%]

var diff OL–CL Post–Pre Index	SS Speed	F Speed
Speed	-2.57	-1.79
Cadence	4.12	-9.44
Stride Length	3.07	3.29
Ankle Power Peak	-32.64	-25.39
Ankle Positive Work	-39.72	-8.12
Ankle Negative Work	-24.47	12.37
Ankle Power Onset From Contralateral HS	-17.37	-20.20

Negative values were found only for the Ankle Power Peak and the Ankle Positive Work, the Ankle Negative Work, and the Ankle Power Onset, thus suggesting a recovery of the contralateral side with respect to the normative bands and the ipsilateral side. These changes were observed to be more definite for the walk at SS speed, rather than at F speed.

Table 3.24: SP2: Third Index: var diff OL–CL Post–Pre, values are expressed in percentage [%]

var diff OL–CL Post–Pre Index	**SS Speed**	**F Speed**
Speed	n.a.	6.04
Cadence	1.14	7.68
Stride Length	-0.07	0.15
Ankle Power Peak	38.73	-2.96
Ankle Positive Work	13.41	-27.49
Ankle Negative Work	97.41	312.61
Ankle Power Onset From Contralateral HS	-10.40	1.24

In this case the index had a positive value for Pre and Post treatment Ankle Negative Work and for the only Pre treatment Ankle Positive Work and Ankle Power Peak. This may be due to the fact that the subject improved the motor outcome by using compensatory strategies by improving the use of the unaffected limb.

The SP3 and SP4 contralateral data were not available, so that the third index could not be evaluated.

3.6.3 Correlation Results

The correlation coefficients results (r) of the analysis with categorical variables as described in section 3.5for each of the four patients are reported in the tables below:

Table 3.25: SP1: Correlation values (r) for the Pre-Post analysis of the fMRI and gait analysis data.

SP1	fMRI and Gait data r value	fMRI data r value	Gait data r value
Pre and Post – Cl and IL sides	0.87	0.99	0.99
Pre and Post – CL side	0.29	0.18	0.99
Pre and Post – IL side	0.51	0.51	0.99

Low correlation ($0.29 \leq r \leq 0.51$) was found between fMRI and gait data together, and the fMRI data for both the two sides. Nice correlations coefficients were found for the fMRI and the gait data as regards the two sides together and for the gait data ($r \geq 0.87$), so SP1 fMRI results did change over time.

Table 3.26: SP2: Correlation values (r) for the Pre-Post analysis of the fMRI and gait analysis data.

SP2	fMRI and Gait data r value	fMRI data r value	Gait data r value
Pre and Post – Cl and IL sides	0.28	0.22	0.99
Pre and Post – CL side	0.17	0.18	0.99
Pre and Post – IL side	0.39	0.26	0.99

The correlation analysis results between fMRI and gait data showed a poor correlation ($0.17 \leq r \leq 0.39$) between all the data for both the two sides together. A poor correlation ($0.18 \leq r \leq 0.26$) for the fMRI data was found, while nice correlations coefficients were found for the gait data ($r \geq 0.99$), this could highlight that most of the changed occurred in the brain activation patterns rather than in the gait.

Table 3.27: SP3: Correlation values (r) for the Pre-Post analysis of the fMRI and gait analysis data.

SP3	fMRI and Gait data r value	fMRI data r value	Gait data r value
Pre and Post – Cl and IL sides	0.34	0.99	-0.99
Pre and Post – CL side	0.21	0.99	-0.99
Pre and Post – IL side	-0.99	0.49 -	0.97

As regards SP3, the categorical variables correlation analysis between fMRI and gait data showed a poor correlation ($0.21 \leq r \leq 0.34$) between all the data for both the two sides together and for the contralateral-affected side, a poor correlation (r=0.49) for the fMRI data only of the ipsilateral side was found. Nice correlations coefficients were found for the gait data and for the remaining fMRI data ($r \geq 0.97$).

Table 3.28: SP4: Correlation values (r) for the Pre-Post analysis of the fMRI and gait analysis data.

SP4	fMRI and Gait data r value	fMRI data r value	Gait data r value
Pre and Post – Cl and IL sides	0.89	0.89	0.99
Pre and Post – CL side	0.84	0.80	0.99
Pre and Post – IL side	0.99	0.99	0.99

SP4 correlation results showed good correlation coefficients ($r \geq 0.80$) for both the fMRI and gait analysis results, suggesting that the overall picture before and after the EMG BFB treatment did not change significantly, a lower correlation (r=0.80) was found for the fMRI data of the affected side.

The results of the quantitative correlation analysis as described in section 3.5 are summarized below. As regards to gait analysis, for each subject the Pearson correlation coefficients (r) between the values of the first index for allthe parameters were evaluated. In particular for each subject the correlation between the first index of the following parameters was evaluated:

the IL and CL limb; the walking at SS and F speed, the IL and CL limb for the SS speed (N CL–OL); the IL and CL limb for the F speed (F CL–OL); the walking at SS and F speed for the CL side (CL N–F), and the walk at SS speed for the IL side (IL N–F). For the third and forth subject only the correlation between the SS speed and the F speed was evaluated (as the IL data were missing). Results are shown in Table 3.29.

Table 3.29: Correlation values (r) between gait analysis first indices results.

Subject	**CL–IL**	**SS–F**	**SS CL–IL**	**F CL–IL**	**CL SS–F**	**IL SS–F**
SP1	0.89	0.80	0.61	0.99	0.93	0.67
SP2	-0.17	0.38	0.98	-0.95	-0.99	0.95
SP3	n.a	0.89	n.a.	n.a.	0.89	n.a.
SP4	n.a.	-0.17	n.a.	n.a.	-0.17	n.a.

The results gave the same information of what it was observed from the individual parameters results. For SP1 the recovery was very similar for both the limbs (CL-OL), an higher r value was found for the F speed data (F CL–OL), the recovery was not uniform at different speeds (SS–F) major differences were found for the ipsilateral side (IL SS–F). SP2 showed a weak negative correlation between the limbs, confirming higher improvements for the unaffected side than for the affected one. Focusing on the correlation coefficients related to the different speeds: for the SS speed both limbs showed a similar improvement (N CL–OL=0.99), while for the F speed the correlation became negative(F CL–OL=-0.95). Furthermore the correlation between the two speed improvements (SS–F) was weak. The correlation coefficient for SP3 showed similar changes for the affected limb at different speeds (CL N–F), while for SP4 different changes were found, showing higher improvement for the affected limb at SS speed than at F speed.

As regards the fMRI data for each subject the Pearson correlation coefficients (r) between the values of the first index for all the parameters were

evaluated. To be more precise, for each subject the correlation between the first index of the following parameters was evaluated: the CL and IL side (CL–IL), the passive task and the active task (P–A), the CL and OL side for the passive task (P CL–IL); the CL and OL side for the active task (A CL–IL), the passive and active task for the CL side (CL P–A), and the passive and active task for the IL limb (IL P–A). Results are shown in Table 3.30.

Table 3.30: Correlation values (r) between fMRI first indices results.

Subject	**CL–IL**	**P–A**	**P CL–IL**	**A CL–IL**	**CL P–A**	**IL P–A**
SP1	0.19	0.67	-0.99	0.54	-0.13	0.83
SP2	-0.56	0.98	-0.90	-0.82	0.89	0.99
SP3	-0.64	0.66	-0.94	-0.87	0.91	0.91

These results confirmed that the neural patterns changes were different if the ankle dorsi-plantarflexion was performed either with the affected or the unaffected side (CL-IL): SP1 showed a nice negative correlation for the passive task, and a weak correlation for the active task. SP2 and SP3 showed a nice negative correlation higher for the passive task. Minor changes (higher r values) were found comparing the changes between the passive and active tasks (P–A), in particular, SP2 showed a strong correlation. So the first quantitative correlation analysis confirmed that the different fMRI and gait acquisitions were suitable for this study. In fact, the results obtained by different tasks did not show strong correlation, confirming that the information carried by the fMRI and gait data were related to different aspects of the motor and neural recovery.

The second quantitative correlation analysis wanted to test if the therapy induced a consistent recovery among the patients. The Pearson correlation matrix evaluated between the first indices values for each couple of the four subjects for the gait analysis parameters are shown in Table 3.31.

Table 3.31: Correlation values (r) between the patients data of the gait analysis results.

Subject	SP1	SP2	SP3	SP4
SP1	1	0.23	0.08	0.79
SP2	0.23	1	-0.04	-0.88
SP3	0.08	-0.04 -	1	-0.004
SP4	0.79	-0.88 -	-0.004	1

The results showed that the changes observed in the gait of SP1 were not comparable with those induced in SP2 and SP3. SP4 showed a comparable gait profile with SP1 and SP2.

The Pearson correlation matrix calculated between the first indices values for each couple of the three subjects for the fMRI data are shown in Table 3.32.

Table 3.32: Correlation values (r) between the patients data of the fMRI results.

SP3	SP1	SP2	SP3
SP1	1	0.40	-0.18
SP2	0.40	1	-0.18
SP3	-0.18	-0.18 -	1

These values confirmed that the changes observed for the neural activation of SP1 were comparable to those of SP2. The changes observed for the SP3 showed a poor correlation with those of the other patients. So the second quantitative correlation analysis confirmed that the EMG BFB treatment led to a not uniform recovery among the different patients both with regard to the motor outcomes,and for the neural activation patterns.

The last statistical test was performed in order to evaluate if the therapy induced the same changes both on the motor patterns and on the neural activation, which is to say if the improvements observed for the gait could

be compared and comparable to those of the brain activity. The Wilcoxon-Mann-Whitney test was performed. The p-values obtained were equal to: 0.03 for the SP1, 0.39 for the SP2, and 0.80 for the SP3. Therefore, assuming a significance level of 5%, the null hypothesis could be accepted for the SP2 and SP3, while it was rejected for the SP1. The low correlation coefficients could suggest that SP2 and SP3 exhibited similar recovery/changes both concerning the fMRI and gait analysis results, conversely the high correlation coefficient of SP1 could underline different developments as regards the two different outcomes.

3.7 Discussion and Conclusion

This thesis aimed at evaluating the correlation between the gait analysis and the neural activity of post-stroke patients before and after a rehabilitation treatment based on the use of electromyographic biofeedback. Gait analysis and functional magnetic resonance imaging data were collected from four recruited subjects, before and after the EMG BFB treatment. In order to describe in a quantitative, objective, accurate and robust way both the brain activity and the motor behavior, the standard methods and innovative techniques of investigation were adopted. The ankle dorsi-plantarflexion is an integral and dominant component in gait, as walking is not feasible during fMRI, the ankle dorsi-plantarflexion was adopted as a motor paradigm, the brain activity during the execution of this task was evaluated and then compared with a subset of the ankle kinematic and dynamic parameters, derived from the gait analysis. Three gait analysis indices were adopted: the first one evaluated the effect of time on the difference between each parameter value and the normative reference bands: a negative value represented a recovery

of the motor function, as the values became closer to the normative bands. The second index tried to quantify the effect of the rehabilitation treatment on the walking at self selected and fast speed, while the third index aimed at determining whether any recovery was due to any improvements related to the affected limb movement or to a compensatory strategy of the unaffected limb. As regards the first index the first patient showed improvements in both the ankle power peak and its timing of onset associated to an increasing energy absorbed by the ankle. The second index showed that the patient recovery was more evident for the walking at self selected speed than for the fast speed. The third index showed that the paretic limb had a pattern more similar to the normative bands. In agreement with the first patient, patient number two showed improvements both in the ankle power peak and its timing, again associated with an increased ankle energy absorption. The second index showed an homogeneous recovery process at different speeds, and a different functionality of the two limbs was assessed by the third index. The third subject indexes of gait did not show significant differences between the values measured before and after rehabilitation treatment. The fourth patient showed improvements as regards the ankle power peak value and onset timing, with an increment of the energy absorption, the improvements involved bot the walking at self selected and fast speed.

In order to analyze the brain activation maps from the fMRI data, the GLM method was first adopted. For some tasks of the first subject, no active areas were found this maybe was due to the patient inability to correctly perform the movement and to follow the experimental design: the recorded signals could have a time course different from the hemodynamic response expected from the set experimental design, so that in this case the GLM method could fail: the compensatory movements involving the leg, the

thigh, and sometimes the upper limbs were observed mainly for the active movements and for those involving the paretic limb.

Given the limitations of the GLM, an innovative method of analysis of the coregistered and normalized images raw signal (in order to obtain comparable results from the different subjects) was adopted. This method could not be performed on the fourth patient's data because of coregistration and normalization problems. This method evaluated the average signal detected for each of the 58 ROI, which the two hemispheres were divided into. Thanks to these data, three indices characterizing the brain activity during the different tasks were evaluated. In particular the primary motor area (MI), the pre-motor area, the somatosensory area, and the cerebellum ROI were considered, as they are the most involved brain areas during motor tasks. The proposed indices evaluated the differences in neural activation during the passive or active task of the affected and of the unaffected limb. For each of the 4 ROI the difference between the average contralateral signal and the average signal ispilateral to the movement were evaluated. Based on the literature and on the control subject data the hemisphere contralateral to the movement was found to be more active than the ipsilateral side. By incrementing the sample of the control subjects this assumption could be confirmed. The first index ws evaluated as the differences of the signals detected before and after the rehabilitation treatment: a positive value showed an increment and an improvement of the difference signal between the two hemispheres. The second index was based on the time changes of the difference signal between the movement of the affected and unaffected limb. As the brain should symmetrically activate during the movement of the two limbs, a correct recovery should result in a index close to zero. The functional images of the movement of both the limbs from the control subject were not available, so thet this

second index could not be derived, a further development would be to verify also this hypothesis. The third index evaluated the percentage change of the difference signal between the active and passive task to determine which of the ROIs are involved in the voluntary movement of the ankle. This index could be evaluated also for the control subject, but no changes were revealed from this analysis, this causing a difficult to discuss and not clear interpretation. With a larger control subjects sample it would be possible to evaluate a threshold to determine a significant activation of the specific ROIs. For the first patient, the first index suggested a trend toward a normal activation and so a recovery of the brain activation patterns as regards the pre-motor and the sensorimotor areas during the movement of the contralateral side, while the activation of the motor area seems even more impaired after treatment (also detected from the activation maps). The cerebellum was characterized by uneven development: during the task B the index got worse, while during task A an improvement was observed, this could be due to the increasing role of the cerebellum by means of an adaptation of the motor pattern to the different external conditions and it appeared to be more relevant during the active task. In agreement with the first index results, the second index showed a generalized recovery of the brain activation, with exception of the motor area during the passive movement. The third index showed significant variations especially as regards the motor area, but only during the paretic limb movement, and with regard to the cerebellum. The overall picture seemed to confirm that these two ROIs were the most involved during the execution of the voluntary task. The first index of the second patient suggested that after the rehabilitation protocol, the activation of the brain areas decreased during the execution of the movement with the affected limb (as seen also with the activation maps). Considering the unaffected limb the

motor area activation seemed not to change, while the other areas showed a greater activation. The second index highlighted a decrement of the motor area activation, while there are no significant changes in the activation of the remaining areas. The third index, in agreement with the first subject, showed an increased involvement of the motor area and the cerebellum ROI during the passive task. As regards the third subject the first index showed the activity of the pre-motor, sensory motor and motor areas assumed pathological values during the execution of the movement with the paretic limb, and a normal activity for the unaffected side. In complete contrast to the first index, the second index suggested an improved brain activation: the index is negative for all the ROIs considered, with the only exception of the motor area especially during task A. The third index had higher values than those found for the other subjects, it could suggest a greater involvement larger areas of the brain, while the activation maps highlighted a more confined activation during task A.

The gait analysis results showed that the EMG BFB treatment could cause different outcomes: the first, the second, and the fourth subjects seemed to have a more correct recovery of the motor patterns, the third patient seemed not to show great changes. Depending on the subject the EMG BFB treatment was able to improve both the walking at self selected and fast speed, but for the fast speed the patients seemed to use compensatory strategies, improving the use of the unaffected limb to overcome their motor difficulties. In agreement with the gait outcomes, also the fMRI results highlighted different rehabilitation processes between the subjects. For the first subject an overall neurological recovery was found, suggesting a possible relearning of the motor functions, in agreement with the related gait analysis data. More precisely, the changes in the activation patterns could

suggest that the unaffected part of M1 was active during the execution of the movement of both the limbs, trying to accomplish the task of the affected side. As regards the second subject, the results showed a different neurological picture after the rehabilitation therapy. The patient seemed to use mainly the unaffected hemisphere of the brain, this could be in agreement with the gait analysis results, which showed the improvement in the motor outcome, basically due to a compensatory strategy of the unaffected limb, which could be reflected by the activation of the unaffected hemisphere. The third subject did not show an improved brain activation.

As regards the relationship between the gait analysis and fMRI data, the changes over time of the relative indices were found to give the same information as regards the second and for the third subject ($p \geq 0.39$), on the contrary, for the first subject the Wilcoxon Rank Sum Test showed a different behavior between the gait and fMRI results, or maybe it suggested a different consequences of the EMG BFB treatment with respect to the central and to the peripheral nervous system. More appropriate statistical tests will be developed and refined once a larger sample of subjects will be available. The qualitative correlation analysis showed that before and after the EMG BFB treatment the changes were mostly related to the fMRI data than to the gait results for all the patients, while the quantitative correlation results showed for the third subject had a poor correlation ($r \leq 0.08$), with the other two subjects, thus indicating that maybe the therapy did not determine the same observed improvements of the first two patients.

In conclusion these preliminary results show that the stroke patients exhibited altered cerebral activation with respect to the control subject, when requested to actively move the ankle of the paretic leg, especially before the EMG BFB treatment. After the rehabilitation treatment changes in brain

activation patterns were found, especially during the active task. These brain functional changes may represent a compensatory strategy designed to maintain a normal performance despite scattered brain lesions. The EMG BFB rehabilitation treatment seemed to improve the neural activation patterns, showing a possible motor re-learning. With regard to the motor area, the activation pattern could suggest that the healthy part of M1 was active during the execution of the task of both the limbs, trying to balance the role previously carried out by the injured area. From the observed values for the control subject and the patients, the cerebellum seemed to be most relevant area between those considered, which was most involved during the execution of the voluntary movement. The significance of this index could need further study, maybe trying to analyze the time evolution.

As regards gait analysis an increased ankle power peak and a more correct power peak onset timing suggested that the overall motor performance improved.

Preliminary correlation analysis revealed that most of the changes were observed for the fMRI data, while gait analysis data did not change so much: this could be related to the possible effects BFB might have on the central as well as on the peripheral nervous system. In conclusion, the combine analysis of fMRI and gait analysis seemed to be valid. The correlation analysis performed between the different index for the different experimental conditions justified the experimental set up. Indeed the Pearson correlation coefficients highlighted a poor correlation between the different sessions. Therefore the different tasks were able to provide different information about the motor and neural recovery. The suggested gait analysis indices were able to perform a more complete characterization of the outcomes of the recovery process. In addition, the proposed method allowed to analyze the acquired fMRI data

that would not have been analyzed with the traditional techniques because of the statistical assumptions on which they rely. For the future fMRI acquisitions it would be necessary to further immobilize the patient in order to minimize the body movements. On the other hand, this way, the patient would still perform the compensatory movements, which would lead to further brain activation. Furthermore, during the early passive tasks the subjects tended to actively move or to resist, a training should be adopted in order to prevent such undesired outcomes. Finally, the protocol should be improved in order to help the patients to achieve a good timing during the active task. Furthermore the evaluation of a normative band also for the fMRI could help to better interpret the different indices and the correlation values between the motor improvements and the outcome of the fMRI. Finally both the T2 and T3 acquisitions would be necessary to assess whether any motor learning induced by the EMG BFB treatment after a short time (T2), would be able to maintain over time (T3).

These results, albeit preliminary, should be considered encouraging in terms of feasibility of the protocol and could be confirmed by incrementing the patients cohort.

Chapter 4

Wearable Technology

4.1 Introduction

Clinical assessment scales to evaluate motor abilities in stroke survivors could be used to individualize rehabilitation interventions thus maximizing motor gains. Unfortunately, these scales are not widely utilized in clinical practice because their administration is excessively time-consuming. Wearable sensors could be relied upon to address this issue. Sensor data could be unobtrusively gathered during the performance of motor tasks. Features extracted from the sensor data could provide the input to models designed to estimate the severity of motor impairments and functional limitations. In previous work, we showed that wearable sensor data collected during the performance of items of the Wolf Motor Function Test (a clinical scale designed to assess functional capability) can be used to estimate scores derived using the Functional Ability Scale, a clinical scale focused on quality of movement. The purpose of the study herein presented was to investigate whether the same dataset could be used to estimate clinical scores derived using the Fugl-Meyer Assessment scale (a clinical scale designed to assess motor im-

pairments). Our results showed that Fugl-Meyer Assessment Test scores can be estimated by feeding a Random Forest with features derived from wearable sensor data recorded during the performance of as few as a single item of the Wolf Motor Function Test. Estimates achieved using the proposed method were marked by a root mean squared error as low as 4.7 points of the Fugl-Meyer Assessment Test scale.

4.1.1 Stroke and Wearable Sensors

Each year about 800,000 people suffer a stroke in the United States alone [129]. Stroke survivors are affected by impairments and limitations of cognitive, language, perceptual, sensory, and motor functions [130]. Rehabilitation interventions are designed to address these impairments and functional limitation. The design of individual rehabilitation programs that target subject-specific motor impairments and functional limitations is of paramount importance to optimize the outcomes of rehabilitation on a subject-by-subject basis.

Clinical Scores Assessment

Several clinical assessment scales have been developed to capture motor impairments and functional limitations in stroke survivors. These scales are based on the observation of a subjects' motor behavior. In the following, we focus on a few of these scales that have been broadly used in stroke rehabilitation. The Wolf Motor Function Test (WMFT) is a clinical scale designed to assess subjects' functional ability. The Functional Ability Scale (FAS) is a clinical scale that captures quality of movement. This scale is based on the observation of a subjects' motor behavior while they perform motor tasks that are part of the WMFT. The Fugl-Meyer Assessment (FMA)

scale is a clinical scale designed to evaluate motor impairments [131].

- **Wolf Motor Function Test** The WMFT quantifies upper extremity movement ability through timed single or multiple-joint motions and functional tasks. The test contains 15 timed and 2 strength tasks (task 7-lifting the weighted limb and task 14 - grip strength, which are scored independently from the rest of the scale). The 15 timed tasks are arranged in order of complexity and performed sequentially: they progress from proximal (shoulder) to distal joints (hand), testing the ability of performing specific movements (e.g. pinch grip), the quality and the speed of such movements [132, 133]. The sequence of the tasks is thought in order to begin selecting simple movements at the shoulder joint, while ending with more complex but functionally relevant tasks, such as turning a key in a lock [133]. Tasks 1 to 6 of the WMFT involve timed joint-segment movements, and tasks 7 to 15 consisted of timed combined functional movements.

- **Functional Ability Scale** Quality of movement during the performance of the 15 timed motor tasks of the WMFT is assessed by using the Function Ability Scale (FAS). The FAS is a six-point scale, where a score of 0 indicates inability to perform the task, while a score of 5 indicates that the task was performed in an ideal way [133], so the FAS is a 75-total point scale. This scale focuses on upper limb motor behavior including movement quality, stage of motor recovery, and use of compensatory movement strategies.

- **Fugl-Meyer Assessment** The Fugl-Meyer Assessment (FMA) is a test based on 155 items designed to assess motor impairments, the FMA test assesses voluntary movement, reflex activity, grasp, and co-

ordination. This clinical scale focuses on multi-joint movements and synergy patterns [134]. Patients are asked to perform movements that are considered to reflect the sequential stages of flexion-extension synergies, and the ability to perform selective movements [135]. The FMA uses a three-point ordinal scale: 0 indicates that the item was not performed, 1 indicates that the item was performed partially, and 2 indicates that the item was performed completely. For this study we considered the upper extremity section of the FMA, which consists of 33 items representing specific movement components; the maximum score achievable for this section of the FMA is 66, inferring optimal recovery.

Both the FAS and the FMA are organized in sections that focus on specific joints (shoulder, elbow, forearm, wrist, and hand), 4.1 shows a summary of the main sections of these two scales.

Unfortunately, the administration of these scales is time-consuming. Given the limited time available for rehabilitation interventions in stroke survivors, therapists often favor increasing the time devoted to therapy at the cost of not performing longitudinal assessments of motor abilities.

Wearable sensors could be used to address this problem [136, 137], they represent a cheap and accurate way to assess movement during motor tasks, by monitor patients' movements in a real-life setting.

Previous studies by our team showed that wearable sensor data can be used to estimate clinical scores of movement ability [138, 139]. Specifically, we collected accelerometer data during the performance of a set of motor tasks selected among the WMFT items, we segmented the data and estimated data features that captured important characteristics of movement patterns observed in stroke survivors (e.g. jerkiness of movement), and we estimated

Table 4.1: Description of the sections of the functional ability scale (FAS) and the Fugl-Meyer clinical (FMA) scores.

Score Section	**Task-Items**	**Range**
Total FAS	1-6, 8-13, 15-17	0-75
Arm FAS	1-6, 8, 17	0-40
Hand FAS	9-13, 15-16	0-35
Total FMA	1-33	0-66
Shoulder–Elbow–Wrist–Hand FMA	3-17, 19-30	0-54
Shoulder–Elbow FMA	3-17	0-30
Shoulder FMA	3-5, 6, 9, 13, 15-16	0-16
Elbow FMA	7-8, 10, 11-12, 14, 17	0-14
Wrist–Hand FMA	19-30	0-24
Wrist FMA	19-23	0-10
Hand FMA	24-30	0-14
Extra12 FMA	1, 2, 18, 31-33	0-12

the total FAS score or each subject undergoing assessment [139]. Results showed that it is possible to achieve estimates of the total FAS score from the analysis of wearable sensor data with a bias of only 0.15 points and a standard deviation of only 2.36 points of the FAS scale.

The purpose of the study herein summarized was to assess if the methodology we previously developed to estimate FAS scores [139] could be extended to the estimation of FMA clinical scores. In other words, we tested the hypothesis that wearable sensor data collected during the performance of motor tasks that are part of the WMFT are suitable to estimate FMA scores.

4.2 Materials and Methods

In order to estimate the FMA scores from the WMFT data we tried to adopt two different methods (see Figure 4.1).

The first one tried to use directly the FAS scores relying on the correlation and the simple linear regression between FAS scores and FMA scores for the FMA scores estimation. The second one try to use the wearable sensor data using the previous proposed algorithm [139], which consists of the following steps: 1) processing by filtering the accelerometer data; 2) derive data segments corresponding to movement components (i.e., reaching, manipulation, and release/return); 3) extract features from the accelerometer data; 4) rank and select features using the ReliefF Algorithm [140] in order to minimize the overlap among classes associated with different clinical scores; and 5) use Random Forests Regression to estimate the FMA clinical scores of movement impairments [141]. The clinical and experimental procedures are detailed described below.

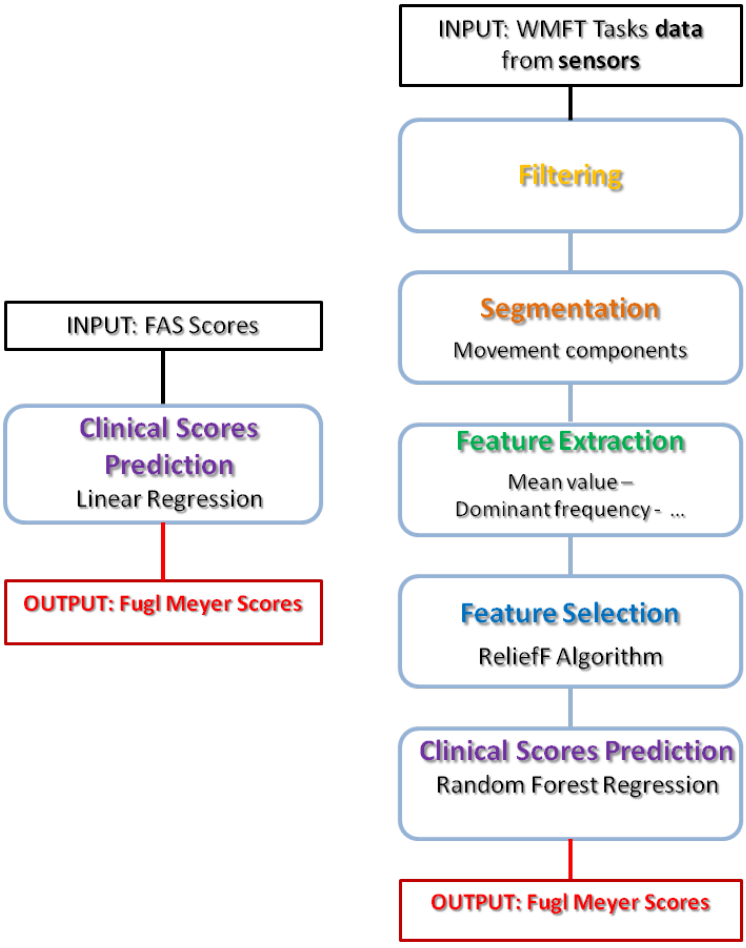

Figure 4.1: Scheme of the two different Methods: Method number one (on the left) and Method number two (on the right).

4.2.1 Subject Recruitment and Clinical Assessment

Twenty-four stroke survivors (mean age: 57.5 11.8 years old, mean years post stroke: 4.2 3.7 years) with residual upper limb weakness (hemiparesis) participated in the study. All experimental procedures were performed according to a protocol approved by the Spaulding Rehabilitation Hospital Internal Review Board. Each subject underwent the WMFT and was evaluated by a clinician using standardized clinical motor performance scales, including the FAS and the FMA (see chapter 4.1). The WMFT consists of 15 timed and 2 strength tasks. The strength tasks are scored independently from the rest of the scale. The 15 timed tasks are arranged in order of complexity, progressing from proximal (shoulder) to distal joints (hand). Quality of movement during the performance of the 15 timed motor tasks of the WMFT is assessed by using the FAS. The FAS is a 75-point scale (see chapter **??**). The FMA is a test designed to assess motor impairments, this clinical scale focuses on multi-joint movements and synergy patterns [134]. The FMA uses a three-point ordinal scale: 0 indicates that the item was not performed, 1 indicates that the item was performed partially, and 2 indicates that the item was performed completely. In this study, we considered the upper extremity section of the FMA, which consists of 33 items. The maximum score achievable for this section of the FMA is 66 (see chapter 4.1). The patients were asked to make movements that are considered to reflect the sequential stages of flexion-extension synergies, and the ability to perform selective movements [135].

4.2.2 Data Collection

Subjects were clinically evaluated for all 15 motor tasks of the WMFT. Sensor data was collected for a subset of eight tasks, the chosen eight motor tasks were shown to capture the main aspects of the FAS [139]. The subset of tasks was dived into two sets of items. Items in the first set were referred to as Reaching Tasks and consisted of item 1 (forearm to table-side), item 4 (extend elbow-weight), item 5 (hand to table), and item 8 (reach and retrieve). Items in the second set were referred to as Manipulation Tasks and consisted of item 9 (lift can), item 10 (lift pencil), item 13 (flip cards) and item 15 (turn key in lock).

Data collection was performed using six accelerometers placed on the affected arm and the trunk. Accelerometers on the hand, forearm, and upper arm were biaxial whereas accelerometers on the index finger, thumb, and sternum were uniaxial (Figure 4.2).

The sensor data was recorded using the Vitaport 3 (Temec BV, The Netherlands) ambulatory recorder but the use of accelerometers is compatible with a wearable sensor implementation of the system, which is our target goal. Therefore, the study should be considered a test of feasibility of an application of wearable sensors. Subjects performed multiple repetitions of each task (between 5 and 20), according to the patients' ability to perform the task and to the difficulty of the task itself.

4.2.3 Data Analysis

FMA scores could be estimated either by 1) first estimating FAS scores via the analysis of wearable sensor data and then relying on the correlation between FAS scores and FMA scores to estimate the FMA scores or by

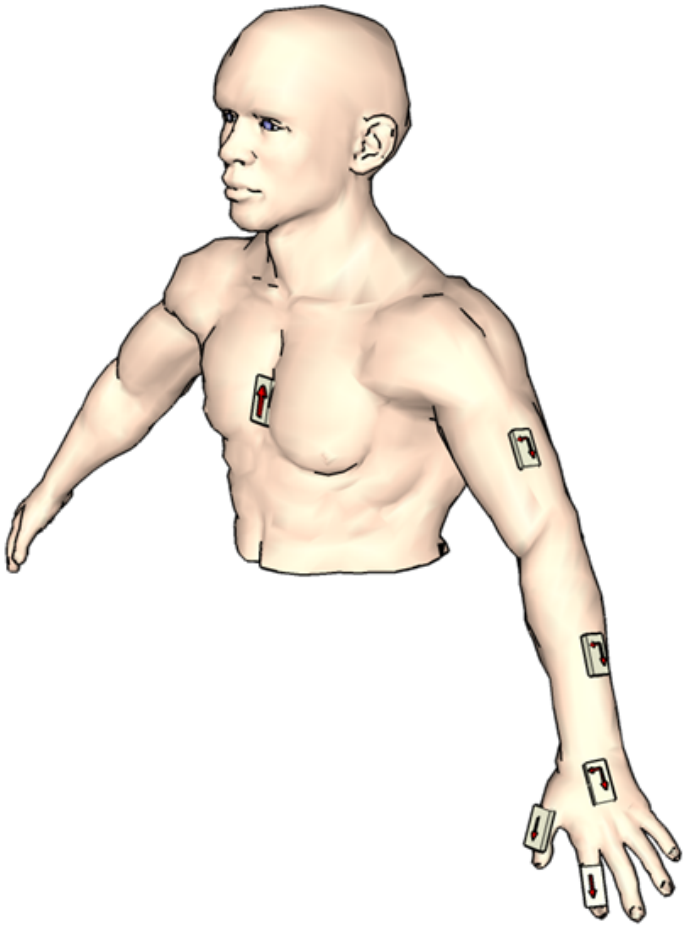

Figure 4.2: Scheme of sensors positioning and axes orientation.

2) developing an algorithm that estimates the FMA scores directly from wearable sensor data. In all the analyses reported below, we focused on estimating the FMA total score.

To compare the above-mentioned approaches, we first assessed the correlation between the FAS total score as well as the scores for sections of the FAS and the FAM total score. Then, we estimated the linear regression line relating sections of the FAS and the FAM total score to estimate the FAM total score given an FAS score. We derived FAM total score estimates and characterized them by means of deriving the root mean squared (RMS) error value of the estimated FAM total scores given that actual scores were known. We set the RMS error values achieved via the method described above as values we had to improve upon to make it worth estimating the FMA scores directly from wearable sensor data. Next, we analyzed the accelerometer data using the method described below, which was designed as an extension of previous algorithms we developed to estimate FAS scores based on the analysis of wearable sensor data [139].

4.2.4 Data Processing, Segmentation and Feature Extraction

Accelerometer time series were low-pass filtered with a cut-off frequency of 15 Hz to remove high frequency noise, and then high-pass filtered with a cut-off frequency of 1 Hz to isolate the acceleration components due to postural adjustments. Both the low-pass and high-pass filtered versions of the data were utilized in the analysis.

Data were segmented to isolate the different movement components that constitute each motor task performed as part of the selected items of the WMFT. The segmentation was performed using digital marks introduced

during the data collection to identify the beginning and the end of each task's repetition, the segmentation of the movement components for the Manipulation Tasks was performed through an additional touch sensor which allowed to detect the contact between the hand of the subject and the object (i.e., the can, the pencil, etc.). The segmentation of Manipulation Tasks consists of detecting three movement components: segment 1 (S1) is the reaching movement component of the task, segment 2 (S2) is the manipulation movement component of the task and segment 3 (S3) is the release/return movement component of the task. Subjects performed between 5 and 20 repetitions of each task according to the nature of the motor task. Subjects performed between 5 and 20 repetitions of each task according to the nature of the motor task. Table 4.2 lists the features extracted from the accelerometer data to capture aspects of movement of interest such as speed, smoothness and coordination.

These features were chosen based on a previous pilot work that allowed us to identify accelerometer data features showing correlation with clinical measures of functional capability [138]. All the features, except the mean value of the accelerometer time series, were derived from a high-pass filtered version of the accelerometer data (with cutoff frequency equal to 1 Hz). All features (except the correlation coefficients) were derived for each axis of the six accelerometers used for the data collection. The correlation coefficients were estimated using the following sensors: forearm and upper arm, hand and forearm, thumb and index finger, thumb and forearm, hand and index finger, forearm and index finger, sternum and upper arm, and sternum and forearm. As regards the Reaching Tasks, features were extracted from the single data segment associated with each of the tasks thus leading to a total of 171 features. on the other hand, for the Manipulation Tasks, features were

Table 4.2: List of the features extracted from the accelerometer data.

Feature extracted
Mean value
Root-Mean-Square value
Dominant frequency
Ratio of energy in 0.2 Hz bin around the dominant frequency to total energy
Range of auto covariance
Root-Mean-Square value of the jerk time series (derivative of acceleration)
Dominant frequency of the jerk time series
Ratio of energy in 0.2 Hz bin around the dominant frequency of jerk to total energy
Peak velocity
Jerk metric (the RMS jerk normalized by the peak velocity)
Approximate entropy
Correlation between pairs of accelerometer time series
Peak correlation within a 1 s window between pairs of accelerometer time series
Lag time of the peak correlation between pairs of accelerometer time series

extracted for each segment (S1, S2, and S3) thus for a total of 513 features. Every repetition of each task was considered an instance. Features derived from all the repetitions performed by all the subjects for a particular motor task were combined together to form a single dataset. Eight datasets, one for each motor task, with different number of instances and features were built. In order to be able to combine the different datasets the SMOTE technique for unbalanced dataset was adopted [142], we built matrices with the same maximum number of instances for each subject. The SMOTE over-sampling approach over-samples the minority class by creating 'synthetic" examples rather than by over-sampling with replacement. The class is over-sampled by taking each class instance and introducing synthetic examples along the line segments joining any/all of the k instances nearest to the neighbors. Depending upon the amount of over-sampling required, the neighbors from the k nearest neighbors are randomly chosen. The implementation we used adopted the five nearest neighbors as suggested in [142]. Synthetic samples are generated by taking the difference between the feature vector of the instance under consideration and its nearest neighbor. The difference is multiplied by a random number between 0 and 1, and added to the feature vector under consideration. This causes the creation of a random point along the line segment between two points in the features space.

4.2.5 Feature Selection

The features from each task were imported into the Waikato Environment for Knowledge Analysis (WEKA) for exploratory analysis. Then we performed feature selection in order to build linear regression models to explore their ability to estimate the clinical scores as well as to examine which feature sets were useful in predicting the scores. The top 10, 20, 30, 40 and 50

features from each of the 8 tasks were selected by the ReliefF feature selection algorithm.

- *ReliefF Algorithm*: The ReliefF algorithm ranks the attributes according to their decreasing importance [140], that is to say according to their ability to maximize the separation among classes associated with different clinical scores. More in details for every instance the algorithm updates the weights assigned to a feature at each iteration. For each instance, the K nearest neighbors from the same class (called nearest hits H), and K nearest neighbors from each of the other classes (called nearest miss M) are searched. Then, the quality of estimation for each attribute is updated and the algorithm moves to the next instance. For our analysis the WEKA implementation of the algorithm was used, the number of nearest neighbors K was set to 10 [143].

4.2.6 Clinical Scores Prediction

To derive estimates of the FMA total scores, we chose to use a regression implementation of the Random Forest method [141].

- *Random Forests*: Random Forests consist of a set of decision trees that are generated via an iterative procedure that is based on the use of a randomized/bagged selection of features at each split, which are replaced at each iteration of the algorithm [141]. We set the number of trees of the Random Forests to 100 [139]. Random Forests were trained and tested using a 10-fold cross-validation method [141].

Table 4.3: Correlation Coefficient and RMS Errors between the different sections of the FAS and the FMA.

FAS Scores	FMA Scores	R Value	RMSE	FMA Score Range	FMA Score Range for Subjects Tested
Total FAS	Total FMA	0.85	6.99	0–66	22-66
Total FAS	Shoulder-Elbow FMA	0.66	3.91	0–30	15–30
Total FAS	Wrist-Hand FMA	0.9	3.14	0–24	1–24
Total FAS	Wrist FMA	0.73	2.23	0–10	0–10
Total FAS	Hand FMA	0.87	2.29	0–14	1–14
Total FAS	Shoulder-Elbow-Wrist-Hand FMA	0.87	5.69	0–54	17–54
Total FAS	Extra 12 FMA	0.63	1.96	0–12	2–12
Arm FAS	Total FMA	0.84	7.25	0–66	22-66
Arm FAS	Shoulder-Elbow FMA	0.71	3.70	0–30	15–30
Arm FAS	Wrist-Hand FMA	0.85	3.85	0–24	1–24
Arm FAS	Wrist FMA	0.73	1.93	0–10	0–10
Arm FAS	Hand FMA	0.79	2.89	0–14	1–14
Arm FAS	Shoulder-Elbow-Wrist-Hand FMA	0.85	5.99	0–54	17–54
Arm FAS	Extra 12 FMA	0.63	1.95	0–12	2–12
Hand FAS	Total FMA	0.66	7.83	0–66	22-66
Hand FAS	Shoulder-Elbow FMA	0.59	4.22	0–30	15–30
Hand FAS	Wrist-Hand FMA	0.90	3.20	0–24	1–24
Hand FAS	Wrist FMA	0.72	2.28	0–10	0–10
Hand FAS	Hand FMA	0.88	2.24	0–14	1–14
Hand FAS	Shoulder-Elbow-Wrist-Hand FMA	0.83	6.37	0–54	17–54
Hand FAS	Extra 12 FMA	0.58	2.06	0–12	2–12

4.3 Results

Correlation coefficients estimated by using different sections of the FAS and the FMA Total score ranged between 0.66 and 0.85. The highest value was found for the correlation between the FAS total score and the FMA total score. The lowest value was found for the correlation between the hand section of the FAS and the FMA total score. Considering the FMA Shoulder-Elbow section the highest correlation coefficient was found with the FAS Arm (0.71) and the lowest value was found using the FAS Hand (0.59). While the FMA Wrist-Hand correlations coefficient ranged from 0.84 to 0.90 (See Table 4.3).

When estimates were then derived using the regression line relating scores

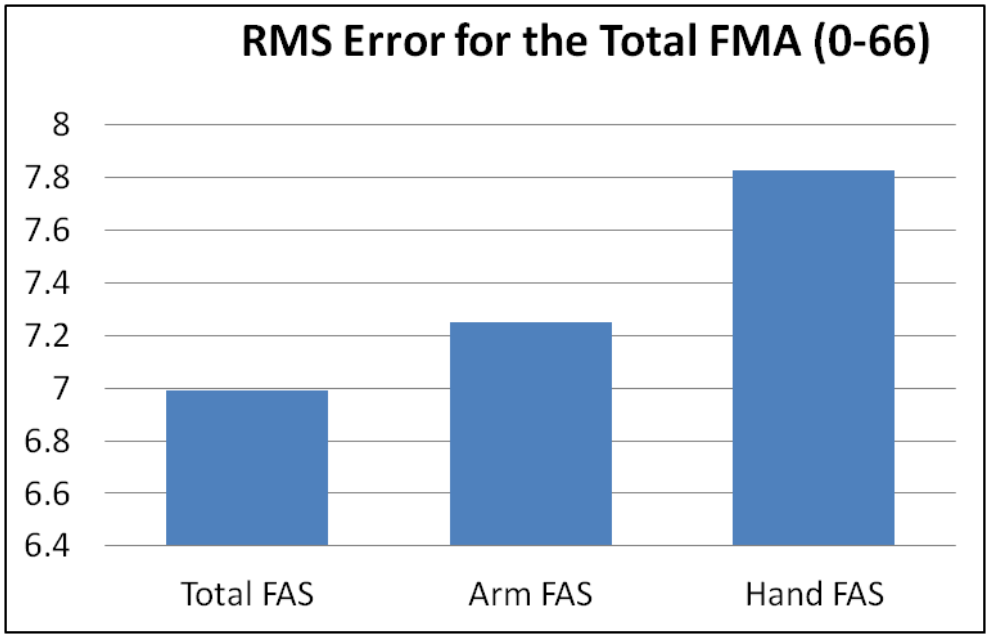

Figure 4.3: RMS Error obtained for the estimates of the Total FMA using the three sections of the FAS.

for the FAS scale (Total and sections of the scale) and the FMA Total score, we observed RMS errors equal to 6.99, 7.25, and 7.83 points of the FMA scale when we used the FAS total score, the FAS arm section and the FAS hand section respectively (Figure 4.3).

It is worth emphasizing that these RMS error values exceed 10% of the FMA upper extremity score range (0-66 points) and is relatively large considering the range observed in patients participating in the study (22-66 points). RMS errors for the Total section of the FMA derived from the Total, Arm and Hand sections of the FAS are shown in 4.4.

It is also worth emphasizing that the regression between the FAS scores derived for each WMFT item and the FMA total scores has not meaning due to the limited range spanned by FAS scores for a single WMFT item (0-5) compared with the 66 points of the upper extremity FMA total score.

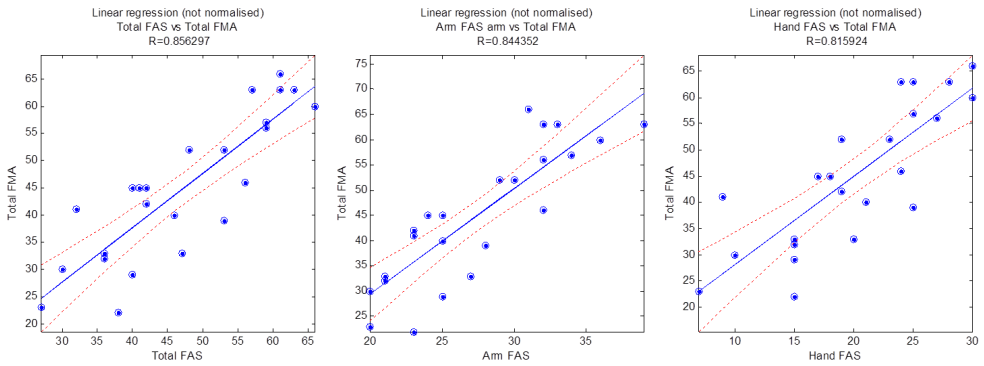

Figure 4.4: Linear Regression between the Total FMA scores and the the three sections of the FAS scores.

Results derived by estimating FMA total scores using wearable sensor data are summarized in 4.5 and 4.6.

The plots shows the RMS error values marking the FAM total score estimates derived from the selected 8 items (4.5) of the WMFT and also including the different sections of the manipulation tasks (WMFT #9, #10, #13 and #15) (Figure 4.6). Results are provided for different numbers of selected features ranging from 10 to 50. Differences in RMS error values marking the FMA total score estimates were found to be lower for certain item of the WMFT (e.g. items 1, 9, and 13) than others (e.g. items 4 and 8) and for different sections (e.g. the manipulation section (section 2) and the reaching sections appears to give better results respect to the retrieving ones). RMS error values appear to decrease significantly when using 20 features compared to using 10 features. Changes in RMS error values when using a larger number of features (30 to 50) appear to be marginal.

Table 4.4 shows the RMS error values marking the FMA total score estimates derived using wearable sensor data from each of the 8 selected items of the WMFT. The best results were achieved using wearable sensor data collected during the performance of items 1, 9, and 13 of the WMFT.

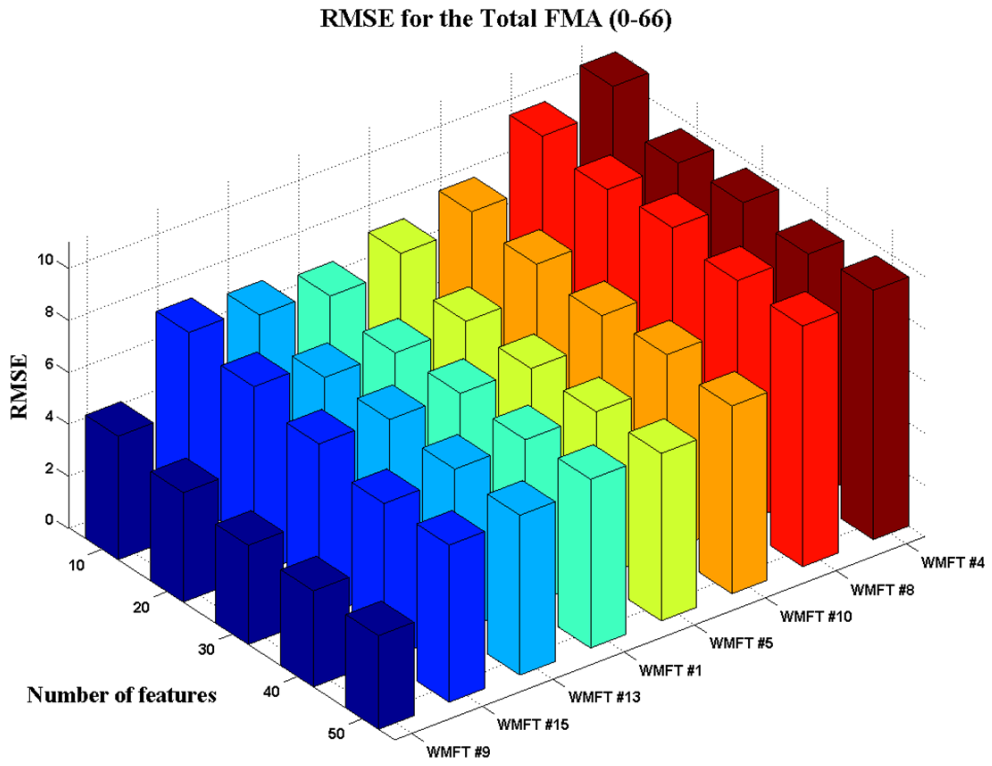

Figure 4.5: Effect of different number of features and choice of WMFT item on the RMS error marking the FMA total score estimates.

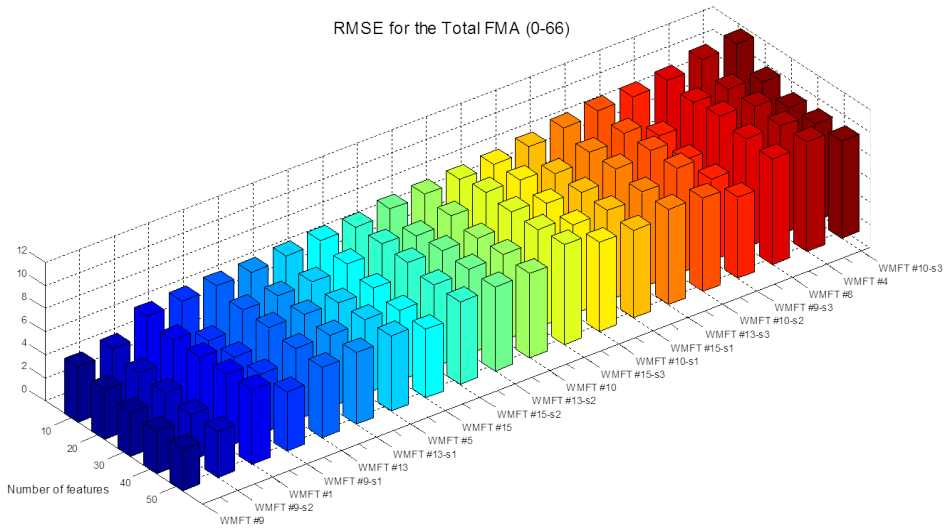

Figure 4.6: Effect of different number of features and choice of WMFT item and sections on the RMS error marking the FMA total score estimates.

Table 4.4: RMS Errors marking the FMA total score estimates derived from the eight selected WMFT items, using 20 wearable sensor data features.

Task	**RMSE Total FMA (0-66)**
	20 features
WMFT item #1	6.33
WMFT item #4	9.64
WMFT item #5	6.72
WMFT item #8	9.61
WMFT item #9	4.27
WMFT item #10	7.83
WMFT item #13	6.62
WMFT item #15	7.13

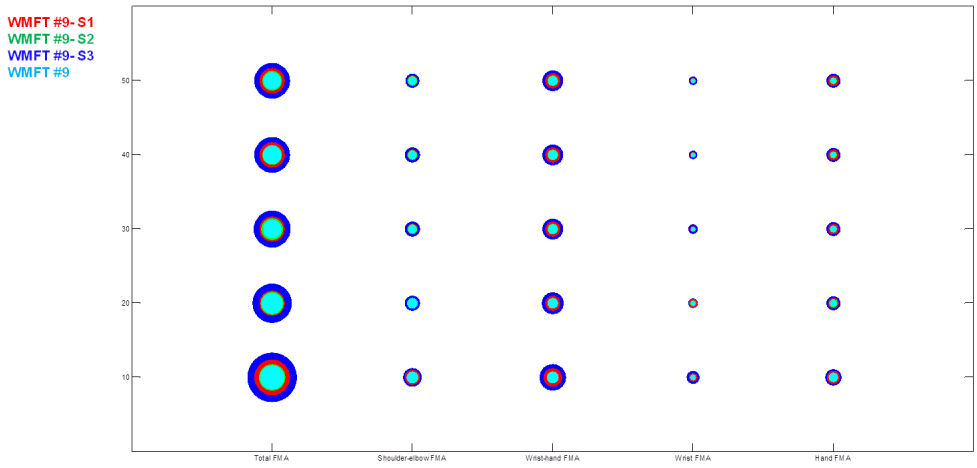

Figure 4.7: RMS error for the Total FMA (0-66) using ITEM #9 and the different section (Reaching–Manipulation–Retrieve).

Focusing of the item with the lowest RMS error (i.e. WMFT #9), figure 4.7 shows that the RMS errors derived using the different segments of the WMFT manipulation task #9 are still higher than the RMSE using all the information provided by using all the segments together.

The estimates given by the item #9 data versus the real scores of the Total FMA (0-66) for the 24 patients are shown in 4.8.

The errors of the estimated different sections of the FMA appeared to be randomly distributed and uncorrelated across the different sections of the FMA, so adding the estimates of the Shoulder-Elbow-Wrist-Hand and the estimated Extra 12 points to estimate the Total FMA scale we obtained better results with lower RMS errors, as expected. An example of the decrease of the RMS errors for the estimate of the Total, Shoulder-Elbow, Wrist-Hand and Shoulder-Elbow-Wrist-Hand FMA, using item #9 of the WMFT is shown in figure 4.9.

As a further step we decided to combine different tasks using the preselected features, as a result we obtained better estimates of the different

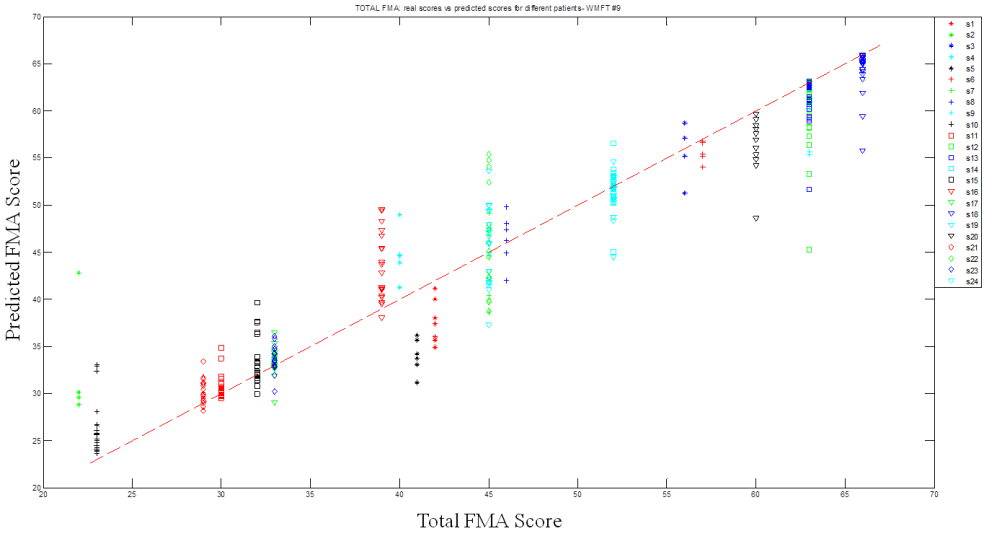

Figure 4.8: Predicted values of the Total FMA Scores vs Real Total FMA (0-66) using item #9 for the 24 subjects.

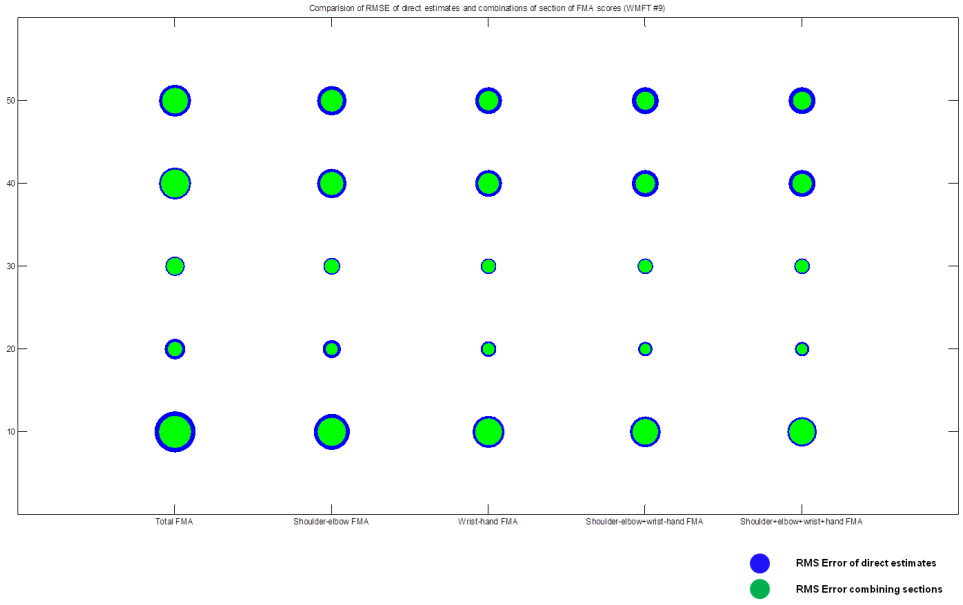

Figure 4.9: Direct estimate of the RMSE for the FMA and RMSE obtained combining different sections for the Total FMA (0-66) using WMFT #9.

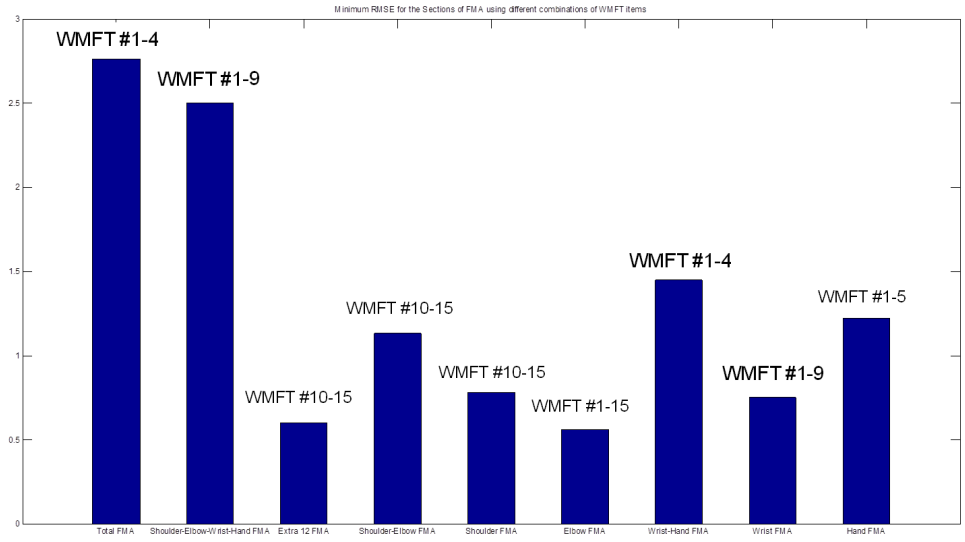

Figure 4.10: Minimum RMS Error for the different Sections of FMA using different pairs of the WMFT Items.

sections of the FMA with different pairs, it's worthy to notice that the pair WMFT #1-4 gave the best results in terms of RMS error for the TOTAL FMA (2.74) and for the Wrist-Hand FMA (1.45), if we consider the remaining FMA sections, the lowest RMS error results were achieved by the WMFT #1-9 for the Shoulder-Elbow-Wrist-Hand and Wrist FMA, the WMFT #10-15 for the Shoulder-Elbow, Shoulder and Extra 12 FMA sections, the WMFT #1-15 gave the minimum value for the Elbow section and the WMFT #1-5 for the Hand section (see figure 4.10).

Considering the Total FMA, the RMS error using all the possible combination of more than two items of the WMFT decreased using three items (WMFT #1-4-9), but was comparable to the RMS error using just items #1 and #4 as shown in figuer 4.11 (2.74 vs 2.71) and as shown before for the single items, a decrease of the RMS error was found adding different sections of the FMA score.

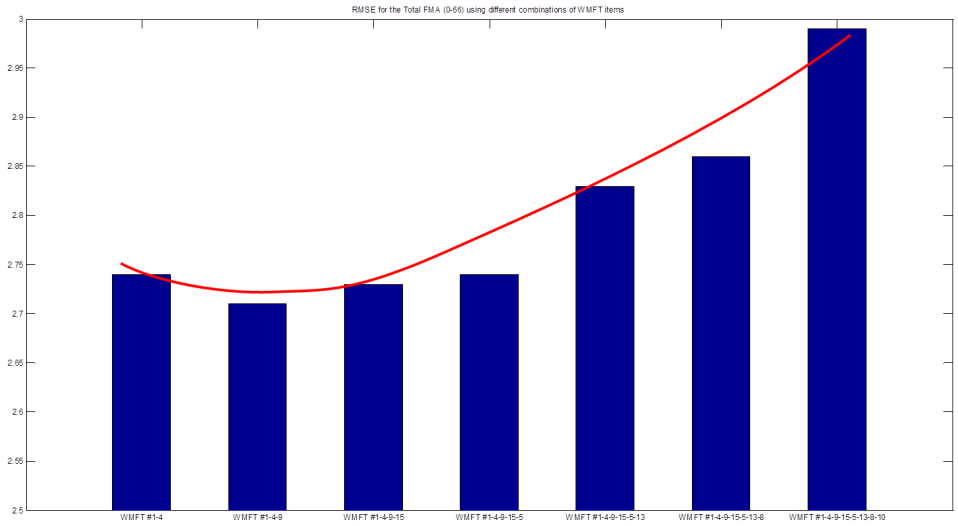

Figure 4.11: Minimun RMS Error for the Total FMA (0-66) using different combination of the WMFT Items.

The last attempt was done to find the minimum number of sensors that gave similar results to when all the 6 sensors are taken into account for the estimation of the scores. On a single item basis, table 4.5 shows the results we obtained for the Total FMA: focusing on WMFT #9 results showed to improve (RMS error 3.74) using just 5 out of the 6 sensors (placed on the Thumb, on the Hand, on the Forearm, on the Upper Arm and on the Sternum). Different trends (RMS error decreasing for WMFT #5, #9, #10, #13, #15 or slightly increasing for WMFT #1, #4 and #8) were obtained using different number of sensors (table 4.5), item #5 decreased the RMS error (6.43, less than the 10% of the Total FMA range (0-66)) using just 2 sensors placed on the Hand and on the Sternum.

While considering the combinations of items using pairs, table 4.6 shows the minimum RMSE obtained with the different sensors combinations which were gave the best results using all the six sensors. A decrease in RMSE for the Elbow section (0.50) of the FMA and the Extra 12 points of the FMA

Table 4.5: Effect of different sensors combination on the RMS Error of the Total FMA (0-66) on an item by item basis.

Task 20 features–6 sensors	RMSE Total FMA (0-66)	Number of Sensors	Sensors Combination	RMSE Total FMA (0-66) 20 features–Combination of Sensors
WMFT item #1	6.33	4	Index–Hand–Upper arm–Sternum	6.93
WMFT item #4	9.64	5	Thumb–Index–Forearm–Upper arm–Sternum	9.79
WMFT item #5	6.72	2	Hand–Sternum	6.43
WMFT item #8	9.61	2	Hand–Sternum	10
WMFT item #9	4.27	5	Thumb–Hand–Forearm–Upper arm–Sternum	3.74
WMFT item #10	7.83	3	Thumb–Index–Upper arm	7.22
WMFT item #13	6.62	4	Thumb–Hand–Forearm–Upper arm	6.54
WMFT item #15	7.13	5	Thumb–Hand–Forearm–Upper arm–Sternum	6.01

Table 4.6: Effect of the number of sensors on the RMS Error for the sections of the FMA using different combinations of WMFT pairs.

Section of FMA with Minimum RMSE	Combination of Task 20 features–Combination of Sensors	RMSE of the FMA Section	Sensors Combination	RMSE of the FMA sections 20 features
Total (0-66)	WMFT item #1-15	2.71	Index–Forearm–Upper arm–Sternum	2.74
Shoulder-Elbow-Wrist-Hand (0-54)	WMFT item #1-9	2.58	Hand–Forearm–Upper arm–Sternum	2.5
Extra12 (0-12) (0-66)	WMFT item #1-9 and #1-5	0.55	Thumb–Forearm–Upper arm–Sternum	0.6
Shoulder-Elbow (0-30)	WMFT item #1-9	1.15	Hand–Forearm–Upper arm–Sternum	1.13
Shoulder (0-16)	WMFT item #10-15	0.8	Thumb–Index–Forearm–Upper arm–Sternum	0.78
Elbow (0-14)	WMFT item #1-15	0.5	Forearm–Sternum	0.56
Wrist-Hand (0-24)	WMFT item #1-15	1.58	Thumb–Index–Forearm	1.45
Wrist (0-10)	WMFT item #1-15	0.75	Thumb–Hand–Forearm–Upper arm–Sternum	0.75
Hand (0-14)	WMFT item #1-15	0.91	Thumb–Index	1.22

(0.58) was observed using the data of just three the sensors placed on the hand, forearm and sternum.

The pair WMFT #1-15 showed the minimum RMSE for different sections: decrease in the RMSE of the Total (2.71), Wrist (0.75) and Hand (0.91) and Elbow (0.50) were observed using respectively combinations of 4, 3 or 2 sensors positioned on the hand, forearm, upper arm and sternum; on the hand, upper arm and sternum, on the thumb and index, and on the forearm and sternum. Table TOT displays the minimum RMSE results achieved with the combinations of sensors and of pairs of items, for the different FMA sections.

Focusing on the best result achieved with the use of the combination of three WMFT items (WMFT #1-4-9), we noticed that there is an increasing trend of the RMSE of the Total FMA if we consider different number of

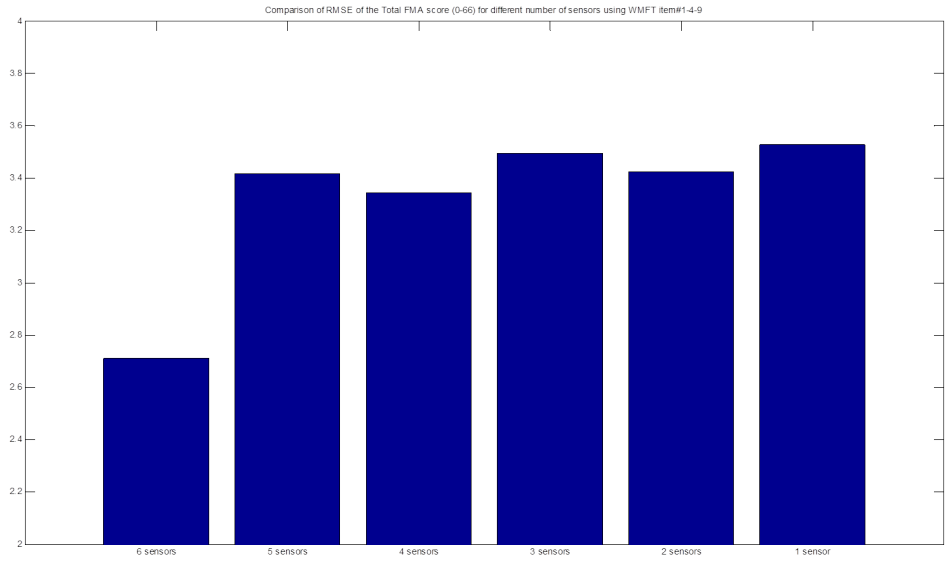

Figure 4.12: Effect of different number of sensors on the RMS error marking the FMA total score estimates using the combination of WMFT #1-4-9.

Table 4.7: Results for the lowest RMS Error for the Total FMA (0-66) using different number of sensors and the combination of WMFT #1-4-9.

WOLF item #1-4-9	**6 sensors**	**5 sensors**	**4 sensors**	**3 sensors**	**2 sensors**	**1 sensor**
RMSE Values	2.71	3.42	3.34	3.49	3.43	3.53
Sensors	Thumb–Index–Hand Forearm–Upper arm–Sternum	Thumb–Hand–Forearm Upper arm–Sternum	Thumb–Hand Upper arm–Sternum	Thumb–Hand–Sternum	Upper arm–Sternum	Sternum

sensors (figure 4.12). The highest RMSE is obtained using only one sensor (3.53) but it's still under the 10% of the Total FMA range. The lowest results (if we don't consider the result achieved by the complete set-up) is obtained with the use of only 4 sensors placed on the Thumb, on the Hand, on the Upper arm and on the Sternum (3.34). All the numerical results are shown in table 4.7.

Considering the best combinations of the WMFT items found for the Total FMA using all the six sensors, we tried to evaluate the influence of the number of sensors on the estimation of the Total FMA, in table 4.8

Table 4.8: Effect of the number of sensors on the RMS Error for the Total FMA (0-66) using the best different combinations of WMFT.

Task and Combination of Task	RMSE Total FMA (0-66) 20 features–Combination of Sensors	Number of Sensors	Sensors Combination	RMSE of the FMA Section 20 features–6 Sensors	Percentage of Increment or Decrement
WMFT item #9	3.74	5	Thumb–Hand–Forearm–Upper arm–Sternum	4.27	-12.41
WMFT item #1-4	3.27	3	Thumb–Index–Sternum	2.74	19.34
WMFT item #1-4-9	3.34	4	Thumb–Hand–Upper arm–Sternum	2.71	23.25
WMFT item #1-4-9-15	2.88	4	Index–Hand–Upper arm–Sternum	2.73	5.49
WMFT item #1-4-9-15-5	2.85	2	Hand–Sternum	2.74	4.01
WMFT item #1-4-9-15-5-13	2.88	3	Hand–Upper arm–Sternum	2.86	10.84
WMFT item #1-4-9-15-5-13-8	3.17	2	Hand–Sternum	2.86	10.84
WMFT item #1-4-9-15-5-13-8-10	3.12	2	Hand–Sternum	2.99	4.35

are shown the sensors chosen for each combination which gave the minimum RMS error, all the RMS error were above the 6% (3.74) of the Total FMA range (0-66) and of the observed range (22-66), as expected we noticed that increasing the number of combined WMFT items, the number of sensors needed is decreasing.

It's worthy to notice that the RMS error obtained with the use of only one sensor is not extremely higher considering the absolute value, compared with the results obtained using the single items with the use of all the six sensors (as previously shown in [139]), all the RMS errors exceeded the 10% of the Total score (6.6 points), except for the WMFT #9.

The lowest RMS error values for the different items are related to the hand, upper arm or thumb sensor: WMFT #1 (hand sensor: 8.56), WMFT #4 (upper arm sensor: 12.18), WMFT #5 (hand sensor: 8.18), WMFT #8 (hand sensor: 10.54), WMFT #9 (hand sensor: 4.46), WMFT #10 (upper arm sensor: 8.21), WMFT #13 (thumb sensor:7.61), WMFT #15 (forearm sensor: 7.24). Conversely, if we consider the RMS error associated to the sternum sensor is usually the highest, this is a good result because it means that the use of only the sternum sensor could not give good information and estimation of the Total scores.

4.4 Discussion and Conclusion

The results of our study indicate that estimates of the FMA total score can be derived by analyzing wearable sensor data collected during the performance of items and the WMFT. The RMS error of the FMA total score estimates that we derived was as low as 4.27 points of the FMA scale. This value is significantly lower than the RMS error value obtained when one relies upon deriving clinical estimates of the FAS score and estimating the FMA total score based on the correlation between the FMA total score and the FAS total score. In fact, in this latter case, the RMS error value marking the FMA total score estimates that we derived in the study was 6.99 points of the FMA scale.

It is worth emphasizing that the RMS error values that we derive to characterize estimates of the FMA total scores derived using wearable sensor data relate to the use of a single item of the WMFT. It is interesting to notice that item #9 of the WMFT was the one, among the 8 items selected for this study, that led to the lowest value of RMS error marking the FMA total score estimates. Item #9 of the WMFT is 'lifting a can'. These tasks require the performance of multiple movement components, namely reaching, manipulation and retrieve. This observation points to the need for analyzing complex movements to capture multiple aspects of the movement characteristics in stroke survivors that are associated with their level of impairment as captured using the FMA scale.

If we consider the use of combinations of different WMFT items, the best results for the total FMA was achieved by using three items (WMFT #1-4-9), but was comparable to the RMS error obtained by using just the pair WMFT #1-4 (2.74 vs 2.71). It is interesting to notice that item #1 and #4 are reaching tasks of the WMFT, while item #9 is a manipulation

task, so the subset of items #1-4-9 would include both the reaching and manipulation aspects–information of the patients' performances.

The performed analyses showed that it is possible to estimate FMA scores for sections of the scale so as to gain a better understanding of the relationships between patients' movement characteristics and specific sections of the FMA scale. As an example the pair WMFT #1-4 gave the best results in terms of RMS error for the TOTAL FMA (2.74) and for the Wrist-Hand FMA (1.45), if we consider the remaining FMA sections, the lowest RMS error results were achieved by the WMFT #1-9 for the Shoulder-Elbow-Wrist-Hand and Wrist FMA, the WMFT #10-15 for the Shoulder-Elbow, Shoulder and Extra 12 FMA sections, the WMFT #1-15 gave the minimum value for the Elbow section and the WMFT #1-5 for the Hand section. This analysis indicated the need for using wearable sensor data to estimate sections of the FMA scale, and that the features derived from wearable sensor data collected during performance of specific movement components such as reaching, manipulation and release could give more precise information about different sections of the FMA, which are related different movement patterns of the patients.

Focusing on the best result achieved with the use of the combination of three WMFT items (WMFT #1-4-9) and using different number of sensors, we noticed that the lowest results (if we don't consider the result achieved by the complete set-up) is obtained with the use of only 4 sensors placed on the Thumb, on the Hand, on the Upper arm and on the Sternum (3.34).

In the future, the methodology herein presented could become part of routine clinical assessments used to monitor patients' response rehabilitation interventions. It would become easy to assess the effectiveness of rehabilitation interventions on the patients by just using four sensors and by

performing a subset of three tasks (i.e. WMFT #1-4-9) of the WMFT, this reducing the time consuming and costs issues of these scales. Moreover with just the performance of a few items of the WMFT would be possible to estimate both the the total FAS score and the total FMA score, assessing not only the functionality, but also the impairment of the patients.

However, several aspects of the proposed methodology require further study before a deployment of this technology in a clinical context can be pursued.

Finally, a study in a larger cohort of stroke survivors should be performed before pursuing clinical assessment of the proposed method.

Bibliography

[1] A. Shumway-Cook, D. Anson, and S. Haller. Postural sway biofeedback: its effect on reestablishing stance stability in hemiplegic patients. *Arch Phys Med Rehabil*, 69:395–400, Jun 1988.

[2] J. Perry, M. Garrett, J. K. Gronley, and S. J. Mulroy. Classification of walking handicap in the stroke population. *Stroke*, 26:982–989, Jun 1995.

[3] N. Neckel, M. Pelliccio, D. Nichols, and J. Hidler. Quantification of functional weakness and abnormal synergy patterns in the lower limb of individuals with chronic stroke. *J Neuroeng Rehabil*, 3:17, 2006.

[4] B. H. Dobkin, A. Firestine, M. West, K. Saremi, and R. Woods. Ankle dorsiflexion as an fMRI paradigm to assay motor control for walking during rehabilitation. *Neuroimage*, 23:370–381, Sep 2004.

[5] G.R. Colborne, S.J. Olney, and M.P. Griffin. Feedback of ankle joint angle and soleus electromyography in the rehabilitation of hemiplegic gait. *Arch Phys Med Rehabil*, 74:1100–1106, 1999.

[6] J.V. Basmajian. *Biofeedback, principles and practice for clinicians.* William and Wilkins, Baltimore (MD), 2nd ed. 1983.

[7] N. Basaglia. *Il Biofeedback in clinica della riabilitazione.* Idelson, Liviana, Napoli, 1992.

[8] C.D. Cozean, W.S. Pease, and S.L. Hubbell. Biofeedback and functional electric stimulation in stroke rehabilitation. *Arch Phys Med Rehabil*, 69:401–419, 1988.

[9] S. J. Olney, G. R. Colborne, and C. S. Martin. Joint angle feedback and biomechanical gait analysis in stroke patients: a case report. *Phys Ther*, 69:863–870, Oct 1989.

[10] J. Perry. *Analisi del movimento.* Elsevier, 2005.

[11] S. Francis, X. Lin, S. Aboushoushah, T. P. White, M. Phillips, R. Bowtell, and C. S. Constantinescu. fMRI analysis of active, passive and electrically stimulated ankle dorsiflexion. *Neuroimage*, 44:469–479, Jan 2009.

[12] D.A. Winter. *The biomechanics and motor control of human gait: normal, elderly and pathological.* 2nd Ed. Waterloo, Ontario: University of Waterloo Press, 1991.

[13] E. Knutsson. Can gait analysis improve gait training in stroke patients. *Scand J Rehabil Med Suppl*, 30:73–80, 1994.

[14] J. Jonsdottir, D. Cattaneo, A. Regola, A. Crippa, M. Recalcati, M. Rabuffetti, M. Ferrarin, and A. Casiraghi. Concepts of motor learning applied to a rehabilitation protocol using biofeedback to improve gait in a chronic stroke patient: an A-B system study with multiple gait analyses. *Neurorehabil Neural Repair*, 21:190–194, 2007.

[15] J. Jonsdottir, D. Cattaneo, M. Recalcati, A. Regola, M. Rabuffetti, M. Ferrarin, and A. Casiraghi. Task-oriented biofeedback to improve gait in individuals with chronic stroke: motor learning approach. *Neurorehabil Neural Repair*, 24:478–485, Jun 2010.

[16] B. J. MacIntosh, R. Mraz, N. Baker, F. Tam, W. R. Staines, and S. J. Graham. Optimizing the experimental design for ankle dorsiflexion fMRI. *Neuroimage*, 22:1619–1627, Aug 2004.

[17] Dobkin B. Recovery of locomotor control. *Neurologist*, 2:239–249, 1996.

[18] C. Casellato, S. Ferrante, M. Gandolla, N. Volonterio, G. Ferrigno, G. Baselli, T. Frattini, A. Martegani, F. Molteni, and A. Pedrocchi. Simultaneous measurements of kinematics and fMRI: compatibility assessment and case report on recovery evaluation of one stroke patient. *J Neuroeng Rehabil*, 7:49, 2010.

[19] No authors listed. The World Health Organization MONICA Project (monitoring trends and determinants in cardiovascular disease): a major international collaboration. WHO MONICA Project Principal Investigators. *J Clin Epidemiol*, 41:105–114, 1988.

[20] A. D. Lopez, C. D. Mathers, M. Ezzati, D. T. Jamison, and C. J. Murray. Global and regional burden of disease and risk factors, 2001: systematic analysis of population health data. *Lancet*, 367:1747–1757, May 2006.

[21] V. L. Feigin, C. M. Lawes, D. A. Bennett, S. L. Barker-Collo, and V. Parag. Worldwide stroke incidence and early case fatality reported in 56 population-based studies: a systematic review. *Lancet Neurol*, 8:355–369, Apr 2009.

[22] G. Cesaroni, N. Agabiti, F. Forastiere, and C. A. Perucci. Socioeconomic differences in stroke incidence and prognosis under a universal healthcare system. *Stroke*, 40:2812–2819, Aug 2009.

[23] B. Stegmayr, K. Asplund, K. Kuulasmaa, A. M. Rajakangas, P. Thorvaldsen, and J. Tuomilehto. Stroke incidence and mortality correlated to stroke risk factors in the WHO MONICA Project. An ecological study of 18 populations. *Stroke*, 28:1367–1374, Jul 1997.

[24] J. Broderick, T. Brott, R. Kothari, R. Miller, J. Khoury, A. Pancioli, J. Gebel, D. Mills, L. Minneci, and R. Shukla. The Greater Cincinnati/Northern Kentucky Stroke Study: preliminary first-ever and total incidence rates of stroke among blacks. *Stroke*, 29:415–421, Feb 1998.

[25] R. D. Brown, J. P. Whisnant, J. D. Sicks, W. M. O'Fallon, and D. O. Wiebers. Stroke incidence, prevalence, and survival: secular trends in Rochester, Minnesota, through 1989. *Stroke*, 27:373–380, Mar 1996.

[26] C. D. Wolfe, A. G. Rudd, R. Howard, C. Coshall, J. Stewart, E. Lawrence, C. Hajat, and T. Hillen. Incidence and case fatality rates of stroke subtypes in a multiethnic population: the South London Stroke Register. *J. Neurol. Neurosurg. Psychiatr.*, 72:211–216, Feb 2002.

[27] E. McFadden, R. Luben, N. Wareham, S. Bingham, and K. T. Khaw. Social class, risk factors, and stroke incidence in men and women: a prospective study in the European prospective investigation into cancer in Norfolk cohort. *Stroke*, 40:1070–1077, Apr 2009.

[28] M. G. Marmot, H. Bosma, H. Hemingway, E. Brunner, and S. Stansfeld. Contribution of job control and other risk factors to social vari-

ations in coronary heart disease incidence. *Lancet*, 350:235–239, Jul 1997.

[29] I. Njolstad, E. Arnesen, and P. G. Lund-Larsen. Body height, cardiovascular risk factors, and risk of stroke in middle-aged men and women. A 14-year follow-up of the Finnmark Study. *Circulation*, 94:2877–2882, Dec 1996.

[30] M. Ezzati, A. D. Lopez, A. Rodgers, S. Vander Hoorn, and C. J. Murray. Selected major risk factors and global and regional burden of disease. *Lancet*, 360:1347–1360, Nov 2002.

[31] D. Leys, D. Deplanque, C. Mounier-Vehier, M. A. Mackowiak-Cordoliani, C. Lucas, and R. Bordet. Stroke prevention: management of modifiable vascular risk factors. *J. Neurol.*, 249:507–517, May 2002.

[32] G. Danaei, C. M. Lawes, S. Vander Hoorn, C. J. Murray, and M. Ezzati. Global and regional mortality from ischaemic heart disease and stroke attributable to higher-than-optimum blood glucose concentration: comparative risk assessment. *Lancet*, 368:1651–1659, Nov 2006.

[33] B. H. Dobkin. Functional MRI: a potential physiologic indicator for stroke rehabilitation interventions. *Stroke*, 34:e23–28, May 2003.

[34] S. Barbay, E. Zoubina, and R.J. Nudo. *Neural Plasticity in Adult Somatic Sensory-Motor Systems.* Neural Plasticy in Adult Motor Cortex, Taylor and Francis, 2005.

[35] T. E. Twitchell. The restoration of motor function following hemiplegia in man. *Brain*, 74:443–480, Dec 1951.

[36] E. S. Lawrence, C. Coshall, R. Dundas, J. Stewart, A. G. Rudd, R. Howard, and C. D. Wolfe. Estimates of the prevalence of acute stroke impairments and disability in a multiethnic population. *Stroke*, 32:1279–1284, Jun 2001.

[37] C. Benaim, D. A. Perennou, J. Villy, M. Rousseaux, and J. Y. Pelissier. Validation of a standardized assessment of postural control in stroke patients: the Postural Assessment Scale for Stroke Patients (PASS). *Stroke*, 30:1862–1868, Sep 1999.

[38] D. K. Sommerfeld, E. U. Eek, A. K. Svensson, L. W. Holmqvist, and M. H. von Arbin. Spasticity after stroke: its occurrence and association with motor impairments and activity limitations. *Stroke*, 35:134–139, Jan 2004.

[39] R.A. Schmidt. *Motor learning and performance. From principles to practice.* Human Kinetics Books, Campaign, Illinois, 1991.

[40] J.H. Carr and R.B. Shepherd. *A motor learning model for rehabilitation.* Heinemann Physiotherapy, London, 1987.

[41] P. Davies. *Steps to follow. The comprehensive treatment of patients with hemiplegia.* 2nd E. Springer-Verlag, Berlin and Heidelberg, 1987.

[42] M. H. Woollacott and A. Shumway-Cook. Changes in posture control across the life span-a systems approach. *Phys Ther*, 70:799–807, Dec 1990.

[43] A. Pollock, G. Baer, P. Langhorne, and V. Pomeroy. Physiotherapy treatment approaches for the recovery of postural control and lower limb function following stroke: a systematic review. *Clin Rehabil*, 21:395–410, May 2007.

[44] C. M. Dean and R. B. Shepherd. Task-related training improves performance of seated reaching tasks after stroke. A randomized controlled trial. *Stroke*, 28:722–728, Apr 1997.

[45] D.A. Perennou and A.M. Bronstein. *Balance disorders and vertigo after stroke: assessment and rehabilitation.* Recovery after stroke, Oxford: Oxford University Press, 2005.

[46] P. Duncan, S. Studenski, L. Richards, S. Gollub, S. M. Lai, D. Reker, S. Perera, J. Yates, V. Koch, S. Rigler, and D. Johnson. Randomized clinical trial of therapeutic exercise in subacute stroke. *Stroke*, 34:2173–2180, Sep 2003.

[47] S. Wood-Dauphinee and G. Kwakkel. *The impact of rehabilitation on stroke outcomes: what is the evidence?* 1st Ed. Recovery after stroke, Cambridge: Cambridge university Press, 2005.

[48] A. M. Moseley, A. Stark, I. D. Cameron, and A. Pollock. Treadmill training and body weight support for walking after stroke. *Cochrane Database Syst Rev*, page CD002840, 2005.

[49] C. J. Winstein, D. K. Rose, S. M. Tan, R. Lewthwaite, H. C. Chui, and S. P. Azen. A randomized controlled comparison of upper-extremity rehabilitation strategies in acute stroke: A pilot study of immediate and long-term outcomes. *Arch Phys Med Rehabil*, 85:620–628, Apr 2004.

[50] Y. R. Yang, R. Y. Wang, K. H. Lin, M. Y. Chu, and R. C. Chan. Task-oriented progressive resistance strength training improves muscle strength and functional performance in individuals with stroke. *Clin Rehabil*, 20:860–870, Oct 2006.

[51] H. S. Jorgensen, H. Nakayama, H. O. Raaschou, J. Vive-Larsen, M. St?ier, and T. S. Olsen. Outcome and time course of recovery in stroke. Part II: Time course of recovery. The Copenhagen Stroke Study. *Arch Phys Med Rehabil*, 76:406–412, May 1995.

[52] R. J. Nudo. Postinfarct cortical plasticity and behavioral recovery. *Stroke*, 38:840–845, Feb 2007.

[53] J. Biernaskie, G. Chernenko, and D. Corbett. Efficacy of rehabilitative experience declines with time after focal ischemic brain injury. *J. Neurosci.*, 24:1245–1254, Feb 2004.

[54] B. Dobkin and T. S. Carmichael. *Principples of recovery after stroke.* Recovery after stroke., Cambridge: Cambridge University Press, 2005.

[55] C. M. Butefisch, R. Kleiser, and R. J. Seitz. Post-lesional cerebral reorganisation: evidence from functional neuroimaging and transcranial magnetic stimulation. *J. Physiol. Paris*, 99:437–454, Jun 2006.

[56] F. C. Hummel and L. G. Cohen. Drivers of brain plasticity. *Curr. Opin. Neurol.*, 18:667–674, Dec 2005.

[57] R. J. Nudo, B. M. Wise, F. SiFuentes, and G. W. Milliken. Neural substrates for the effects of rehabilitative training on motor recovery after ischemic infarct. *Science*, 272:1791–1794, Jun 1996.

[58] S. C. Cramer, G. Nelles, R. R. Benson, J. D. Kaplan, R. A. Parker, K. K. Kwong, D. N. Kennedy, S. P. Finklestein, and B. R. Rosen. A functional MRI study of subjects recovered from hemiparetic stroke. *Stroke*, 28:2518–2527, Dec 1997.

[59] C. J. Perkins, E. Kahya, C. T. Roque, P. E. Roche, and G. C. Newman. Fluid-attenuated inversion recovery and diffusion- and perfusion-weighted MRI abnormalities in 117 consecutive patients with stroke symptoms. *Stroke*, 32:2774–2781, Dec 2001.

[60] H. Johansen-Berg. Functional imaging of stroke recovery: what have we learnt and where do we go from here? *Int J Stroke*, 2:7–16, Feb 2007.

[61] A. Krainik, M. Hund-Georgiadis, S. Zysset, and D. Y. von Cramon. Regional impairment of cerebrovascular reactivity and BOLD signal in adults after stroke. *Stroke*, 36:1146–1152, Jun 2005.

[62] P. M. Rossini, C. Altamura, A. Ferretti, F. Vernieri, F. Zappasodi, M. Caulo, V. Pizzella, C. Del Gratta, G. L. Romani, and F. Tecchio. Does cerebrovascular disease affect the coupling between neuronal activity and local haemodynamics? *Brain*, 127:99–110, Jan 2004.

[63] C. Calautti and J. C. Baron. Functional neuroimaging studies of motor recovery after stroke in adults: a review. *Stroke*, 34:1553–1566, Jun 2003.

[64] S. C. Cramer and K. R. Crafton. Somatotopy and movement representation sites following cortical stroke. *Exp Brain Res*, 168:25–32, Jan 2006.

[65] D. Tombari, I. Loubinoux, J. Pariente, A. Gerdelat, J. F. Albucher, J. Tardy, E. Cassol, and F. Chollet. A longitudinal fMRI study: in recovering and then in clinically stable sub-cortical stroke patients. *Neuroimage*, 23:827–839, Nov 2004.

[66] I. Loubinoux, C. Carel, J. Pariente, S. Dechaumont, J. F. Albucher, P. Marque, C. Manelfe, and F. Chollet. Correlation between cerebral reorganization and motor recovery after subcortical infarcts. *Neuroimage*, 20:2166–2180, Dec 2003.

[67] C. Gerloff, K. Bushara, A. Sailer, E. M. Wassermann, R. Chen, T. Matsuoka, D. Waldvogel, G. F. Wittenberg, K. Ishii, L. G. Cohen, and M. Hallett. Multimodal imaging of brain reorganization in motor areas of the contralesional hemisphere of well recovered patients after capsular stroke. *Brain*, 129:791–808, Mar 2006.

[68] A. Thiel, B. Aleksic, J. C. h. Klein, J. Rudolf, and W. D. Heiss. Changes in proprioceptive systems activity during recovery from post-stroke hemiparesis. *J Rehabil Med*, 39:520–525, Sep 2007.

[69] J. D. Schaechter and K. L. Perdue. Enhanced cortical activation in the contralesional hemisphere of chronic stroke patients in response to motor skill challenge. *Cereb. Cortex*, 18:638–647, Mar 2008.

[70] Y. Iwamura, M. Taoka, and A. Iriki. Bilateral activity and callosal connections in the somatosensory cortex. *Neuroscientist*, 7:419–429, Oct 2001.

[71] J. Doyon, V. Penhune, and L. G. Ungerleider. Distinct contribution of the cortico-striatal and cortico-cerebellar systems to motor skill learning. *Neuropsychologia*, 41:252–262, 2003.

[72] E. J. Plautz, G. W. Milliken, and R. J. Nudo. Effects of repetitive motor training on movement representations in adult squirrel monkeys: role of use versus learning. *Neurobiol Learn Mem*, 74:27–55, Jul 2000.

[73] J. W. Krakauer. Motor learning: its relevance to stroke recovery and neurorehabilitation. *Curr. Opin. Neurol.*, 19:84–90, Feb 2006.

[74] M. K. Stehling, R. Turner, and P. Mansfield. Echo-planar imaging: magnetic resonance imaging in a fraction of a second. *Science*, 254:43–50, Oct 1991.

[75] G. H. Glover and S. Lai. Self-navigated spiral fMRI: interleaved versus single-shot. *Magn Reson Med*, 39:361–368, Mar 1998.

[76] J. Hennig. K-space sampling strategies. *Eur Radiol*, 9:1020–1031, 1999.

[77] J. Hennig, O. Speck, M. A. Koch, and C. Weiller. Functional magnetic resonance imaging: a review of methodological aspects and clinical applications. *J Magn Reson Imaging*, 18:1–15, Jul 2003.

[78] S. Ogawa, T. M. Lee, A. S. Nayak, and P. Glynn. Oxygenation-sensitive contrast in magnetic resonance image of rodent brain at high magnetic fields. *Magn Reson Med*, 14:68–78, Apr 1990.

[79] S. Ogawa, R. S. Menon, D. W. Tank, S. G. Kim, H. Merkle, J. M. Ellermann, and K. Ugurbil. Functional brain mapping by blood oxygenation level-dependent contrast magnetic resonance imaging. A comparison of signal characteristics with a biophysical model. *Biophys. J.*, 64:803–812, Mar 1993.

[80] D. G. Norris. Principles of magnetic resonance assessment of brain function. *J Magn Reson Imaging*, 23:794–807, Jun 2006.

[81] R. S. Menon. Imaging function in the working brain with fMRI. *Curr. Opin. Neurobiol.*, 11:630–636, Oct 2001.

[82] M. S. Cohen. Parametric analysis of fMRI data using linear systems methods. *Neuroimage*, 6:93–103, Aug 1997.

[83] X. Hu, T. H. Le, T. Parrish, and P. Erhard. Retrospective estimation and correction of physiological fluctuation in functional MRI. *Magn Reson Med*, 34:201–212, Aug 1995.

[84] E. Seto, G. Sela, W. E. McIlroy, S. E. Black, W. R. Staines, M. J. Bronskill, A. R. McIntosh, and S. J. Graham. Quantifying head motion associated with motor tasks used in fMRI. *Neuroimage*, 14:284–297, Aug 2001.

[85] K. J. Friston, S. Williams, R. Howard, R. S. Frackowiak, and R. Turner. Movement-related effects in fMRI time-series. *Magn Reson Med*, 35:346–355, Mar 1996.

[86] S.A. Huettel, A.W. Song, and G. MCCarthy. *Functional Magnetic Resonance Imaging.* Associates S Editor, 2004.

[87] K. J. Friston, P. Fletcher, O. Josephs, A. Holmes, M. D. Rugg, and R. Turner. Event-related fMRI: characterizing differential responses. *Neuroimage*, 7:30–40, Jan 1998.

[88] A. Cappozzo, F. Catani, A. Leardini, M. G. Benedetti, and U. D. Croce. Position and orientation in space of bones during movement: experimental artefacts. *Clin Biomech (Bristol, Avon)*, 11:90–100, Mar 1996.

[89] E. J. Alexander and T. P. Andriacchi. Correcting for deformation in skin-based marker systems. *J Biomech*, 34:355–361, Mar 2001.

[90] A. Cappozzo, U. Della Croce, A. Leardini, and L. Chiari. Human movement analysis using stereophotogrammetry. Part 1: theoretical background. *Gait Posture*, 21:186–196, Feb 2005.

[91] U. Della Croce and A. Cappozzo. A spot check for estimating stereophotogrammetric errors. *Med Biol Eng Comput*, 38:260–266, May 2000.

[92] L. Chiari, U. Della Croce, A. Leardini, and A. Cappozzo. Human movement analysis using stereophotogrammetry. Part 2: instrumental errors. *Gait Posture*, 21:197–211, Feb 2005.

[93] A. Leardini, L. Chiari, U. Della Croce, and A. Cappozzo. Human movement analysis using stereophotogrammetry. Part 3. Soft tissue artifact assessment and compensation. *Gait Posture*, 21:212–225, Feb 2005.

[94] Aurelio Cappozzo. Three-dimensional analysis of human walking: Experimental methods and associated artifacts. *Human Movement Science*, 10(5):589–602, 1991.

[95] T. P. Andriacchi and E. J. Alexander. Studies of human locomotion: past, present and future. *J Biomech*, 33:1217–1224, Oct 2000.

[96] A. Cappozzo, A. Cappello, U. Della Croce, and F. Pensalfini. Surface-marker cluster design criteria for 3-D bone movement reconstruction. *IEEE Trans Biomed Eng*, 44:1165–1174, Dec 1997.

[97] T. P. Andriacchi, E. J. Alexander, M. K. Toney, C. Dyrby, and J. Sum. A point cluster method for in vivo motion analysis: applied to a study of knee kinematics. *J Biomech Eng*, 120:743–749, Dec 1998.

[98] A. Cappello, A. Cappozzo, and T.E. Prampero. *Bioingegneria della postura e del movimento.* Patron Editore, 2003.

[99] Y.I. Abdel-Aziz and H.M. Karara. Direct linear transformation into object space coordinates in close-range photogrammetry. *Proc ASP Symp Close Range Photogram - Urbana - IL*, 1971.

[100] J. Dapena, E. A. Harman, and J. A. Miller. Three-dimensional cinematography with control object of unknown shape. *J Biomech*, 15:11–19, 1982.

[101] P. K. Weng and J. S. Shie. Self-directioning with the revolving retroreflection technique. *Appl Opt*, 31:4365–4370, Aug 1992.

[102] Z. Zhang. A flexible new technique for camera calibration. *IEEE Transactions on Pattern Analysis and Machine Intelligence*, 22(11):1130–1134, 2000.

[103] P. Cerveri, N. A. Borghese, and A. Pedotti. Complete calibration of a stereo photogrammetric system through control points of unknown coordinates. *J Biomech*, 31:935–940, Oct 1998.

[104] Gennery Donald B. Visual tracking of known three-dimensional objects. *International Journal of Computer Vision*, 7:243–270, 1992.

[105] D.M. Gavrila and L.S. Davis. Towards 3-D model-based tracking and recognition of human movement: a multi-view approach. In *In International Workshop on Automatic Face- and Gesture-Recognition. IEEE Computer Society*, pages 272–277, 1995.

[106] P. R. Cavanagh. A technique for averaging center of pressure paths from a force platform. *J Biomech*, 11:487–491, 1978.

[107] A. Cappozzo, F. Catani, U. D. Croce, and A. Leardini. Position and orientation in space of bones during movement: anatomical frame definition and determination. *Clin Biomech (Bristol, Avon)*, 10:171–178, Jun 1995.

[108] G. Wu, S. Siegler, P. Allard, C. Kirtley, A. Leardini, D. Rosenbaum, M. Whittle, D. D. D'Lima, L. Cristofolini, H. Witte, O. Schmid, and I. Stokes. ISB recommendation on definitions of joint coordinate system of various joints for the reporting of human joint motion–part I: ankle, hip, and spine. International Society of Biomechanics. *J Biomech*, 35:543–548, Apr 2002.

[109] M. Rabuffetti, M. Ferrarin, P. Mazzoleni, F. Benvenuti, and A. Pedotti. Optimised procedure for the calibration of the force platform location. *Gait Posture*, 17:75–80, Feb 2003.

[110] Aurelio Cappozzo. Gait analysis methodology. *Human Movement Science*, 3(1-2):27–50, 1984.

[111] I. Davis, S. Ounpuu, D. Tyburski, and J.R. Gage. A gait analysis data collection and reduction technique. *Human Movement Science*, 10(5):575–587, Oct 1991.

[112] M. P. Kadaba, H. K. Ramakrishnan, and M. E. Wootten. Measurement of lower extremity kinematics during level walking. *J. Orthop. Res.*, 8:383–392, May 1990.

[113] U. Della Croce, A. Cappozzo, and D. C. Kerrigan. Pelvis and lower limb anatomical landmark calibration precision and its propagation to bone geometry and joint angles. *Med Biol Eng Comput*, 37:155–161, Mar 1999.

[114] E. Stindel, J. L. Briard, P. Merloz, S. Plaweski, F. Dubrana, C. Lefevre, and J. Troccaz. Bone morphing: 3D morphological data for total knee arthroplasty. *Comput. Aided Surg.*, 7:156–168, 2002.

[115] G.T. Rab, J. Rose, and J.G. Gamble. *Human Walking. 2nd Edition.* Williams and Wilkins, Baltimore, 1994.

[116] C.L. Vaughan, B.L. Davis, and J.C. O'Connor. *Dynamics of human gait.* Number v. 2 in Dynamics of Human Gait. Human Kinetics Publishers, 1992.

[117] M. G. Benedetti, F. Catani, A. Leardini, E. Pignotti, and S. Giannini. Data management in gait analysis for clinical applications. *Clin Biomech (Bristol, Avon)*, 13:204–215, Apr 1998.

[118] A. Leardini, Z. Sawacha, G. Paolini, S. Ingrosso, R. Nativo, and M. G. Benedetti. A new anatomically based protocol for gait analysis in children. *Gait Posture*, 26:560–571, Oct 2007.

[119] Z. Sawacha, G. Gabriella, G. Cristoferi, A. Guiotto, A. Avogaro, and C. Cobelli. Diabetic gait and posture abnormalities: a biomechanical investigation through three dimensional gait analysis. *Clin Biomech (Bristol, Avon)*, 24:722–728, Nov 2009.

[120] C. Frigo, M. Rabuffetti, D. C. Kerrigan, L. C. Deming, and A. Pedotti. Functionally oriented and clinically feasible quantitative gait analysis method. *Med Biol Eng Comput*, 36:179–185, Mar 1998.

[121] M. Rabuffetti and P. Crenna. A modular protocol for the analysis of movement in children. *Gait Posture*, 20:S77–S78, 2004.

[122] A. Ferrari, M. G. Benedetti, E. Pavan, C. Frigo, D. Bettinelli, M. Rabuffetti, P. Crenna, and A. Leardini. Quantitative comparison of five current protocols in gait analysis. *Gait Posture*, 28:207–216, Aug 2008.

[123] L.G. Portney and M.P. Walkins. *Foundations of clinical research: application to practice.* Prentice Hall Health, Upper Saddle River (NJ), 1999.

[124] C. Frigo and M. Rabuffetti. Multifactorial estimation of hip and knee joint centres for clinical application of gait analysis. *Gait Posture*, 8:91–102, Oct 1998.

[125] K.J. Friston, K.J. Worsley, R.S.J. Frackowiak, J.C. Mazziotta, and A.C. Evans. Assessing the significance of focal activations using their spatial extent. *Human Brain Mapping*, 1:214–220, 1994.

[126] K.J. Friston, J. Ashburner, C.D. Frith, J.B. Poline, J.D. Heather, and R.S.J. Frackowiak. The spatial registration and normalisation of images. *Human Brain Mapping*, 3:165–189, 1995.

[127] J. Jonsdottir, M. Recalcati, M. Rabuffetti, A. Casiraghi, S. Boccardi, and M. Ferrarin. Functional resources to increase gait speed in people with stroke: strategies adopted compared to healthy controls. *Gait Posture*, 29:355–359, Apr 2009.

[128] R Development Core Team. *R: A Language and Environment for Statistical Computing.* R Foundation for Statistical Computing, Vienna, Austria, 2011. ISBN 3-900051-07-0.

[129] V. L. Roger, A. S. Go, D. M. Lloyd-Jones, R. J. Adams, J. D. Berry, T. M. Brown, M. R. Carnethon, S. Dai, G. de Simone, E. S. Ford, C. S.

Fox, H. J. Fullerton, C. Gillespie, K. J. Greenlund, S. M. Hailpern, J. A. Heit, P. M. Ho, V. J. Howard, B. M. Kissela, S. J. Kittner, D. T. Lackland, J. H. Lichtman, L. D. Lisabeth, D. M. Makuc, G. M. Marcus, A. Marelli, D. B. Matchar, M. M. McDermott, J. B. Meigs, C. S. Moy, D. Mozaffarian, M. E. Mussolino, G. Nichol, N. P. Paynter, W. D. Rosamond, P. D. Sorlie, R. S. Stafford, T. N. Turan, M. B. Turner, N. D. Wong, and J. Wylie-Rosett. Heart disease and stroke statistics–2011 update: a report from the American Heart Association. *Circulation*, 123:e18–e209, Feb 2011.

[130] National Institute of Neurological Disorders and Stroke (NINDS). Stroke: Hope through research. NINDS, Washington, DC, 2004.

[131] V. M. Pomeroy, A. Pramanik, L. Sykes, J. Richards, and E. Hill. Agreement between physiotherapists on quality of movement rated via videotape. *Clin Rehabil*, 17:264–272, May 2003.

[132] S. L. Wolf, P. A. Catlin, M. Ellis, A. L. Archer, B. Morgan, and A. Piacentino. Assessing Wolf motor function test as outcome measure for research in patients after stroke. *Stroke*, 32:1635–1639, Jul 2001.

[133] S. L. Wolf, J. P. McJunkin, M. L. Swanson, and P. S. Weiss. Pilot normative database for the Wolf Motor Function Test. *Arch Phys Med Rehabil*, 87:443–445, Mar 2006.

[134] J. Sanford, J. Moreland, L. R. Swanson, P. W. Stratford, and C. Gowland. Reliability of the Fugl-Meyer assessment for testing motor performance in patients following stroke. *Phys Ther*, 73:447–454, Jul 1993.

[135] J. H. van der Lee, H. Beckerman, G. J. Lankhorst, and L. M. Bouter. The responsiveness of the Action Research Arm test and the Fugl-

Meyer Assessment scale in chronic stroke patients. *J Rehabil Med*, 33:110–113, Mar 2001.

[136] P. Bonato. Advances in wearable technology and applications in physical medicine and rehabilitation. *J Neuroeng Rehabil*, (1):2, Feb 2005.

[137] P. Bonato. Advances in wearable technology for rehabilitation. *Stud Health Technol Inform*, 145:145–159, 2009.

[138] T. Hester, R. Hughes, D. M. Sherrill, B. Knorr, M. Akay, J. Stein, and P. Bonato. Using wearable sensors to measure motor abilities following stroke. *Third Annual Workshop on Wearable and Implantable Body Sensor Networks (BSN)*, pages 5–8, 2006.

[139] S. Patel, R. Hughes, T. Hester, J. Stein, M. Akay, J. Dy, and P. Bonato. Tracking motor recovery in stroke survivors undergoing rehabilitation using wearable technology. *Conf Proc IEEE Eng Med Biol Soc*, 98(3):6858–6861, 2010.

[140] M. Robnik-Sikonja and I. Kononenko. Theoretical and Empirical Analysis of ReliefF and RReliefF. *Machine Learning*, pages 23–69, 2003.

[141] L. Breiman. Random forests. *Mach Learn*, 45:5–32, 2001.

[142] N.V. Chawla, K.W. Bowyer, L.O. Hall, and W.P. Kegelmeyer. Smote: Synthetic minority over-sampling technique. *Journal of Artificial Intelligence Research*, 16:321–357, 2002.

[143] IH. Witten and E. Frank. *Data Mining: Practical machine learning tools and techniques.* Morgan Kaufman, San Francisco, 2005.